

## INFORMATION TO USERS

This manuscript has been reproduced from the microfilm master. UMI films the text directly from the original or copy submitted. Thus, some thesis and dissertation copies are in typewriter face, while others may be from any type of computer printer.

**The quality of this reproduction is dependent upon the quality of the copy submitted.** Broken or indistinct print, colored or poor quality illustrations and photographs, print bleedthrough, substandard margins, and improper alignment can adversely affect reproduction.

In the unlikely event that the author did not send UMI a complete manuscript and there are missing pages, these will be noted. Also, if unauthorized copyright material had to be removed, a note will indicate the deletion.

Oversize materials (e.g., maps, drawings, charts) are reproduced by sectioning the original, beginning at the upper left-hand corner and continuing from left to right in equal sections with small overlaps. Each original is also photographed in one exposure and is included in reduced form at the back of the book.

Photographs included in the original manuscript have been reproduced xerographically in this copy. Higher quality 6" x 9" black and white photographic prints are available for any photographs or illustrations appearing in this copy for an additional charge. Contact UMI directly to order.

# U·M·I

University Microfilms International  
A Bell & Howell Information Company  
300 North Zeeb Road, Ann Arbor, MI 48106-1346 USA  
313/761-4700 800/521-0600



**Order Number 9303403**

**Geochemical studies of fumarolic systems in the eastern  
Aleutian Volcanic Arc: Applications for understanding  
magmatic and volcanic processes**

**Kodosky, Lawrence Gerard, Ph.D.**

**University of Alaska Fairbanks, 1992**

**Copyright ©1993 by Kodosky, Lawrence Gerard. All rights reserved.**

**U·M·I**

300 N. Zeeb Rd.  
Ann Arbor, MI 48106



**GEOCHEMICAL STUDIES OF FUMAROLIC SYSTEMS  
IN THE EASTERN ALEUTIAN VOLCANIC ARC:  
APPLICATIONS FOR UNDERSTANDING  
MAGMATIC AND VOLCANIC PROCESSES**

**A  
THESIS**

**Presented to the Faculty of the University of Alaska  
in Partial Fulfillment of the Requirements  
for the Degree of**

**DOCTOR of PHILOSOPHY**

**By  
LAWRENCE G. KODOSKY, B.S., M.S.**

**Fairbanks, Alaska**


**May 1992**

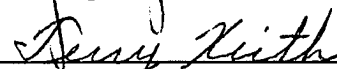
**GEOCHEMICAL STUDIES OF FUMAROLIC SYSTEMS  
IN THE EASTERN ALEUTIAN VOLCANIC ARC:  
APPLICATIONS FOR UNDERSTANDING  
MAGMATIC AND VOLCANIC PROCESSES**

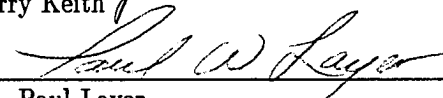
by

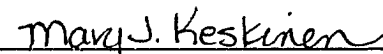
Lawrence G. Kodosky

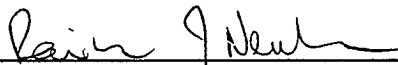
RECOMMENDED:

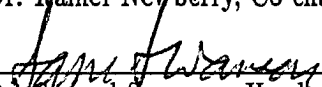
  
\_\_\_\_\_  
Dr. Juergen Kienle

  
\_\_\_\_\_  
Terry Keith


  
\_\_\_\_\_  
Dr. Paul Layer


  
\_\_\_\_\_  
Dr. Mary Keskinen, Co-chairman, Advisory Committee

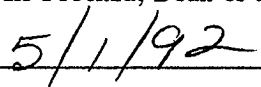
  
\_\_\_\_\_  
Dr. Rainer Neuberry, Co-chairman, Advisory Committee

  
\_\_\_\_\_  
Dr. Samuel Swanson, Head, Department of Geology and Geophysics

APPROVED:

  
\_\_\_\_\_  
Dr. Paul Reichardt, Dean, College of Natural Sciences

  
\_\_\_\_\_  
Dr. Luis Proenza, Dean of the Graduate School

  
\_\_\_\_\_  
Date

## Abstract

Geochemical studies of active and fossil fumaroles were conducted at Mount St. Augustine and the Valley of Ten Thousand Smokes (VTTS) to investigate fumarolic systems for providing information on volcanic and magmatic processes. Gases and condensates collected from high-temperature rooted fumaroles at Mount St. Augustine in 1979, 1982, and 1984 are characterized by systematic long-term trends in gas composition and stable isotopes that can be best explained by progressive magmatic outgassing coupled with increasing proportions of seawater in the fumarolic emissions. Seawater-magma interaction may initiate some of the early explosive phases of Mount St. Augustine eruptions.

The distribution and morphology of rootless fumaroles formed on pyroclastic flows and a lava flow emplaced during the 1986 eruptive cycle of Mount St. Augustine were controlled by pre-eruption drainage and topography, as well as by the thickness, compaction, and settling of the flow deposits. The majority of chemical components present in encrustations collected from these active fumaroles were derived by acidic condensate leaching of the eruptive deposits. Trace-element distribution apparently followed a pattern of isomorphic substitution in the encrustation phases.

A reconnaissance survey of surface  $Hg^0$  contents in the VTTS supports the presence of a shallow intrusion beneath the dome-like feature known as the Turtle. Based on the  $Hg^0$  data, the preferred model of the 1912 Novarupta vent is one generated by collapse of supporting vent walls into a cored-out explosive vent after the major eruptive phase. Vent morphology is funnel-like with subsidence concentrated in the narrow funnel center. The magnitude of the Novarupta Basin  $Hg^0$  anomalies implies that a shallow ( $\approx 1$  km depth) incipient hydrothermal system has developed beneath the vent.

Although the VTTS primary fumarolic deposits have been severely degraded by weathering, the fossil encrustations preserve a signature of their initial formation processes and subsequent evolution. Statistical analysis of chemical data suggests alteration of the VTTS ejecta as the primary source for the encrustation chemical components. Vapor phase transport of elements, probably as halide or oxyhalide species, occurred in the VTTS fumaroles and was significant for As, Sb, and Br.



## Table of Contents

	Page
Abstract	iii
Table of Contents	v
List of Figures	vii
List of Tables	x
Acknowledgments	xi
<b>CHAPTER 1: INTRODUCTION</b>	<b>1</b>
Assumptions, Techniques, and Limitations of Fumarole Studies	2
Some Applications of Fumarole Studies	7
Thesis Study Objectives	10
<b>CHAPTER 2: FUMAROLIC EMISSIONS AT MOUNT ST. AUGUSTINE: 1979-1984</b>	<b>15</b>
Introduction	15
Mount St. Augustine	16
Previous Studies of Volatiles at Mount St. Augustine	17
Fumarolic Activity, Sampling Sites and Collection Procedures	20
Analytical Methods	21
Results	23
Discussion	42
<b>CHAPTER 3: ROOTLESS FUMAROLIC DEPOSITS OF THE 1986 MOUNT ST. AUGUSTINE ERUPTIVE DEPOSITS</b>	<b>62</b>
Introduction	62
Characteristics of the 1986 Lava and Pyroclastic Flows	62
Fumarole Distribution and Morphology	63
Fumarolic Encrustation Mineralogy and Chemistry	68
Discussion	78

<b>CHAPTER 4: RECONNAISSANCE Hg<sup>o</sup> SURVEY OF THE VTTS</b>	84
Introduction	84
The 1912 Katmai Eruption	86
Nature of the 1912 Vent	88
Mercury Geochemistry	94
Sampling and Analytical Procedures	96
Data Analysis	97
Results	101
Discussion	106
<b>CHAPTER 5: EVALUATION OF THE VTTS ALTERATION SAMPLES</b>	111
Introduction	111
Nature of the 1912 Ash-Flow Sheet	113
Fumarole Evolution, Distribution and Morphology	115
Previous Studies of the VTTS Encrustations	117
Mineralogy and Chemistry of the Alteration Samples	120
Discussion	148
<b>CHAPTER 6: DISCUSSION AND CONCLUSIONS</b>	155
<b>CHAPTER 7: RECOMMENDATIONS FOR FUTURE WORK</b>	166
References	171
Appendix 1      Results of X-ray Diffraction Analyses	185
Appendix 2      Geochemistry of the Mount St. Augustine Samples*	187
Appendix 3      VTTS Hg <sup>o</sup> and Au Data	189
Appendix 4      Geochemistry of the VTTS Samples	194

## List of Figures

		Page
Fig. 1	Location map for lower Cook Inlet, Alaska.	18
Fig. 2	Oxygen fugacity - temperature relationships for the summit dome gas samples.	27
Fig. 3	$\delta D$ - $\delta^{18}O$ plot for summit fumarolic condensates and local surface waters from 1979-1984.	38
Fig. 4	Changes in $H_2O$ content from 1979 through 1984 for the summit gas samples.	43
Fig. 5a-b	Atomic ratio plots for the summit gas samples.	44
Fig. 6	Log H/C versus Log H/S for the summit gas samples.	45
Fig. 7	Changes in $CO_2/H_2$ ratios in the summit gas samples.	46
Fig. 8	Explosive event duration (26 March - 2 April 1986) at Augustine volcano.	54
Fig. 9a-c	Fumarole vent types and measured fumarole temperatures in the 1986 eruptive deposits.	64
Fig. 10	Example of pre-eruption drainage control on fumarole distribution.	67
Fig. 11	Fumarole sample sites at Augustine volcano.	70
Fig. 12a-g	SEM photographs of observed encrustation mineralogies and morphologies.	72
Fig. 13	Chemical variation between two fumarole types.	75
Fig. 14a-b	Scatter plots illustrating the isomorphic substitution of elements.	76
Fig. 14c-d	Scatter plots illustrating the isomorphic substitution of elements.	77
Fig. 15	Log $fO_2$ - temperature of formation conditions estimated for the encrustations.	79
Fig. 16	Location map for the upper Alaska Peninsula.	85

Fig. 17	Location map for the Valley of Ten Thousand Smokes.	87
Fig. 18	Map showing the concentric and radial fractures which outline the 1912 vent in the area around Novarupta dome (N).	89
Fig. 19a-b	Proposed models for the 1912 Novarupta vent.	91
Fig. 20a-b	Novarupta Basin sample traverse lines and fumarole sample sites.	98
Fig. 21	Fumarole sample sites in the VTTS.	99
Fig. 22	Hg <sup>o</sup> contrast values for fumarole sample sites within the VTTS.	102
Fig. 23	Hg <sup>o</sup> contrast values for fumarole sample sites within Novarupta Basin.	103
Fig. 24	Hg <sup>o</sup> contrast profiles across sample traverse line A-A'.	105
Fig. 25	Hg <sup>o</sup> contrast profile across sample traverse line B-B'.	105
Fig. 26	Modified version of the cylindrical 1912 vent model of Figure 19b assuming a shallow intrusion beneath the Turtle.	109
Fig. 27	Preferred 1912 vent model based on results of the Hg <sup>o</sup> survey and available geological and geophysical data.	109
Fig. 28	Fumarole sample sites in the VTTS.	114
Fig. 29a-b	Box plots of the VTTS encrustation chemistry.	124
Fig. 29c-d	Box plots of the VTTS encrustation chemistry.	125
Fig. 29e-f	Box plots of the VTTS encrustation chemistry.	126
Fig. 30a-b	Mean enrichment factors (EF) for the VTTS alteration products.	130
Fig. 30c-d	Mean enrichment factors (EF) for the VTTS alteration products.	131
Fig. 31a-b	Scatter plots illustrating elemental covariance in the VTTS encrustations.	136
Fig. 31c-d	Scatter plots illustrating elemental covariance in the VTTS encrustations.	137

- Fig. 32 Cross-plot of the canonical variable derived from factor 1 of the major oxides (CNVRF1) against the canonical variable derived from factor two of the trace elements (CNVRF2). 146
- Fig. 33 Cross-plot of the canonical variable derived from factor 4 of the major oxides (CNVRF1) against the canonical variable derived from factor 1 of the trace elements (CNVRF2). 147

## List of Tables

		Page
Table 1	Analyses of high-temperature fumarolic gases.	24
Table 2	Gas analyses recalculated after removal of N <sub>2</sub> , Ar and O <sub>2</sub> .	25
Table 3	Estimated gas compositions for the 1979 NaOH samples.	30
Table 4	Estimated water compositions, equilibrium temperatures and <i>f</i> O <sub>2</sub> values for the dry flask samples.	33
Table 5	Anion analysis of a 1982 summit fumarolic condensate.	34
Table 6	Correspondence temperatures and restored gas compositions for the 1984 NaOH samples.	36
Table 7	Isotopic analyses of fumarolic emissions from the 1976 dome.	39
Table 8	Isotopic fractionation temperatures for Δ (H <sub>2</sub> -H <sub>2</sub> O).	40
Table 9	Whole rock oxide and trace-element analyses of lavas, pumice, unaltered ash and fumarolic encrustations from Mt. St. Augustine.	65
Table 10	Characteristics of pyroclastic and lava flow fumaroles.	68
Table 11	Summary of F test statistics for Hg <sup>0</sup> data set.	100
Table 12	Calculated Hg <sup>0</sup> threshold values.	101
Table 13	XRD-determined minerals in the VTTS alteration samples.	122
Table 14	Correlation matrix for the encrustation samples.	134
Table 15	Factor loadings and scores for the major oxide data.	140
Table 16	Factor loadings and scores for the trace-element data.	141
Table 17	Example of statistical parameters for canonical correlation.	145
Table 18	Percentage of data variance explained by the individual factors.	150

## Acknowledgments

This thesis is jointly dedicated to my parents and family who have always encouraged me in my academic pursuits, and to my students in China, very few of which will probably ever have an opportunity to pursue a graduate education. My committee members, Dr. Rainer Newberry, Dr. Mary Keskinen, Terry Keith, Dr. Juergen Kienle and Dr. Paul Layer, have helped to guide this study and bring it to fruition. Special thanks go to Dr. Sam Swanson for sharing his technical expertise as well as for his repeated attempts to secure funding for this project. Partial financial support in the form of teaching assistantships and field travel grants from the Department of Geology and Geophysics is greatly appreciated. Upon returning to this work after a one year leave of absence, the Alaska Volcano Observatory, through Dr. Juergen Kienle, provided financial support which enabled me to concentrate on finishing a thesis draft.

Material from three of the thesis chapters has been published as scientific journal articles. A footnote at the beginning of the appropriate chapter details the publication source and authorship of these articles. The manuscript examining Mount St. Augustine gas chemistry (Chapter 2), co-authored with Roman Motyka and Robert Symonds, would not have been possible without Dr. Roman Motyka of the Alaska Division of Geological and Geophysical Surveys, who gave me access to his gas chemistry data set. Dr. Motyka also helped with the data reduction and manuscript preparation. During a four day visit to the Michigan Technological University in January, 1990, Robert Symonds assisted me in thermodynamic modeling of the Mount St. Augustine gas data using his computer code SOLVGAS. This allowed Dr. Motyka and me to check our earlier more crude thermodynamic modeling of the gas data. Dr. Sam Swanson, Dr. Mary Keskinen and Dr. Dan Hawkins provided thoughtful reviews of this manuscript.

During preparation of the Mount St. Augustine fumarolic encrustation manuscript (Chapter 3), my co-author Dr. Mary Keskinen served as an advisor and editor. While I

was in China, Dr. Keskinen also took the lead in completing the final editorial revisions for this manuscript. Her help is highly appreciated. Dr. Sam Swanson critically reviewed this manuscript.

Although the manuscript on surficial Hg<sup>0</sup> chemistry derived from Chapter 4 was solely authored by myself, Dr. Mary Keskinen aided in part with the sample collection and contributed insight on the behavior of Hg in geothermal systems. Tom and Cheryl Dyehouse also helped in part with the sample collection.

Many other faculty, staff and students at the University of Alaska Fairbanks have helped to facilitate this study. Although too numerous to mention, the advice, moral support and friendship of these individuals allowed me to persevere and bring this work to completion. Finally, the love and support of Laura Cates enabled me to view life in a more beneficial way and to find inner peace.



## CHAPTER 1:

### INTRODUCTION

---

The physiochemical properties of magmas, the transport and deposition of many ore-forming elements, volcanic eruption mechanisms, and the origin and evolution of the Earth's atmosphere and hydrosphere are intimately tied to the actions of magmatic volatiles. Studies of fumarolic gases, condensates and solid deposits have provided insights on the role of dissolved volatiles in magmatic systems.

Volcanic fumaroles are vents of various size and morphology which emit gases and water vapor. Rooted fumaroles have a direct connection to a degassing magma body and are commonly located on the flanks or summit of volcanic edifices. In contrast, rootless fumaroles develop on cooling eruptive deposits (e.g., lava and pyroclastic flows) and have no direct connection to a degassing magma. Analyses of volcanic fumarolic gases reveal them to be dominantly composed of  $H_2O$ ,  $CO_2$ ,  $SO_2$ ,  $H_2$ ,  $H_2S$ ,  $HCl$ ,  $CO$ ,  $HF$  and  $S_2$  (White and Waring 1963; Gerlach and Nordlie 1975a,b,c; Giggenbach and LeGuern 1976; Gerlach 1980; Gerlach and Casadevall 1986a,b; Symonds et al. 1990). These gas compositions vary with time, volcanic setting, fumarole type, and magma composition (Heald et al. 1963; Gerlach and Nordlie 1975b; Anderson 1975; Gerlach 1982; Gerlach and Casadevall 1986a,b). Gerlach (1982,1983) reported that tholeiitic and alkaline mafic magmas may exhibit a wide range of gas compositions from  $H_2O$ -rich to  $CO_2$ -rich to  $SO_2$ -rich, and that  $H_2O$  and  $CO_2$  are the principal hydrogen and carbon species at any reasonable gas temperature and oxygen fugacity.

Volcanic fumarole condensates are composed chiefly of acidic water formed by condensed volcanic gas. Alkalis, alkaline earths, halogens and sulfates are the major dissolved

species (Stoiber and Rose 1970). Of the metallic or metalloid elements, Fe, Zn, As, Sb, Mo, V, Ni, Cu, W and Bi predominate (Symonds et al. 1987).

Encrustations are the colorful solid deposits that often surround and line the throats of fumarolic vents. Gas phase sublimates and their alteration products, as well as chemically altered vent materials, comprise encrustations (Keith et al. 1981; Keith 1983). Sulfates, chlorides and oxides, in various states of hydration, are the dominant encrustation mineral groups (Stoiber and Rose 1974; Naughton et al. 1976; Oskarrson 1981; Keith et al. 1981). The encrustation suites of many fumarolic systems, particularly active, low-temperature ( $\leq 150^{\circ}\text{C}$ ) vents, are mostly composed of water-rich amorphous phases (Keith et al. 1981; Kodosky and Keskinen 1990). With the exception of Fe, the metallic elements normally comprise trace to minor amounts of the encrustations and sublimates. Though the relative metallic element abundances in these deposits vary widely between different volcanic centers, the more abundant metals and metalloids are usually Fe, As, Zn, Cu, Pb, Mn, W and Sn, while Ag, Ni, Au, Cs, V, Mo, Ga, Ge, Ti, Zr, Cr, Cd, Te, Hg and Bi normally occur in smaller amounts (Krauskopf 1979; Keith 1984; Symonds et al. 1987; this thesis).

### **Assumptions, Techniques, and Limitations of Fumarole Studies**

The study of active and fossil fumarolic systems proceeds from the premise that analyses of fumarolic gases, condensates and solid deposits can be correlated with volatiles released by degassing magmas and eruptive products and may reflect post-magmatic processes as well. The applicability of fumarole studies, however, depends not only on how correlative fumarolic product volatile contents are with those in silicate melts but also on the acquisition of representative and satisfactory samples (Krauskopf 1979; LeGuern et al. 1982).

The hazardous and uncontrollable situations under which most volcanic gases are collected give rise to many of the difficulties associated with evaluation and interpretation of

volcanic gas data. Although analytical error and crude sampling methods plagued the earliest attempts at volcanic gas sampling (see review by Shepherd 1938), improved sampling and analytical techniques (Giggenbach 1975; Cioni and Corazza 1981; LeGuern et al. 1982; Sheppard and Giggenbach 1985) have allowed geochemists studying volcanic gases to focus on problems beyond collection and analytical methods.

Fumarolic gases are typically collected in evacuated glass bottles; the most commonly used technique employs evacuated glass flasks charged with 50 ml of 4 Normal (N) NaOH solution. Sampling tubes made of titanium or silica are inserted as deeply into the fumarolic orifices as conditions will permit and connected to the sampling flasks with tygon tubing. The major volcanic gases (e.g., H<sub>2</sub>O, CO<sub>2</sub>, H<sub>2</sub>S, SO<sub>2</sub>, HCl, HF) are readily absorbed in the NaOH solution enabling concentration of the non-condensable gases (e.g., H<sub>2</sub>, N<sub>2</sub>, CH<sub>4</sub>, CO and Ar) in the flask headspace. Head space gases are routinely analyzed by gas chromatography, while the NaOH solutions are analyzed by a variety of techniques including acid titration, ion chromatography, Mohr titration, specific ion electrode and gravimetry. A comprehensive review of these collection and analytical techniques is provided by Sheppard and Giggenbach (1985).

Studies to date (Heald et al. 1963; Gerlach and Nordlie 1975a; Gerlach and Casadevall 1986a) support the assumption that high-temperature volcanic gases initially exist in a state of internal chemical equilibrium. Secondary alteration processes (e.g., atmospheric oxidation, reactions with the sampling apparatus, H<sub>2</sub>O gain or loss, contamination by wall rock or surface materials) typically modify these gas species, resulting in most sampled gases being disequilibrium assemblages. For example, thermodynamic calculations show that hydrocarbons and halogenated hydrocarbons should not be stable under most volcanic conditions (Gerlach 1980), but these compounds have been reported (Stoiber et al. 1971) in volcanic gas analyses. If reasonably complete analytical data are available, the equilibrium hypothesis can be tested. If disequilibrium is found, then using procedures developed by

Gerlach (1979,1980) and Gerlach and Casadevall (1986a) it is often possible to identify the alteration processes, remove their effects, and restore the analytical data to an assemblage reflecting an inferred temperature of last equilibrium in the exhaled gas. Less complete analyses may still provide useful (though less reliable than the restored compositions) information on the distribution of gas species and processes modifying the gaseous assemblage (Gerlach and Casadevall 1986a).

Condensates are most readily collected by inserting stainless steel or aluminum condensing tubes or silica tubes into the vent and connecting these to a nalgene or pyrex flask through tygon tubing. Immersion of the condensing coils in cold water, snow or dry ice-ethanol slush speeds up the collection process. Mechanically or manually operated pumps connected to the end of the collection apparatus have also been utilized (Symonds et al. 1990) to increase the efficiency of the condensation process. The gas condensation procedure traps the majority of trace elements present in the volcanic gas (Symonds et al. 1987), and the resulting liquid is suitable for common wet chemical analytical techniques. Within the condensates, anions are usually determined by ion chromatography and cations by either atomic absorption spectrophotometry (AAS) or inductively coupled plasma atomic emission spectrometry (ICPAES). Because of the potential for reaction of the condensates with the collection materials, the condensate data must be carefully evaluated for contamination. To circumvent this problem, analytical data for elements which compose part of the condensate collection apparatus are often discarded from the data set (Symonds et al. 1987). Although the condensates efficiently trap most of the trace elements in the volcanic gas, some of the more volatile elements (e.g., sulfur) may pass through the collection apparatus (Symonds et al. 1987).

Encrustations often exhibit crude to well-developed color zonation outward from the fumarole mouth (Stoiber and Rose 1974; Keith 1983,1984; Kodosky and Keskinen 1990). Encrustation samples are usually collected with non-metallic scoops and sealed in plastic

storage bags until analysis. If water condenses in these storage bags, soluble phases may be dissolved or change their state of hydration. As previously reviewed, encrustations are composed of both sublimates and phases generated by gas or liquid phase reaction with the underlying matrix (e.g., wall rock, ash). In delineating the source of the chemical components which make up the encrustations, it is difficult to determine which chemical components were derived from the volcanic gas and which from acid attack on the fumarolic vent materials (White and Waring 1963). To try and overcome this difficulty, several techniques have been employed. Naughton et al. (1974) isolated volcanic gas sublimates by suspending quartz tubes filled with quartz wool above vents of fountaining lava at Kilauea volcano. LeGuern and Bernard (1982) inserted silica tubes directly into fumarolic orifices to collect sublimates at Merapi volcano, Indonesia. Additional studies employing the silica tube technique have been undertaken by Bernard and LeGuern (1986), Symonds et al. (1987) and Symonds et al. (in press).

X-ray powder diffraction (XRD), scanning electron microscopy (SEM) and transmission electron microscopy (TEM) are commonly used to identify the mineral phases in the encrustations. Chemical compositions of these samples are routinely obtained by sample dissolution followed by AAS, ICPAES, direct current plasma atomic emission spectrometry (DCPAES), or by application of X-ray fluorescence (XRF) or electron microprobe techniques to the solid sample.

Much caution needs to be taken in the interpretation of encrustation analyses. Because of the typical intimate relationship between the encrustations and underlying matrix, it may be impossible to collect a pure encrustation sample. The use of silica tubes at active vents to collect sublimates largely overcomes this problem. A second concern, how correlative the elemental contents of encrustations are with the volatile contents of silicate melts, depends on the degree of equilibrium maintained between the fumarolic gas, encrustations and near-surface and surface environments. With the exception of lower halogen contents, Naughton

et al. (1974) found ionic ratios in sublimates at Kilauea similar to the compilation of condensate analyses reported by Stoiber and Rose (1970), suggesting a high degree of equilibrium had been maintained between the gases and the solid phases. Hampton and Bailey (1985), during fusion of volcanic glasses, produced sublimate types and patterns very similar to natural phases collected inside silica tubes by LeGuern and Bernard (1982). According to Symonds et al. (1987), thermodynamic modeling of sublimate deposition from saturated gases agrees well with the highest temperature occurrence of each silica tube sublimate phase collected from active fumaroles by LeGuern and Bernard (1982) and Bernard (1985), although some noteworthy differences were observed. Naughton et al. (1976) reported that although equilibrium calculations applied to condensates at Kilauea volcano quantitatively approximated elemental concentrations in natural volcanic systems, these same condensates showed little relation in component content to encrustations collected at the same site.

As mentioned earlier, the primary phases developed early in the life of an active fumarole may undergo a range of chemical reactions (e.g., attack by condensed acid, hydration/dehydration, solution, etc.) in the later stages of fumarolic development or after fumarolic activity has ceased. The net result of these reactions is the removal of water-soluble compounds and the formation of an assemblage of insoluble, resistant minerals (Keith 1983). It seems logical that the more weathered the primary fumarolic deposits, the more difficult it will be to correlate elemental components in the encrustations with those that may have been carried in the fumarolic gases. A more detailed discussion of elemental transport and concentration mechanisms operative in fumaroles and the secondary alteration processes affecting the primary fumarolic deposits will be given in Chapters 3 and 5.

## Some Applications of Fumarole Studies

Despite some of the problems associated with the collection, analysis and interpretation of fumarolic gases and deposits, data from the study of fumarolic systems have been applied to a wide range of geological problems. Active fumaroles are associated with a majority of geothermal sites (Henley et al. 1984), and their presence, along with other related phenomena such as mudpots, geysers, hot springs and silica terraces, has long been utilized as an exploration tool for geothermal resources. Empirical gas geothermometers have been used (D'Amore and Panichi 1980; Tedesco and Sabroux 1987) to estimate the temperature in the geothermal reservoir feeding the overlying fumaroles. Trace-element (e.g., Hg, As, Sb, Be, Li) contents in fumarolic deposits or fumarolically altered materials may also provide evidence of anomalous subsurface thermal activity and the structures (faults/fractures) responsible for its localization (Christensen et al. 1983; Bingqiu et al. 1986; Kodosky 1989).

Researchers have long sought a link between fumarolic processes and ore-forming processes. Metallic element-rich encrustations and sublimates have been observed from a variety of volcanic settings and magma types (Allen and Zies 1923; Kennedy 1948; Naughton et al. 1974; Oskarsson 1981; Hughes and Stoiber 1985; Bernard and LeGuern 1986; Symonds et al. 1987; Symonds et al. in press). Such observations led Zies (1929) to suggest movement of hydrothermal fluids as a metal transport mechanism. Further work (White 1955; Silberman et al. 1979; Henley and Ellis 1983; Henley 1985; Silberman and Berger 1985) recognized the similarity in alteration mineralogies, trace-element patterns, temperatures, fluid compositions and stable isotopes between epithermal precious metal deposits and geothermal and fumarolic systems.

Early attempts to investigate the relationship between fumarolic processes and ore formation, particularly the role of vapor phase transport of metallic species (Krauskopf

1964; Iwasaki et al. 1964), were hampered by incomplete and imprecise thermodynamic data as well as unsatisfactory collection and analytical techniques for the fumarolic products. More complete, revised thermodynamic data along with collection methods for separating out sublimates (the silica tube technique) has allowed a more rigorous approach to this problem. Symonds et al. (1987) reported that vapor phase transport of metals occurs primarily as chloride species and that sublimation from a high temperature, high velocity carrier gas is probably not efficient enough to form a sizable ore deposit. Additional work is needed to test this hypothesis, particularly for silica-rich magmatic systems.

Studies of the stable isotopes of oxygen, carbon, sulfur and hydrogen in fumarolic gases and condensates have been used (Matsuo et al. 1974; Sakai et al. 1981; Mizutani and Sugira 1982; Kiyosu and Kurahashi 1983; Barnes 1984; Symonds et al. 1990; Kodosky et al. 1991) to suggest the source(s) and evolution of volatiles in volcanic emissions. Ratios of  $^3\text{He}/^4\text{He}$  in fumarolic gases (Poreda and Craig 1989) have also been used to differentiate between mantle and crustal sources of helium in arc volcano gases. Recent advances in the analysis of the stable isotopes of chlorine (Kauffman et al. 1988) suggest that  $^{37}\text{Cl}/^{35}\text{Cl}$  ratios may prove to be useful for determining the origins of chloride species in volcanic systems.

Volcanic hazard monitoring and prediction is a fast-growing, potentially important application of fumarole and volcanic gas studies. Since dissolved magmatic volatiles have different solubilities (Burnham 1979), time-measured changes in their ratios may reflect changes (e.g., magma ascent, assimilation of wall rock) in the underlying magma. Increases in the ratios of  $\text{SO}_2/\text{CO}_2$  (Harris et al. 1980) and  $\text{S}/\text{Cl}$  (Noguchi and Kamiya 1963) and decreases in  $\text{He}/\text{CO}_2$  ratios (Thomas and Naughton 1979) in fumarolic gases have been observed immediately prior to volcanic eruptions and probably represent gas solubility changes resulting from lower confining pressures on the magma during ascent. In addition, Stoiber and Rose (1970) reported significant decreases in  $\text{Cl}/\text{SO}_4$  ratios in fumarolic condensates



at the beginning of an eruptive cycle. Such variations in gas chemistry and/or condensate stable isotope patterns have been hypothesized to coincide with the injection of fresh magma or hotter gases into the volcanic system (Stoiber et al. 1981) or with a change in the fraction of magmatic volatiles in the fumarolic emissions (Gerlach 1981; Viglino et al. 1985; Gerlach and Casadevall 1986a; Kodosky et al. 1991). These types of studies show potential for aiding in the modeling of the magmatic plumbing networks beneath volcanic centers.

Further advances in volcanic hazard monitoring will depend on safe, cost effective, reliable and frequent monitoring of fumarolic discharges at many volcanic centers. Improvements in airborne analytical techniques (correlation spectrometry (COSPEC), infrared analysis) have enabled frequent, reliable monitoring of volcanic emanations (Casadevall et al. 1982) but at a high unit cost. Technological advances in chemical sensors may be the answer. A gas sensor is an electrochemical device which transmits an electrical signal as a function of the concentration of gas contacting the sensor (Gantes et al. 1983). Although widely used in the monitoring of industrial processes, air pollution and fuel cell technology, only solid electrolyte sensors have proven capable of working in the high temperature, usually acidic environment of volcanic gases (Sato and Wright 1966; Sato and Moore 1973; Benhamou et al. 1988). These devices are composed of a reversible electrochemical fuel cell using a selective ionic conductor as the electrolyte. The models currently in use measure oxygen fugacity and temperature variations in fumarolic vents. Benhamou et al. (1988) have suggested using such a device to monitor magma ascent and gas - magma separation within volcanoes. Other solid electrolyte sensors of halogens, carbon dioxide, sulfur and hydrogen are in various stages of development or testing (Gantes et al. 1983). Refinement of these sensors would allow for continuous, "real time" monitoring of fumarolic gases and drastically reduce the need for perilous ground and airborne sampling of volcanic gases.

A heightened interest in the atmospheric impact of volcanism has prompted additional studies of volcanic gases. Johnston (1980) first suggested that gaseous HCl injected into the stratosphere by explosive volcanism may seriously reduce stratospheric ozone levels. Direct (correlation spectrometry) (Rose et al. 1985, 1988a,b) and indirect (satellite) measurements of volcanic gas plumes have led to a better understanding of the global contribution of volcanic SO<sub>2</sub> to the atmosphere. Sulphuric acid-rich volcanic aerosols have also been shown to perturb stratospheric chemistry (Hoffmann and Rosen 1983; Rose et al. 1983). Positive correlation between sulfur-rich explosive volcanic events and post-eruption temperature drops has been theorized (Devine et al. 1984; Rampino and Self 1984; Strothers and Rampino 1983). Report of iridium in gaseous emissions at Kilauea volcano (Zoller et al. 1983) even led some researchers to speculate that mass extinctions at the Cretaceous-Tertiary boundary resulted from widespread volcanism at the close of the Cretaceous (Officer and Drake 1985). These and related studies point out the necessity of considering volcanic sources during attempts to negotiate multinational agreements for reduction in anthropogenic levels of chlorofluorocarbons and carbon and sulfur gases.

### **Thesis Study Objectives**

Two locations, Mount St. Augustine and Katmai National Park, were chosen to evaluate fumarolic systems as sources for information on volcanic and magmatic processes in the eastern Aleutian volcanic arc. These sites presented a rare opportunity to compare and contrast data from extinct (fossil) and active rooted and rootless fumaroles. Results derived from these studies are presented as separate chapters. Detailed location maps and the geological setting of these sites are provided within the appropriate chapters.

Mount St. Augustine is historically the most active volcano of the Aleutian arc which lies in close proximity to significant population centers and established air and sea transport

routes. Beginning in March 1986, Mount St. Augustine underwent a series of volcanic eruptions. Because of its strategic location, Mount St. Augustine was chosen for the study of active fumaroles. In the summer of 1986, approximately three months after the peak eruptive period, Mount St. Augustine was visited for the purpose of sample collection. A number of unsuccessful attempts were made to reach the volcano's summit and collect high-temperature rooted fumarolic gases. These gases were targeted for collection in the hope that their analyses would provide information on the evolution of Mount St. Augustine's magmatic system and would serve as baseline data for a volcanic hazard monitoring program of this site utilizing volcanic gas data.

Although post-1986 eruption gases were not obtained, following the 1976 eruption of Mount St. Augustine gas and condensate samples were collected from high-temperature summit rooted fumaroles in 1979, 1982 and 1984 by members of the United States Geological Survey (USGS) and the Alaska Division of Geological and Geophysical Surveys (ADGGS). Analytical data from these samples were made available to the author and incorporated into the thesis study. The gas sample evaluation techniques described earlier were applied to these data. Results of this study are discussed in Chapter 2. The specific objectives of this work included:

- (1) description of any degassing trends following the 1976 eruption,
- (2) explanation of any degassing trends in terms of evolution of the Mount St. Augustine magmatic system,
- (3) determination of the source(s) of volatiles in the Mount St. Augustine fumarolic emissions, and
- (4) speculation on the role of volatiles in Mount St. Augustine eruption mechanisms.

Numerous rootless fumaroles developed on pyroclastic flows and a lava flow generated during the March 1986 eruptive cycle of Mount St. Augustine. Rootless fumaroles play a

critical role in the degassing and cooling of pyroclastic and lava flows. However, few published studies (e.g., Keith et al. 1981) focus on the parameters controlling the formation and evolution of rootless fumaroles. Therefore, during the 1986 summer field season, encrustation samples were collected from cooling, rootless fumaroles on pyroclastic flows and a lava flow emplaced on the north side of Mount St. Augustine. Chapter 3 presents the results of phase characterization and chemical analyses of these samples. This work was conducted in order to:

- (1) better constrain the physical and chemical factors affecting the formation of fumarolic systems, and
- (2) determine if the chemical components contained in the encrustations were derived from direct sublimation or from acidic condensate leaching of the eruptive deposits and therefore whether the encrustations can be used to interpret fumarolic gas chemistry.

Samples of fumarolic encrustations were also collected in the summers of 1986 and 1987 from the Valley of Ten Thousand Smokes (VTTS), Katmai National Park. The 1912 eruption of Novarupta, located near the head of the VTTS, is, to date, the most voluminous of the twentieth century and the only eruption of rhyolitic composition in the last 1800 years (Hildreth 1983). The VTTS is also unique in the number of fossil fumarolic vents present on a large ( $\approx 120 \text{ km}^2$ ) ash-flow sheet emplaced during the 1912 eruption. No comparable site exists where the volcanic vent and eruptive products of such a voluminous eruption are as well preserved as at Katmai (Eichelberger and Hildreth 1986). The importance of this site for addressing a wide array of problems concerning young magmatic systems and explosive volcanism is highlighted by its inclusion as a target for the U.S. Continental Scientific Drilling Program (Eichelberger and Hildreth 1986; Eichelberger et al. 1990).

The morphology and size of the 1912 Novarupta eruptive vent is obscured by large volumes of fall-back tephra (Hildreth 1983, 1987). Knowledge of the vent shape and size is

critical for reconstructing the eruption mechanism of the 1912 event as well as for determining the nature of any developing geothermal system beneath the vent surface. Unfortunately, only several patchy areas of warm ground and wispy, low-temperature fumaroles still persist near Novarupta. However, since volatile element (e.g., Hg<sup>0</sup>, As, Rn) surveys of surface materials have shown promise in locating geothermal resources (Matlick and Buseck 1976; Klusman and Landress 1979) and subsurface geologic structures (Crenshaw et al. 1982), a reconnaissance survey of surface Hg<sup>0</sup> contents in the VTTS ash-flow sheet was conducted. Results of this study are discussed in Chapter 4. It was hoped that the results of this study would enable the:

- (1) modeling of the 1912 vent structure, with emphasis on the process of vent formation and the detection of any near-surface igneous intrusives and,
- (2) location of zones of anomalously high subsurface thermal activity that may be related to a developing hydrothermal system beneath the 1912 eruptive site.

Shipley (1920), Allen and Zies (1923), Zies (1924, 1929) and Keith (1984, 1991) described significant enrichment of metallic elements in the VTTS fumarolic encrustations. As previously stated, researchers have long sought to unravel the relationship between geothermal/fumarolic processes and ore-forming processes in volcanic terranes. From a practical standpoint, this research is pertinent because a significant proportion of recent increases in U.S. gold production (Ivosevic 1987) has come from volcanic rock-hosted precious metal epithermal ore deposits (Henley 1985, Morgan 1986). A better knowledge of the nature and efficiency of element transport and deposition mechanisms operative in fumaroles could increase our understanding of the genesis of volcanic rock-hosted epithermal ores. A collection of encrustations from the VTTS fossil fumaroles was therefore compiled. Chapter 5 discusses the results of phase characterization and chemical analyses of these samples. This work was performed with the goals of:

- (1) determining the elemental source, transport and deposition mechanisms for the fumarolic deposits, and
- (2) evaluating the applicability of fumarolic deposits for modeling epithermal ore-forming processes.

Although data from each of the thesis study locations can be, and was, applied to specific geologic problems at those sites, it was hoped that integration of these data would provide a broad overview of the long-term evolution of fumarolic systems and their utility for geologic problem solving. For instance, whereas the study of Mount St. Augustine's active rootless fumaroles can be used to evaluate the conditions responsible for fumarole formation and early development, the VTTS fossil rootless fumarolic deposits can indicate the extent to which these systems and their deposits are modified by exposure to surface conditions. Of particular interest to this study was whether the VTTS fossil fumarolic deposits would preserve a signature of their initial formative processes (e.g., vapor phase transport of elements) and therefore could be used to reconstruct fumarolic processes operative during the early cooling history of the 1912 ash-flow sheet. These data are important for determining how useful fumarolic encrustations, particularly those encrustations collected from fossil vents, are for modeling volcanic fluid (gas, liquid) chemistries.

During this study, a moderate amount of confidence was held that samples of Mount St. Augustine's summit rooted fumarolic gases would provide useful, interpretable information. Whether surface Hg<sup>0</sup> contents, which are largely the result of vapor phase transport and deposition (Jonsson and Boyle 1972, Varekamp and Buseck 1983a,b) would, in the absence of any vigorous fumarolic activity, provide information on crystallizing magma bodies or hydrothermal systems beneath Novarupta Basin was not known. This particular study was also done to ascertain if such volatile element surveys are applicable to recently active volcanic centers with minor or no surface expressions of hydrothermal or magmatic activity.

## CHAPTER 2:

### FUMAROLIC EMISSIONS AT MOUNT ST. AUGUSTINE: 1979-1984

#### Introduction

The study of volcanic volatiles has received increased attention because of their potential for increasing our understanding of the origin of magmas, metallogenesis, and the origin of the atmosphere, biosphere and hydrosphere. Concerns over the atmospheric impact of volcanism and the need for eruption prediction and monitoring technology have also contributed to an interest in the chemistry of volcanic gases. Because of their less hazardous nature and easier accessibility, gas emissions from tholeiitic and alkaline magmas have been studied extensively (e.g., Gerlach 1982), while emanations from calcalkaline lavas of volcanic arcs and continental margins, which are probably responsible for a majority of Earth's volcanic emissions (Stoiber et al. 1987), are less well characterized.

This study† focuses on medium- to high-temperature (300° – 800°C) fumarolic emissions from Mount St. Augustine, a very active calcalkaline volcano located in the eastern Aleutian volcanic arc of Alaska. The data include chemical and isotopic compositions of gases and condensates collected in 1979, 1982 and 1984 from fumaroles rooted in an andesite-dacite dome emplaced at Mount St. Augustine's summit following its 1976 eruption. The

---

† Portions of this chapter comprise a manuscript authored by Lawrence G. Kodosky, Roman J. Motyka and Robert B. Symonds published in the *Bulletin of Volcanology* (1991) 53: 381-394.

1979 gas samples were collected by Dr. David A. Johnston. These samples, as well as Johnston's personal field notes, were made available to Roman Motyka of the ADGGS by the USGS after Johnston's untimely death in the 1980 eruption of Mount St. Helens. Dr. Motyka allowed the author of this thesis access to the complete data set and also participated in the data reduction and evaluation.

The purpose of this work is to evaluate degassing trends of Mount St. Augustine's summit fumaroles following the 1976 eruption. Recently, Symonds et al. (1990) have completed a related study of fumarolic gases for an eighteen month period following the 1986 eruption of Mount St. Augustine. Knowledge of the consistency of Mount St. Augustine's post-eruptive degassing trends will prove to be useful in future volcanic hazard prediction and monitoring at this site. In addition, speculation is made on the sources of the volatile components and on how the sequence of incorporation of these components into the volcanic system may influence Mount St. Augustine's eruptive style.

### **Mount St. Augustine**

Mount St. Augustine, a roughly 90 km<sup>2</sup> calcalkaline island stratovolcano situated approximately 285 km southwest of Anchorage, Alaska (Figure 1), is one of over 40 historically active volcanoes of the Aleutian volcanic arc. This volcanic arc extends over 3000 km from Mt. Buildur in the west, where it overlies Tertiary oceanic crust, to Mt. Spurr in the east, where it is built upon Mesozoic and younger continental crust. Mount St. Augustine lies in the easternmost segment of the arc and is built upon continental crust about 105 km above a seismically active Benioff zone dipping 45° to the northwest (Kienle and Swanson 1983).

Mount St. Augustine consists of a core of overlapping lava domes surrounded by an apron of pyroclastic and debris flows and minor lava flows on its northwest flank (Detterman 1973; Kienle and Swanson 1980; Beget 1986). The present volcanic edifice postdates



the last glaciation in Cook Inlet (35,000 - 17,000 years b.p.; Johnston 1979) and is built upon a sequence of uplifted Jurassic and Tertiary marine and terrestrial sedimentary rocks (Detterman 1973; Buffler 1976; Johnston 1979). An 80-m section of these older units crops out on the west side of the island (Viglino et al. 1985). High seismic compressional wave velocities ( $\approx 5.1$  km/s) recorded from the subvolcanic sediments led Kienle et al. (1979) to suggest that sediments as shallow as 900 m beneath the volcano base have been extensively zeolitized.

Since the island was charted and named by James Cook in 1778, Pelean-type eruptions of Mount St. Augustine have occurred in 1812, 1883, 1935, 1963-64, 1976 and 1986. Eruptions typically commence as vent-clearing explosions with ash-rich eruption plumes reaching altitudes of 10 - 14 km. Eruption column collapse in turn generates numerous pyroclastic flows. The eruptive cycle ends with extrusion of a viscous dome. Merapi-style (i.e., by partial dome collapse) pyroclastic flows accompany dome emplacement and growth. Generally, eruption volumes of  $0.3 - 0.4 \text{ km}^3$  are produced from approximately  $0.2 \text{ km}^3$  dense rock equivalent magma (Johnston 1978; Swanson and Kienle 1988). As an example, the 1976 initial explosive activity lasted three days (January 22-25) and produced at least 12 major eruptions with several ash clouds penetrating the stratosphere (Lepel et al. 1978; Kienle and Shaw 1979). On February 6 violent activity resumed for several days. By February 12, a new dome began to intrude the January crater and pyroclastic flow activity changed from eruption column collapse to dome collapse, with dome building continuing into April (Kienle and Swanson 1980).

### **Previous Studies of Volatiles at Mount St. Augustine**

The nature and chemistry of Mount St. Augustine gaseous emissions have received intermittent study since the 1976 eruption. Airborne sampling of the 1976 eruption plumes

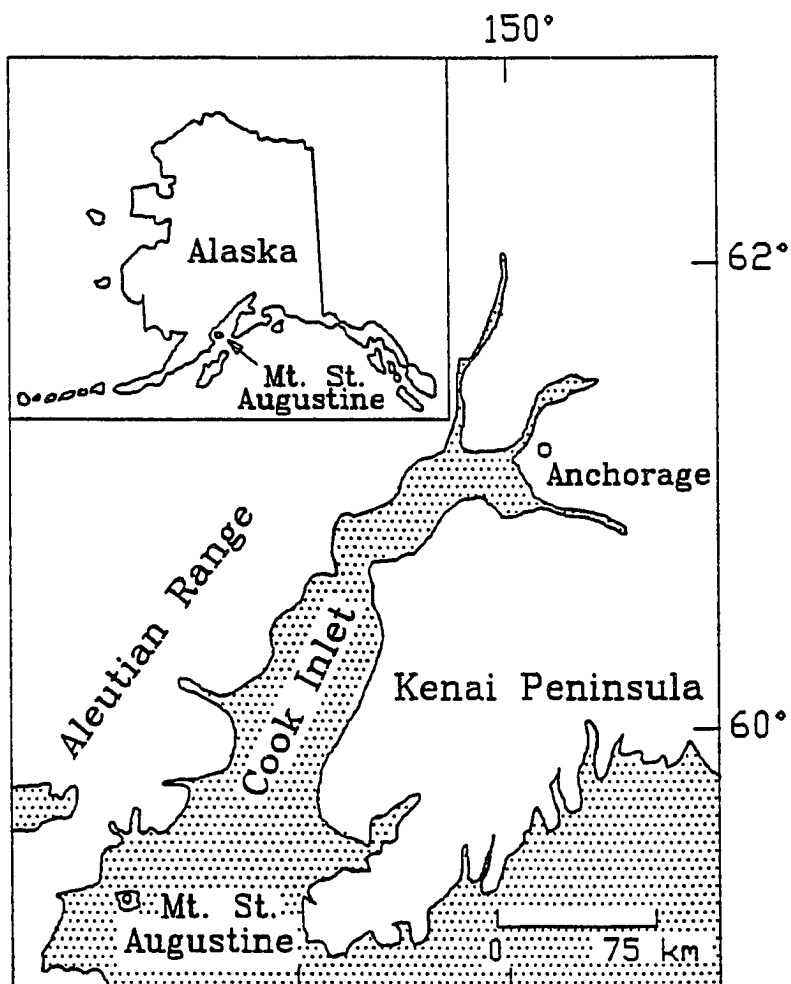


Fig. 1 Location map for lower Cook Inlet, Alaska.

provided evidence for release of large amounts of HCl and SO<sub>2</sub> (Hobbs et al. 1977; Lepel et al. 1978) to the atmosphere. By comparison of chlorine concentrations of crystal-hosted glass inclusions to those of quenched ash, Johnston (1980) provided further evidence of the Cl-rich nature of Mount St. Augustine emissions and suggested that up to  $525 \times 10^6$  kg of chlorine was released into the atmosphere during the 1976 eruption, of which  $82 \times 10^6$  to 175

$\times 10^6$  kg may have been injected into the stratosphere as hydrogen chloride. Viglino et al. (1985) used stable isotope data to identify a magmatic component in fumarolic condensates from high-temperature ( $> 450^\circ\text{C}$ ) summit vents. Based on summit gas samples collected in 1982 and 1984, Motyka et al. (1986) speculated that progressive magmatic outgassing could explain significant shifts in dry gas ( $\text{H}_2\text{O}$  - free recalculated) compositions over this two year period. Rose et al. (1988a,b) measured aerosol and gas fluxes following the 1986 eruption. They estimated the HCl emission rate one week after the major explosive phase at 10,000 tonnes/day and the peak eruptive emission rates of HCl and  $\text{SO}_2$  at 160,000 tonnes/day and 375,000 tonnes/day, respectively. Continuation of their airborne and ground-based sampling program allowed Symonds et al. (1990) to conclude that, compared to other convergent plate volcanoes, the Mount St. Augustine system is very Cl-rich (e.g., HCl gas contents an order of magnitude greater than any previously reported) and S-rich, and that the fluid components of the fumarolic emissions were derived from varying mixtures of primary magmatic water, meteoric water and seawater. Symonds et al. (1990) interpreted the decrease in airborne correlation spectrometry (COSPEC)  $\text{SO}_2$  emission rates measured between April 1986 and August 1987 to be the result of progressive magmatic degassing following Mount St. Augustine's 1986 eruption. Poreda and Craig (1989) reported that  $^3\text{He}/^4\text{He}$  ratios from Mount St. Augustine summit fumaroles and other volcanic centers in the Aleutian arc are consistent with the idea that the mantle is the dominant source of helium in volcanic arc fluids. Kodosky and Keskinen (1990) studied encrustations developed around rootless fumaroles in the 1986 pyroclastic flows and concluded that condensed acidic vapors promoted leaching of andesitic ash and provided the primary source for chemical components contained in the low-temperature encrustations.

### Fumarolic Activity, Sampling Sites and Collection Procedures

In 1975, fumarolic activity at Mount St. Augustine was confined to the margins of an andesitic dome emplaced during the 1963-64 eruption. The most active fumaroles were concentrated along the western side of the dome, and emissions consisted mainly of water vapor at sub-boiling temperatures (D. Johnston pers. field notes 1978, 1979). Extrusion of the 1976 lava dome initiated vigorous summit fumarolic activity. In August 1978 David Johnston (pers. field notes 1978, 1979) observed dull-red incandescence in active fumaroles located at the base of an apical spine emplaced on the dome's northeastern rim during the final phase of eruptive activity in April, 1976. On a return visit in July, 1979, Johnston noted that fumarolic temperatures at this site ranged from 721° to 754°C. At this time Johnston collected gas samples by inserting a titanium tube into the fumarolic orifices and connecting the tube to sample bottles with tygon tubing. The samples were collected in 300 ml evacuated flasks containing 50ml of 4 Normal (N) solution which during the collection procedure were kept cool by cold water baths. Using this method the predominant volcanic gases (e.g., H<sub>2</sub>O, CO<sub>2</sub>, H<sub>2</sub>S, SO<sub>2</sub>, HCl, HF) are readily absorbed in the NaOH solution, allowing concentration of the non-condensable gases (e.g., H<sub>2</sub>, N<sub>2</sub>, CH<sub>4</sub>, CO and Ar) in the flask headspace. The sample flask solutions stopped bubbling after only a few minutes, suggesting the fumarolic gases were no longer being absorbed and the samples were being contaminated with air. An additional sample was collected from a 648°C fumarole located several meters below the apical spine.

The fumaroles at the base of the apical spine were resampled in August, 1982. The fumaroles remained highly pressurized with good flow. The gases were noted to be very acidic (pH < 2), and vent temperatures had declined to 472°C. Two samples (82A1 and 82A2) were collected using a glass tube inserted into the vent and connected to a condensing dewar filled with dry ice-ethanol slush. Water and other condensibles were frozen in a cold

trap with the flow of the remaining residual dry gases collected in an uncharged (dry bottle), evacuated 100 cc glass bottle with vacuum stopcocks. This collection procedure was used to reduce the potential for reactions between sulfur gases and H<sub>2</sub>O within the sampling flask. Sample 82A4 was also collected with an uncharged evacuated flask but the sampling tube was connected directly to the flask. In this technique (wet bottle), water condenses in the sampling flask.

By 1984 temperatures of the fumaroles at the base of the spine had declined to 357°C. Sample 84A4 was collected at this location using a glass tube inserted into the vent and connected directly to a NaOH-charged evacuated flask. Sample 84A6 was taken from a nearby vent (338°C) using the same method. Flasks were cooled with snow during the approximately 30 minute collection time. Because of the long sample collection periods, any minor water loss should have been insignificant with respect to the total amount of water collected. Wet bottle backup samples (84A12 at site 84A4, 84A9 at site 84A6) were also collected at these sites. All samples of fumarolic condensates for isotopic and anion analyses were collected using aluminum condensing coils immersed in cold water, water-ice slush or in cold traps of dewars filled with dry ice-ethanol slush.

## **Analytical Methods**

### **Gases and condensates**

The gas samples collected by D. Johnston in 1979 were analyzed between 1982 and 1984, up to five years after collection. The 1982 and 1984 samples were analyzed three to six months after acquisition. All sample analyses were performed by personnel of the USGS in Menlo Park, California, the ADGGS in Fairbanks, Alaska, the Southern Methodist University in Dallas, Texas, and the Scripps Institute of Oceanography in La Jolla, California.

Analyses of gases collected in evacuated flasks charged with NaOH generally followed the procedures outlined in Sheppard and Giggenbach (1985). Head space gases were analyzed on dual-column gas chromatographs using argon and helium carrier gases. The NaOH solutions were analyzed by gravimetric methods ( $\text{H}_2\text{O}$ ), acid titration ( $\text{CO}_2$ ), ion chromatography (total sulfur,  $\text{Br}^-$ ,  $\text{Cl}^-$  in sample 84A6), Mohr titration (for  $\text{Cl}^-$  in all but sample 84A6) and specific ion electrode ( $\text{F}^-$ ).

Samples in the uncharged evacuated glass flasks were analyzed by gas chromatography for all gases except  $\text{SO}_2$ . Levels of  $\text{SO}_2$  were measured using a Teflon column packed with polyphenyl ether and phosphoric acid on Chrom T as described by Stevens et al. (1971).

Sample 82A4 was analyzed differently. Following  $^3\text{He}/^4\text{He}$  isotope analysis at the Scripps Institute of Oceanography, total moles of gas were measured. Carbon dioxide and sulfur gases were then frozen in a cold trap at  $-195^\circ\text{C}$  and the residual gases collected in an evacuated flask. Next, splits of both the condensed and non-condensed gases were analyzed by gas chromatography. Sulfur dioxide was determined by difference between the measured mole percentage of  $\text{CO}_2$  plus  $\text{H}_2\text{S}$  in the condensed split.

Stable isotope values of  $\delta^{13}\text{C}$  in  $\text{CH}_4$  and  $\delta\text{D}$  in  $\text{H}_2$  were determined by the Stable Isotope Laboratory, Southern Methodist University, Dallas, Texas. Measurements of  $\delta^{13}\text{C}$  and  $\delta^{18}\text{O}$  in  $\text{CO}_2$  were made by the USGS in Menlo Park, California.

Anion concentrations in steam condensates collected in 1982 were determined by the ADDGS using ion chromatography. Condensate values of  $\delta^{18}\text{O}$  and  $\delta\text{D}$  were measured by the Stable Isotope Laboratory, Southern Methodist University. All (gas and condensate) stable isotope analyses were conducted on separate sample splits taken from the original sample flasks.

## Results

### Gas chemistry and adjustments to compositions

Analyzed gas compositions are given in Table 1. Samples 79A4Ga and 79A4Gb as well as samples 82A1, 82A2 and 82A4 are duplicate field samples. Because sulfur gas species collected in NaOH-charged flasks could not be distinguished, the absorbed sulfur gases, originally calculated as SO<sub>2</sub>, are reported as total sulfur, S<sub>t</sub>. Oxygen is highly reactive at the vent temperatures involved and should be present in only minute amounts in equilibrium assemblages ( $\approx 10^{-6} - 10^{-8}$  mole %, Heald et al. 1963). The presence of detectable O<sub>2</sub> in the sample flasks probably indicates atmospheric contamination. The N<sub>2</sub>/Ar and N<sub>2</sub>/(O<sub>2</sub>+Ar) ratios are similar to or larger than atmospheric values (Table 1), supporting the premise that N<sub>2</sub> and Ar are mostly of atmospheric origin and that some atmospheric O<sub>2</sub> may have reacted with reduced gas species and/or fumarole wall rocks. Since Ar, N<sub>2</sub> and O<sub>2</sub> are assumed to be of atmospheric origin, the gas data were normalized after their removal (Table 2).

#### *1979 gases*

The 1979 NaOH flask gas samples have large concentrations of N<sub>2</sub> and Ar but no detectable O<sub>2</sub>, which implies significant oxidation of reduced gas species, fumarole wall rocks, or, perhaps, reaction of O<sub>2</sub> with the titanium sampling tube. The main deficiencies of these analyses are 1) non-differentiation of the sulfur gas species and 2) lack of detectable CO. Carbon monoxide is typically present in high-temperature reduced volcanic gases (the lower temperature 1982 and 1984 samples contain measurable CO). Absence of CO in the 1979 samples suggests the CO has been oxidized to CO<sub>2</sub>. Reactions with ferrous iron in incandescent wall rocks and oxidation of sulfur gases absorbed in the NaOH solutions to sulfates seem the most likely candidates for the removal of large amounts of O<sub>2</sub>. Such

Table 1 Analyses of high-temperature fumarole gases. All data in mole percent.

Sample	Date sampled	T <sub>v</sub> , °C	H <sub>2</sub> O	CO <sub>2</sub>	SO <sub>2</sub> (or S <sub>T</sub> )	H <sub>2</sub> S	H <sub>2</sub>	CH <sub>4</sub>	CO	HF	HCl	HBr	N <sub>2</sub>	O <sub>2</sub>	Ar	N <sub>2</sub> /Ar <sup>1</sup>	N <sub>2</sub> /(O <sub>2</sub> +Ar) <sup>2</sup>
NaOH flasks																	
79A3G	7-79	648	92.00	1.80	0.08	as S <sub>T</sub>	0.361	<8.x10 <sup>-6</sup>	<8.x10 <sup>-6</sup>	0.053	0.348	<0.002	5.28	<8.x10 <sup>-6</sup>	0.103	51.5	51.5
79A4Ga	7-79	746	95.53	1.22	0.49	as S <sub>T</sub>	0.560	<3.x10 <sup>-6</sup>	<3.x10 <sup>-6</sup>	<0.003	0.155	0.076	1.94	<3.x10 <sup>-6</sup>	0.032	60.2	60.2
79A4Gb	7-79	746	95.24	1.11	0.48	as S <sub>T</sub>	0.679	<3.x10 <sup>-6</sup>	<3.x10 <sup>-6</sup>	<0.003	0.222	0.062	2.17	<3.x10 <sup>-6</sup>	0.036	60.9	60.9
79A6G	7-79	721	98.42	0.727	0.17	as S <sub>T</sub>	0.513	<3.x10 <sup>-6</sup>	<3.x10 <sup>-6</sup>	<0.003	0.235	0.013	1.88	<3.x10 <sup>-6</sup>	0.035	54.5	54.5
84A4	7-84	357	99.63	0.033	0.018	as S <sub>T</sub>	0.091	0.00016	2.9x10 <sup>-5</sup>	0.001	0.0232	0.0008	0.005	0.00017	6.4x10 <sup>-5</sup>	77.4	21.1
84A6	7-84	338	99.75	0.058	0.022	as S <sub>T</sub>	0.102	<1.x10 <sup>-7</sup>	2.4x10 <sup>-5</sup>	0.002	0.0544	<0.0004	0.0111	0.00055	1.5x10 <sup>-4</sup>	78.4	15.9
Evacuated flasks (d = dry; w = wet)																	
82A1-d	8-82	472	nd	14.4	0.03	0.060	6.50	<0.01	0.092	nd	nd	nd	59.4	16.6	(as O <sub>2</sub> )	-	3.6
82A2-d	8-82	472	nd	22.8	1.58	0.250	12.1	<0.01	0.140	nd	nd	nd	49.5	13.0	0.59	83.6	3.6
82A4-w	8-82	472	nd	56.3	5.43	<0.01	36.5	<0.01	<0.01	nd	nd	nd	1.85	0.130	(as O <sub>2</sub> )	-	12.7
84A12-w	7-84	357	nd	7.12	1.40	<0.01	62.0	<0.01	0.035	nd	nd	nd	23.6	7.40	0.38	66.1	3.1
84A9-w	7-84	336	nd	4.12	0.39	<0.01	32.0	<0.01	0.008	nd	nd	nd	52.0	14.0	0.62	76.4	3.6

T<sub>v</sub> = measured vent temperature    nd = not determined    S<sub>T</sub> = total sulfur  
<sup>1</sup> atmospheric ratio: 83.6    <sup>2</sup> atmospheric ratio: 3.57



Table 2 Gas analyses recalculated after removal of N<sub>2</sub>, Ar, and O<sub>2</sub>. All data in mole percent, normalized to 100 percent.

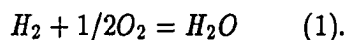
Sample	Date sampled	T <sub>v</sub> , °C	H <sub>2</sub> O	CO <sub>2</sub>	SO <sub>2</sub> (or S <sub>t</sub> )	H <sub>2</sub> S	H <sub>2</sub>	CH <sub>4</sub>	CO	HF	HCl	HBr
<b>NaOH flasks</b>												
79A3G	7-79	648	97.23	1.90	0.06	as S <sub>t</sub>	0.381	<6.x10 <sup>-6</sup>	<6.x10 <sup>-6</sup>	0.056	0.366	<0.002
79A4Ga	7-79	746	97.46	1.24	0.50	as S <sub>t</sub>	0.571	<3.x10 <sup>-6</sup>	<3.x10 <sup>-6</sup>	<0.003	0.158	0.077
79A4b	7-79	746	97.39	1.14	0.49	as S <sub>t</sub>	0.695	<3.x10 <sup>-6</sup>	<3.x10 <sup>-6</sup>	<0.003	0.227	0.064
79A6G	7-79	721	98.30	0.741	0.18	as S <sub>t</sub>	0.524	<3.x10 <sup>-6</sup>	<3.x10 <sup>-6</sup>	<0.003	0.239	0.013
84A4	7-84	357	99.83	0.033	0.016	as S <sub>t</sub>	0.092	0.00016	0.000029	0.001	0.0232	0.0008
84A6	7-84	338	99.76	0.058	0.022	as S <sub>t</sub>	0.103	<1.x10 <sup>-7</sup>	0.000024	0.002	0.0544	<0.0004
<b>Evacuated flasks (d = dry; w = wet)</b>												
82A1-d	8-82	472	nd	62.4	0.13	0.260	36.8	<0.01	0.399	nd	nd	nd
82A2-d	8-82	472	nd	61.8	4.28	0.677	32.8	<0.01	0.379	nd	nd	nd
82A4-w	8-82	472	nd	57.3	5.53	<0.01	37.2	<0.01	<0.01	nd	nd	nd
84A12-w	7-84	357	nd	10.1	1.98	<0.01	87.9	<0.01	0.050	nd	nd	nd
84A9-w	7-84	338	nd	11.3	1.07	<0.01	87.6	<0.01	0.016	nd	nd	nd

T<sub>v</sub> = measured vent temperature

S<sub>t</sub> = total sulfur

reactions would have no effect on total sulfur gas contents since oxidation of sulfur gases in the NaOH solution was part of the analytical procedure for total sulfur determination. Concentrations of O<sub>2</sub> proportional to the N<sub>2</sub> and Ar atmospheric contents would have been more than adequate to convert all the analyzed sulfur to sulfates.

It is also possible that some H<sub>2</sub> may have been oxidized to H<sub>2</sub>O. The extent of atmospheric oxidation of H<sub>2</sub> in the fumarolic conduits can be assessed to some degree by examining the oxygen fugacity relationship:



The equilibrium quotient for this reaction can be rearranged into an equation solving for log  $fO_2$ . By substituting the concentrations of H<sub>2</sub> and H<sub>2</sub>O from Table 2 into the rearranged equation and determining the equilibrium constant for the temperature of interest from available thermodynamic data, the oxygen fugacity for the written reaction can be calculated.

Reaction (1) only provides estimates of the oxygen fugacities of the 1979 gases because their exact H<sub>2</sub>O contents (determined by mass difference) cannot be determined without knowing the S species distribution in these gases. Regardless, atmospheric oxidation of H<sub>2</sub> should result in anomalously high apparent oxygen fugacities. However, oxygen fugacities calculated for the measured vent temperatures using (1) plot very near the nickel-nickel oxide (NNO) buffer (Figure 2), an oxygen fugacity buffer curve that many andesitic to dacitic magmas follow (Gerlach and Casadevall 1986a). In addition, oxygen fugacities near NNO are consistent with those obtained by Symonds et al. (1990) from two restored gas samples collected in 1987 from 870°C fumaroles located on the 1986 Mount St. Augustine dome. With the possible exception of sample 79A3G, similar ratios of H<sub>2</sub>O/H<sub>2</sub> in the

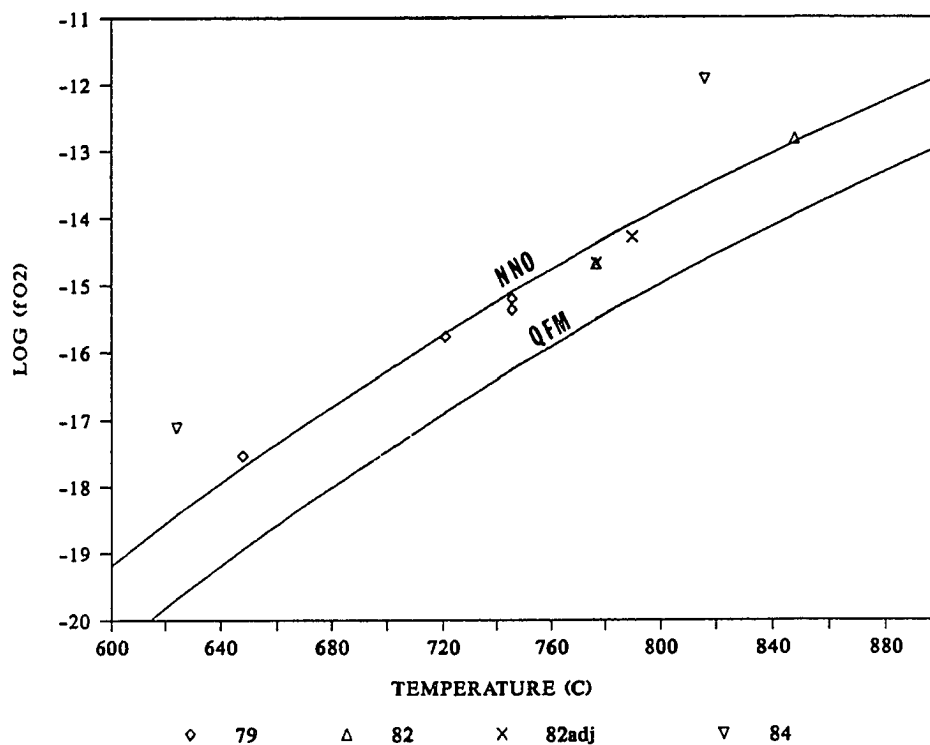


Fig. 2 Oxygen fugacity - temperature relationships for the summit dome gas samples. The 1979 data are calculated for assumed equilibrium at the vent temperatures, the 1982 data represent estimated equilibrium conditions corrected (triangle symbols) and uncorrected (X symbols) for sulfur deposition in the intake tube of the sampling apparatus, and the 1984 data are for restored equilibrium compositions. See text for full explanation. Shown for reference are the nickel-nickel oxide (NNO) and quartz-fayalite-magnetite (QFM) buffer curves (Huebner and Sato 1970; Wones and Guilbert 1969).

1979 gases (Table 3) also imply that oxidation of  $H_2$  was not a factor for these samples. Atmospheric oxidation of  $H_2$  in the 1979 samples therefore appears to have been minimal.

Giggenbach (1987) reported that for vent temperatures above 650°C, titanium is subject to acid gas attack. The sampled 1979 gases may have reacted with the titanium sampling tube, but there is no independent way to evaluate whether this process occurred. Given the high gas pressures and temperatures of the sampled vents, loss of water from the sample flask via condensation in the sampling tube seems unlikely.

The incomplete analyses do not allow a rigorous testing of the equilibrium hypothesis and calculation of restorable analyses. However, an estimate of the original CO, H<sub>2</sub>S and SO<sub>2</sub> present in these gases was made by assuming chemical equilibrium at the measured vent temperatures and using the computer code SOLVGAS (Symonds et al. 1987) which calculates homogeneous equilibria in ideal gases. SOLVGAS calculates the distribution of 142 gas species in the system C-O-H-S-Cl-F-Br as a function of temperature and pressure by simultaneously solving a series of mass balance and mass action equations using a Newton-Raphson method. The calculations are constrained by the thermochemical data base GASTHERM (Symonds et al. 1987; Symonds and Reed, unpublished). The gas species included in the final calculations are the ones reported in the estimated and restored gas compositions; species with concentrations of  $< 10^{-25}$  mole % were suppressed from the final calculations.

To estimate the equilibrium compositions of the 1979 gases, the total moles of O, S, C, Cl, F, and Br were fixed using the mass balances for the normalized compositions (Table 2). Then, the distribution of species and the total moles of H for each gas composition were computed using the approximate oxygen fugacities from reaction (1). However, redistributing some of the SO<sub>2</sub> and CO<sub>2</sub> as H<sub>2</sub>S and CO, respectively, results in a different mass balance for O and more H<sub>2</sub>O than reported in the original analyses, because H<sub>2</sub>O was determined by mass difference. To correct for this problem, the revised estimates for SO<sub>2</sub>, H<sub>2</sub>S, CO<sub>2</sub>, and CO, the analyzed amounts of HCl, HF, and HBr, and the weighted normalized gas compositions were used to calculate new H<sub>2</sub>O concentrations by mass difference. The

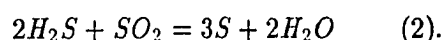
whole procedure was then repeated, using the revised estimates for H<sub>2</sub>O and total moles of O, until a convergent set of values for H<sub>2</sub>O, SO<sub>2</sub>, H<sub>2</sub>, CO<sub>2</sub>, CO and fO<sub>2</sub> was obtained. Finally, the converged gas compositions were normalized to 100%. These results (Table 3) suggest H<sub>2</sub>S/SO<sub>2</sub> ratios of 2 - 10 and CO<sub>2</sub>/CO ratios of 193 - 543 in these gases if they are assumed to be in chemical equilibrium at the vent temperatures.

#### *1982 gases*

The N<sub>2</sub>/(O<sub>2</sub> +Ar) ratio for 82A4 indicates atmospheric oxygen may have reacted with reduced gas species and probably accounts for the lack of detectable CO and H<sub>2</sub>S in this sample. In contrast, although highly air contaminated, the two dry bottle samples (82A1 and 82A2) have N<sub>2</sub>/(O<sub>2</sub> +Ar) and/or N<sub>2</sub>/Ar ratios that are nearly that of air indicating these samples were minimally modified by reactions with atmospheric O<sub>2</sub>.

The head space gases in the NaOH sample 82A3 (not listed in Tables) were lost during analysis. However, the molar concentrations of CO<sub>2</sub> and total sulfur absorbed in the NaOH solution were determined and yielded an S/C ratio of approximately 0.3, compared to ratios of about 0.1 in samples 82A2 and 82A4 and 0.01 in 82A1. The comparatively low S/C ratio in sample 82A1 may result from analytical errors in the sulfur species determination; evidence for this is found in the relatively low concentrations of sulfur species in this sample (Table 1). Ratios of S/C in the two 1984 wet bottle samples (0.1 to 0.2) are also significantly lower than ratios in the two NaOH samples collected at the same vents (0.4 to 0.5).

The cause of these differences may be the deposition of elemental sulfur in the collection apparatus or sampling flasks as a result of the reaction:



Evans et al. (1981) used the dry bottle sampling technique for fumaroles located on the 1980 Mount St. Helens eruptive dome and estimated that about 20% of the sulfur gases entering

**Table 3** Estimated equilibrium gas compositions for the 1979 NaOH samples. Gas data in mole percent.

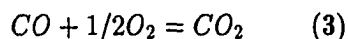
Sample	$T_v, ^\circ\text{C}$	H <sub>2</sub> O	CO <sub>2</sub>	SO <sub>2</sub>	H <sub>2</sub> S	H <sub>2</sub>	CO	HF	HCl	HBr	log $f_{\text{O}_2}$	S/C	H/C	H <sub>2</sub> O/H <sub>2</sub>
79A3G	648	97.24	1.90	0.006	0.058	0.381	0.0035	0.056	0.366	<0.002	-17.54	0.03	103	256
79A4Ga	746	97.46	1.23	0.171	0.329	0.571	0.0053	<0.003	0.158	0.077	-15.20	0.40	159	171
79A4Gb	746	97.38	1.13	0.109	0.381	0.695	0.0059	<0.003	0.227	0.064	-15.37	0.43	173	140
79A6G	721	98.30	0.74	0.046	0.133	0.524	0.0026	<0.003	0.239	0.013	-15.77	0.24	267	188

$T_v$  = measured vent temperature

their collection tube as  $H_2S$  and  $SO_2$  could have gone unanalyzed because of reaction (2). Wet bottle samples would be even more susceptible to loss of sulfur gas species via water-gas reactions. An anion analysis of a 1982 fumarolic condensate (cf. Table 5) is relatively rich in the sulfate anion, implying a total S concentration of 0.035 mole% in the bulk gas and loss of S from the gases by water-gas reactions.

Sulfur deposition and water-gas reactions should have much less effect on analyses of NaOH samples. The analytical techniques employed are able to detect the total amount of sulfur collected. The much greater volume of gases typically collected using the NaOH technique would also tend to dilute the effects of any sulfur condensation in the sampling tube.

Of the 1982 samples, fairly complete data exist only for the dry bottle samples (82A1 and 82A2). These samples lack  $H_2O$  data and may involve an underestimation of sulfur gases. Water contents in equilibrium with the dry bottle compositions can be inferred by assuming equilibrium at the vent temperatures, estimating  $fO_2$  via the reaction:



and calculating the  $H_2O$  content using reaction (1) and the measured  $H_2$  concentration (Gerlach and Casadevall 1986a). However, evaluation of reaction (3) for the dry bottle samples at the vent temperature of  $472^\circ C$  yields  $\log fO_2$  values of -26.3 and -26.4. These values lie very near the Quartz-Fayalite-Magnetite (QFM) buffer curve, which seems unlikely for Mount St. Augustine gases and implies equilibrium at a temperature greater than the measured vent temperature.

If the analyzed dry flask compositions are assumed to represent an equilibrium assemblage at some higher temperature, SOLVGAS can be used to test whether a quantity of  $H_2O$  can be found that would produce an equilibrium assemblage. Trial amounts of  $H_2O$  were added to the analyses and for each trial a new element mass balance was calculated

and used to compute the distribution of equilibrium gas species over a range of temperatures. These equilibrium distributions were used to determine correspondence temperatures (CT) of the gas species for the trial  $H_2O$  amounts. A CT is the temperature at which the analytical concentration of a gas species is equal to its calculated equilibrium concentration, the equilibrium concentrations being derived from the element mass balance defined by the analysis. If the CTs for all the gas species are equal, this is strong evidence that the gas is an equilibrium mixture (Gerlach 1980; Gerlach and Casadevall 1986a). The CTs determined for each trial  $H_2O$  value were used as a test of the degree of equilibrium in the gaseous assemblage and as a guide for making closer estimates of the  $H_2O$  content in subsequent trials. When an  $H_2O$  content was found that caused the CTs for all the gas species to converge at a single temperature, this procedure was terminated.

Table 4 lists the convergence compositions. Although the oxygen fugacity calculated for sample 82A2 plots very near NNO, the estimated equilibrium temperature ( $T_e$ ) appears unreasonably high compared to that of its duplicate field sample (82A1) and the 1979 vent temperatures. To test the effects of the possible underestimation of sulfur gases in the 1982 analyses, the S/C ratio determined from the NaOH sample and reaction (2) were used to adjust (by reversing the reaction) the dry gas  $SO_2$  and  $H_2S$  contents (Table 4). Trial amounts of  $H_2O$  were added to these adjusted compositions and the previously described procedure repeated until the CTs converged at a single temperature. The resulting  $T_e$  values are closer to each other and more reasonable in comparison to the 1979 vent temperatures. Log  $fO_2$  values plot very near the NNO buffer curve (Figure 2).

The preceding thermodynamic analysis suggests that the gases were in chemical equilibrium at temperatures substantially higher than the vent temperatures. It should be noted that successful convergence of CTs for the dry bottle samples is a required but not conclusive test of the equilibrium hypothesis. It is possible that an amount of  $H_2O$  could be found that would give the false appearance of overall equilibrium. In particular, the absence



**Table 4 Estimated water compositions, equilibrium temperatures and  $fO_2$  values for the dry flask samples.  
Gas data in mole percent.**

Sample	$T_v, ^\circ C$	H <sub>2</sub> O	CO <sub>2</sub>	SO <sub>2</sub>	H <sub>2</sub> S	H <sub>2</sub>	CO	$T_e, ^\circ C$	log $fO_2$	S/C	H/C	H <sub>2</sub> O/H <sub>2</sub>
82A1	472	97.94	1.29	0.003	0.005	0.758	0.0082	777	-14.68	0.01	150	128
82A2	472	98.27	1.07	0.074	0.012	0.568	0.0066	848	-12.82	0.08	182	173
Gas composition adjusted until C/S = 3.42 by adding 2H <sub>2</sub> S + SO <sub>2</sub> to compensate for estimated sulfur deposition:												
82A1	472	97.58	1.28	0.125	0.251	0.755	0.0082	777	-14.68	0.29	149	126
82A2	472	97.63	1.30	0.182	0.199	0.688	0.0079	790	-14.29	0.29	148	138

$T_v$  = measured vent temperature  
 $T_e$  = estimated equilibrium temperature

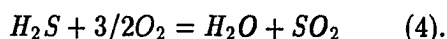
**Table 5 Anion analysis of a 1982 summit fumarolic condensate.**

Anion	Concentration (ppm)
SO <sub>4</sub>	1850
F	120
Cl	3430
Br	3

of H<sub>2</sub>O data does not allow a unique solution for the procedure involving the adjustment of sulfur gas species via the reversal of reaction (2). However, the fact that the results are also very plausible for this system allows some confidence to be placed in the estimated compositions. Although the 1982 sampling procedures precluded analysis of halogen gas species, anion analysis of a fumarolic condensate acquired at the same time shows that HCl was present in significant amounts (Table 5).

#### 1984 gases

Though the 1984 NaOH samples contained extremely small amounts of O<sub>2</sub>, the N<sub>2</sub>/(O<sub>2</sub> + Ar) ratios show that some oxygen was consumed in oxidation reactions thereby producing a disequilibrium assemblage. If all of the N<sub>2</sub>, Ar and O<sub>2</sub> are assumed to be of atmospheric origin, the amount of atmospheric O<sub>2</sub> which may have reacted with the gas species can be estimated. This is done by calculating the amount of O<sub>2</sub> required to lower the N<sub>2</sub>/(O<sub>2</sub> + Ar) ratio to the atmospheric ratio of 3.57. For samples 84A4 and 84A6 these values are 26.3 and 26 micromoles, respectively. Gerlach (1980) reported that oxidation of H<sub>2</sub>S may occur as a result of the reaction:



As stated earlier, such oxidation reactions would have no effect on total sulfur gas contents in the NaOH samples due to the analytical technique employed. Consumption of all of the oxygen by reaction of H<sub>2</sub> to H<sub>2</sub>O would increase the H<sub>2</sub>O content in 84A4 by only 0.002% and that of 84A6 by 0.006%. Oxygen fugacities calculated at the vent temperatures from

reaction (1) plot slightly above the NNO buffer curve. In addition, the  $\text{H}_2\text{O}/\text{H}_2$  ratios in the NaOH samples are very similar. All of these lines of evidence imply that oxidation of  $\text{H}_2$  to  $\text{H}_2\text{O}$  was insignificant in samples 84A4 and 84A6.

The minute amounts of measured CO (84A4 - 1.16 micromoles, 84A6 - 0.33 micromoles) have the greatest potential to show the effects of oxidation. Oxidation of CO to  $\text{CO}_2$  via reaction (3) is a likely mechanism for removing CO. Since the total measured moles of gases in sample 84A4 were more than 2.5 times greater than that of 84A6, sample 84A4 is considered to be the most representative of the 1984 samples. The two wet bottle samples (84A9, 84A12) were noticeably air contaminated, analytically less complete and may also have suffered post-acquisition reactions between sulfur gases and water condensed within the sample flasks. They are considered less reliable data than the NaOH samples.

Correspondence temperatures (Table 6) calculated for the NaOH samples indicate they are disequilibrium assemblages. Reactions (3) and (4) were employed to test if the disagreement in the CTs was due to oxidation of  $\text{H}_2\text{S}$  and/or CO. For sample 84A6 trial amounts of  $\text{SO}_2$  were converted to  $\text{H}_2\text{S}$  by reversing reaction (4) and the CTs then recalculated with the new mass balance. However, no amount of  $\text{SO}_2$  could be found, which, when converted to  $\text{H}_2\text{S}$ , would produce overall CT convergence. This suggests that sample 84A6 underwent additional disequilibrium modifications. To test if this sample also experienced oxidation of CO, trial amounts of  $\text{CO}_2$  were converted to CO by reversing reaction (3). These values and the trial amounts of  $\text{SO}_2$  converted to  $\text{H}_2\text{S}$  were then used to recompute the CTs. All the CTs converged at  $624^\circ\text{C}$  after conversion of  $5.9909 \times 10^{-3}$  moles of  $\text{SO}_2$  to  $\text{H}_2\text{S}$  and  $1.102 \times 10^{-6}$  moles of  $\text{CO}_2$  to CO.

The low CTs for  $\text{CO}_2$  and  $\text{CH}_4$  (Table 6) in sample 84A4 imply that the relatively high concentration of  $\text{CH}_4$  in this sample is a contaminant. Support for this assumption comes from the exceedingly minute amount of  $\text{CH}_4$  present in the restored equilibrium gas composition of sample 84A6 (Table 6). Additional support for the  $\text{CH}_4$  being a contaminant

**Table 6 Correspondence temperatures and restored gas compositions for the 1984 NaOH samples.**

Correspondence temperatures, °C.

Sample	H <sub>2</sub> O	CO <sub>2</sub>	SO <sub>2</sub>	H <sub>2</sub> S	H <sub>2</sub>	CH <sub>4</sub>	CO
84A4	>1200	152	>1000	>1200	733	162	813
84A6	1200	645	>1025	>1200	1159	-	635

Restored Gas Compositions, mole percent.

Sample	T <sub>v</sub> , °C	H <sub>2</sub> O	CO <sub>2</sub>	SO <sub>2</sub>	H <sub>2</sub> S	H <sub>2</sub>	CH <sub>4</sub>	CO	HF	HCl	HBr	T <sub>θ</sub> , °C	log fO <sub>2</sub>	S/C	H/C	H <sub>2</sub> O/H <sub>2</sub>
84A4	357	99.83	0.0330	0.0160	2.1x10 <sup>-5</sup>	0.092	9.7x10 <sup>-18</sup>	2.9x10 <sup>-5</sup>	0.001	0.023	8.0x10 <sup>-4</sup>	816	-11.92	0.49	5951	1109
84A6	338	99.76	0.0580	0.0160	0.0060	0.103	2.4x10 <sup>-14</sup>	2.5x10 <sup>-5</sup>	0.002	0.054	<0.0004	624	-17.11	0.37	3390	969

T<sub>v</sub> = measured vent temperature

T<sub>θ</sub> = restored equilibrium temperature

is found in the stable isotope patterns (discussed below) of gases and condensates collected from this vent. Therefore the  $\text{CH}_4$  was removed from the raw data and the CTs recalculated. The new CT for  $\text{CO}_2$  increased markedly and moved toward those of the other gas species. Testing of the oxidation hypothesis then proceeded as for sample 84A6. Conversion of  $2.1453 \times 10^{-5}$  moles of  $\text{SO}_2$  to  $\text{H}_2\text{S}$  caused all of the CTs for sample 84A4 to converge at  $816^\circ\text{C}$  (it was not necessary to convert any  $\text{CO}_2$  to  $\text{CO}$ ). The high  $\text{SO}_2/\text{H}_2\text{S}$  ratios in the restored compositions (Table 6) are consistent with analyses of their corresponding wet bottle samples in which  $\text{H}_2\text{S}$  was below the limits of detection. Log  $f\text{O}_2$  values for the restored equilibrium conditions plot considerably above NNO (Figure 2). The possible significance of these data will be examined in a later section (cf., Degassing Trends).

### Stable isotopes

#### $\delta\text{D}$ and $\delta^{18}\text{O}$

Table 7 lists all available  $\delta\text{D}$  and  $\delta^{18}\text{O}$  data for high-temperature fumarolic condensates from Mount St. Augustine prior to 1986. Isotope data up through 1982 were published in Viglino et al. (1985). New data include the 1984 fumarolic condensates and 11 additional 1984 surficial water samples. Interpretation of these data are postponed to a later section in which the potential sources for water being emitted from the Mount St. Augustine fumaroles are re-examined. Note here that the 84A6 fumarolic condensate plots along an apparent mixing trend between local seawater and prior year high-temperature fumarolic condensates (Figure 3). In contrast, sample 84A4 condensate is significantly richer in  $\delta^{18}\text{O}$  than either sample 84A6 or most of the other condensates.

#### $\delta\text{D} - \text{H}_2$

Table 7 gives the results of  $\delta\text{D}-\text{H}_2$  analyses for five selected gas samples. Actual measured yields of  $\text{H}_2$  from samples 79A3G and 79A6G were substantially lower than the predicted yields from gas chromatographic analyses and gas pressure measurements, indicating

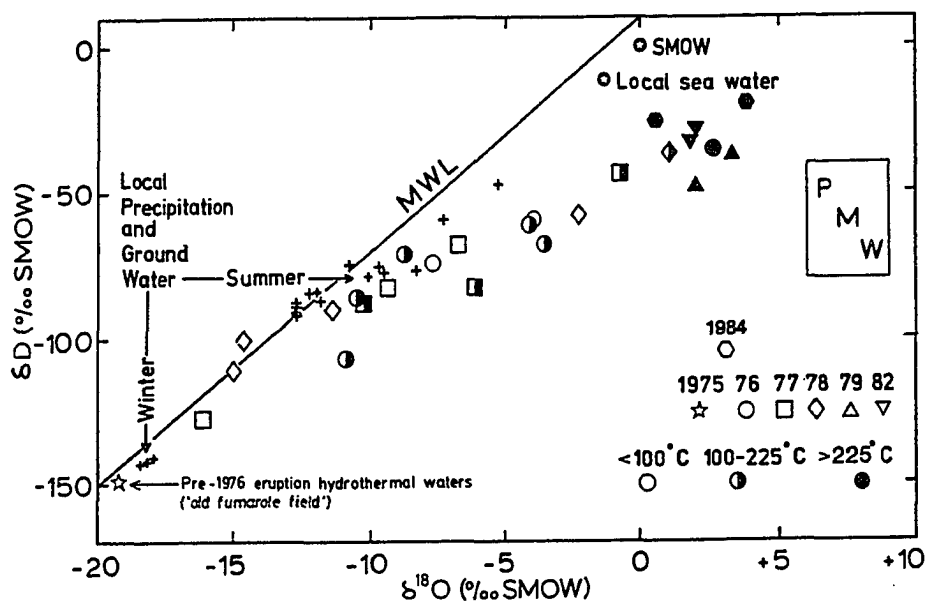


Fig. 3  $\delta D$ - $\delta^{18}O$  plot for summit fumarolic condensates and local surface waters from 1979-1984. The Meteoric Water Line (MWL) (Craig 1961), the Primary Magmatic Water (PMW) field (Sheppard et al. 1969), Standard Mean Ocean Water (SMOW) and local seawater are included for reference. Modified slightly from Viglino et al. (1985).

that  $H_2$  had escaped from the glass bottles in which these sample splits were stored. This  $H_2$  loss is reflected in the high magnitude  $\delta D$ - $H_2$  values for these samples. In contrast, the measured yield for the other three samples equaled or exceeded predicted amounts. The most significant difference between the two sample sets was the seal on the gas split storage flasks: 79A3G and 79A6G had a single o-ring seal while the remaining samples had double

**Table 7. Isotopic analyses of fumarolic gases from the 1976 dome. The values for  $\delta^{13}\text{C}$  are per mil PDB,  $\delta^{18}\text{O}$  and  $\delta\text{D}$  values are per mil SMOW.**

Sample	$\delta^{18}\text{O}$	H <sub>2</sub> O $\delta\text{D}$	$\delta^{13}\text{C}$	CO <sub>2</sub> $\delta^{18}\text{O}$	CH <sub>4</sub> $\delta^{13}\text{C}$	H <sub>2</sub> $\delta\text{D}$	R/R <sub>a</sub> <sup>1</sup>
79A3G	2.7	-48	-8.8	-	-	7930 <sup>2</sup>	-
79A4Ga	3.3	-37	-9.2	-	-	-	-
79A4Gb	-	-	-7.7	-	-	-134	-
79A6G	-	-	-7.7	-	-	6940 <sup>2</sup>	-
82A1	1.8	-32	-5.6	9.1	-	-	7.6
82A2	2.0	-28	-5.2	10.1	-	-	-
84A9	0.7	-27	-8.6	-	-	-300	-
84A12	4.0	-20	2.4	53.3	-22.3	-311	-

<sup>1</sup> Ratio of  $^3\text{He}/^4\text{He}$  in sample (R) to  $^3\text{He}/^4\text{He}$  in atmosphere (R<sub>a</sub>).

<sup>2</sup> Suspect analyses due to probable air leakage.

**Table 8 Isotopic fractionation temperatures for  $\Delta$  ( $H_2$ - $H_2O$ ).**

Sample	$T_f, ^\circ C$	$T_v, ^\circ C$
79A4Gb	>1000	746
84A9	580	338
84A12	550	357

$T_f$ , fractionation temperatures from Richet et al. (1977);  $T_v$ , measured vent temperatures.

o-ring seals. The extremely heavy  $\delta D$  values of 79A3G and 79A6G are therefore discounted because of possible fractionation and diffusion effects due to apparently weak o-ring seals.

Hydrogen used for standard calibration in isotopic analyses at the Scottish Universities Reactor Centre has been kept in Corning pyrex glassware for periods of up to eight months without having any noticeable effect on analytical results (< 2 per mil; J. Borthwick, pers. commun. 1986). Therefore the effects of any relative diffusion of  $H_2$  vs.  $D$  through glass with time are probably minor.

The  $\delta D$ - $H_2$  values for the three accepted samples (79A4Gb, 84A9, 84A12) are relatively heavy, indicative of probable high-temperature fractionation with the co-existing steam in the fumarolic vent. Table 8 provides the apparent equilibrium fractionation temperatures calculated from data compiled from Richet et al. (1977). Comparison to the empirical data of Richet et al. (1977) suggests that the apparent isotopic fractionation temperature calculated for  $D$  between  $H_2$  and  $H_2O$  in the 1979 sample was much greater than  $740^\circ C$ , the highest temperature for which empirical data are available. Although this shows that the 1979 gases were originally substantially hotter than the measured vent temperatures, the  $\delta D$ - $H_2$  fractionation temperature in excess of  $1000^\circ C$  is questionable because it exceeds or is near the upper temperature estimate of the 1976 magma by two-pyroxene geothermometry ( $830^\circ$ - $1050^\circ C \pm 60^\circ C$ , Johnston 1978;  $950^\circ C \pm 50^\circ C$ , Johnson 1986).

The fractionation of  $D$  between  $H_2$  and  $H_2O(v)$  is very rapid, and  $H_2$  -  $H_2O(v)$  is commonly found to be at or near isotopic equilibrium for the outlet temperatures of lower temperature fumarolic vents and geothermal wells (Truesdell and Hulston 1980). Kiyosu



(1983), however, reported several low- to medium-temperature fumarolic vents in Japan in which the  $\delta D$  in  $H_2$  and  $H_2O(v)$  indicated isotopic equilibrium  $100^\circ C$  to  $200^\circ C$  higher than the outlet temperatures, a situation which also appears to be the case at Mount St. Augustine.

### $\delta^{13}C$

Results of  $\delta^{13}C-CO_2$  analyses for selected Mount St. Augustine gases are listed in Table 7. Values for mantle-derived  $CO_2$  are considered to range from -4 to -9 per mil (Pineau and Javoy 1983). Ohmoto and Rye (1979) report that the  $\delta^{13}C$  values of carbon in magmas formed by partial melting of average mantle rocks lie between -3 to -7 per mil. For nonmagmatic systems,  $\delta^{13}C$  values of reduced carbon in sediments, coal, petroleum and graphite typically vary between -10 to -35 per mil with a mean of -25 per mil, while the  $\delta^{13}C$  values of most marine carbonates are constant at  $0 \pm 4$  per mil (Ohmoto and Rye 1979). All but one of the Mount St. Augustine samples lie within the mantle range of  $\delta^{13}C$  values, suggesting a mantle source for most if not all of the fumarolic  $CO_2$ .

The only fumarole emitting measurable  $CH_4$  (84A4) yielded a  $\delta^{13}C-CH_4$  value of -22.3 per mil for the wet bottle sample (84A12) taken from this site. This value is lower than the range of -20 to -15 per mil reported by Welhan (1981) as indicative of mantle-derived methanes; a more likely source for the methane is thermogenic breakdown of marine sedimentary country rock incorporated into the Mount St. Augustine magmatic system (see below).

## Discussion

### Degassing trends

The estimated and restored compositions allow examination of the 1979-1984 degassing trends for the Mount St. Augustine system. Samples 79A4Ga, 79A4Gb, 82A1, 82A2, 84A4 and 84A6 were all taken from the same or adjacent fumaroles and should provide the best illustration of compositional changes with time. The most dramatic long-term trend in these analyses is the large increase in the proportion of H<sub>2</sub>O (Figure 4) accompanied by decreasing proportions of the residual gases. Apparently, H<sub>2</sub>O contents in these fumarolic gases stayed relatively constant through 1982 ( $\approx 97.4$  mole%) but by 1984 became extremely water-rich ( $\approx 99.8$  mole%). The constancy of H<sub>2</sub>O/H<sub>2</sub> ratios within these 1979 and 1984 NaOH analyses supports minimal oxidation of H<sub>2</sub> to H<sub>2</sub>O in these samples and that the observed water-enrichment trend is real. The influence of H<sub>2</sub>O is also clearly shown in plots of atomic ratios (Figures 5a-b, 6) where the vertical trends for H/C versus S/C and H/S versus S/C and the diagonal trend for H/S versus H/C indicate that the variations are chiefly related to water content. Carbon dioxide fractions remain relatively constant (or even increase slightly) through 1982 but by 1984 have decreased by a factor of 25 to 40. The same trend is observed for H<sub>2</sub> but the decline is much less steep than that for CO<sub>2</sub>. Gerlach and Casadevall (1986a, 1986b) reported similar, but more constant trends in the CO<sub>2</sub> and H<sub>2</sub>O contents of dome gas samples at Mount St. Helens after the May 1980 eruption. They attributed these trends to a decline in the magmatic volatile fraction (i.e., progressive magmatic degassing) and an increase in the hydrothermal steam proportion of the fumarolic gases as a result of continued infiltration of meteoric water into the solidifying magma.

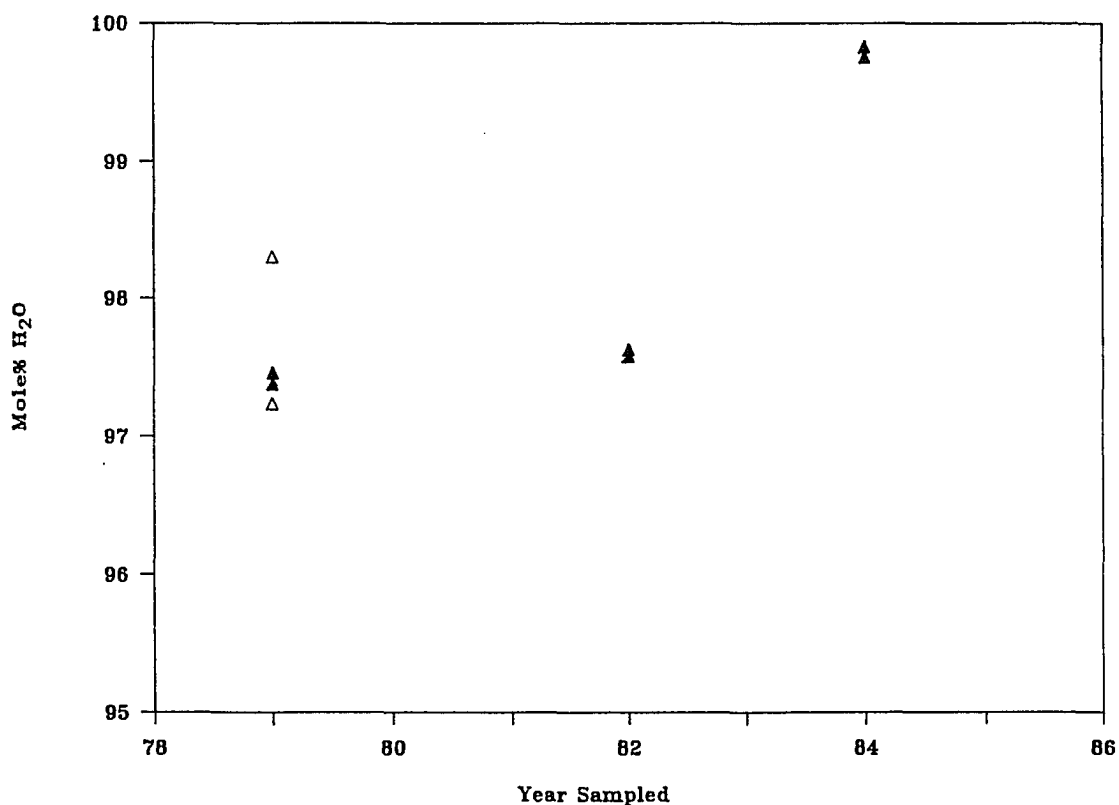


Fig. 4 Changes in H<sub>2</sub>O content from 1979 through 1984 for the summit gas samples. Filled symbols are for resampled or adjacent vents.

Dry gas (H<sub>2</sub>O-free recalculated) mole proportions in the resampled or adjacent vents changed from being CO<sub>2</sub>-dominated ( $\approx 45\%$  CO<sub>2</sub>, 24% H<sub>2</sub> in 1979) to H<sub>2</sub>-dominated ( $\approx 49\%$  H<sub>2</sub>, 22% CO<sub>2</sub> in 1984) (Figure 7). As previously reviewed, Motyka et al. (1986) suggested that these shifts in dry gas composition were indicative of progressive (ongoing) magmatic degassing. The dry gas proportion of HCl at these sites increased by 1.6 to 3 fold from 1979 through 1984 while the total mole% of HCl decreased by a factor of 3 to 10. The ratio

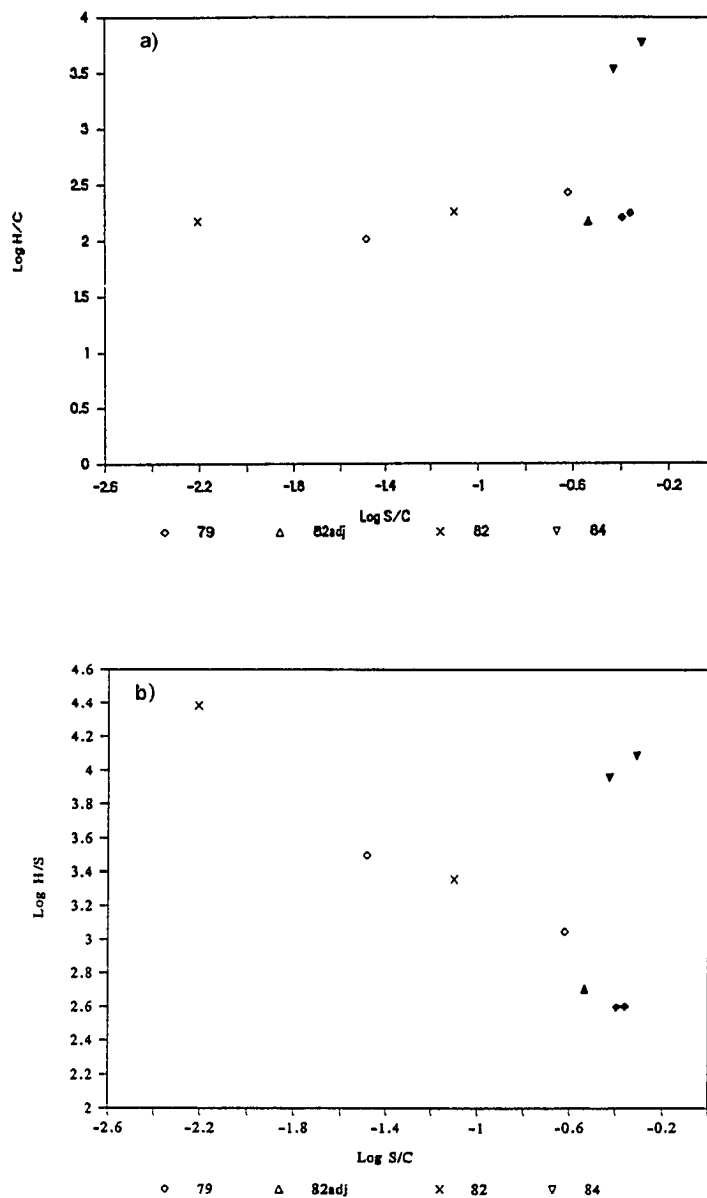


Fig. 5a-b Atomic ratio plots for the summit gas samples. a) Log H/C versus Log S/C. b) Log H/S versus Log S/C. In both figures the triangle symbol represents two 1982 data points and reflects correction for the apparent deposition of sulfur in the intake tube of the sampling apparatus (see text for discussion). The X symbols represent 1982 samples uncorrected for sulfur deposition. Filled symbols are for resampled or adjacent vents.

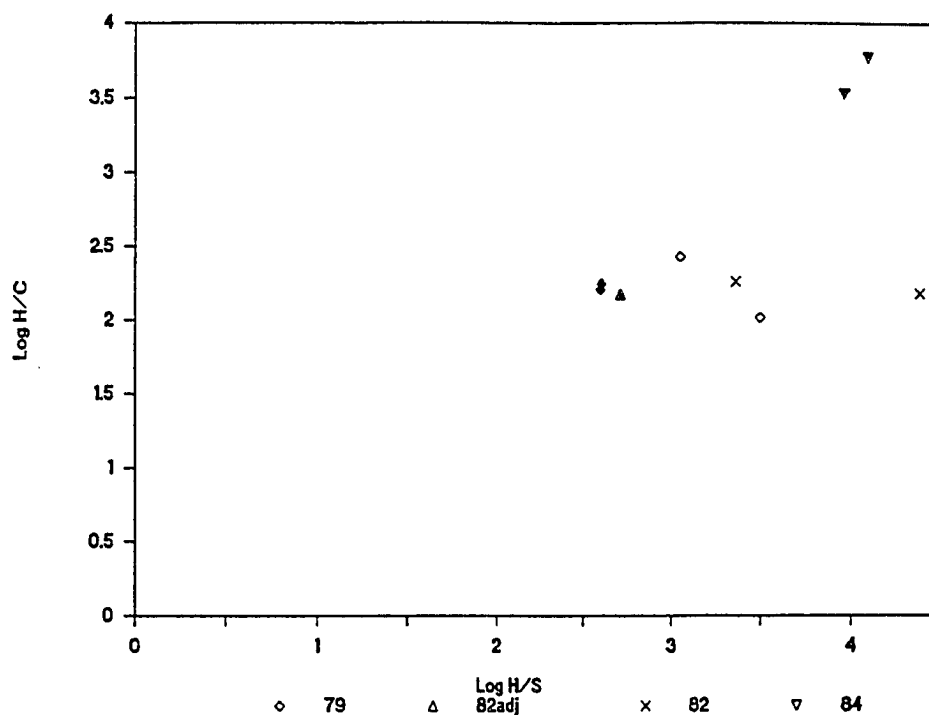


Fig. 6 Log H/C versus Log H/S for the summit gas samples. The triangle symbol represents two 1982 data points and reflects correction for the apparent deposition of sulfur in the intake tube of the sampling apparatus (see text for discussion). The X symbols represent 1982 samples uncorrected for sulfur deposition. Filled symbols are for resampled or adjacent vents.

of  $H_2S$  to  $SO_2$  appears to have decreased moderately from 1979-1982 whereas by 1984 the sulfur gases were almost entirely  $SO_2$ .

Decreases in  $H_2$  and  $CO$  in the Mount St. Augustine gases from 1979-1984 are consistent with a shift in volcanic gas equilibria with decreasing measured fumarole temperatures. However, readjustment of gas equilibria with falling temperatures does not adequately account for the magnitude of the  $H_2O$  increase, the decreases in  $CO_2$  and  $H_2S$ , and the relative

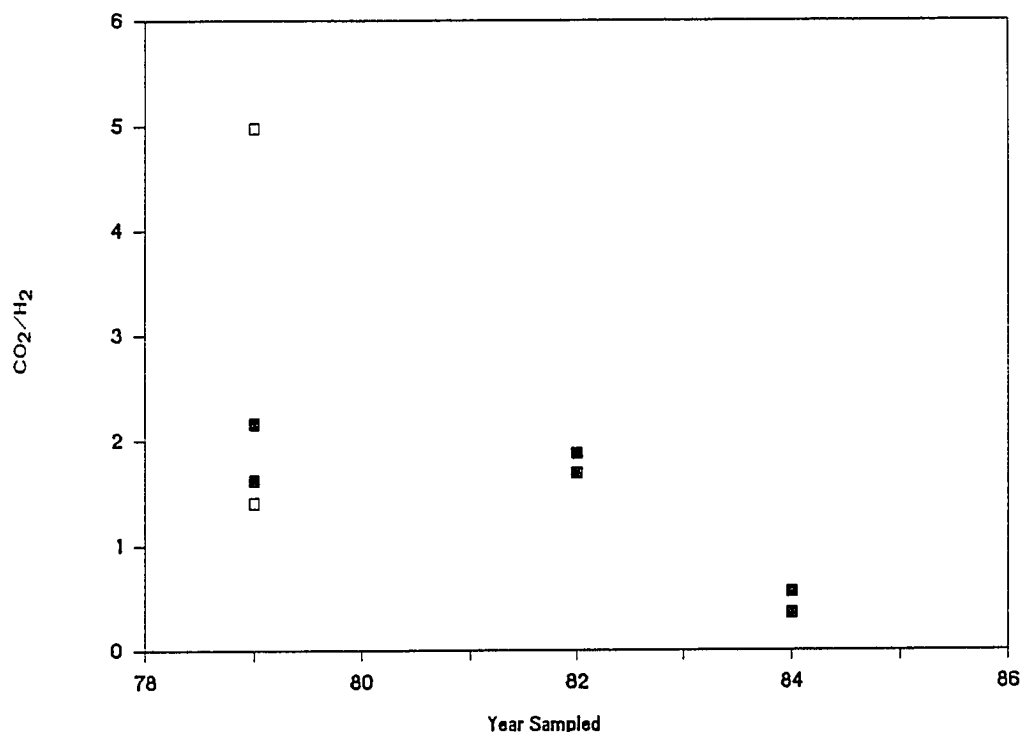


Fig. 7 Changes in CO<sub>2</sub>/H<sub>2</sub> ratios in the summit gas samples. Filled symbols are for resampled or adjacent vents.

increase in SO<sub>2</sub> over this period. Neither do declining fumarole temperatures adequately explain the apparent distribution of points on a log  $fO_2$ -T plot (Figure 2). Gases undergoing closed system cooling with high C/S and low C/H values such as the 1979-1984 Mount St. Augustine samples should have log  $fO_2$  values which parallel or closely follow the NNO or QFM buffer curves with falling temperatures (Gerlach and Nordlie 1975c; Gerlach 1982). Instead, the restored equilibrium temperatures and log  $fO_2$  values for 1984 plot well above NNO suggesting open system cooling of the gases in an increasingly O<sub>2</sub>-rich environment.

The log  $fO_2$ -T trend in the sampled high-temperature gases deserves more attention. The 1984 restored gas sample oxygen fugacities are very similar ( $\approx 1.5$  to 2 log units above NNO) to log  $fO_2$ -T values determined from coexisting Fe-Ti oxides in analyses of the 1976 and 1986 domes and 1986 explosive phases and lava flow (Harris in prep). However, the 1979 and 1982 gas sample oxygen fugacities plot very near NNO. This apparent discrepancy is perplexing, and limited information concerning this problem exists in the literature. Gerlach and Casadevall (1986a) report that most of their gas samples collected during 1980-1982 after the Mount St. Helens eruption yield  $fO_2$  values which lie along NNO and are similar to  $fO_2$  values determined from Fe-Ti oxides in the 1980 eruption products and dome samples. Some of their gases, however, have oxygen fugacities which plot considerably below NNO. They suggest the samples plotting below NNO may have had their  $fO_2$  lowered through buffering of the gases by the volcanic wall rock, or, that the  $CO_2$ -CO equilibrium quench temperatures were higher than those used to estimate  $fO_2$  in these samples. Benhamou et al. (1988) note that gas samples collected between 1978-1985 from Momotombo volcano have  $fO_2$  (near NNO) much higher than the intrinsic  $fO_2$  (near QFM) of fresh and altered lavas from the last eruption of this volcano in 1905. In their opinion, this indicates that Momotombo gases, after being released from magma, suffered variable oxidation during their ascent by both unbuffered cooling and reactions with wall rock and surface waters.

As presented earlier,  $fO_2$  values for the restored 1987 gas samples collected from the 1986 Mount St. Augustine dome plot almost exactly on NNO (Symonds et al. 1990). This implies that the analytical data and temperatures used in the  $fO_2$  estimation procedure for the 1979 and 1982 gas samples of this study are not unreasonable and gives credibility to the 1979-1984  $fO_2$ -T trend. Determination of  $fO_2$  in summit gas samples collected at Mount St. Augustine in 1989 by Robert Symonds (unpublished) may shed more light on this problem. Perhaps the lower  $fO_2$  of the 1979 and 1982 gas samples represents a lowering of the gas  $fO_2$  by wall rock - gas reactions. By 1984 this wall rock - gas equilibria may have

shifted due to changes in magmatic properties or contaminant influx into the volatile source region. If this is the case, then variations of  $fO_2$  in summit fumarolic gases at Mount St. Augustine may prove useful in hazard monitoring at this site.

Gerlach and Nordlie (1975b) investigated compositional changes in volcanic gases resulting from atmospheric oxidation,  $H_2O$  addition (meteoric  $H_2O$ ),  $SO_2$  depletion,  $H_2$  diffusion,  $S_2$  depletion or Cl addition for the system C-O-H-S. Of the processes they reviewed which increase the  $fO_2$  of the gases, only  $H_2O$  addition can explain all of the compositional trends observed in the gas samples of this study. Gerlach and Nordlie (1975b) report that at high temperatures ( $\approx 1000^\circ C$ ) this mechanism is inefficient, except when high relative volumes of  $H_2O$  (e.g., ratios of added moles of  $H_2O$  to total moles of initial gas  $\approx 250$ ; log C/H values  $\approx 10^{-3}$  or less) are added to the system. However, the log C/H trend seen in the Mount St. Augustine gases (high of  $1 \times 10^{-2}$  in 1979, low of  $2 \times 10^{-4}$  in 1984) suggests  $H_2O$  addition as a viable mechanism for generating the higher  $fO_2$  of the 1984 gases. Gerlach and Nordlie (1975b) also note that the efficiency of the  $H_2O$  addition process increases with falling temperature. Chlorine addition also has an oxidizing effect because the chlorine will react with  $H_2O$  to form HCl and in doing so release  $O_2$  (Gerlach and Nordlie 1975b). According to Gerlach and Nordlie (1975b), this process is also inefficient except when Cl is added in large amounts ( $\approx 3$  mole% HCl or greater). These workers report that addition of elemental chlorine maximizes its influence.

There is no independent, conclusive evidence to confirm that copious quantities of  $H_2O$  have been added to the Mount St. Augustine system. The explanation most consistent with the gas composition changes, atomic ratio trends and  $fO_2$ -T behavior is that the 1976 magma was becoming progressively degassed (decreasing the magmatic volatile fraction) and that nonmagmatic waters were increasing proportionately in the high-temperature fumarolic emissions.



## Sources of volatile components

### *CH<sub>4</sub> in fumarole 84A4*

Fumarole 84A4 was the only vent emitting measurable amounts of CH<sub>4</sub> (Table 1), a gas which theoretically should be present in only trace amounts in high-temperature magmatic volatile assemblages (Gerlach and Casadevall 1986a). The restored equilibrium concentration of CH<sub>4</sub> in sample 84A4 (Table 6) is below analytical detection, suggesting a nonmagmatic source for the measured CH<sub>4</sub> of this sample. The CH<sub>4</sub> is unlikely to have formed through reactions in the sample flask since CO<sub>2</sub> would have been absorbed in the NaOH, solution and no methane-producing material is known to be present in the flask.

The  $\delta^{13}\text{C}$  values of coexisting CO<sub>2</sub> and CH<sub>4</sub> (84A12 was collected from the same vent as 84A4) provide further evidence for a nonmagmatic source for the methane. The time required for equilibrium fractionation of  $^{13}\text{C}$  between CO<sub>2</sub> and CH<sub>4</sub> is extremely long at lower temperatures (e.g., > 20 ka at 400°C and > 10 Ma at 300°C) but relatively short at magmatic and sub-magmatic temperatures (e.g.,  $\approx$ 1min. at 750°C) (Sackett and Chung 1979; Giggenbach 1982). Therefore the high-temperature isotopic equilibrium composition of magmatic methane would be expected to be "frozen in" upon rapid ascent and quenching of magmatic gases. However, application of Bottinga's (1969) calculated equilibrium fractionation factor to sample 84A4 yields a CO<sub>2</sub>-CH<sub>4</sub> equilibrium temperature of approximately 300°C, well below the measured vent temperature. This implies the CH<sub>4</sub> came from a nonmagmatic source.

The  $\delta^{13}\text{C}$ -CO<sub>2</sub> and  $\delta^{18}\text{O}$ -H<sub>2</sub>O values for this same vent (2.4 o/oo PDB and 3.5 o/oo SMOW, respectively) are much heavier than those found in the emissions from the other fumaroles. The observed differences may have been produced by mixing or isotopic exchange with exotic materials not present in the source region of the other vents. One potential candidate for generating these differences is the reaction between the magma and a xenolith of

marine sedimentary rock. Marine sedimentary formations are known to underlie Mount St. Augustine, and xenoliths of argillaceous rocks have been found in the dacite dome (Johnson 1986). Marine carbonate rocks in particular may be enriched in both  $^{13}\text{C}$  (0 to +6 o/oo) and  $^{18}\text{O}$  (up to +20 o/oo) (Craig 1953; Magaritz and Gat 1981). High-temperature thermogenic decarbonation of such rocks coupled with isotopic exchange reactions can produce  $\text{CO}_2$  and  $\text{H}_2\text{O}$  enriched in  $^{13}\text{C}$  and  $^{18}\text{O}$  (Shieh and Taylor 1969).

Data for  $\text{CH}_4$  in sample 84A4 illustrate the caution needed in interpreting fumarolic gas data, particularly when potential disequilibrium processes have not been evaluated and isotopic data are unavailable. Vents sampled in 1984 were only several meters apart but yielded some noticeable differences in gas chemistry and isotopic compositions for methane.

#### $\text{H}_2\text{O}$

Deuterium-Oxygen isotope ratios measured in low-temperature fumarolic condensates (Figure 3) support meteoric water as the major fluid source in these vents. Apparently, these vents are rooted to very shallow levels beneath the summit and their emissions dominated by meteoric water seeping into the dome complex. Viglino et al. (1985) showed that boiling of local meteoric waters below  $220^\circ\text{C}$  with attendant steam separation could explain the isotopic enrichment seen in the low-temperature fumarolic condensates. Viglino et al. (1985) also argued for a significant magmatic water fraction in high-temperature fumarolic emissions at Mount St. Augustine. They contended that the waters in these gases were a mixture of magmatic and meteoric fluids with the proportion of magmatic waters decreasing systematically following the 1976 eruption. These same workers suggested, but discounted, that a  $\delta\text{D}-\delta^{18}\text{O}$  trend within the high-temperature fumarolic condensates indicated a mixture of local seawater and PMW (Primary Magmatic Water); instead, they argued that the magmatic  $\text{H}_2\text{O}$  was a mixture of subducted ocean water and mantle  $\text{H}_2\text{O}$ .

Lepel et al. (1978) noted extremely high concentrations of seawater-abundant (Na, Cl, Br) elements on aerosols of the 1976 eruptive plumes and argued that seawater was the source for all the Cl and Br in plumes following the second major eruptive phase of the 1976 event. Symonds et al. (1990) note that Cl/Br ratios are near the seawater ratio in condensates collected in 1986 from fumaroles situated on remains of the 1976 lava dome. However, Cl/Br ratios similar to the seawater ratio were not found in either the gas or condensate analyses of this study. As mentioned earlier, condensate from sample site 84A6 plots along the apparent mixing trend between local seawater and prior year high-temperature fumarolic condensates (Figure 3). Similarly, Symonds et al. (1990) report a 1986 dome high-temperature fumarolic condensate which falls along this same mixing trend, and that another high-temperature fumarolic condensate collected in August 1987 from the same fumarole field plots within the PMW field. Symonds et al. (1990) suggest that only PMW escapes from the magma itself. These workers concluded that a logical way to explain the isotopic enrichment of the high-temperature fumarolic condensates was by mixing of PMW with variable amounts of local seawater. The position of 84A6 condensate along the apparent PMW - local seawater mixing trend supports this conclusion.

Extensive isotopic exchange between meteoric waters and the volcanic wall rock, leading to  $^{18}\text{O}$ -enrichment in the fluids, is another potential mechanism for producing the  $\delta\text{D}$ - $\delta^{18}\text{O}$  pattern observed in the high-temperature fumarolic condensates at Mount St. Augustine. However, all but one of the high-temperature condensates (Figure 3) are moderately to highly enriched in  $\delta\text{D}$  relative to the most  $\delta\text{D}$ -enriched local precipitation measured. Though contamination of the high-temperature emissions by meteoric waters cannot categorically be ruled out, the 1976 aerosol, 1986 condensate anion, and stable isotope data strongly support a seawater component in the high-temperature fumarolic gases at this site. A three-component mixture (magmatic water, meteoric water and seawater) may be appropriate for modeling these high-temperature condensates. Addition of a seawater component to

the source region for Mount St. Augustine's volatiles can also explain the changes in gas chemistry observed in the 1979 to 1984 gas samples.

### *Cl and S*

The origin of chlorine and sulfur in the gaseous emissions at Mount St. Augustine is problematic. Johnston (1978) reported that all historic pumices erupted through 1976 are banded and consist of dark andesitic and light dacitic layers. Johnston (1978) proposed that the andesitic ejecta resulted from the mixing of a deeply-derived (25-75 km below sea level) basaltic magma with a shallowly-ponded (2-10 km below sea level) dacitic magma. An estimate of the crystallization pressures for hornblende inclusions in olivine phenocrysts (assumed to have come from the basaltic magma) within the andesitic ejecta was used by Johnston (1978) to constrain the source depth of the basaltic component. Microprobe analyses of Cl in glass inclusions within olivine crystals in the andesitic ejecta led Johnston (1980) to estimate the pre-eruption Cl content of the basaltic magma at 0.25 wt.% Cl. This high Cl content implies a deep source for some of the chlorine. Anderson (1975) suggested that Cl derived from subducted oceanic lithosphere might explain the generally Cl-rich nature of convergent zone magmas. Johnson et al. (in press) report that the presence of a subduction component, in the form of sediments or a fluid phase (dehydrated subducted slab), is supported by chondrite-normalized Ba/La ratios and time-integrated  $^{10}\text{Be}$  concentrations in Mount St. Augustine's lavas and pyroclastic samples. Subducted oceanic lithosphere therefore seems a likely source for some of the deep Cl component at Mount St. Augustine. The previously discussed  $^3\text{He}/^4\text{He}$  data of Poreda and Craig (1989) and the majority of  $\delta^{13}\text{C}-\text{CO}_2$  values of this study also support derivation of a portion of Mount St. Augustine's volatile budget from a mantle source.

The  $\text{SO}_2$  degassing patterns following the 1986 eruption may provide insight into the nature and magnitude of any shallower Cl and S sources at this volcano. Sulfur dioxide

fluxes were measured using COSPEC by Rose et al. (1988b) on 3 April 1986, during low-level eruptive activity one week after the 1986 eruption commenced, and by Symonds et al. (1990) on 24 July 1986, 24 May 1987, and 24 August 1987, during times of passive degassing. These four values fit an exponential decay equation of the form:

$$y = B1(e^{B2*x}) + B3 \quad (5)$$

quite well ( $R^2 = 0.980$ ), where  $y$  equals the  $SO_2$  flux,  $x$  equals the time elapsed in days and  $B1$ ,  $B2$  and  $B3$  are constants. Integration of this function for the approximately 508 days between the 4/3/86 and 7/24/87 COSPEC analyses suggests that 553,848 tonnes of  $SO_2$  were emitted over this time period. This value does not include the  $SO_2$  released during the peak eruptive periods covering the seven days prior to the first COSPEC sample. Rose et al. (1988b) estimated that the  $SO_2$  emission rate during the peak eruptive episodes may have been as high as 375,000 tonnes  $SO_2$ /day. The duration of 1986 individual explosive events at Mount St. Augustine are shown in Figure 8. From 28 March through 2 April these total about 95 minutes. To estimate the  $SO_2$  released during this period, the peak eruptive rate estimate of Rose et al. (1988b) was multiplied by this 95 minute span; it was further assumed that over this seven day period the background  $SO_2$  flux was at least as high as the 3 April 1986 COSPEC eruptive degassing determination (24,000 tonnes/day). These further estimates add approximately 192,740 tonnes to the volume of degassed  $SO_2$  for a total of 746,588 tonnes.

These results must be used with caution due to the limited number of COSPEC data, the long time period between COSPEC samples, the uncertainties involved in scaling-up the low-level eruptive degassing rates to those of the peak eruptive episodes and the natural variations which may result within individual eruption plumes. However, the total degassed  $SO_2$  estimate can be used to compare to what could be released upon complete degassing of the 1986 erupted magma volume. To make this calculation, the dense rock equivalent of the

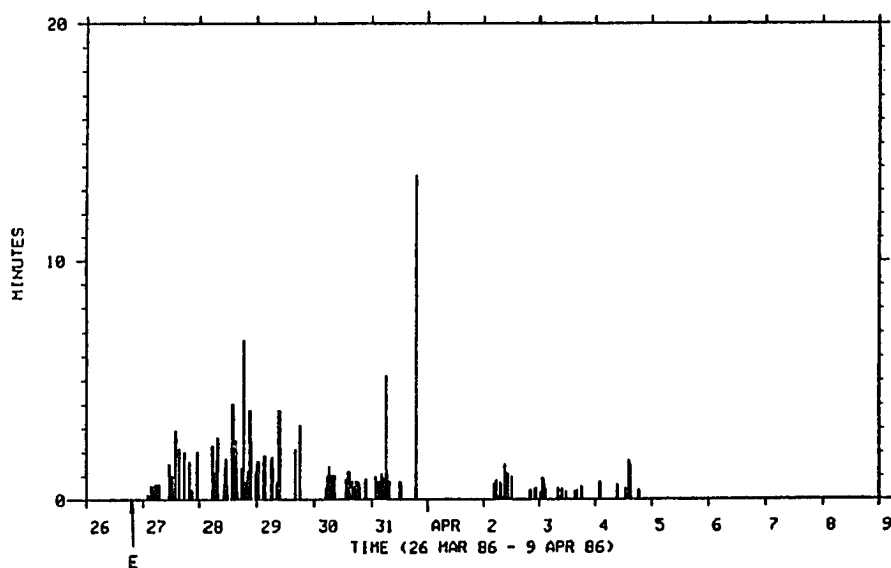


Fig. 8 Explosive event duration (26 March - 2 April 1986) at Augustine volcano. Measured at station OPT approximately 25 km northeast of the volcano. The "E" indicates start of the 1986 eruptions. Modified slightly from Power (1988).

1986 eruptive products was assumed to be the same as that reported by Johnston (1980) for the 1976 eruption ( $0.19 \text{ km}^3$ ). Although Johnston (1978) measured pre-eruptive magma sulfur contents of 100-700 ppm in crystal-hosted glass inclusions at this site, he recognized that these values may have been significantly underestimated due to the presence of sulfide globules in both the andesitic and dacitic eruptive products. Therefore, Johnston (1978) estimated the S content of the 1976 basalt using the S-FeO trend for MORB basalts of Mathez (1976) and his FeO analyses of glass inclusions in the 1976 andesitic ejecta, assuming

that the S-FeO trend is the same for both systems. Johnston's (1978) corrected estimate of 1400-2200 ppm S was used in the calculations. Lastly, Johnston's (1980) estimate of crystals (30%) to melt (70%) was employed, and it was assumed that all the sulfur in the melt was converted to SO<sub>2</sub> and that the melt density was 2.56 g/cm<sup>3</sup>.

Results of this calculation show that a maximum of 748,500 tonnes of S, equivalent to 1,497,000 tonnes SO<sub>2</sub>, could have been released upon complete degassing of the erupted magma. Corresponding minimum values are 476,280 tonnes S and 952,560 tonnes SO<sub>2</sub>. In addition, Symonds et al. (in press) have recently computed Cl flux estimates for the four COSPEC sampled dates. These flux estimates were derived using the ratio of Cl/S in a restored 1987 dome gas sample (Symonds et al. in press) and the COSPEC SO<sub>2</sub> fluxes. Because they are derived with the COSPEC data, the Cl flux estimates fit the same exponential decay equation as the SO<sub>2</sub> fluxes. Applying the same technique as for the SO<sub>2</sub> data yields an estimate of 438,400 tonnes of Cl outgassed over the period 3/27/86 - 7/24/87. Johnston (1978, 1980) measured average Cl contents of 0.25 wt. % and 0.50 wt. %, respectively, in crystal-hosted glass inclusions within the 1976 andesitic and dacitic ejecta. Using these as bounding values for the 1986 event, 850,000 - 1,700,000 tonnes Cl could have been released upon complete degassing of the 1986 erupted magma. However, based on measurements made on the glassy groundmass in degassed pumices and blocks from the 1976 eruption, Johnston (1980) also suggested the eruptive products may have retained 0.25 wt.% Cl (measurements were not reported for S). Similar Cl contents in the glassy groundmass of the 1986 eruptive products (ave. 0.24 wt.%,  $\sigma=0.11$  for 76 microprobe measurements) imply that eruptive product degassing could have contributed a maximum of 850,000 tonnes Cl to the atmosphere.

Bacon (1989) has recently proposed that igneous rock phenocryst-hosted crystal inclusions may form within a zone of local element saturation adjacent to the growing host

crystal. This requires that the inclusion mineral components exist in elevated concentrations, relative to the bulk magma, at the advancing crystal/liquid interface. If this is a viable crystal inclusion formation mechanism, then crystal-hosted glass inclusions may not be appropriate for estimating equilibrium bulk melt elemental concentrations. The glass inclusions that Johnston (1978) microprobed were hosted dominantly within plagioclase, with a few measurements also coming from glass inclusions within olivine. Since Cl and S do not readily substitute within the lattice of these minerals, these crystal-hosted inclusions may not be a good first-order estimate of the pre-eruptive magma Cl and S contents at Mount St. Augustine, but may actually signify the maximum pre-eruptive magma levels of these components. The COSPEC-derived HCl fluxes of Rose et al. (1988a, b) and the restored 1987 summit gas samples of Symonds et al. (1990) definitely show that the Mount St. Augustine volcanic system is very Cl-rich. Similar levels of Cl retained in the 1976 and 1986 eruptive products suggest a constancy to the pre-eruptive magma Cl contents at Mount St. Augustine.

Limited literature exists on pre-eruptive magma Cl contents for convergent plate volcanoes. Of the few published studies, all based on microprobe analyses of glass inclusions in minerals, pre-eruptive magma Cl content estimates range from a low of 800 ppm for the 1974 basaltic Fuego eruption (Woods et al. 1985) to a high of 3299 ppm for the 1963 basaltic-andesite eruption of Agung (Devine et al. 1984). In the absence of further experimental or observational constraints, microprobe analyses of the 1976 and 1986 Mount St. Augustine eruptive products will be used as the best current estimate of pre-eruptive magma Cl concentrations at this site.

The preceding calculations imply that degassing of the eruptive products and near-surface magma could account for all of the Cl and SO<sub>2</sub> vented at Mount St. Augustine. If this is the case, then most of any Cl and S derived from near-surface sources must have entered the system before extensive magmatic crystallization. The  $\delta D$ - $\delta^{18}O$  trend observed



in the high-temperature summit fumarolic condensates, the 1976 eruptive plumes aerosol chemistry, the 1986 summit fumarole condensate chemistry and the 1979-1984  $fO_2$ -T degassing trend are permissive evidence for a seawater component of S and Cl which did not reequilibrate with the magmatic system. This Cl and S might be derived via assimilation (without reequilibration) of near-surface seawater-bearing sediments or dehydration of seawater contained in these sediments. As magmatic crystallization proceeds, the total amount of Cl and S generated from this process should diminish along with the total volume of fumarolic emissions. This effect, coupled with a steep decline in the magmatic volatile fraction, could explain why HCl total gas contents in the samples decrease from 1979 to 1984 whereas dry gas HCl proportions in these samples increase over the same period. In this model, continued seawater influx through subvolcanic fractures or permeable sediments would act to recharge the seawater-depleted zone and provide a near-surface Cl and S source for the next eruptive cycle.

Unfortunately, insufficient data exist to properly evaluate the subvolcanic fracture characteristics (e.g., fracture density, length, diameter) and hence the magnitude of any seawater influx at this volcanic center. According to Power (pers. commun. 1989) the low magnitude (maximum of 2 on the Richter scale) shallow earthquakes that occurred beneath Mount St. Augustine prior to the 1976 and 1986 eruptions would probably generate a high-density fracture network of limited linear extent. Such a fracture network would not be favorable for large volume seawater influx. However, the fact that Mount St. Augustine is built upon uplifted sedimentary basement (an 80-m-thick section of which crops out on the south side of the island) and the volcanic edifice is deeply fractured leaves open the possibility that large-scale tectonism may have generated a significant subvolcanic fracture system. Seawater might also enter the volatile source region through permeable zones within the near-surface volcanic pile.

### **Eruption mechanisms**

Johnston (1978) contended that the 1976 eruption resulted from rapid volume increase and vesiculation upon mixing of the deeply-derived basaltic magma with the shallowly-ponded dacitic magma. Work in progress (S. Swanson pers. commun. 1989) suggests that magma mixing is still a viable trigger for the initial explosive phases at Mount St. Augustine but that the batches of magma undergoing mixing may be compositionally more similar than previously thought. Various lines of evidence suggest a phreatomagmatic component in Mount St. Augustine eruptions. Lepel et al. (1978) measured high concentrations of seawater-abundant elements (relative to earlier samples) in post-1976 eruption plumes and argued for two distinctive eruption mechanisms. In their opinion, the first 1976 eruptive phase was the result of explosive magmatic outgassing, whereas the second eruptive phase resulted from seawater interacting with hot magma to initiate a phreatomagmatic eruption. Johnston (1978) reported an "olivine" ash layer in the 1976 eruptive deposits which he presumed was laid down following the first 2 or 3 major explosive events of the initial eruptive phase. According to Johnston (1978), the physical characteristics of this ash layer argue against an air-fall origin and may support a base-surge origin (phreatomagmatic generated?) for this deposit. This ash layer, however, has not been verified by any of the later investigators of the 1976 eruptive products. Ash characteristics (e.g., presence of blocky tephra) have also been used to support a phreatomagmatic component in both the 1976 and 1986 eruptions (Johnston 1978; Kienle et al. 1986). In addition, Rose et al. (1988a) report that the distribution of the 1986 ash fallout is consistent with a phreatomagmatic origin. Power (1988), based on analysis of 1986 pre- and post-eruption seismicity patterns, theorized that near sea level groundwater in the volcanic cone interacted with ascending magma bodies. In his view, this groundwater - magma interaction resulted in a phreatomagmatic component in the initial 1986 vent-clearing explosions.

Eruption patterns may also reflect a phreatomagmatic component. The duration of individual 1986 explosive events (Figure 8) roughly correlates with relative explosive energies (J. Power pers. commun. 1989). Individual event length and explosion intensity increased slowly to a 28 March maximum and then slowly decreased. On 31 March the largest single explosion occurred; this event lasted over 13 minutes and generated an eruption column which rose to greater than 12 km above sea level (Power 1988). The fact that no significant duration explosive event preceded this large explosion for about 10 hours (nor followed it over the studied period) implies a different eruption mechanism than that operative from March 27 through March 30. The large March 31 eruption may indicate phreatomagmatic processes; a highly-charged, rapid energy release would be expected if water came into contact with an already water-saturated magma. If as suggested by Power (1988) the physical behavior of Mount St. Augustine's magmatic system was approximately the same for the 1976 and 1986 eruptions, then similar processes were probably operative during the 1976 eruptive cycle.

The major fluid source (meteoric or seawater) for any phreatomagmatic component in the Mount St. Augustine eruptions remains unclear. Lepel et al.'s (1978) plume chemistry data suggest that seawater enters the volatile source region sometime during the initial explosive phase of the eruptions. Perhaps the high energy 31 March 1986 eruption is indicative of seawater - magma interaction. Regardless, the stable isotope signature, the high collection temperatures and implied equilibrium in their 1986 and 1987 summit complex gas samples led Symonds et al. (1990) to propose that seawater must enter a high-temperature volatile source region. The accumulated data therefore suggest that seawater is already present in or begins to enter the volatile source region during the initial explosive phase and may generate some of the explosive activity associated with eruptions of Mount St. Augustine. This seawater component apparently continues to influence high-temperature

fumarolic emissions long after the eruptive activity has ceased and as the volcanic/magmatic system continues to cool.

### **Study applications and additional questions**

Data from this study illustrate the applicability of fumarolic gas samples to geologic problem solving. These data also raise broader questions about the relationships between fumarolic gases, dissolved magmatic volatiles, and retained volatiles in lavas or intrusive rocks.

This study shows that volcanic gas data must be carefully evaluated. Gas and condensate stable isotope patterns support Mount St. Augustine's summit fumaroles being rooted to different levels beneath the dome complex. Low-temperature vents are apparently shallowly rooted, with their fumarolic emissions dominated by meteoric waters (Vigilino et al. 1985), whereas high-temperature vents are apparently more deeply rooted with fumarolic emissions contaminated by seawater. A simple two-component (primary magmatic water and local seawater) isotopic mixing model suggests the high-temperature fumarolic emissions may be composed of 40 - 75 % seawater. In addition, fumarole 84A4 was the only vent ever sampled at Mount St. Augustine that emitted measurable methane. Equilibrium testing of the gas data, coupled with stable isotope gas values, suggest the CH<sub>4</sub> emanating from this vent was from a nonmagmatic source. Therefore, an integrated approach, utilizing gas chemistries and gas and condensate stable isotope data will produce the most valid and useful fumarolic emissions data. Fumarolic gas analyses should never be interpreted before testing the gaseous assemblage for disequilibrium.

The correlation between fumarolic gases and dissolved magmatic volatiles remains sketchy. The recent work of Bacon (1989) reveals that measurements of crystal-hosted glass inclusions may not be appropriate for estimating pre-eruptive magma volatile contents. A restored 1987 summit fumarole gas sample collected at Mount St. Augustine

in 1987 contained 5.6 mole% HCl (Symonds et al. 1990); this HCl value is an order of magnitude greater than that in any previously reported volcanic gas analysis. Similar high concentrations of Cl ( $\approx 0.25$  wt.%) retained in the glassy groundmass of the 1976 and 1986 eruptive products confirm the very Cl-rich nature of the Mount St. Augustine volcanic system. Whole-rock volcanic and crystalline plutonic rock Cl and S contents, however, are typically an order of magnitude lower (Krauskopf 1979) than Cl contents measured in Mount St. Augustine's eruptive products. If Mount St. Augustine's gas and eruptive product Cl and S data are truly representative of some magmatic systems, this would imply a radical, efficient loss of volatiles (e.g., Cl, S) from these magmas during volcanic eruptions and/or plutonic cooling. Such a large-scale loss of magmatic volatiles has significant implications for atmospheric chemistry and ore deposits generated by plutonic activity.

Discrepancies between the 1979, 1982 (this study), and 1987 (Symonds et al. 1990) fumarolic gas  $f_{O_2}$  (near NNO), and  $f_{O_2}$  values ( $\approx 1.5 - 2$  log units above NNO) determined from Fe-Ti oxides in the 1976 and 1986 eruptive phases (Harris: in prep), need further study. The intermittent gas sampling record following the 1976 and 1986 eruptions of Mount St. Augustine suggests the post-eruption summit fumarolic gases become increasingly oxidized with time (1984 gas sample oxygen fugacities are 1.3 to 1.8 log units above NNO) as a result of greater proportions of seawater in the high-temperature fumarolic emissions. This seawater influx may actually trigger some of the explosive phases of ensuing eruptions.

To clarify the relationship between gas and solid phase (and possibly magmatic)  $f_{O_2}$ , a continuous yearly record of gas samples from Mount St. Augustine's high-temperature summit fumaroles would be required. Data from the summit gas samples collected in 1989 at Mount St. Augustine by R. Symonds remain unpublished. Verifiable, consistent changes in the  $f_{O_2}$  of the high-temperature fumarolic gases could possibly be useful in volcanic hazard monitoring at this site.

## **CHAPTER 3:**

### **ROOTLESS FUMARoles OF THE 1986 MOUNT ST. AUGUSTINE ERUP- TIVE DEPOSITS**

---

#### **Introduction**

The 1986 eruptions of Mount St. Augustine generated extensive pyroclastic deposits and a small lava flow through which numerous rootless fumaroles vented. This event provided an opportunity to study fumarole development and deposits in the early stages of cooling and degassing of the eruptive products. This chapter† reports on the fumarole distribution, morphology, and alteration chemistry associated with these 1986 Augustine deposits. Data gathered in this study can be used to evaluate the physical and chemical parameters responsible for the formation and evolution of fumarolic systems, particularly rootless vents.

#### **Characteristics of the 1986 Lava and Pyroclastic Flows**

The 1986 eruptions of Mount St. Augustine included three major episodes: March 27-April 2, April 23-28, and August 22-September 1. Eruptive activity commenced on March 27, and was characterized by ash-rich eruption plumes ranging in height from 3000-12200 m (Yount et al. 1987). During this initial phase hundreds of small pyroclastic flows generated by the collapse of vertical eruption columns moved down the north flank of the volcano.

---

† Portions of this chapter comprise a manuscript authored by Lawrence Kodosky and Mary Keskinen published in the *Bulletin of Volcanology* (1990) 52:175-185.

The largest pyroclastic flows terminated on the north shore of the island, approximately 5 km from the summit vent. A small lava flow also formed on the north flank of the volcano during early April. The areal extent of the 1986 Mount St. Augustine eruptive products as of early June and July, 1986, is shown in Figure 9b. Minor pyroclastic activity was associated with the late August eruptions, most of which was generated by partial collapse of the newly emplaced dome complex. This activity modified the morphologies of the previously formed north flank deposits but did not change their areal distribution. Flow depth varies considerably with geographic position, but the 1986 deposits have been estimated to be up to 10-15 m thick high on the cone, thinning irregularly with distance downslope (S. Swanson pers. commun. 1989). Lithologically, the pyroclastic flows are comprised of a series of block and ash flows and monolithologic pumice flows (Limke and Beget 1986). The lava flow consists of a two-pyroxene andesite, which is mineralogically and geochemically similar to other historic Augustine lavas (Swanson and Kienle 1988). Table 9 provides bulk-rock chemistry determined for selected 1986 lava and pyroclastic flow pumice and ash samples.

### **Fumarole Distribution and Morphology**

Numerous fumaroles developed on the lava and pyroclastic flows generated during the March-April eruptive phase. All of the eruptive deposit fumaroles are rootless. During the first field visit in early June, the majority of the pyroclastic and lava flow fumaroles emitted a strong halogen and sulfurous odor. Field pH values of condensates from these sites were always lower than 2.

Four types of fumarolic vents were distinguished based on morphology. *Fissure vents* range 2.5-12.5 cm in width and are up to 4.5 m long and linear in form. *Phreatic explosion craters* are funnel-shaped vents which range 1.5-3.7 m in diameter and taper down to a

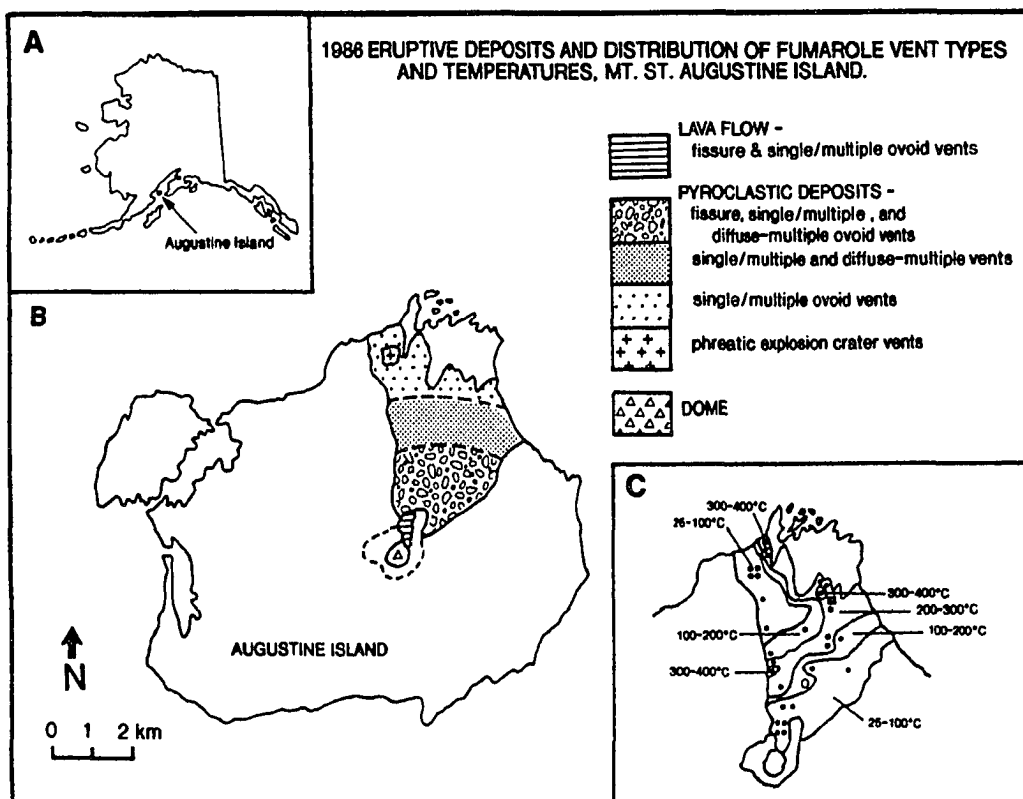


Fig. 9a-c Fumarole vent types and measured fumarole temperatures in the 1986 eruptive deposits. a) Location map for Augustine Island, southern Alaska. b) Distribution of fumarole vent types. Areal distribution of the 1986 deposits modified from Swanson and Kienle (1988). c) Measured fumarole temperatures in the 1986 eruptive deposits. Open circle and filled square show location of fissure fumarole PF4.5 ( $T=106^{\circ}\text{C}$ ) and single, ovoid opening fumarole PF4.2 ( $T=242^{\circ}\text{C}$ ), respectively, which are discussed in the text.



Table 9 Whole Rock Oxide and Trace Element (XRF, ICP, DCP) Analyses of 1986 Lavas, Pumice, Unaltered Ash, and Fumarolic Encrustations from Mt. St. Augustine. See text for details.

	Lava		Pumice		Unaltered Ash		Sublimate	Fissure		Single Ovoid	
	Range	Average	Range	Average	Range	Average		Z1	Z2	Z2	Z1
SiO <sub>2</sub>	58.3-61.7	60.3	61.0-62.2	61.8	57.79-59.42	58.79	4.61	46.74	63.52	62.31	56.31
Al <sub>2</sub> O <sub>3</sub>	16.4-17.0	16.6	16.3-16.7	16.4	16.62-17.21	16.91	3.11	14.75	10.82	11.48	15.59
Fe <sub>2</sub> O <sub>3</sub> *	5.91-7.02	6.38	5.75-6.35	6.01	5.52-6.32	6.02	0.72	5.34	3.57	6.34	5.34
CaO	6.68-7.96	7.27	6.49-6.99	6.72	7.36-7.62	7.50	3.00	7.10	3.92	3.44	5.64
MgO	3.15-4.17	3.64	3.23-3.62	3.38	3.70-4.04	3.87	1.46	3.63	2.69	2.26	3.34
Na <sub>2</sub> O	3.58-3.86	3.75	3.75-3.98	3.85	2.65-3.52	2.96	41.30	2.04	2.47	2.13	2.33
K <sub>2</sub> O	0.87-1.03	0.96	0.97-1.03	1.01	0.73-0.78	0.75	0.87	0.71	0.87	0.95	0.82
MnO	0.13-0.14	0.14	0.12-0.13	0.13	0.12-0.14	0.13	0.10	0.12	0.09	0.08	0.11
TiO <sub>2</sub>	0.55-0.65	0.59	0.52-0.57	0.54	0.60-0.63	0.61	0.08	0.35	0.48	0.62	0.54
P <sub>2</sub> O <sub>5</sub>	0.13-0.14	0.14		0.14	0.15-0.19	0.16	0.22	0.01	0.02	0.10	0.10
Ba					337-366	350	127	399	417	445	398
Sr					277-311	301	274	345	174	214	275
Cr					69-74	72	22	59	31	47	71
Ni					35-39	37	99	25	21	22	45
Co					110-176	135	211	52	82	93	124
V					149-170	163	25	175	83	151	117
Cu					n.d.	n.d.	b.d.	n.d.	n.d.	n.d.	n.d.
Pb					n.d.	n.d.	60	n.d.	n.d.	n.d.	n.d.
Zn					n.d.	70	99	1245	222	82	97
# analyses		3		3	65-75+	4	1	1	1	1	1

## Oxides - Wt.%; elements - ppm

\* Total Fe as Fe<sub>2</sub>O<sub>3</sub>

n.d. - not determined

b.d. - below detection

+ based on 3 samples

Sources: Pumice and lava by Harris (1988) unpublished data and Swanson and Kienle (1988) - ash and encrustation data from this study.

depth of 0.6-0.9m. *Singular/multiple ovoid opening* types consist of individual or clustered vents with a maximum diameter of 0.6 m and often extend deep into the flows. *Diffuse, multiple opening* types are areas up to 20 m<sup>2</sup> of shallow, randomly oriented and shaped vents.

The morphologic type and distribution of the fumaroles directly reflect their mode of formation (Figure 9b). Fissure fumaroles are confined to the lava flow and to the steeper, upper third of the pyroclastic flows. The fissures are primarily oriented transverse to the flow direction and appear to have formed as the result of extensional forces associated with the settling and draping of the flows. Phreatic explosion craters are restricted to a 0.4 x 0.4 km area approximately 0.8 km inland from the island's northern coast. Prior to the 1986 eruption this site contained a shallow freshwater lake. The phreatic craters formed by explosive cavitation of the pyroclastic deposits as the result of rapid water vaporization.

Single and multiple ovoid opening vents are randomly distributed throughout the lava and pyroclastic deposits. They appear to have no single major factor controlling their formation and distribution. However, in the lower portion of the pyroclastic flows, two nearly 0.4 km long linear segments were observed that host single ovoid fumaroles along their length (Figure 10). These trends align with the predominant trend of pre-eruption drainage channels. The lack of any contraction features and the smoothness of the pyroclastic flow surface in this area supports pre-eruption drainage control on fumarole morphology and distribution. Diffuse, multiple opening vents form around larger (> 1 m diameter) lithic blocks partially submerged within the pyroclastic flows. Apparently, differential settling and compaction of the flows around these buried blocks creates zones of weakness that allow easy access for gases to the flow surface. The majority of the diffuse vents are found in the upper two-thirds of the pyroclastic flows since this coincides with the areal distribution of



Fig. 10 Example of pre-eruption drainage control on fumarole distribution. The white fumarolic mounds in the distance define an approximately 0.4 km linear segment which aligns with the predominant trend of pre-eruption drainage channels on this section of the island.

most of the larger lithic blocks. Some of these factors were also suggested by Keith et al. (1981) for distribution of rootless fumaroles on Mount St. Helens.

Temperatures of rootless fumaroles measured in June-July 1986 ranged from 75°-394°C. Fumarole temperatures were taken with a platinum resistance thermometer calibrated through a working range up to 950°C. Figure 9c shows the erratic distribution of the fumarole surface temperatures. The highest temperatures were found in the single ovoid

**Table 10 Characteristics of pyroclastic and lava flow fumaroles.**

Fumarole Shape	Single/multiple ovoid	Diffuse, multiple opening	Fissure	Phreatic explosion crater
Fumarole size	Diameter up to 0.6 m	Up to 20 m <sup>2</sup> of randomly oriented and shaped vents	Width 2.5-12.5 cm Length up to 4.5 m	Diameter 1.5-3.7 m Depth 0.6-0.9 m
Temperature range(°C)	50-394	189-274	54-141	90-98
Alteration mineralogy, chemistry	Gypsum, sulfur, amorphous Fe-Al-Cl and Al-Cl hydroxides	Gypsum, tridymite, amorphous Fe-Al-Cl and Al-Cl hydroxides	Sulfur, tridymite, halite, amorphous Fe-Al-Cl and Al-Cl hydroxides	Gypsum, anhydrite, soda alum
Areal distribution	Ubiquitous; typically extend very deep into flows	Primarily in upper 2/3 of pyroclastic flows around large lithic blocks	Confined to upper 1/3 of pyroclastic flows and to the lava flow	Confined to site of a small, preeruption freshwater lake
No. of sites	17 (15 pyroclastic flow, 2 lava flow)	4	8 (4 pyroclastic flow, 4 lava flow)	4

vents, which confirms their deeper subsurface extension into the cooling, degassing deposits. In contrast, the lowest fumarole temperatures were consistently taken from fissure fumaroles and reflect their shallow subsurface extent. Characteristics of the different fumarole types are summarized in Table 10.

### Fumarolic Encrustation Mineralogy and Chemistry

#### Sampling procedure

All of the 1986 Mount St. Augustine eruptive deposit fumaroles showed some degree of development of encrustations. Encrustation samples were collected at 24 sites from the four fumarole types. Figure 11 shows these sites along with their sample designations. Encrustation development at these sites ranged from a very thin and narrow monochrome coating within the vent to up to three relatively wide, crudely zoned and variably colored deposits extending up to a meter from the main fumarolic vent. The single/multiple ovoid

opening and diffuse, multiple opening vents typically hosted a roughly concentric, three-zone alteration pattern: a reddish-orange innermost zone surrounding the fumarolic orifice, a greenish-yellow or reddish-green middle zone, and a white outermost zone. The white zone was usually of the greatest relative width. Fissure vents usually contained the same inner and middle colored alteration zones but never developed an outer white zone. The phreatic explosion crater fumaroles contained only a white alteration zone which formed around the fumarole opening.

At each examined site individual samples were taken from as many differently colored zones as were present. Due to extreme thinness of some of these zones, sample sizes ranged from 1-50 g. The thinness of these zones also precluded taking a pure encrustation sample in most cases; therefore, most samples represent a mixture of encrustation and altered volcanic ash. The encrustation samples were collected in sealed plastic bags and stored until sample preparation and analysis. Some soluble phases may have dissolved or changed their hydration state in water which condensed in the plastic bags. No color changes in the bagged encrustations were observed during storage, suggesting that phases present did not undergo significant post-collection oxidation.

### **Analytical techniques**

Wet-chemistry, XRD and SEM techniques were employed in the study of the encrustations. Phase identification was accomplished by XRD and SEM energy dispersive X-ray analysis (EDAX).

Encrustation chemistry was determined by wet-chemical analysis using DCPAES and ICPAES. The sample dissolution procedure was that described by Suhr and Gong (1983). A 0.2-g split of -200 mesh material, obtained by crushing the bulk sample in a tungsten-carbide shatterbox, was thoroughly mixed with 1 g of lithium metaborate. After fusion at 1050°C for ten minutes, the resulting molten bead was dissolved in a 4% HNO<sub>3</sub> solution.

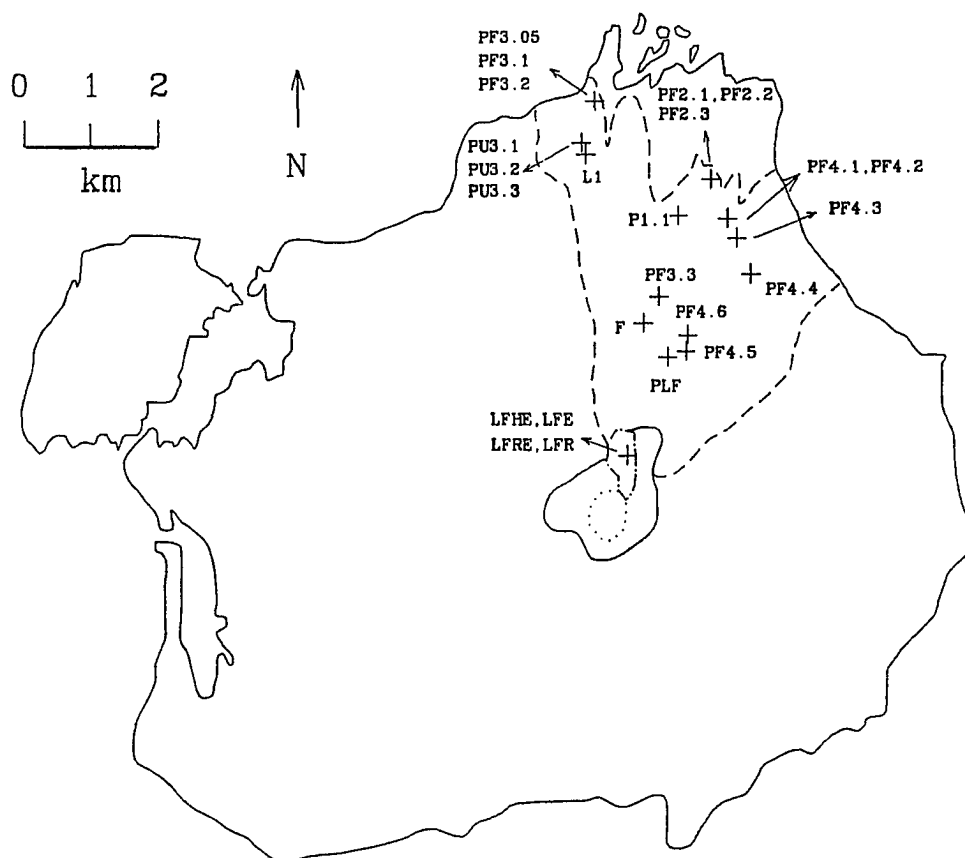


Fig. 11 Fumarole sample sites at Augustine volcano. Dashes outline the areal extent of the 1986 pyroclastic flows, the dashed-dot pattern outlines the 1986 lava flow and the dot pattern outlines the summit dome complex.

These solutions were subsequently analyzed for major and minor oxides and six to eight trace elements. Analytical accuracy and precision were monitored through analysis of selected geologic reference samples from the U.S. National Bureau of Standards (plastic clay, limestone, and basalt) and the Canada Center for Mineral and Energy Technology (MRG-1, Mount Royal Gabbro). Total accuracy and relative precision (determined by duplicate sample analyses) for the trace elements fell within  $\pm 5\%$ . For the major and minor oxides,

accuracy and relative precision were  $\pm 4\%$  or less, except for  $\text{SiO}_2$  for which both accuracy and relative precision were  $\pm 8\%$ .

### Analytical results

Six crystalline phases were identified by XRD in the encrustations. Sulfates are the most abundant mineral group found in these deposits (Table 10) but were not observed at the fissure fumaroles on either the pyroclastic or lava flows. Gypsum is the most common mineral phase followed in order of decreasing abundance by anhydrite, sulfur (orthorhombic), tridymite, halite, and soda alum. Although cristobalite is the  $\text{SiO}_2$  polymorph most commonly described from fumarolic deposits (e.g., Keith et al. 1981), tridymite has been reported from zones of vapor phase crystallization in fumarolic channels (Sheridan 1970; Stoiber and Rose 1974), often in metastable association with cristobalite. Trace amounts of cristobalite may have been present but below XRD detection limits in the samples of this study. Soda alum  $[\text{NaAl}(\text{SO}_4)_2 \cdot 12\text{H}_2\text{O}]$  was found only at one sample site, a phreatic explosion crater. SEM and EDAX confirmed the presence of the XRD-identified phases and revealed a number of additional amorphous and crystalline phases present in quantities too minor for XRD detection. A list of the X-rayed samples and their identified minerals are given in Appendix 1.

Figure 12 (a-g) illustrates the morphologies of some of these phases. Three crystalline phases remain unidentified. The platelets of Figure 12a yield EDAX spectra of Zn, S, and Cl, although the S and Cl X-ray counts were extremely minor relative to those of Zn and probably represent absorbed acidic condensate. Thomas et al. (1982) described zincite ( $\text{ZnO}$ ) platelets from the phreatic ashes of Mount St. Helens. The intersecting plates in Figure 12b contain only Ca and relatively minor Cl. Stoiber and Rose (1974) list hydrophyllite ( $\text{CaCl}_2$ , orthorhombic) as a mineral common to Central American fumaroles. The bladed habit of Figure 12b is consistent with orthorhombic hydrophyllite, but the relative intensities of the



Fig. 12a-g SEM photographs of observed encrustation mineralogies and morphologies. a) Zn-Cl-S platelets. b) Intersecting plates of a Ca-Cl phase. c) Bladed gypsum. d) Halite cubes forming on ash matrix. e) Bulbous noncrystalline Al-Cl hydrate; this sample contains 56% nonstructural water. f) Noncrystalline Al-Cl hydrate showing dehydration cracks and containing 21% nonstructural water. g) Al-Cl crystalline phase (chloroaluminate ?) containing 17% nonstructural water.



Ca and Cl peaks on the EDAX spectra do not completely corroborate this identification. Figure 12g shows cubelike forms which yield only Cl and Al peaks on EDAX scans. Chloroaluminate ( $\text{AlCl}_3 \cdot 6\text{H}_2\text{O}$ ), a common low-temperature mineral in fumarolic systems (Stoiber and Rose 1974), appears to be a reasonable if tentative identification. Although the crystal symmetry of chloroaluminate is hexagonal-rhombohedral, it is possible for a rhombohedral form, when viewed in some orientations, to appear cubelike. It should be kept in mind that the nondetectability of elements lighter than sodium affects the interpretation/identification of these minor phases.

Figure 12e-g illustrates the metastability of some of the encrustation phases. Amorphous phases are much more abundant than crystalline phases in the Mount St. Augustine encrustations studied. EDAX analyses of the sample surfaces in Figures 12e and 12f yielded only large Cl and Al peaks. Their bulbous and curved morphologies support the presence of abundant water. Keith et al. (1981) have suggested that, as fumarolic systems cool, dehydration cracks develop in the amorphous phases, followed by incipient crystallization to a more stable product. Figure 12e is a sample whose nonstructural water  $[(\text{H}_2\text{O}^-/\text{H}_2\text{O}^- + \text{H}_2\text{O}^+) \times 100\%]$  content is 56%. The nonstructural water component of the sample in Figure 12f is 21%. Dehydration cracks are evident, and the bulbous habit has been modified. The final stage in this transition is shown in Figure 12g. This sample contains only 17% nonstructural water. Crystallization to a more stable phase Al-Cl phase (chloroaluminate?) appears complete.

Figure 13 and Table 9 examine the variations in major and minor oxide and structural and nonstructural water contents between the differently colored alteration zones and unaltered ash for two fumaroles, one a pyroclastic flow fissure (PF4.5) and the other a single, ovoid fumarole (PF4.2). These sample locations are shown in Figure 9c and Figure 11. Mineral assemblages most commonly found in these two fumarole types are presented in Table 10. Geochemical data are presented in Table 9 as oxides, following the convention for

rock chemical data. This facilitates comparison between unaltered lava flow and ash compositions and fumarole encrustation chemistry, but is not meant to suggest that oxide species predominate in the fumarolic deposits. Chemical data for all of the analyzed encrustations are tabulated in Appendix 2.

Fumaroles PF4.2 and PF4.5 had two similarly colored alteration zones outward from their respective vent mouths, an innermost red to reddish-orange zone (Z1) surrounded by a greenish-yellow to greenish-orange zone (Z2). The ovoid vent also had an outermost zone of almost pure gypsum which has been excluded from Figure 13. At each fumarole site the remaining two alteration zones consisted of thin, colored coatings on an ash matrix. The unaltered ash samples were always collected well outside of any visibly altered material, but they may have experienced slight alteration from large-scale degassing of the pyroclastic flows.

With the exception of  $\text{Fe}_2\text{O}_3$ ,  $\text{TiO}_2$ ,  $\text{P}_2\text{O}_5$ , V, and Co, the chemical variation patterns between the unaltered ash and the two altered zones are quite similar for the two fumaroles. Overall, the outermost alteration zones (Z2) of Figure 13 show the greatest range of chemical component enrichment and depletion relative to the unaltered ash. Comparison of the trace-element patterns with those of the major and minor oxides suggests that the trace-element contents of the encrustations are controlled by isomorphic substitution (e.g., for elements with similar ionic charge, electronegativity, and/or ionic radius;  $\text{Sr}^{2+}$  for  $\text{Ca}^{2+}$ ,  $\text{Ni}^{2+}$  for  $\text{Mg}^{2+}$ ,  $\text{Ba}^{2+}$  for  $\text{K}^+$ , etc.) for more abundant cations in the alteration phases. Elemental scatter plots (Figure 14a-d) suggest that Cr and V may substitute in this manner for Fe, Ba substitutes for K, and Cr substitutes for Mg. Naughton et al. (1976) similarly recognized this substitution behavior in fumarolic encrustations and condensates from Kilauea volcano in Hawaii. The high content of structural and nonstructural water relative to unaltered ash in both fumarole types suggest that reactions involving a liquid phase are the dominant mechanism of fumarolic alteration. Although no chemical analyses were made of

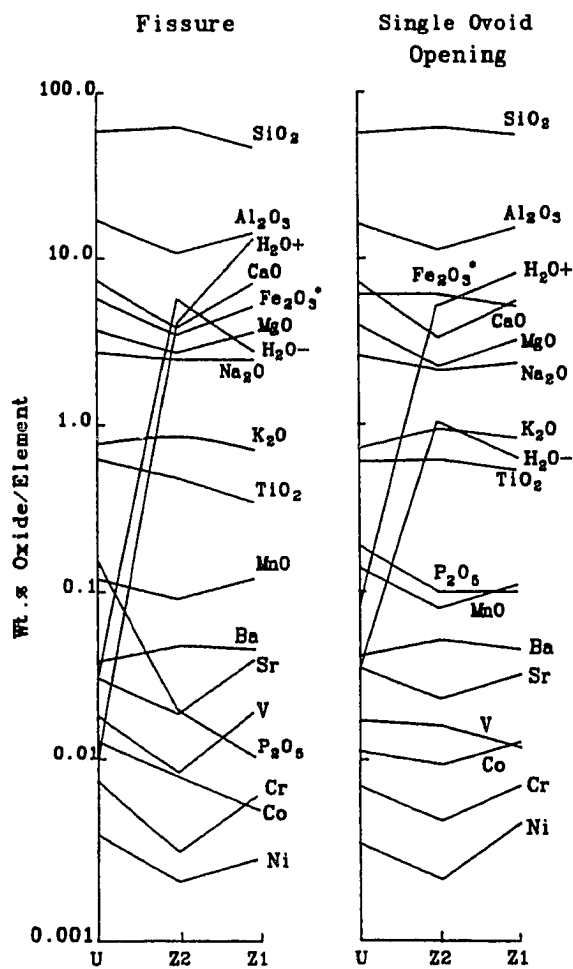


Fig. 13 Chemical variation between two fumarole types. Zone Z1 surrounds the fumarole mouth; zone Z2 lies outward from Z1; "U" refers to unaltered ash collected well outside of these vents. \*Total Fe expressed as  $\text{Fe}_2\text{O}_3$ .

encrustations from the lava flow, the similarity of encrustation mineralogy and morphology between the lava and pyroclastic flow samples supports similar alteration mechanisms for these two flow types.

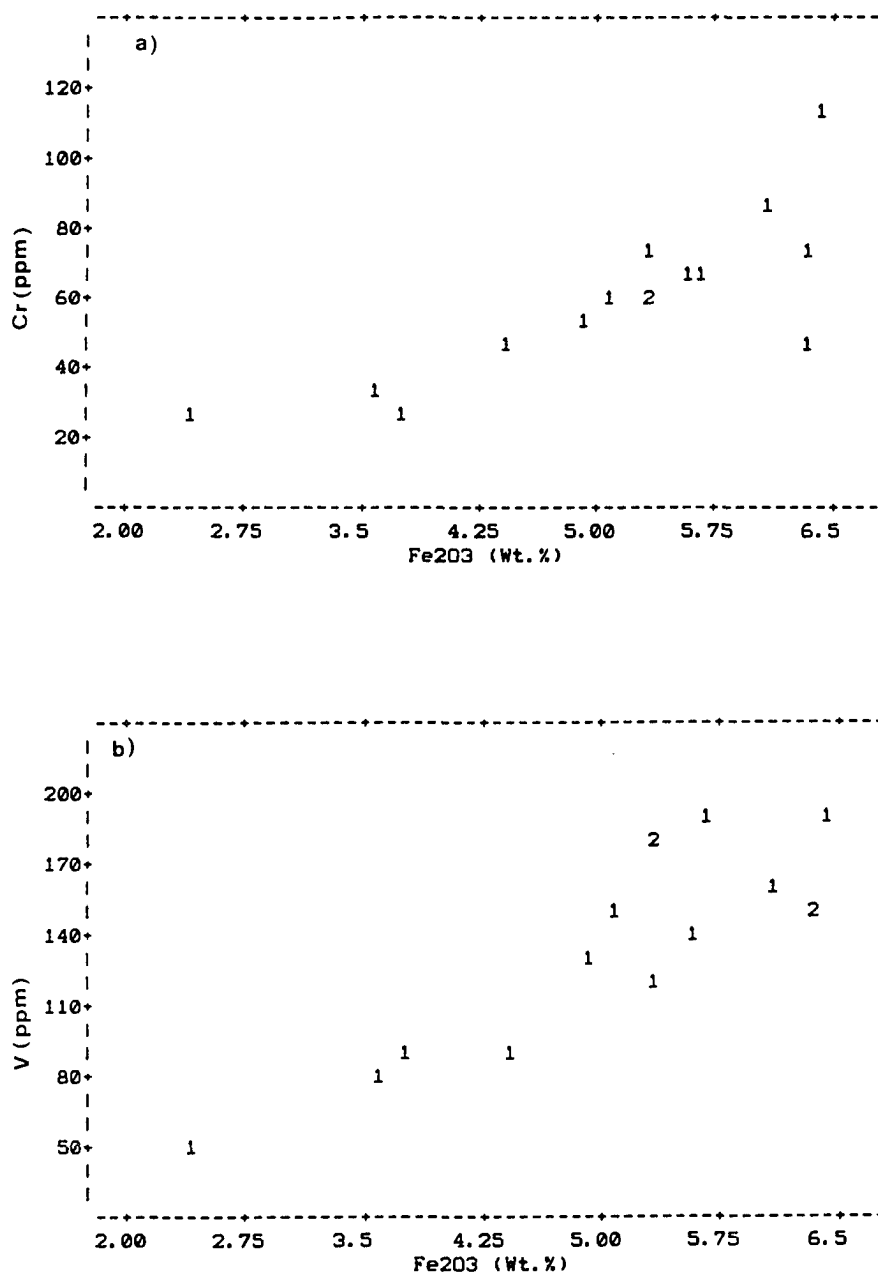


Fig. 14a-b Scatter plots illustrating the isomorphous substitution of elements. a) Cr vs. Fe<sub>2</sub>O<sub>3</sub>. b) V vs. Fe<sub>2</sub>O<sub>3</sub>. Numerals correspond to the number of plotted points.

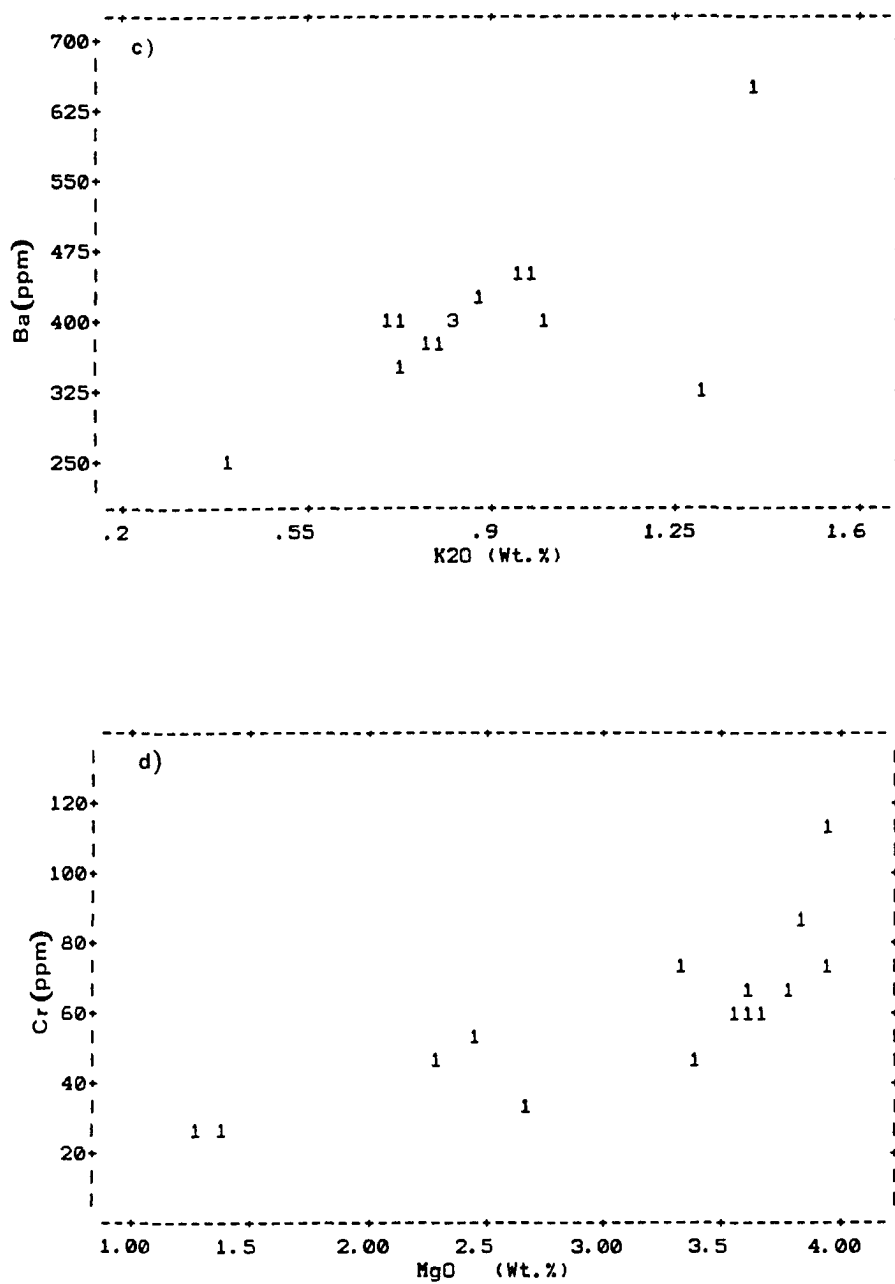


Fig. 14c-d Scatter plots illustrating the isomorphous substitution of elements. c) Ba vs. K<sub>2</sub>O. d) Cr vs. MgO. Numerals correspond to the number of plotted points.

## Discussion

The mineralogies observed in the Augustine encrustations are consistent with those collected at other low-temperature, oxidized fumaroles (e.g., Stoiber and Rose 1974; Naughton et al. 1976; Keith et al. 1981) where sulfates, chlorides, and oxides dominate the range of primary and secondary phases. Stoiber and Rose (1974) identified 47 minerals in encrustations deposited at nearly 100 different high-temperature (400°-900°C) fumaroles from 14 Central American volcanoes. Of these 47 minerals, 30 were sulfates, 10 halides, 6 oxides, and one a native element. Sulfides (e.g., Cu-Pb- and Zn-sulfides described by Zies 1929 from the Valley of Ten Thousand Smokes, Alaska), vanadates (Hughes and Stoiber 1985), and a host of rare and/or subordinate minerals have been described as well from other fumaroles, as has been comprehensively summarized by Stoiber and Rose (1974).

The mineralogy and geochemistry of the encrustations allow insight into the processes occurring in and around the fumarolic vent. The observed Augustine encrustation mineralogy, chemistry, and morphology are very similar to those found by Keith et al. (1981) around relatively low temperature, oxidized, rootless fumaroles developed on the 1980 Mount St. Helens pyroclastic and debris flows. More quantitative estimates of conditions of deposition can be obtained by comparison to the encrustation mineral assemblages described by Stoiber and Rose (1974) from Central American fumaroles. They found that the zonal arrangement of encrustations around the vent develops in response to the rapidly changing temperature and  $fO_2$  at the mouth of the fumarole. Matching the Augustine mineral assemblages to basically similar mineralogies from Central American volcanoes on a modification of the  $fO_2$ -T plot (Figure 15) by Stoiber and Rose (1974) yields a range of  $\log fO_2/T$  (0 at 25°C to -12 at 250°C) compatible with the observed low-temperature, oxidizing conditions.

As outlined earlier, in delineating the source of the components which make up the encrustations, the major problem is determining which components precipitated from the

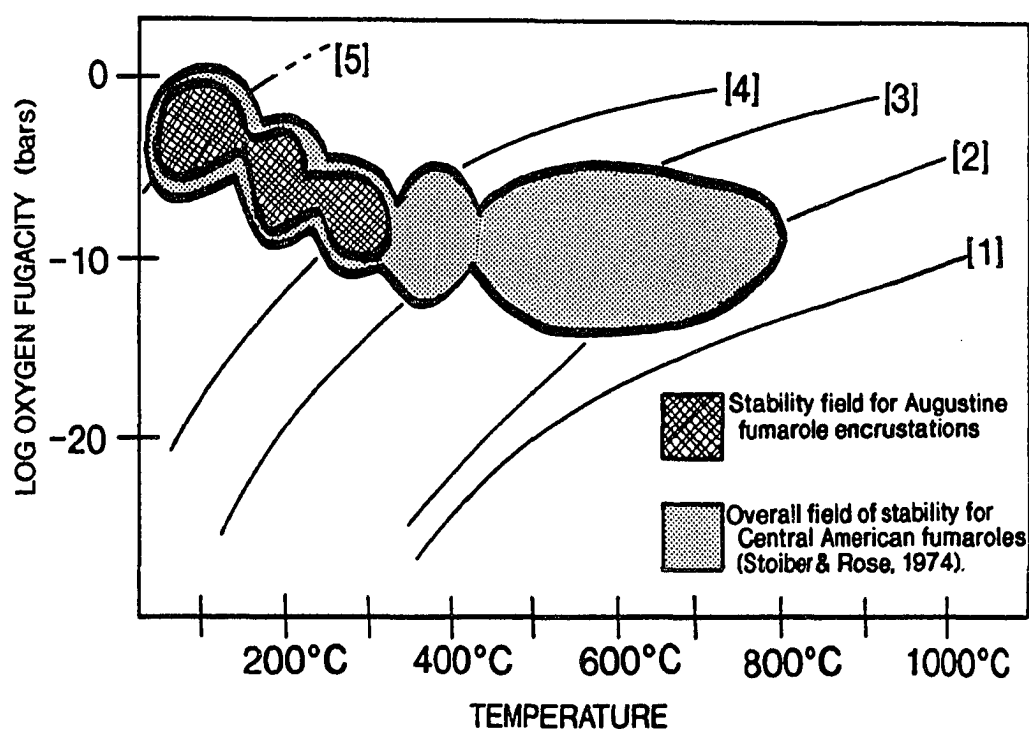
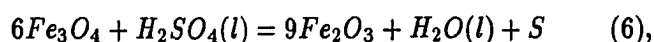


Fig. 15 Log  $f_{O_2}$  - temperature of formation conditions estimated for the encrustations. Modified from Stoiber and Rose (1974). Numbered curves represent the following oxide buffer curves plotted for reference: 1,  $SO_2-S_2$ ; 2,  $Fe_2O_3-Fe_3O_4$ ; 3,  $CuO-Cu_2O$ ; 4,  $SO_3-SO_2$ ; 5,  $MnO_2-Mn_2O_3$ . Total pressure=1 bar. Cross-hatched area is a rough approximation of formation conditions for mineral assemblages similar to those found in the 1986 Mount St. Augustine eruptive deposits, derived by comparison to the relations estimated by Stoiber and Rose (1974) for similar Central American fumarole encrustations. Stippled area shows the full range of Stoiber and Rose's encrustation stabilities.

vapor phase and which were derived by acid attack on the underlying matrix. A number of lines of evidence support condensation of acidic vapors and subsequent leaching of the andesitic ash as the primary elemental source for and mechanism by which the Mount St. Augustine encrustations formed. As previously mentioned, the high structural and

nonstructural water contents of the alteration zones (Figure 13) as well as the morphologies of the encrustation phases (Figures 12e,f) support liquid phase - solid phase reactions as the dominant mechanism of fumarolic alteration. These data, together with the sulfurous and halogen-rich odors noted emanating from the fumaroles during early June 1986, the low pH values and high halogen contents (7800-41000 ppm Cl<sup>-</sup>; 50-1100 ppm F<sup>-</sup>; n=3) of the fumarolic condensates (Symonds et al. 1990), and the encrustation mineralogies, all support leaching of the andesitic ash by acid condensate as the primary elemental source for the encrustations. Stoiber and Rose (1974) provide two possible low temperature (< 200°C) reactions by which sulfur and gypsum, common minerals in the Mount St. Augustine encrustations, may form from the acid alteration of fumarolic wall rock material:



In their opinion hydrated and hydroxyl-bearing crystalline and amorphous phases also probably result from halogen acid alteration of wall rock material in reactions analogous to equations (6) and (7). Similar reactions may be taking place in the Mount St. Augustine deposits although the actual mechanisms may vary slightly due to the high halogen content of the condensates. Reactions involving hydrolysis and the boiling of acid solutions may also play an important role in the alteration process (Lovering 1957).

The degree of involvement of gas phase reactions and vapor phase transport of elemental species in the rootless fumaroles at Mount St. Augustine is poorly constrained. Table 9 contains analytical results for a sample which most closely approximates a true "sublimate" phase in the eruptive deposits. This sample was collected from the surface of a large lithic block in the pyroclastic flow which extended over and about one meter above the mouth of an active fumarole. This orientation of the lithic block served to shield this deposit from most surficial weathering processes.

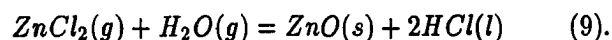
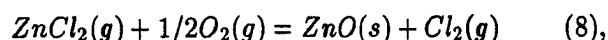


The only mineral phases identified in the apparent sublimate by either XRD or SEM techniques were abundant quantities of halite and minor amounts of native sulfur. Both LeGuern and Bernard (1982) and Symonds et al. (1987) identified halite in sublimate samples collected in quartz tubes from rooted fumaroles at Merapi volcano, Indonesia. LeGuern and Bernard (1982) point out that Na and K compounds are sufficiently volatile as halide or oxyhalide gas species to form true sublimate deposits. For comparison, Table 9 also contains major and minor oxide and trace-element data for four unaltered andesitic ashes as well as the corresponding chemistry for the fumarolic encrustation samples of Figure 13. The  $\text{Na}_2\text{O}$  in the "sublimate" sample (expressed as the oxide for consistency but likely present as a chloride) is nearly 14 times the average  $\text{Na}_2\text{O}$  content in the unaltered ash; this apparent enrichment is consistent with the prevalence of halite in this deposit. Stoiber and Rose (1974) report that Ca and Mg compounds are typically not volatile enough to generate substantial concentrations via sublimation. If so, then the relatively large amounts of CaO and MgO in the apparent sublimate sample suggests that gas-liquid alteration of the lithic host may have contributed chemical components to this deposit.

In terms of trace elements, Ba, Cr, and V have markedly lower concentrations in the "sublimate" when compared to unaltered ash. Symonds et al. (1987) contend that Ba and Cr are derived from wall rock interactions. High concentrations of these elements, which is not the case here, would imply that alteration of the lithic host was supplying the majority of the chemical components for the formation of the apparent sublimate deposit. Relatively high Ni and Co values suggest that a significant portion of these elements in the "sublimate" may have been carried in the vapor phase.

In addition, the innermost alteration zone (Z1) of the fissure fumarole is enriched in Zn relative to the average unaltered ash by nearly a factor of 18. The Zn-rich platelets tentatively identified as zincite of Figure 12a are present in this alteration sample. Thomas

et al. (1982) contend that zincite observed in the phreatic ashes of Mount St. Helens formed by the oxidation of magmatic vapor-transported  $ZnCl_2$  according to the following reactions:



High chloride contents in the pyroclastic flow condensates at Mount St. Augustine (Symonds et al. 1990) suggest that similar vapor phase transport of Zn may have also occurred there. Symonds et al. (1987) report that vapor phase Zn is concentrated in or very close to the fumarole mouth, which may explain why it is only slightly enriched in the apparent sublimate sample and present at fairly high concentrations in the encrustations nearer the fumarolic orifice.

Whether encrustation chemistries are representative of fumarolic gas compositions is a long-standing question. Unfortunately, the Mount St. Augustine rootless fumarolic encrustations cannot be properly compared to gaseous emissions of either the rooted summit fumaroles of this study or those of Symonds et al. (1990). Emissions from the rootless fumaroles were heavily contaminated by air incorporated into the flows during emplacement and meteoric water infiltration into the thin flows. Two gas samples collected from pyroclastic flow fumaroles in the summer of 1986 were too highly air-contaminated for proper chemical analysis. The rootless fumaroles also have a much more rapid cooling history (months) compared to the rooted summit vents (years). In addition, volatiles from the sampled rooted and rootless fumaroles were released during much different stages of Mount St. Augustine's eruptive cycle; a period of extremely low-level passive degassing three to five years after an eruption (rooted fumaroles) versus high-level degassing immediately following a major vent-clearing eruption (rootless fumaroles).

Of the six most abundant crystalline phases revealed by XRD analysis of the rootless fumarolic encrustations, three of these phases were sulfates, one was native sulfur, and

the other was a chloride. The amorphous phases in these deposits are dominantly Cl-rich. Because of the limited concentration period resulting from the rapid cooling of the rootless fumaroles, the encrustation phase chemistries suggest the rootless fumarolic gases were also rich in Cl and S. The extremely high Cl concentrations (7800 ppm, 28000 ppm and 41000 ppm) measured in condensates collected in July 1986 from three low-temperature (202°C - 247°C) pyroclastic flow fumaroles (Symonds et al. 1990) is further evidence of the very Cl-rich nature of the rootless fumarolic gases.

The marked enrichment of Na in the halite of the apparent sublimate sample suggests that the rootless fumarolic gases were not only Cl-rich, but that they were also efficient transporters of some trace elements. The high concentration of Zn (1245 ppm) found in the innermost alteration zone of fissure fumarole PF4.5 (Table 9), and the tentative identification of the Zn-Cl-S platelets of this alteration zone (Figure 12a) as zincite support efficient vapor phase metal transport in the rootless fumaroles.

The importance of volatile compounds in ore metal transport and concentration was first investigated by Krauskopf (1964). Whether vapor phase transport of metallic species can produce a sizable ore deposit, or whether magma devolatilization and vapor phase transport of metals serve as an ore preconcentration stage preceding hydrothermal remobilization, remains problematic. Symonds et al. (1987) have recently suggested that sublimation from a high-temperature, high-velocity carrier gas may not be efficient enough to form a large ore deposit. Work in progress by Symonds (pers. commun. 1987) on sublimate samples collected in quartz tubes from high-temperature, rooted, summit fumaroles at Mount St. Augustine will serve as a high-temperature endpoint for such studies. Studies of this type will more closely constrain volatile element fluxes at Mount St. Augustine and in general will allow better evaluation of the importance of metal volatility in the generation of ore deposits associated with igneous and volcanic activity.

## CHAPTER 4:

### RECONNAISSANCE Hg<sup>o</sup> SURVEY OF THE VTTS

---

#### Introduction

Mercury soil/regolith geochemical surveys have been successfully utilized in locating favorable areas for geothermal resources in a variety of bedrock types (Matlick and Buseck 1976; Phelps and Buseck 1978; Klusman and Landress 1979; Varekamp and Buseck 1983a; Van Kooten 1987). Elemental mercury (Hg<sup>o</sup>) anomalies have been reported in the surface deposits overlying a broad range of lava types from basalt (Crenshaw et al. 1982) through rhyolite (Varekamp and Buseck 1983a). Alone, or complemented by surface radon geochemistry, Hg<sup>o</sup> surveys have also been used to delineate structures (faults/fractures, dikes) associated with geothermal sites and volcanic centers (Klusman and Landress 1979; Crenshaw et al. 1982) and to postulate renewed magmatic activity beneath volcanic centers (Cox 1983; Varekamp and Buseck 1984; Williams 1985).

The purpose of this study† is to use surface mercury geochemistry to model vent structure of the 1912 eruption at Novarupta in Katmai National Park, Alaska (Figure 16). This was the most voluminous volcanic eruption, to date, of the twentieth century and the largest eruption of rhyolitic composition in 1800 years (Hildreth 1983, 1987). Large volumes of fall-back tephra mask the nature of the eruptive vent and intravent structures (Hildreth 1983). Due to its unique eruptive history and enigmatic nature, this area was chosen for the application of reconnaissance Hg<sup>o</sup> surveys. The primary objectives of this study

---

† Portions of this chapter comprise a manuscript authored by Lawrence G. Kodosky published in the *Journal of Volcanology and Geothermal Research* (1989) 38:227-242.

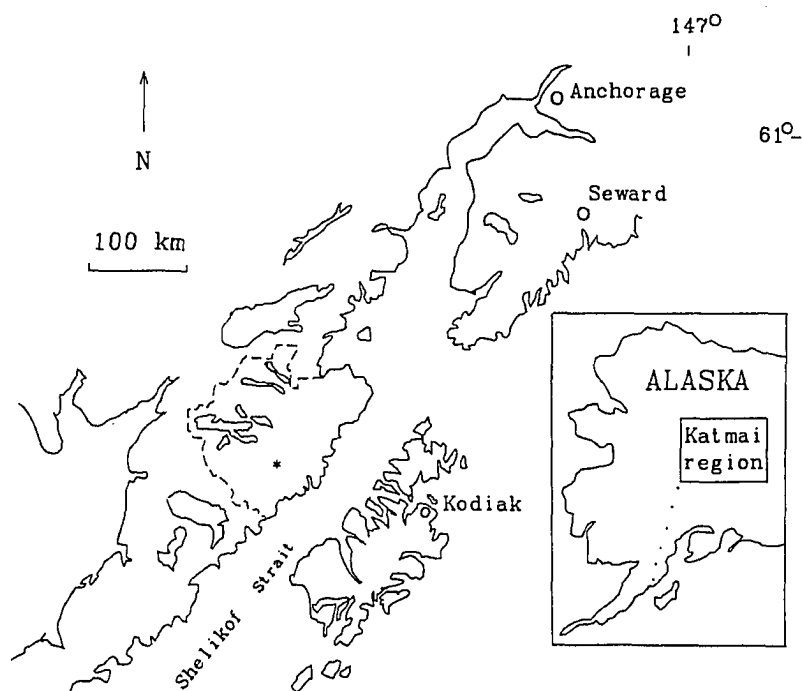


Fig. 16 Location map for the upper Alaska Peninsula. Dashed line is the boundary of Katmai National Park and Preserve. Asterisk denotes the 1912 vent at Novarupta.

were to 1) test the viability of the  $Hg^0$  technique in further constraining the nature of the 1912 eruptive center (size, shape) and in defining intravent structures (e.g., faults/fractures, presence/absence of feeder dikes or intrusions), and 2) locate zones of near-surface high heat flow which may be related to the establishment of hydrothermal circulation in response to magmatic intrusion beneath the 1912 eruptive site.

Both of the goals of this study are primary goals of the previously mentioned Continental Scientific Drilling Program (CSDP) activity planned for the VTTS. Samples for elemental mercury surveys require little preparation prior to analysis, and the typical method of Hg<sup>o</sup> analysis (gold-film detectors) is quick, simple, and of low unit cost for large (hundreds) sample sets. The reconnaissance Hg<sup>o</sup> survey was also undertaken to test whether volatile element surveys would be a useful, cost-effective tool in areas of recent volcanism that currently exhibit little or no surface manifestations of geothermal or magmatic activity. It was hoped that the Hg<sup>o</sup> survey would produce interpretable data which could be compared to models of the Novarupta vent region generated from planned CSDP-sponsored gravity, magnetic, and heat flow studies.

### **The 1912 Katmai Eruption**

Over a 60 hour period commencing on June 6, 1912, a series of Plinian eruptions generated approximately 20 km<sup>3</sup> of air-fall tephra and 11-15 km<sup>3</sup> of ash-flow tuff from 12-15 km<sup>3</sup> of magma (dense rock equivalent) (Hildreth, 1983, 1987). Among historic eruptions, Katmai is unique in the large volume of pumiceous pyroclastic flows that came to rest on land and the associated widespread and intense fumarolic activity that accompanied degassing of the ash-flow sheet. The ash-flow sheet extends more than 20 km from the eruptive source, covers an area of nearly 120 km<sup>2</sup> filling a pre-existing glacial valley in some places to estimated depths of 200 m (Curtis 1968; Hildreth 1983). The intense fumarolic activity (e.g., measured temperatures up to 645°C, plume heights to 300 m) in the ash-flow prompted Griggs (1922) to name the area encompassed by the ash-flow sheet the "Valley of Ten Thousand Smokes" (VTTS) (Figure 17).

Early workers in the VTTS (Shipley 1920; Fenner 1920, 1923; Griggs 1922) recognized that the source of the ash-flow was somewhere in the VTTS other than at Mt. Katmai.

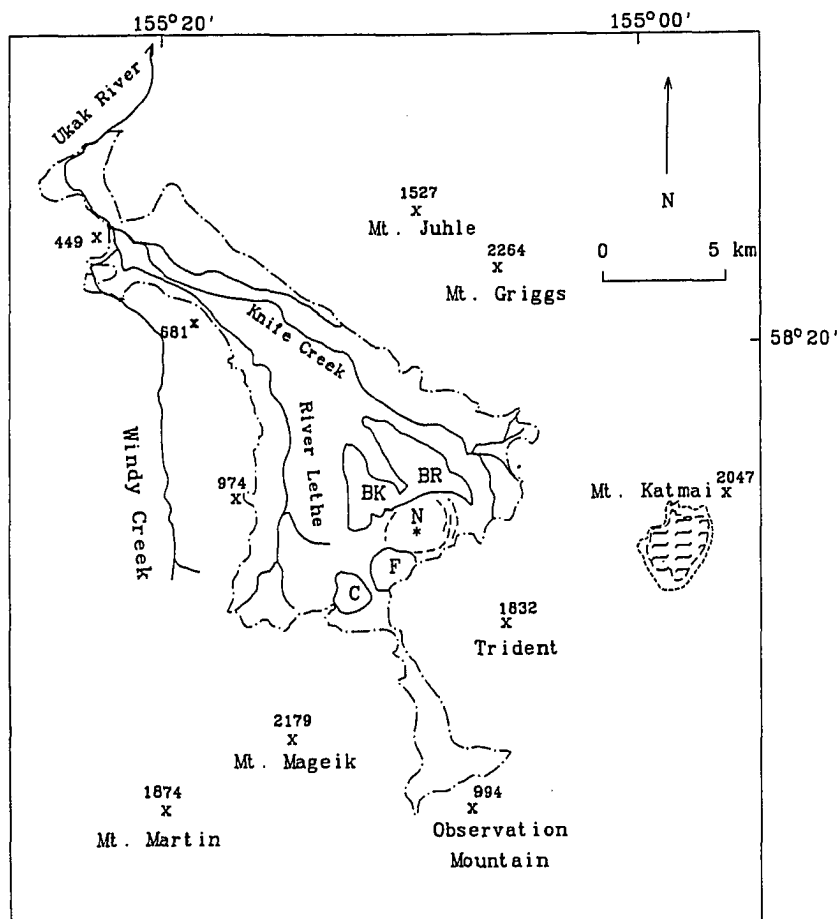


Fig. 17 Location map for the Valley of Ten Thousand Smokes. The dash-dot line shows the approximate  $120 \text{ km}^2$  extent of the 1912 ash-flow sheet. Mts. Martin, Mageik, Trident, Katmai, and Griggs are Holocene andesite-dacite stratovolcanoes. Mt. Cerberus (C) and Falling Mtn. (F) are Holocene dacite domes. Dashed fracture pattern circumscribes Novarupta Basin (N). The asterisk locates Novarupta's extrusive dome. Baked Mtn. (BK) and Broken Mtn. (BR) consist of Jurassic sedimentary rocks of the Naknek Formation. X with corresponding numbers indicates approximate summit elevations in meters. The dashes enclosing the bent-line pattern locate Katmai caldera and its associated lake (revised from Hildreth 1983).

In addition, these investigators observed Katmai Caldera ( $\approx 6.5 \text{ km}^2$ , 600 m deep) and suggested that a large fraction of the tephra falls vented there and at Novarupta. However,

Curtis (1968) convincingly showed that most, if not all, of the 1912 ejecta vented within the 2-km-wide subsidence structure encircling the Novarupta dome. Novarupta dome, a 65-m-high, 380-m-diameter exposure of rhyolitic composition, and its surrounding ejecta ring were emplaced near the center of this subsidence structure (Hildreth 1983) sometime after the June 6th eruption (Figure 18). Further studies suggest that compensatory caldera collapse occurred at Mount Katmai ( $\approx 10$  km east of Novarupta dome) as a result of hydraulic transfer of magma from beneath nearby stratovolcanoes (Curtis 1968; Hildreth 1983, 1987).

Abundant, colorful encrustations were deposited around a large number of the VTTS fumaroles (Shiple 1920; Griggs 1922; Keith 1984). Crude chemical studies of the metallic element-rich encrustations (Shiple 1920; Allen and Zies 1923; Zies 1924, 1929) led Zies (1929) to propose hydrothermal fluids as a metal transport mechanism. The ash-flow fumaroles died out by the 1930s, and current evidence confirms that they were nearly all rootless in nature. Several areas of warm ( $50^{\circ}$ - $90^{\circ}$ C), wispy fumaroles presently exist along the west side of Baked Mountain and within Novarupta Basin.

### Nature of the 1912 Vent

The mechanics of the 1912 eruption, while allowing preservation of the vent structure, have obscured its size and morphology as a result of the large volumes of air-fall tephra which filled the caldera (Hildreth 1983). Arcuate and radial fissures outline a 2-km-wide, 6 km<sup>2</sup> depression known as Novarupta Basin (Hildreth 1983), which is bordered by the truncated faces of Falling Mountain and Baked Mountain (Figure 18).

Two simplified end-member models have been proposed for the 1912 vent. Hildreth (1983, 1987) suggested that the vent is a flared, funnel-like structure (Figure 19a) produced by explosive ejection of country rock coupled with inward slumping of the vent walls and continuous reaming of the orifice during eruption. Abundant inclusions of the Mesozoic



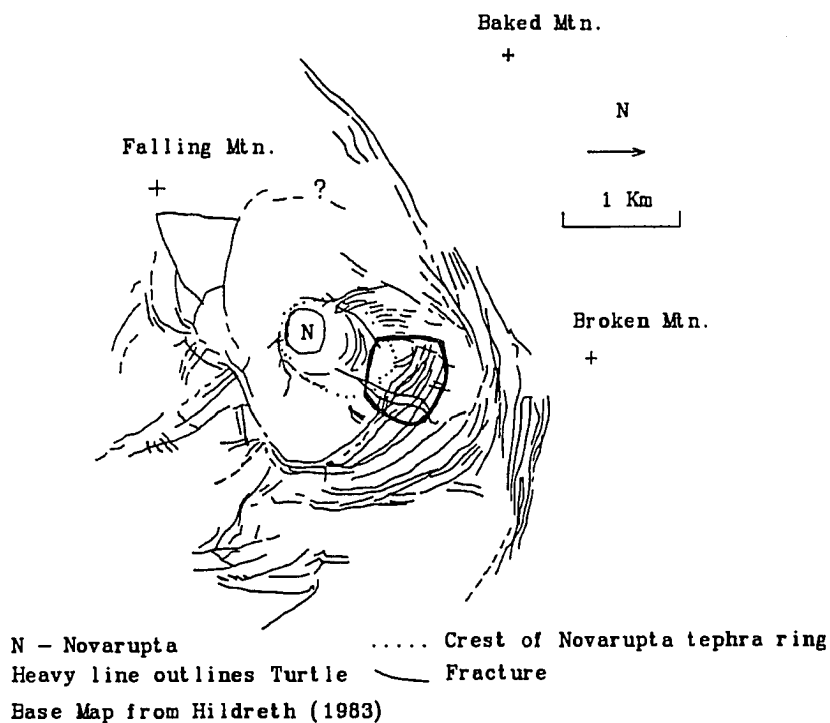


Fig. 18 Map showing the concentric and radial fractures which outline the 1912 vent in the area around Novarupta dome (N).

sandstones and shales in the ash-flow deposits confirm that country rock was involved in the eruption. According to Hildreth (1983, 1987) this sequence of processes generated a vent with a funnel base at  $< 1.5$  km depth which flares shallowly to a surface diameter of 2 km. In this model the concentric fractures around Novarupta Basin are ascribed to compaction of the fall-back tephra. Geothermal drilling and geophysical studies at some Quaternary Japanese calderas (e.g., Nigorikawa) have defined funnel-like vents (Donhan Geothermal Energy Company 1984; Walker 1984). However, Hildreth (1987) reports that

a lithic budget (calculated from available surface data) falls markedly short of what would be necessary to account for explosive excavation of a funnel-shaped vent filled with 1912 fall-back tephra and ash-flow deposits.

A cylindrical morphology (Figure 19b) is the other end-member model proposed for the 1912 vent (Eichelberger and Hildreth 1986; Hildreth 1987). In this model, the concentric fractures surrounding Novarupta Basin correspond to a bounding ring fault/fracture system; the process of vent formation is one of piston-like collapse along the ring fractures. Although the Novarupta Basin resembles a resurgent caldera complete with a ring fault system and central uplift, no calderas this small ( $\approx 2$  km in diameter) formed by piston-like collapse have been recognized in the geologic record (Walker 1984; Eichelberger and Hildreth 1986). In addition, Walker (1984) notes that most known ring dikes occur in Precambrian crust and theorizes that the subsiding piston mechanism operates most efficiently where the crust is rigid and strong, with other mechanisms of caldera growth predominating in younger, weaker crust such as that found at Katmai.

Hildreth (1987) notes that the adjacent stratovolcanoes, Martin, Mageik, Trident, and Katmai, exhibit at least twelve vents which align along a linear volcanic front striking N65°E. He observed linear fractures lying just outside of the 1912 vent which trend nearly perpendicular to the volcanic front. In the opinion of Hildreth (1987), these linear fractures might indicate dike transport of magma previously stored beneath Trident; hydraulic transfer of Katmai magma toward Novarupta by way of reservoir components under Trident may have precipitated Katmai's caldera collapse. Hildreth (1987) reports that the fracture trend from Novarupta to Trident corresponds with that predicted for dike azimuths by Nakamura (1977) for this portion of the Alaska Peninsula. A survey of 160 Quaternary calderas by Walker (1984) showed that the most common caldera type is one where a vent or line of vents extends outside the caldera to intersect with a linear zone of precaldera vents. In contrast, Hildreth (1987) also reports that the Mt. Cerberus - Falling Mtn. - Novarupta

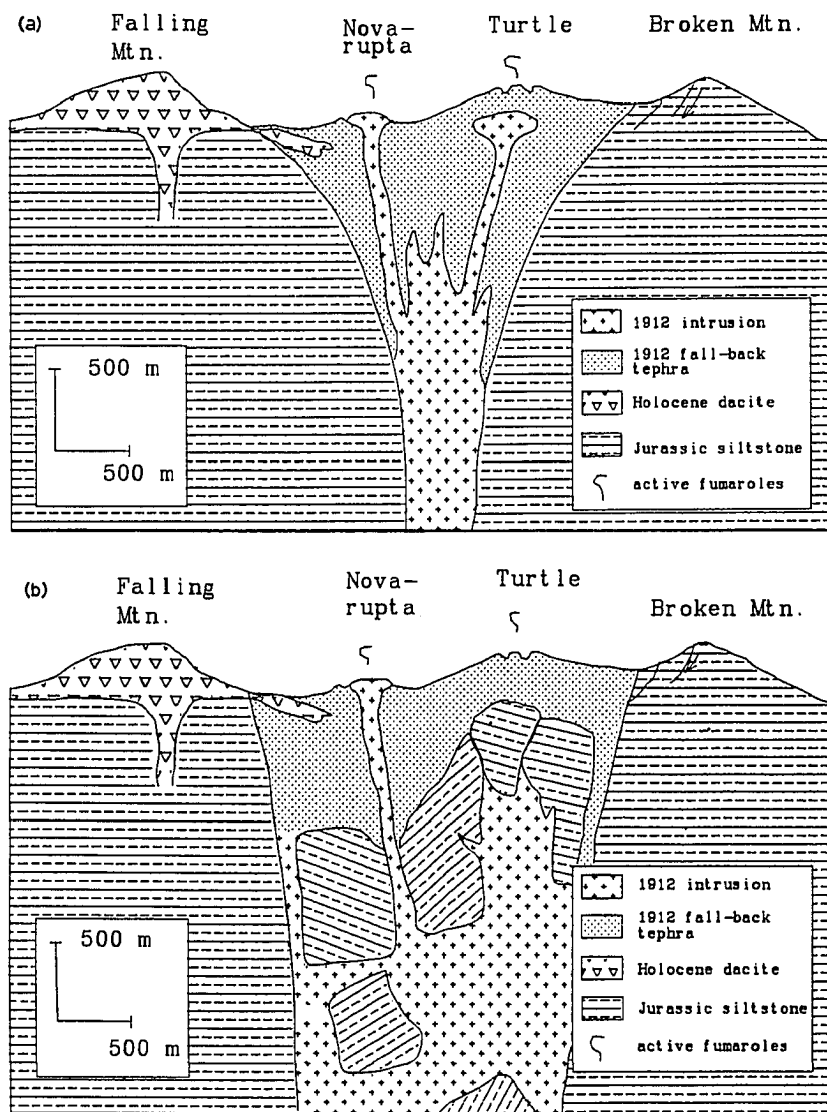


Fig. 19a-b Proposed models for the 1912 Novarupta vent. a) Preferred model of Hildreth (1983, 1987) for the 1912 vent assuming a funnel-like morphology (modified slightly from Eichelberger and Hildreth 1986). b) Alternative configuration proposed for the 1912 vent. The morphology is cylindrical and is generated by piston-like collapse along a ring fault/fracture system (modified slightly from Eichelberger written commun. 1986).

alignment is approximately 4 km behind and roughly parallel to the volcanic front and may reflect local behind-the-front extension and/or extension above an upper-VTTS silicic magma chamber.

Novarupta Basin also contains the Turtle, a 225-m-high, 1-km-long ejecta-covered, dome-like feature which lies approximately 1 km northeast of the Novarupta extrusive dome (Figure 18). The summit of the Turtle is cut by nearly perpendicular sets of grabens and other related faults and fractures. Weak fumarolic activity (temperatures as high as 90°C, Keith 1991) exists on the Turtle summit, mostly located along the fault/fracture systems.

The Turtle's fault system was totally developed when visited in 1917 by members of the National Geographic Society expedition to Katmai (Griggs 1922). This surface deformation may be the result of extensional faulting accompanying shallow emplacement of a cryptodome. Based on the small fault displacements ( $< 1$  to  $\approx 8$  m) on the Turtle's summit, topographic and stratigraphic continuity with Novarupta's ejecta ring, and the minor fumarolic activity found at this site by early (1917-1922) expeditions to Katmai, Hildreth (1987) contends that an intrusion is not present. Hildreth (1987) considers the Turtle an asymmetrical accumulation of near-vent fall-back tephra. The Turtle's fault pattern would then be the result of compaction and welding of the fall-back tephra.

Hildreth (1987) states that, " a low-level positive aeromagnetic anomaly coinciding in part with the Turtle " was observed by Anna (1971). Although he recognizes that this anomaly may indicate a concealed intrusion, Hildreth (1987) feels the anomaly is more likely to be related to " 1) the much higher proportion on the Turtle of andesitic ejecta (vis-a-vis the silicic, relatively Fe-poor ejecta dominant elsewhere), 2) the thicker accumulation of welded fall-back material there, and 3) intravent concentration of fumarolic magnetite."

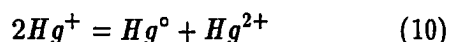
The magnetic data permit no unique solution. Therefore, though it is a possibility that the aeromagnetic anomaly over the Turtle may be the result of a thick accumulation of

relatively Fe-rich andesitic ejecta, it is as equally likely to be the result of a shallow intrusion (D.Stone pers. commun. 1988). Inspection of Anma's (1971) M.S. thesis reveals two separate positive aeromagnetic anomalies of similar magnitude at three different flight levels (915, 975 and 1065 m above sea level). Profiles of these aeromagnetic anomalies take the form of a broad peak coinciding with the Novarupta dome and a narrower peak overlying part of the Turtle. The Turtle was a site of only minor post-eruption fumarolic discharge (Hildreth, 1987). Zies (1929) found that the fumarolic magnetite deposited in the VTTS was essentially associated with intense, high temperature ( $\approx 250^{\circ}$ - $500^{\circ}$ C) fumarolic activity. It seems unlikely that a sufficient intravent concentration of fumarolic magnetite could have been built up to make a significant contribution to the Turtle's observed aeromagnetic anomaly. The 1912 eruption extruded through relatively flat-lying, low magnetic susceptibility sediments (Tribble 1972) of the Upper Jurassic Naknek Formation. An uplifted block of Naknek basement overlain by fall-back tephra is also not a likely candidate for producing the Turtle's aeromagnetic signature.

Regional gravity (Berg et al. 1967), local gravity (Kienle 1969), and local seismicity patterns (e.g., S-wave attenuation patterns associated with microearthquakes; Matumoto 1971) support the presence of magma at shallow (< 10 km) depths under a number of the volcanic centers in the VTTS region. The active fumaroles in Novarupta Basin are located along subsidence fractures suggesting they are maintained by residual heat (i.e., rooted) from an underlying magma reservoir (Keith 1984). Based on the temperatures (up to  $90^{\circ}$ C) of the active fumaroles and the distribution of warm ground within Novarupta Basin, Keith (1991) suggested that meteoric water is heated to boiling beneath the surface and subsequently condenses in the near-surface vent region. Therefore, sufficient cooling is likely to have occurred to have allowed the initiation of a hydrothermal convection system within 1-2 km of the surface in the vent region.

## Mercury Geochemistry

Elemental mercury ( $\text{Hg}^{\circ}$ ) is strongly partitioned into the vapor phase during vapor exsolution from subsurface geothermal/hydrothermal systems (Varekamp and Buseck 1983b). Anomalous concentrations of  $\text{Hg}^{\circ}$  observed in the sediments surrounding actively outgassing volcanoes (Cox 1983; Varekamp and Buseck 1984) support a magmatic source for the  $\text{Hg}^{\circ}$ . Jonasson and Boyle (1972) contend that  $\text{Hg}^{\circ}$  may also be produced during the hydrothermal alteration of rocks or sediments, in particular of those materials containing sulfides. According to these workers, during hydrothermal alteration of sediments mercury is released as  $\text{Hg}^{2+}$  and can be subsequently reduced by  $\text{Fe}^{2+}$  or organic matter to  $\text{Hg}^{+}$  and/or  $\text{Hg}^{\circ}$ . Any  $\text{Hg}^{+}$  may further undergo a disproportionation reaction of the form:



which results in a net production of  $\text{Hg}^{\circ}$  that diffuses upward through the weathered regolith. It should be noted, however, that an anonymous reviewer of the manuscript published from this chapter stated that the Jonasson and Boyle (1972) model for  $\text{Hg}^{\circ}$  generation was too simplistic and that the systematics (mass balance, mass action) of the disproportionation reaction were incorrect.

Regardless of its source (degassed magma or hydrothermally altered sediments),  $\text{Hg}^{\circ}$  is concentrated in the low temperature (< 45°C) environment of the soil/regolith overlying geothermal/hydrothermal sites, primarily by adsorption onto organic matter, clay minerals, and clay-size particles (McNeal and Rose 1974; Fang 1978; Landa 1978). Klusman and Landress (1978, 1979) showed that even though variations within soil/regolith properties (e.g., pH, clay content, organic content) influence  $\text{Hg}^{\circ}$  concentrations in surface deposits,

geothermal/hydrothermal activity at depth supplies sufficient  $\text{Hg}^0$  to overwhelm local background variations in the overlying soil/regolith. Anomalous concentrations of  $\text{Hg}^0$  in surface deposits are therefore indicative of zones of active/fossil vertical convective heat flow.

The magnitude and areal distribution of the surface  $\text{Hg}^0$  anomalies reflect both the characteristics (e.g., size, depth) of the underlying geothermal/hydrothermal system and the migration pathways (Van Kooten 1987). Processes (e.g., silicification) resulting in sealed or relatively impermeable structures eliminate or greatly reduce the transfer of  $\text{Hg}^0$  to the surface (Crenshaw et al. 1982; Cox 1983). Positive correlation has been shown between the magnitude of  $\text{Hg}^0$  surface anomalies and measured geothermal gradients (Matlick and Shiraki 1981).

The formation of mercury soil/regolith anomalies is a dynamic process. After an initial period of non-equilibrium, a steady-state system is set up (Varekamp and Buseck 1983a). The period of non-equilibrium may be very short. Varekamp and Buseck (1984) noted that when ash from the 1980 eruption of Mt. St. Helens fell on a 'concealed' mercury deposit, the mercury anomaly superimposed itself on the ash within a few days.

The conditions of weathering and the chemical state of the mercury present dictate its rate of removal from surface deposits. Revolatilization, biogenic uptake, and simple dissolution processes continuously remove mercury from the soil/regolith (Kama and Siegel 1980). Bowen (1979) estimated the residence time of mercury in soils to be between 500 and 1,000 years. However, from observations on the duration of hydrothermal activity at Lassen Peak, California, Varekamp and Buseck (1983a) suggested that adsorbed ( $\text{Hg}^0$ ) or organically bound mercury will be released to the atmosphere perhaps within a few decades after termination of hydrothermal activity. Christensen et al. (1983) reported that remobilization of adsorbed mercury is initiated by any moderate temperature increase, with complete removal of  $\text{Hg}^0$  by  $300^\circ\text{C}$ . If the mercury is fixed in the surface deposits as cinnabar or as a trace element in other sulfides (i.e., mercury is in the  $\text{Hg}^{2+}$  state), normal

weathering processes and atmospheric volatilization will not dramatically decrease mercury contents (Varekamp and Buseck 1983a).

### **Sampling and Analytical Procedures**

One-hundred twelve samples were collected from relatively unaltered air-fall ejecta along two Novarupta Basin traverse lines (Figure 20a). Presently the 1912 intravent region and ash-flow sheet remain almost exclusively free of any deep-rooted vegetation. Although lichen development is extensive throughout the vent region, the resulting organic mat was never observed to extend more than 1.5 cm beneath the surface. Therefore, the term 'regolith' is most appropriate for the material sampled in the upper reaches of the VTTS and ash-flow. Samples were collected from both 5 and 15 cm depths within this regolith to see if a particular depth interval would optimize the survey results. A typical sample spacing along the traverses was 100 m; areas of special interest were sampled at 50 m spacings. Thick snow accumulations prevented sampling in certain parts of Novarupta Basin.

One hundred eighty-two samples were taken from active/fossil fumaroles in Novarupta Basin (24 sites, Figure 20b), fossil fumaroles (41 sites) and air-fall tephra (2 sites) within and immediately adjacent to the remainder of the VTTS (Figure 21). These samples enabled  $Hg^0$  background levels in the VTTS to be determined. The differently colored alteration zones surrounding the VTTS fumaroles consist mainly of insoluble, secondary minerals (e.g., various iron oxides/hydroxides and clays) formed by low temperature alteration and surficial weathering of primary fumarolic encrustations (Keith 1984). At the fumarole sites, samples were collected from each of the differently colored alteration zones. This was done in order to constrain the range of  $Hg^0$  values resulting from the different mineralogies, clast



types and degrees of alteration present within each zone. Up to four samples were taken at a fumarole site; most sites are represented by two samples.

In total, 294 samples were collected from 127 sites and stored in sealed plastic bags. Mercury analyses were performed on air-dried (< 80 mesh fraction) samples using the Jerome Instrument Corporation 301 Au-film Hg<sup>0</sup> detector. The analytical procedures for this device are detailed by McNerney et al. (1972) and Matlick and Buseck (1976). During routine analysis the lower limit of detection is 10 ppb.

### Data Analysis

Measured Hg<sup>0</sup> concentrations ranged from 12 - 6913 ppb. Forty replicate analyses, performed to monitor both the variance within and between analytical sessions, yielded an average relative precision of  $\pm 11.8\%$ . The manufacturer claims a reproducibility limit of  $\pm 10\%$  for homogeneous samples using the Au-film Hg<sup>0</sup> detector. Based on the replicate analyses the data of this study were therefore assumed to be homogeneous. A complete listing of the sample Hg<sup>0</sup> values and replicate analyses are given in Appendix 3.

Raw data were analyzed by a four step procedure. In the first step Hg<sup>0</sup> values of the fumarolic deposits and relatively unaltered regolith were statistically evaluated (by means of an F test) to reveal whether they should be treated as two distinct sample populations. Because of the large number of randomly collected samples, it is reasonable to assume (Central Limits Theorem, see Davis 1986) that parametric statistical tests can be applied to both sets of data. However, since this assumption may be compromised by samples whose values lie well outside the sample population mean, both sets of data were also log transformed. Table 11 provides a summary of the F test statistics for both the raw data and log-transformed data. From these tests it was concluded that the fumarolic deposits and relatively unaltered regolith represent two distinct sample populations.

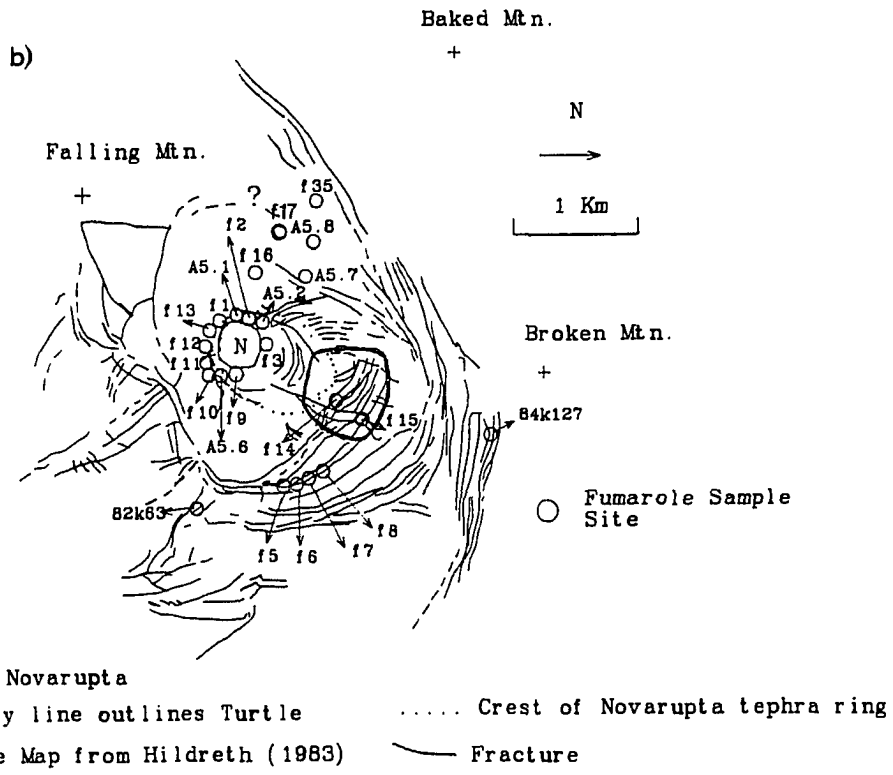
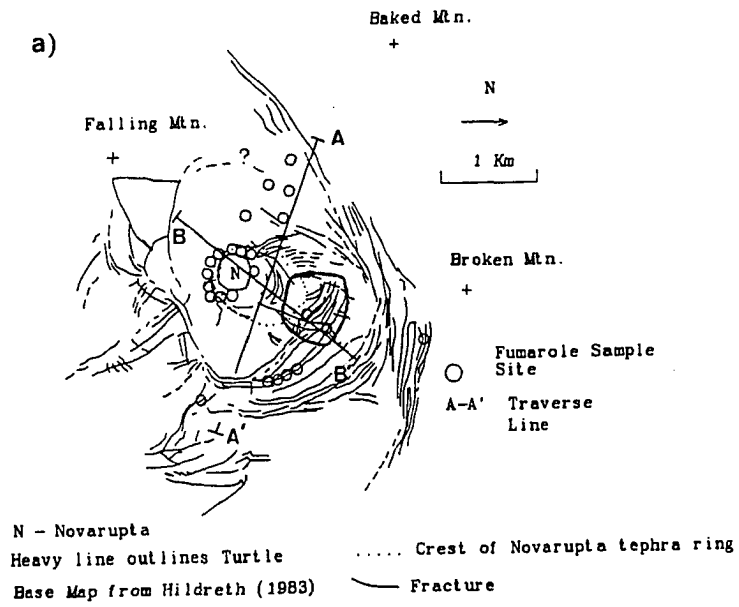


Fig. 20a-b Novarupta Basin sample traverse lines and fumarole sample sites.  
a) Sample traverse lines. b) Fumarole sample site designations.

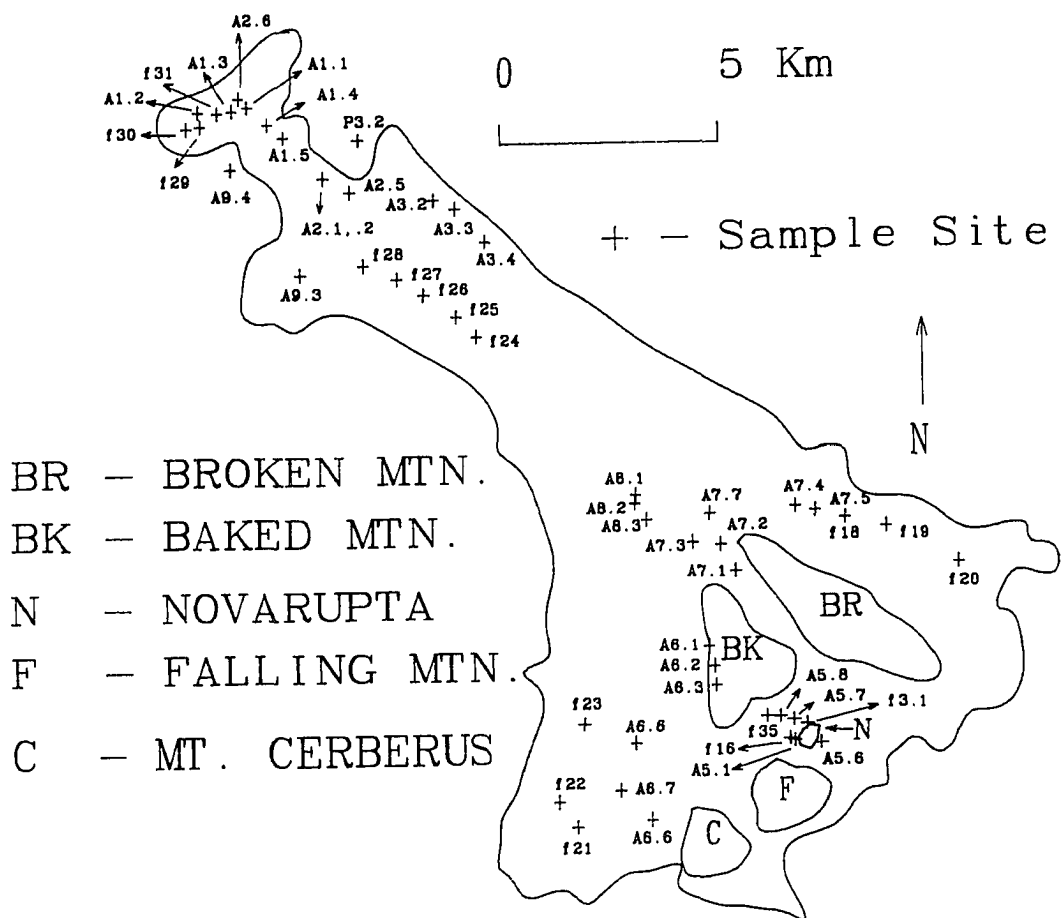


Fig. 21 Fumarole sample sites in the VTTS. For clarity, only 7 of 24 sample sites within Novarupta Basin are shown. A complete view of Novarupta Basin is given in Figure 20a-b. Two air-fall tephra sample sites lie adjacent to the VTTS near its northwestern terminus.

In the next step threshold  $Hg^0$  concentration values were determined for each of the sample populations. The threshold is defined as the concentration above which all samples are considered anomalous (i.e., the upper limit of background). Thresholds were derived by visual assessment of lognormal probability plots after the methods of Sinclair (1974) and by

**Table 11 Summary of F test statistics for Hg<sup>o</sup> data set.**

	Fumarolic deposits (F)	Relatively unaltered regolith (U)
<b>Raw Data</b>		
Number of samples	182	112
Degrees of freedom	181	111
Mean Hg <sup>o</sup> content (ppb)	432	130
Hg <sup>o</sup> range (ppb)	12-6913	14-3313
Standard deviation	1171.1	383.4
Variance ( $\sigma^2$ )	1373818	146996
<b>Lognormal Data</b>		
Mean Hg <sup>o</sup> content	1.927	1.672
Hg <sup>o</sup> range	1.079-3.840	1.146-3.520
Standard deviation	0.661	0.460
Variance ( $\sigma^2$ )	0.437	0.212
F test:		
Null hypothesis: $\sigma^2$ (F) = $\sigma^2$ (U)		
F test = variance (F) / variance (U)		
F statistic $\approx$ 1.71 at $\alpha = 0.025$ (level of significance)		
Raw data: F test = 9.34		
Lognormal Data: F test = 2.06		

F test in both cases > F statistic therefore reject null hypothesis and assume that fumarolic deposits and unaltered regolith represent two different sample populations.

visual inspection of log-transformed data histograms. An average threshold was calculated from the two techniques (Table 12).

The process of continuous Hg<sup>o</sup> depletion from the soil/regolith allows differentiation between actively accumulating Hg<sup>o</sup> and Hg<sup>o</sup> deposited from fossil fumarole or fossil hydrothermal/geothermal activity (Varekamp and Buseck 1983a). To facilitate this discrimination, contrast values (sample value/threshold) were calculated for the two sample populations using the average thresholds of Table 12. A contrast of one represents the upper limit of Hg<sup>o</sup> background. The higher the contrast above one the greater the probability that the Hg<sup>o</sup> from a particular site is related to present-day vertical convective heat flow.

The final step of data analysis included the construction of contrast range maps and contrast geochemical profiles. To simplify comparison between sites on the contrast range maps, the maximum contrast values at each sample site were used in the constructions.

**Table 12** Calculated Hg<sup>0</sup> threshold values for the VTTS samples.

Method	Threshold (ppb)	
	Fumarolic deposits (N=182)	Relatively unaltered regolith (N=112)
Lognormal probability plots	339	120
Histogram	363	100
	Ave.(ppb)=351	Ave.(ppb)=110

Three sample sites along traverse line A-A' fell on fumarolically altered regolith which exhibited no indication of current surface fumarolic activity. In these instances the contrast was calculated using the threshold of the fumarolic deposits.

## Results

Early chemical studies (Shipley 1920; Allen and Zies 1923; Zies 1924, 1929) of the VTTS eruptive deposits detected neither cinnabar nor trace levels of mercury. However, these investigators were limited by rather crude analytical techniques. Subsequent studies (Keith 1984; Kodosky and Keskinen 1987) verified the presence of mercury in the VTTS regolith. Neither of these later works identified the presence of cinnabar or mercury-bearing sulfides. The nature of the mercury depositional process (concentration from a vapor phase), the probable lack of any mercury-bearing sulfides, and the absence of any deep-rooted vegetation in the VTTS regolith supports mercury being dominantly present as Hg<sup>0</sup> adsorbed to clays and clay-size particles.

Figure 22 shows Hg<sup>0</sup> contrast ratios for fumarole sites within the VTTS and two adjacent air-fall sites. For clarity of presentation only seven of the twenty-four fumarole sites of Novarupta Basin are included. Those listed exhibit the range of contrast values present. Only two fumarole sites outside of Novarupta Basin (near Broken Mtn.) possess contrast

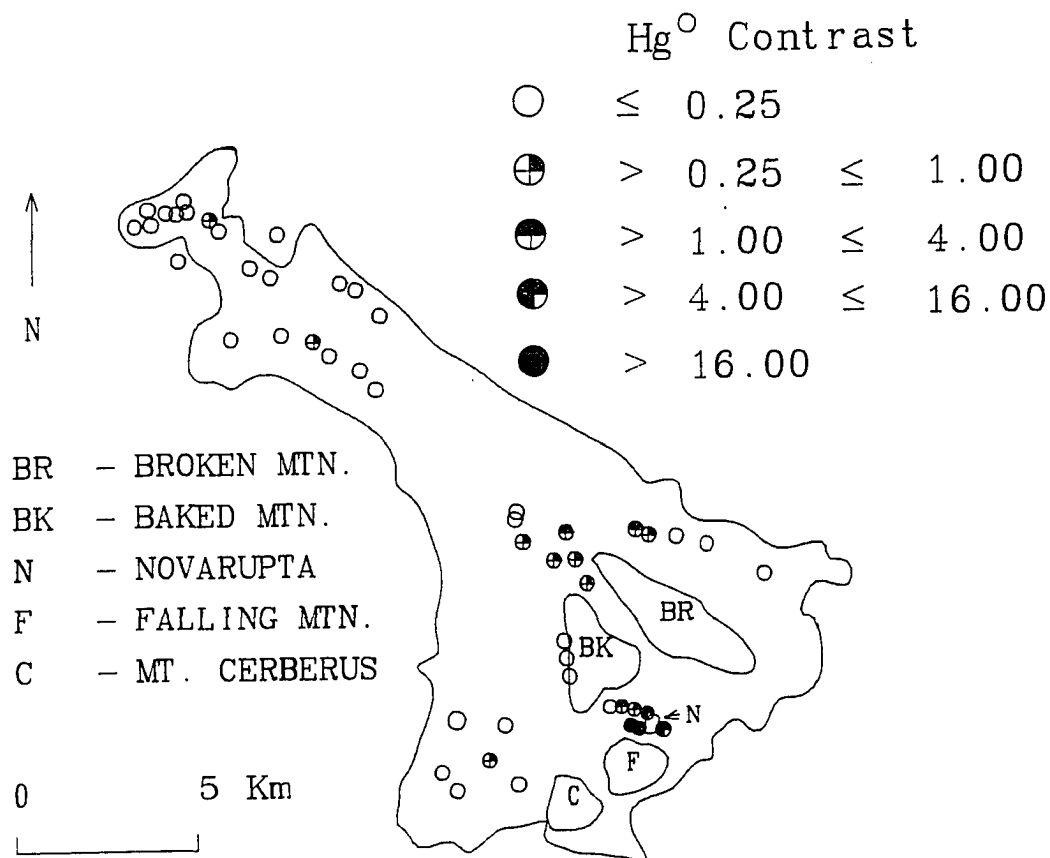


Fig. 22  $\text{Hg}^{\circ}$  contrast values for fumarole sample sites within the VTTs. Contrast codes correspond to the maximum value calculated for a given site. The seven fumarole sample sites shown for Novarupta Basin exhibit the range of contrast values present in this area.

values greater than one (1.07 and 1.09). Because of their low contrast values, the  $\text{Hg}^{\circ}$  concentrations of these fumaroles are still considered to be near the upper background limit and not to be indicative of actively accumulating  $\text{Hg}^{\circ}$ .

All significant  $\text{Hg}^{\circ}$  anomalies (contrast values  $> 1.5$ ) occur within Novarupta Basin (Figure 23). Contrast values for fumaroles within Novarupta Basin range from 0.09 to 19.7.

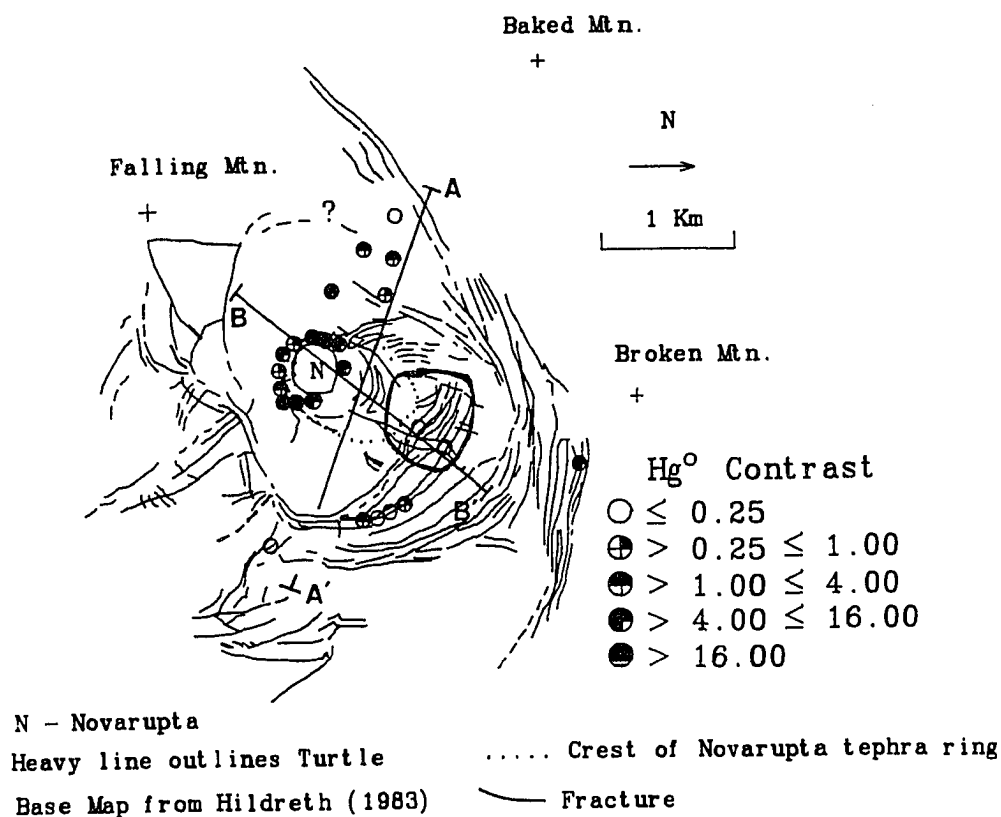


Fig. 23 Hg<sup>0</sup> contrast values for fumarole sample sites within Novarupta Basin. Contrast codes correspond to the maximum value calculated for a given site.

The second highest Hg<sup>0</sup> contrast (17.5) at a fumarole site was measured from a location west of and well outside of Novarupta's tephra ring but within the vent region. This area gave no indication of current surface fumarolic activity or high heat flow and may be fracture-related. A high Hg<sup>0</sup> contrast at a Broken Mtn. fumarole site situated along the concentric fracture system may also represent a deep-extending fracture/fault. The wide variability in sample contrast within Novarupta Basin, particularly inside Novarupta's tephra ring, confirms the Hg<sup>0</sup> technique as an aid for locating zones of near-surface high heat flow.

Understanding the nature of the concentric fractures outlining Novarupta Basin is critical for delineating the 1912 vent morphology. Compaction fractures ( flared funnel model) should exhibit lower magnitude, less continuous  $Hg^0$  anomalies than a set of deeper-extending ring faults (cylindrical vent model) which had provided or are providing permeable pathways to a crystallizing magma. Comparison of the Novarupta and Turtle surficial  $Hg^0$  patterns was also considered a possible means of discerning whether the Turtle is supported by a cryptodome or not.

Contrast profiles of  $Hg^0$  across the two Novarupta Basin traverse lines are shown on Figures 24 and 25. The 5- and 15-cm sample depth profiles show a strong positive correlation to each other on both sample traverse plots. This allows a higher degree of confidence to be placed on the traverse line data. The 15-cm sample depth should more closely mirror the true surface  $Hg^0$  contents as it will be less affected by wind erosion and mechanical creep than will the 5-cm samples.

No significant  $Hg^0$  enrichments are seen along traverse line A-A'(Figure 24). Two slight  $Hg^0$  spikes overlie the northwestern and southeastern intersections of the traverse with the tephra ring margin. The northwestern anomaly corresponds to a fossil, intensely altered fracture/fumarole system and is most likely reflecting relict  $Hg^0$  accumulations. Although the southeastern  $Hg^0$  anomaly is found within relatively unaltered regolith, its magnitude (maximum contrast of 1.34) is inconclusive for determining if it represents a location of active  $Hg^0$  deposition.

The western terminus of line A-A' crosses a portion of the concentric fracture system (see Figure 20a). Only normal background levels of  $Hg^0$  were observed in this zone. Shallow-depth compaction fractures or effectively sealed deeper-extending structures could both contribute to the observed  $Hg^0$  pattern. Sampling in the zone of concentric fractures from the eastern end of the traverse was prevented by thick snow accumulations.



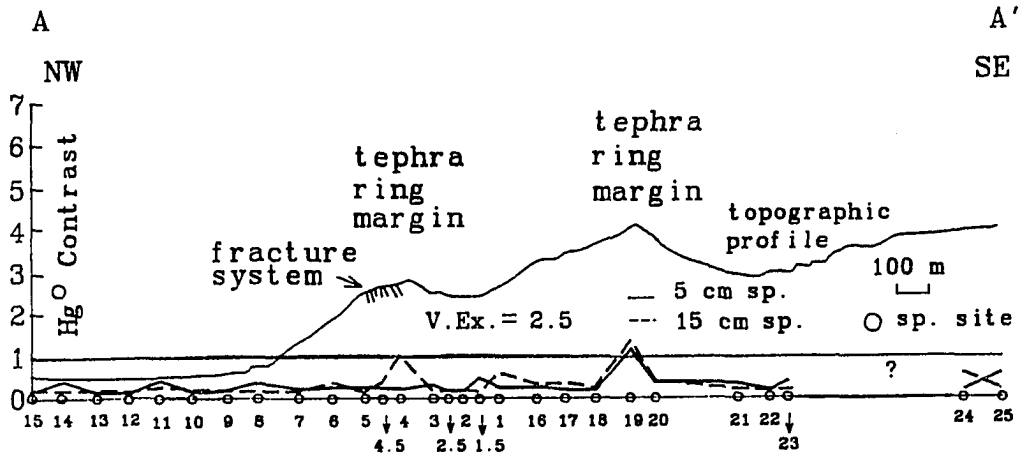


Fig. 24  $Hg^0$  contrast profiles across sample traverse line A-A'. A solid horizontal line has been drawn through a contrast value of 1.0. Contrast values above this are considered anomalous.

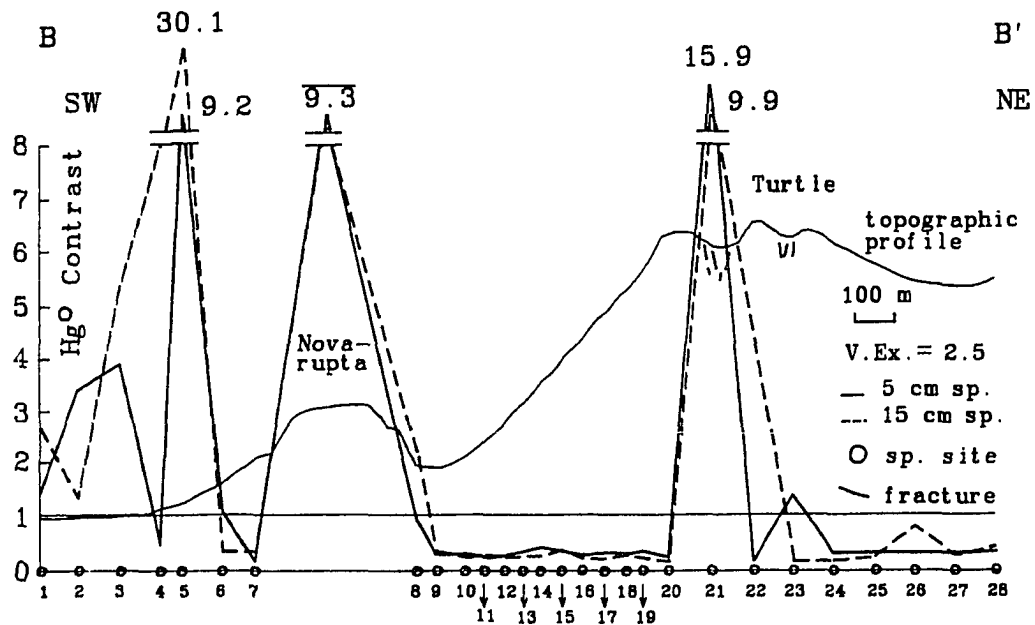


Fig. 25  $Hg^0$  contrast profile across sample traverse line B-B'. A solid horizontal line has been drawn through a contrast value of 1.0. Contrast values above this are considered anomalous. The  $Hg^0$  contrast value above Novarupta represents an average calculated from eleven fumarole sites located within Novarupta's tephra ring.

Traverse line A-A' was oriented under the assumption that a shallow intrusion underlies the Turtle. Line A-A' strikes essentially perpendicular to the direction a northeast-trending magma feeder dike connecting Novarupta and the Turtle would take. If the Turtle is supported by a cryptodome, the background levels of  $Hg^0$  found between Novarupta's tephra ring margins do not support the presence of a near-surface lateral feeder dike connecting Novarupta with this body (i.e., a feeder dike roughly parallel to the VTTS regional volcanic front and representing behind-the-front extension). Therefore, sub-vertical to vertical intrusion with separate apophyses under both the Turtle and Novarupta would be required.

Profile B-B' (Figure 25) shows two major zones of  $Hg^0$  enrichment. With the exception of one 5-cm sample, the portion of the traverse extending from the base of Falling Mountain northeast to midway up the slope of Novarupta's tephra ring is highly anomalous. This region contains the highest contrast (30.1) measured. The high contrast site may represent a caldera-bounding fault and is significant since no surface expressions of faults/fractures exist in this section of Novarupta Basin. An extremely high (15.9) and slightly high ( $\approx 1.5$ )  $Hg^0$  contrast coincide with fracture sets cutting the summit of the Turtle. The contrast of 15.9 is the second highest measured in the relatively unaltered regolith. For comparison, an average contrast of 9.3 was calculated from the fumarole contrasts (11 sites) within the Novarupta tephra ring.

## Discussion

The following lines of evidence together provide tentative support for the presence of a shallow intrusion beneath the Turtle: (1) the morphology and distensional faulting of the Turtle; (2) the aeromagnetic profiles of Anna (1971); (3) the widespread patches of minor fumarolic activity and warm ground present on the Turtle, and (4) the observed  $Hg^0$  enrichments on the Turtle's summit. Hildreth (1987) cites the antithetic displacement

sense of faults on the lower slopes of both the Turtle and Broken Mountain as evidence that the Turtle's fault pattern reflects compaction fractures of near-vent fallout. However, the high  $Hg^0$  contrast present on the Turtle's summit is definitely not consistent with a set of shallow-depth compaction fractures. Compaction fractures in the regolith undoubtedly exist; this study, however, suggests they are a secondary component superimposed on the original fault pattern formed by a shallow intrusion.

In defense of Hildreth's (1987) conclusion that an intrusion does not underlie the Turtle, two areas of warm ground sampled on the Turtle's summit show no  $Hg^0$  enrichment (see Figure 23). A similar situation was observed at four warm ground sites southeast of and off of the Turtle. No evidence exists that these areas had been recently hot enough to remobilize the major portion of earlier-accumulated  $Hg^0$ . Two of these sites were excavated, and amorphous silica (identified by energy dispersive X-ray analysis) was encountered. Effective sealing of once-permeable structures by silicification may be inhibiting the migration of  $Hg^0$  to the surface at these locations.

In contrast to the zone of  $Hg^0$  enrichment seen near the southwest boundary of Novarupta Basin, no  $Hg^0$  anomalies were found along traverse line B-B' near Novarupta Basin's northeast boundary. Three alternatives could be responsible for the lack of  $Hg^0$  enrichment: (1) traverse line B-B' did not extend far enough to the northeast to intersect a possible deep-extending, caldera-bounding fault; (2) the fractures crossed by the traverse northeast of the Turtle are shallow-depth compaction fractures; or (3) the fracture sets immediately northeast of the Turtle have been sealed to  $Hg^0$  leakage. The first alternative seems the most plausible, especially in light of the high  $Hg^0$  contrast present at a fumarole site along the portion of the concentric fracture system which cuts the lower slope of Broken Mountain. This  $Hg^0$  anomaly provides support for a deep-extending fracture and possible caldera-bounding fault in the immediate vicinity.

In terms of vent morphology, the  $Hg^{\circ}$  data are far from unequivocal. However, the pattern and magnitude of  $Hg^{\circ}$  anomalies seen between Falling Mountain and the Novarupta extrusive dome, and the  $Hg^{\circ}$  anomaly located on the southern slope of Broken Mtn., are not compatible with shallow-depth compaction fractures and a simple flared funnel vent model. Figures 26 and 27 illustrate two alternatives. The cylindrical vent model (Figure 26) differs from that of Figure 19b in possessing a shallow intrusion beneath the Turtle. Previously discussed evidence concerning the small size of the 1912 vent and accompanying mechanical problems for cylindrical collapse do not make this an attractive vent model.

The preferred vent model is shown in Figure 27. This vent type is generated through collapse of supporting walls into a cored-out explosive vent (Escher 1929). The resulting vent morphology is funnel-like with subsidence concentrated in the narrow funnel center. Deep-extending fracture sets provide multiple  $Hg^{\circ}$  migration pathways interconnected to a crystallizing magma body. This model is consistent with the funnel-shaped vents observed and predicted for many Quaternary Japanese calderas (Aramaki 1984; Walker 1984). It is also consistent with the morphology proposed for the 1912 vent by Hildreth (1983, 1987). The process of collapse into a cored-out vent, subsequent to the major pulses of the 1912 eruption, would generate a smaller amount of ejected lithics than Hildreth's (1987) mechanism of slumping coupled with continuous reaming of the 1912 eruption orifice. Therefore the cored-out vent model could also explain why the surface lithic budget of Hildreth (1987) falls well short of that required for a simple flared funnel vent type.

During the summer of 1989, as part of preliminary studies for the proposed Continental Scientific Drilling Program at Novarupta, detailed gravity and magnetic data were collected from a 150-point surveyed grid spanning the area outlined by the Novarupta Basin concentric fracture system (Eichelberger et al. 1990). An aeromagnetic survey of the vent area was also flown during this preliminary study. Analysis of these data led Goodliffe et al. (1991) to suggest that the Turtle is underlain by an andesitic intrusion with dimensions similar to

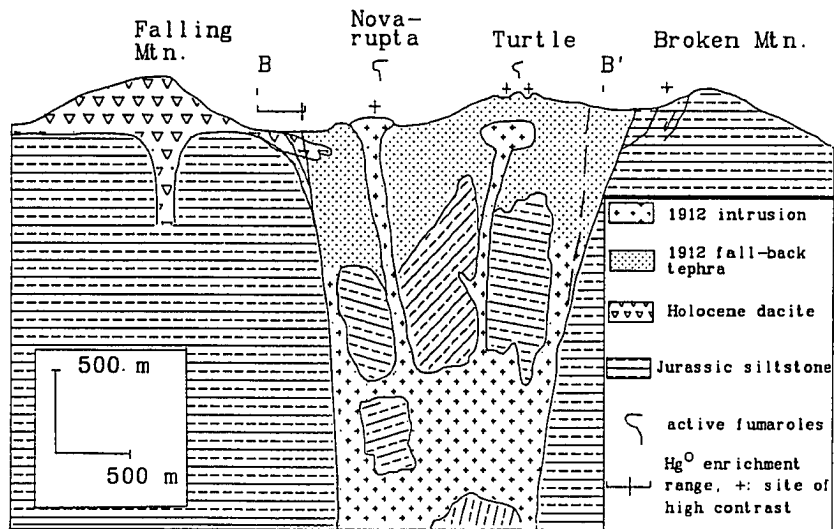


Fig. 26 Modified version of the cylindrical 1912 vent model of Figure 19b assuming a shallow intrusion beneath the Turtle. Cross-sectional view is projection essentially parallel to traverse line B-B'.

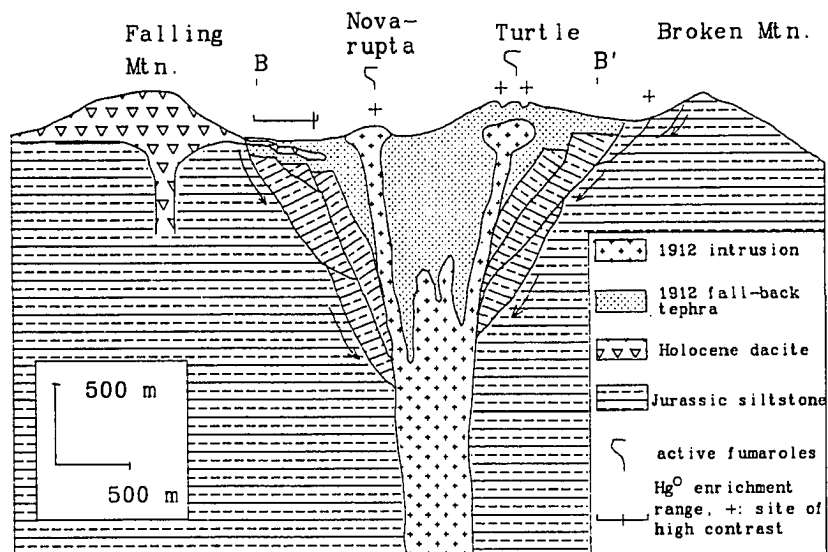


Fig. 27 Preferred 1912 vent model based on results of the  $Hg^{\circ}$  survey and available geological and geophysical data. Cross-sectional view is projection essentially parallel to traverse line B-B'.

or slightly larger than the Novarupta dome. Goodliffe et al. (1991) further suggested that the aeromagnetic data define an eruptive vent that flares from depth and has a structural boundary that lies inside of the concentric fracture system. The gravity and magnetic data thus support the preferred vent model (Figure 27) proposed by Kodosky (1989).

In addition to the recent gravity and magnetic surveys of the Novarupta vent region, Wallmann (1991) has completed detailed mapping and numerical analysis of the Turtle's structural features. According to Wallmann (1991), numerical modeling supports the theory that the Turtle's observed topography was generated through intrusion of an igneous body with similar dimensions to Novarupta dome. The work of Goodliffe et al. (1991) and Wallmann (1991) therefore provide independent evidence to support the preferred vent model derived from the Hg<sup>o</sup> survey data. This suggests that Hg<sup>o</sup> regolith surveys are a reliable, cost-effective tool for locating subsurface geological structures and zones of anomalously high near-surface heat flow in the VTTS.

## CHAPTER 5:

### EVALUATION OF THE VTTS ALTERATION SAMPLES

---

#### Introduction

Early workers in the VTTS (e.g., Shipley 1920; Griggs 1922; Allen and Zies 1923) were fascinated by the multi-colored encrustations surrounding the VTTS fumaroles. Studies of the VTTS encrustations and fumarolic gases (Shipley 1920; Allen and Zies 1923; Zies 1924, 1929) detected the presence of abundant metallic elements in the encrustations and allowed an estimate to be made of the volume of gases released during the initial degassing stages of the ash-flow sheet.

As previously described, works by White (1955), Silberman et al. (1979), Henley and Ellis (1983), Henley (1985) and Silberman and Berger (1985) recognized the similarities in alteration mineralogies, trace-element distributions, fluid compositions and stable isotope patterns between many epithermal precious metal deposits and geothermal/fumarolic systems. The Goldfield, Nevada, and Round Mountain, Nevada, ore deposits are two examples of volcanic rock-hosted precious metal epithermal ores. Gold reserves at these sites are 4.3 million and 8.7 million troy ounces, respectively (Henley 1985). Although actively-mined epithermal precious metal ore deposits may possess low gold grades (as low as 0.05 troy ounces Au/tonne), other characteristics (e.g., very fine-grained disseminated mineralization, shallow deposit depths) make them suitable for bulk mining and therefore very attractive mining targets. The growing number of recently discovered volcanic rock-hosted epithermal ore deposits and their potential for large reserves of gold illustrate the important role of magmatic/volcanic processes in ore formation. Fossil and active fumarolic systems may

provide a small-scale analog of the larger epithermal systems. A better understanding of fumarolic processes may therefore contribute to improved genetic and exploration models for volcanic rock-hosted precious metal epithermal ore deposits.

Zies (1924) reported that the 1919 VTTS expedition observed a series of fissure fumaroles where significant quantities (up to 10 tons) of magnetite were being actively deposited. The distribution and morphology of the magnetite crystals suggest it was a vapor phase sublimate. Subsequent crude chemical analyses of the magnetite revealed high concentrations of Cu, Zn, and Mo, and moderate to minor concentrations of many other metal and metalloid elements (Zies 1924, 1929). Detailed chemical analysis of the primary fumarolic magnetite should therefore be the best way to constrain the role of vapor phase metal and metalloid transport in the VTTS fumaroles. Unfortunately, as the VTTS fumaroles cooled, subsequent acid dissolution reactions effectively removed the magnetite. According to Keith (1991), primary fumarolic magnetite is now very scarce in the fossil fumaroles of the lower VTTS, while at other scattered vents it commonly exists as a thin coating covering fallout clasts.

Without the ability to collect significant quantities of fumarolic magnetite in the VTTS, this study concentrated on the collection, phase characterization and chemical analysis of the preserved fossil fumarolic encrustations. Of particular interest to this study was whether the fossil fumarolic encrustations would preserve a signature of their initial formation processes seventy-five years after emplacement of the ash-flow sheet. These data are necessary for further constraining the elemental source, transport and deposition mechanisms for the VTTS encrustations and for evaluating the applicability of bulk fossil fumarolic deposits for modeling epithermal ore-forming processes in volcanic terranes.



### Nature of the 1912 Ash-Flow Sheet

Pumice counts in surface exposures from the distal portion of the 1912 ash-flow sheet are nearly 100% rhyolite ( $77 \pm 0.6\%$   $\text{SiO}_2$ ), but progressive increases toward Novarupta of dacite (64.5-66%  $\text{SiO}_2$ ) and andesite (58.5-61.5%  $\text{SiO}_2$ ) eventually reduce the near-surface component to less than 2% (Hildreth 1983). The rhyolitic ejecta is phenocryst-poor (1-2% phenocrysts), but the andesitic and dacitic ejecta are relatively phenocryst-rich (30-45% phenocrysts) (Hildreth 1983). Hildreth (1983) notes that all pumice compositions contain phenocrysts of plagioclase, orthopyroxene, titanomagnetite, ilmenite, apatite and pyrrhotite; quartz is present and augite absent only in the rhyolite while rare olivine occurs in the andesite.

Hildreth (1983) speculated that all three ejecta compositions were derived from a single magmatic system. The emplacement temperature of the ash-flow sheet is unknown, but Fe-Ti oxide data reported by Hildreth (1983) yielded the following pre-eruptive magma temperatures: rhyolite (805-850°C), dacite (855-955°C), and andesite (955-990°C). Except in the extreme distal portions of the ash-flow sheet, the true and relative thicknesses of the ash-flow sheet are poorly constrained. Published estimates of the maximum thickness for the same site in the ash-flow sheet (middle VTTS) range from 25 meters (Gedney et al. 1970) to 295 meters (Curtis 1968). Due to incomplete knowledge of the density contrasts within the ash-flow materials and sediments underlying the ash-flow sheet, Kienle (1970) proposed two end-member models of the ash-flow sheet thicknesses based on analysis of VTTS gravity traverses. According to Kienle (1991), later density determinations of VTTS materials favor a gravity model of the ash-flow sheet thickness that fits the estimates of Curtis (1968) quite well.

Apparently, the degree of welding in the ash-flow sheet varies widely (Keith 1984, 1991). According to Keith (1991), the exposed distal portion (15-20 km from Novarupta,

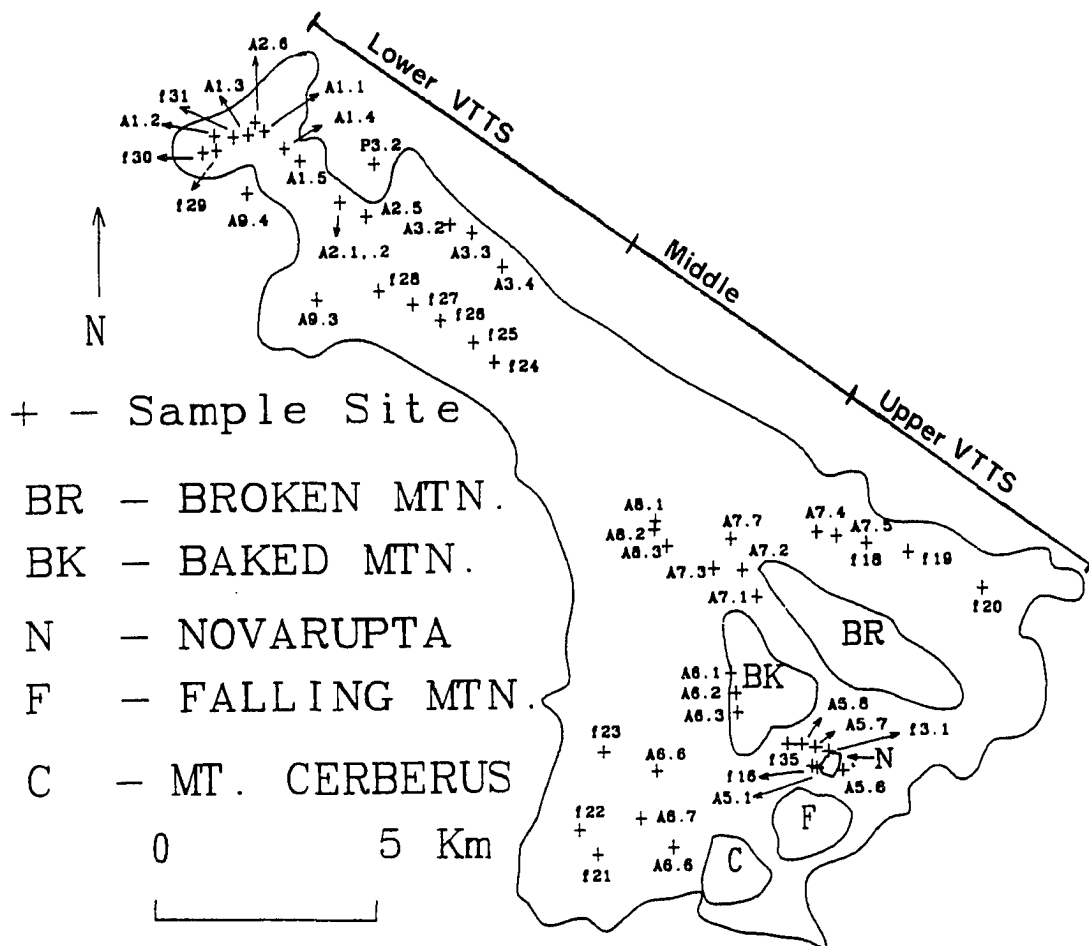


Fig. 28 Fumarole sample sites in the VTTS. For clarity, only 7 of 24 Novarupta Basin sample sites are shown. Division of the ash-flow sheet into lower, middle, and upper segments is after Keith (1991).

Figure 28) of the ash-flow sheet is predominantly rhyolitic and nonwelded while in the upper VTTS the exposed ash-flow sheet is a partially welded, rhyolite-poor mixture of dacite and andesite. Overlying the ash-flow sheet are Plinian fall layers ( $\approx 5\text{-}8$  m thick,  $> 98\%$  dacite) which are coarsest and thickest toward Novarupta. Black andesitic scoria is common in the near-vent air-fall tephra (Hildreth 1983, 1987; Keith 1991).

## Fumarole Evolution, Distribution and Morphology

The most serious shortcoming of the 1917 expedition into the VTTS was the inability, due to inadequate equipment, to accurately measure fumarole temperatures. Eighty-six vents measured in 1918 by Sayre and Hagelbarger (1919) exhibited temperatures greater than 190°C (maximum of 432°C), while in 1919 Allen and Zies (1923) measured 54 fumaroles with temperatures exceeding 200°C (maximum of 645°C). In nearly every instance, vents resampled in 1919 showed a considerable decline in temperature from the previous year (Allen and Zies 1923). Infiltration and subsurface lateral flow of surface waters, while promoting the initial vigorous fumarolic activity, acted to cool the ash-flow sheet. Allen and Zies (1923) conservatively estimated that only 1/11th of the water entering the upper VTTS exited at Three Forks (see Figure 17, lower VTTS), the intersection of Knife Creek, Windy Creek and the River Lethe. Allen and Zies (1923) contended that while a small portion of this water was lost to evaporation, the remainder was contributed to fumarolic emissions. This cooling action resulted in nearly all of the ash-flow fumaroles having died out by the 1930s. Cementation by their deposits has favored the preservation of the fossil fumaroles as colorful, resistant rubble-like outcrops or isolated mounds (Keith 1984). Patches of warm ground and a few wispy fumaroles ( $T \approx 90^\circ\text{C}$ ) still persist in Novarupta Basin. The warm ground patches frequently appear as bright blue-gray- and red-streaked muds.

Current evidence confirms that nearly all of the ash-flow fumaroles were rootless (Williams 1954; Keith 1984, 1991). The location and morphology of these rootless fumaroles were probably controlled by pre-eruption surface drainage, differential permeability and welding within the ash-flow sheet, and post-eruption fractures generated by cooling and/or settling of the ash-flow (Keith 1991). The alignment of some of the fumaroles along these post-eruption fractures led Griggs (1919) to erroneously propose that all of the ash-flow fumaroles were rooted to a degassing magma body. As previously stated, the few remaining

active fumaroles in Novarupta Basin are located along subsidence fractures suggesting they are maintained by residual heat (i.e., rooted) from the Novarupta magma reservoir (Keith 1984).

Allen and Zies (1923) classified the active fumaroles of the VTTS into six categories based on fumarole morphology and activity level: 1) fissure vents; the commonest class of fumarole, these ranged from a few feet up to 800 feet in length and a few inches to five feet in width, 2) crater vents; openings on the sides or bottom of craters up to 225 feet in diameter and that nowhere reached down to the original VTTS floor, 3) small mounds; also described as "pimples"; these fumaroles when active were fairly quiescent, 4) low-temperature vents accompanied by little or no chemical action; these vents very rarely produced encrustations, 5) mud pots; fairly uncommon, these shallow features sputtered mud to the height of a few inches, and 6) mud fields; sticky, steamy mud of a few inches depth which often covered an area of acres in the Valley. More recently, Keith (1991) has described the distribution and types of fossil fumarolic orifices found in the VTTS. Keith (1991) reports that three types of abundant relict fissure fumaroles are preserved in the middle and upper VTTS: 1) fissures which developed parallel to the enclosing valley walls during compaction of the ash-flow sheet, 2) fissures that extend nearly perpendicular to the flow direction and formed through cooling and settling of the flow deposits, and 3) randomly oriented fractures generated as cooling contraction cracks during vapor phase devitrification. Keith (1991) states that some of these fissures can be traced (via their resistant encrustations) for many tens of meters at the surface and that some fumarolic deposits extend almost entirely across the width of the ash-flow sheet.

Crudely circular orifices, color zoned and up to 3 m across, are common in the lower VTTS (Figure 28). In cross-section these are flared, funnel-shaped vents which originate in the non-welded tuff and whose irregularly-shaped conduits become more sharply defined upwards (Keith 1991). Many of the "crater" fumaroles of Allen and Zies (1923) are, in the

opinion of Keith (1991), better classified as funnel vents. During this study, fissure and funnel vents were observed in the VTTS which fit the distribution noted by Keith (1991). What appear to be phreatic explosion craters along the upper reaches of Knife Creek (Figure 17) were also sampled. The "mud pots" and "mud fields" of Allen and Zies (1923) were preferentially removed by erosion, although Keith (1991) has recognized some relict mud pots.

### **Previous Studies of the VTTS Encrustations**

#### **Encrustation mineralogies**

Shiple (1920) reported that in 1917 the most characteristic deposit of fumarolic activity was amorphous silica, with many fumaroles having built up mounds of almost pure  $\text{SiO}_2$  several feet high. Magnetite and amorphous Fe-oxides were also abundant. Chlorides and fluorides were found in nearly all of the encrustations examined, but only ammonium chloride ( $\text{NH}_4\text{Cl}$ ) and halite could be identified. Many fumaroles, particularly those on the western rim of Novarupta, were depositing significant amounts of  $\text{NH}_4\text{Cl}$ . Gypsum, as well as other unidentified sulfate phases, potassium alum, pyrite, vivianite ( $\text{Fe}_3\text{P}_2\text{O}_8 \cdot \text{H}_2\text{O}$ ), sulfur, and sulfides of arsenic were also noted (Shiple 1920).

Zies (1924) states that in 1919 very few distinct minerals were found in the encrustations; most of the samples were apparently amorphous. The most interesting discovery of 1919 was the presence of large amounts of fumarolic magnetite in fissure vents of the middle and upper Valley. Zies (1929) estimated that in 1919 up to ten tons of fumarolic magnetite was present as the lining on the roof of a series of fissure vents which covered an area of approximately 30 x 30 m in the middle VTTS. Octahedral crystals of  $\text{Cu}_2\text{S}$  and  $\text{CuS}$  were frequently found on the surface of the magnetite crystals. Encrustations found at this

site, and in practically all of the sampled vents, contained chloride and fluoride phases. In some cases the concentration of chlorides and fluorides was quite astounding; many encrustations, for instance, possessed fluoride contents in excess of a few weight percent with the highest concentration being 15 weight percent F. Kryptohalite  $[(\text{NH}_4)_2\text{SiF}_6]$  was observed in relatively large amounts at several fumaroles. Erythrosiderite  $(2\text{NH}_4\text{Cl}\cdot\text{FeCl}_3\cdot\text{H}_2\text{O})$  was also noted in the 1919 encrustation samples (Zies 1924).

Zies (1929) reported that no magnetite was found when the magnetite-rich vents were revisited in 1923. Instead, well-developed crystals of galena, sphalerite, and copper sulfides had replaced the magnetite. The fumarole temperatures in this area had declined below  $100^\circ\text{C}$  enabling the condensation of acidic gases and subsequent magnetite decomposition. As the fumarolic activity waned, surficial weathering processes operated to convert the primary fumarolic deposits to more stable, secondary phases. Lovering (1957) studied the fumarolic alteration for a vent in the extreme distal portion of the ash-flow sheet and reported that magnetite, hematite, goethite, hydromica, opal, montmorillonite and kaolinite were the chief alteration minerals. Utilizing reflected light microscopy, Ramdohr (1962) found that some of the primary fumarolic magnetite contained tiny Cu-, Fe- and Zn-sulfide inclusions.

Based on their mineralogical suites, Keith (1991) has classified the VTTS fossil fumaroles into "magnetite-rich" and "hematite-rich" vents. Magnetite-rich vents have conspicuous black cores of a thin coating of primary fumarolic magnetite encrusting fallout clasts. Later-stage deposits of  $\alpha$ -cristobalite, illite, fluorite, hydrated aluminum hydroxy-fluoride (AHF - a ralstonite-like phase, Desborough and Rostad 1980), and kaolinite cement the magnetite-encrusted ejecta. The outer portions of these vents are typically composed of encrusted fall deposits of limonite, goethite, hematite, AHF, fluorite, alunite,  $\alpha$ - and  $\beta$ -

cristobalite, opal, pyrite, sulfur, kaolinite and illite (Keith 1991). In contrast, hematite-rich fumaroles have dark-red or orange-red cores of hematite- or hematite plus magnetite-encrusted ejecta. Goethite, limonite, AHF, fluorite,  $\alpha$ - and  $\beta$ -cristobalite, kaolinite, and mixed-layer illite-smectite cement the core region. According to Keith (1991), hematite-rich fumaroles usually have larger amounts of later-stage minerals deposited at their outer edges than the magnetite-rich fumaroles. For instance, the surface expression of fissure fumaroles, particularly the hematite-rich vents, typically host leached ejecta encrusted with deposits of sulfur, alunite, fluorite, AHF,  $\alpha$ - and  $\beta$ -cristobalite and pyrite (Keith 1991). The large volumes of primary fluorides, chlorides and sulfates reported by the early VTTS investigators have been removed via dissolution and weathering processes (Keith 1991).

#### **Encrustation trace-element chemistries**

Chemical analysis of the encrustations collected by the early workers in the VTTS revealed the encrustation phases to be highly metalliferous. Unfortunately, even the best quantitative analytical techniques of the day proved inadequate for the analysis of a number of metallic constituents. Of particular interest to these early analytical efforts was the chemistry of the high-temperature fumarolic magnetite. Quantitative analysis of a 10 g sample of the magnetite revealed significant concentrations of other metallic elements such as Cu (2300 ppm), Zn (4700 ppm), Mo (400 ppm), Sn (40 ppm) and Pb (50 ppm) (Zies 1924). Zies (1929) noted that encrustations from a distal ash-flow fumarole contained appreciable concentrations of Sn (190 ppm), Pb (540 ppm) and Zn (340 ppm). Small areas within the ash-flow sheet were also found to be enriched in Mo (0.1-0.5 wt.% MoO<sub>3</sub>) and Bi and Tl ( $\approx$ 100 ppm). Selenium and tellurium were detected in nearly all the analyzed encrustations but actual contents were not determined. Arsenic routinely exhibited the highest concentration of any of the metallic or metalloid elements; values of 5000 ppm or

greater, 500 times more than the average pumice As concentration, were not uncommon (Zies 1929), implying that As was extremely mobile in the alteration fluids.

Keith (1984) reported the trace-element chemistry for two VTTS fossil fumarole deposits. Significant concentrations of As (3000 ppm maximum), Bi (20 ppm maximum), Sn (1000 ppm maximum), Tl (50 ppm maximum), Se (50 ppm maximum) and Sb (50 ppm maximum) were found in these encrustations. Analyses of patches of warm altered ground from within Novarupta Basin yielded Hg contents of 15-20 ppm (Keith 1984). Verification of the presence of Hg was important since the earlier studies (e.g., Zies 1929) contended that Hg was not present in either the encrustations or unaltered ejecta.

## **Mineralogy and Chemistry of the Alteration Samples**

### **Sampling and analytical techniques**

Crudely zoned deposits of black, gray, purple, red, orange, pink, or yellow encrustations can be observed around many of the VTTS fossil fumarole orifices. As discussed in Chapter 4, 182 samples were collected from the differently-colored zones of 65 active/fossil fumarole and warm ground sites within the VTTS. Phase identification was undertaken for powdered mounts of 50 samples from 32 different fumaroles using XRD techniques. Chemical analyses for fifty samples of encrustations and unaltered and altered samples of regolith and Naknek Formation were obtained from Bondar-Clegg analytical services in Vancouver, B.C., Canada. The data for the contracted "gold + 46 elements" package as well as the analytical methods used for the analyses are given in Appendix 4. For both the XRD scans and chemical analyses of the encrustations, attempts were made to provide as pure a sample of encrustations as possible. Keith (1991), however, reports that the VTTS fossil fumarolic deposits typically include 50-90% ejecta in various stages of alteration. Therefore even in



the best case scenario these samples represent mixtures to some degree of encrustation and ejecta.

In addition to the Bondar-Clegg analyses, Au analyses were performed on 26 encrustation samples and 6 other altered and unaltered VTTS samples at the University of Alaska Fairbanks. Sample splits ranging in size from 7 to 50 g were dissolved for 1-2 hours in heated ( $T \approx 85^{\circ}\text{C}$ ) pyrex beakers containing approximately 50 ml of aqua regia (3 parts  $\text{HNO}_3$ , 1 part  $\text{HCl}$ ). The aqua regia effectively dissolves glass and most mineral phases, with the exception of the more strongly bonded silicates. After cooling, the beaker contents were filtered through Whatman no. 42 filter paper. The filter paper was washed repeatedly with distilled  $\text{H}_2\text{O}$  until the percolating solution became clear. Ten milliliters of the filtrate were then extracted into 2 ml of dimethyl isobutyl ketone which quantitatively extracts the Au from the filtrate. The organic solvent was then analyzed by flame atomic absorption spectrometry. Analytical accuracy was monitored through the Canadian Metallurgical Association gold ore standard (CMA-1).

## Results

### *Phase identification*

Table 13 lists XRD-identified minerals grouped by location of the fumaroles and warm ground patches into the categories of lower VTTS, middle and upper VTTS, and Novarupta Basin. Of the 33 samples taken from 22 fumarole sites in the lower and middle and upper VTTS, hematite-rich vents were the most common. Magnetite was identified in only one sample, a lower VTTS fumarole. This is in stark contrast to the early studies of the VTTS deposits. Mineralogies of the individually X-rayed samples are provided in Appendix 1.

Relatively abundant in the lower, and middle and upper VTTS X-rayed samples are  $\alpha$ -cristobalite and AHF. Keith (1984) suggests that AHF formed during the late stages of fumarolic activity by the reaction of hydrofluoric acid and pumice. Although fumarolic

**Table 13 XRD-determined minerals in the VTTS alteration samples.**

Location	Mineral Suite
Lower VTTS (n=12)	Fluorite, hematite, $\alpha$ -cristobalite, magnetite, sulfur, alunite
Middle and upper VTTS (n=21)	Sulfur, $\beta$ -cristobalite, $\alpha$ -cristobalite, hydrated aluminum hydroxy-fluoride (AHF), hematite
Novarupta Basin (n=17)	Kaolinite, goethite, alunite, pyrite, natroalunite, hematite, mixed layer illite-smectite

gas samples collected by the early VTTS investigators were extremely water-rich (Allen and Zies 1923), HF was detected in minor amounts. The relative abundance of AHF in the encrustations is further evidence that the VTTS fumaroles emitted significant quantities of F.  $\beta$ -cristobalite was noted in two middle and upper VTTS samples. Fournier (1973) used the term  $\beta$ -cristobalite to describe poorly crystalline cristobalite and opal-CT. Poorly crystalline cristobalite shows broad XRD peaks centered around 4.1 and 2.5 Å (Fournier 1985).

Supergene, advanced argillic (Rose and Burt 1979) alteration assemblages are abundant in the warm ground patches within Novarupta Basin (Table 13). In addition to alunite, natroalunite was tentatively identified in a few of the X-rayed samples. This mineral has not been reported in any of the earlier studies of the VTTS alteration deposits. Advanced argillic alteration is common at many active volcanoes (Henley 1985); low pH fluids formed by the mixing of exsolved H<sub>2</sub>S, HCl, and SO<sub>2</sub> with surface waters are the active agents of alteration. The interaction of fumarolic gases with condensed steam is responsible for the advanced argillic alteration suites within Novarupta Basin. Keith (1991) notes that the advanced argillic alteration was already well developed in the Novarupta vent region as early as 1919 and that it now appears confined to the shallow portions of the Novarupta Basin concentric fracture system.

Sixteen of the 50 XRD samples were apparently amorphous. This is not uncommon for the VTTS fumarolic alteration products. Papike et al. (1991) analyzed the alteration suites

of three lower VTTS fossil fumaroles. Using a combination of the XRD reference intensity ratio (RIR) technique and the optical investigation of grain mounts, they estimated that amorphous phases composed the bulk (79-94 wt. %) of their samples.

#### *Chemistry of the VTTS alteration products*

Chemical data for the VTTS alteration products were evaluated via a series of comparative chemical ratios and univariate and multivariate statistical techniques. The statistical techniques employed assume a normal data distribution. Therefore, the analytical data base was investigated with the goal of producing a valid, consistent data subset for these subsequent tests. Samples of encrustations, warm ground muds, and altered and unaltered regolith and Naknek Formation were grouped separately. As the result of this grouping, only the encrustation category contained more than ten samples. The encrustation data distributions for the 47 analyzed species were then checked by normal probability plots, box plots and data histograms. Elements with five or more observations below the lower analytical detection limit were discarded from the data set. Those species exhibiting a significant departure from a normal data distribution (LOI, As, Br, Sb, Cu, Ni, Pb, Zn) were log-transformed. The mean of the respective element was substituted for below detection values or missing data in the remaining elements. This procedure resulted in the selection of 17 trace and minor elements (As, Ba, Br, Ce, Cr, La, Rb, Sb, Sc, Sm, Th, U, Cu, Ni, Pb, Zn, Li) and the 10 major oxides (plus loss on ignition) for detailed analysis. Six of the 25 encrustation samples lacked sufficient material to analyze for the major oxides. Figure 29 (a-f) shows untransformed data box plots for the 28 selected chemical species. All chemical data for the VTTS alteration products are listed in Appendix 4.

#### *Au concentrations*

Of the data obtained from Bondar-Clegg, only 4 samples contained Au in concentrations above the lower analytical detection limit, with the highest value being 12 ppb. This would

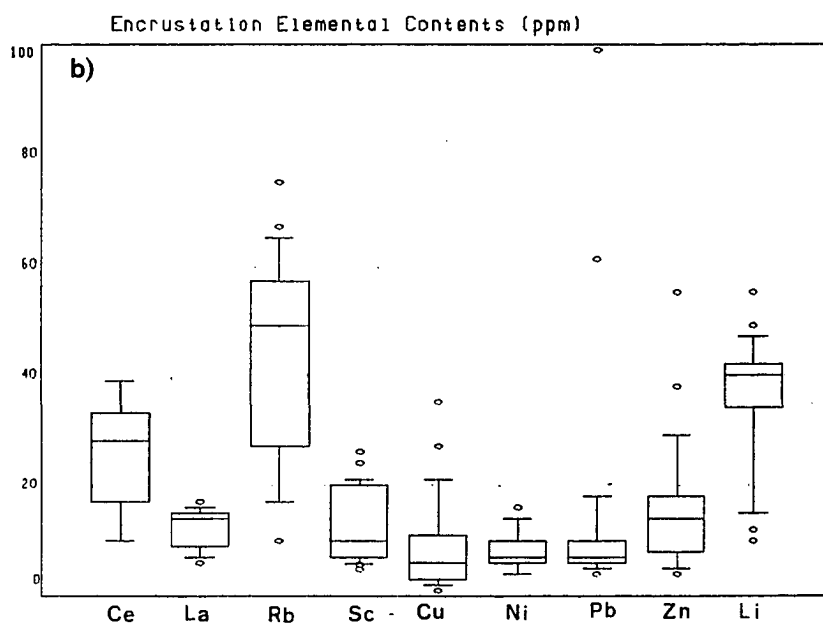
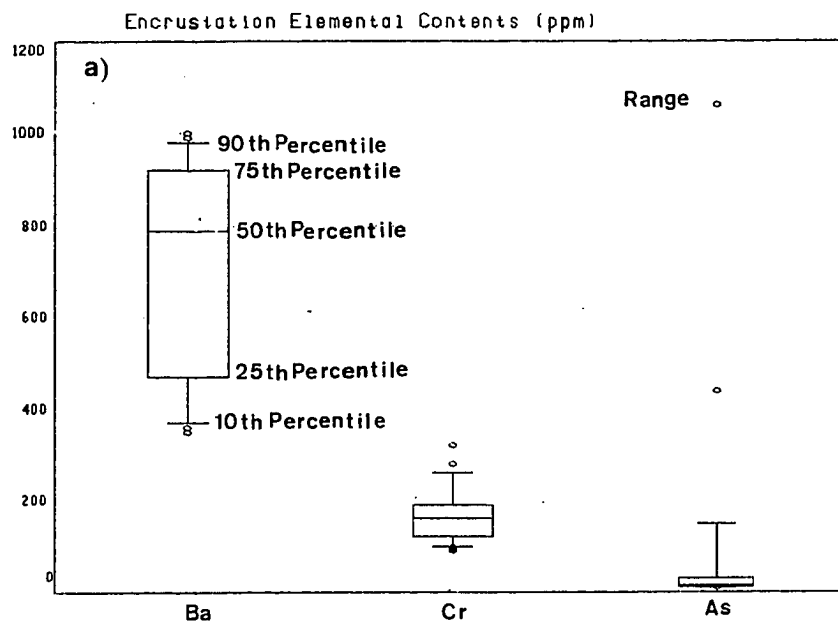


Fig. 29a-b Box plots of the VTTS encrustation chemistry. a) Ba, Cr, As. b) Ce, La, Rb, Sc, Cu, Ni, Pb, Zn, Li.

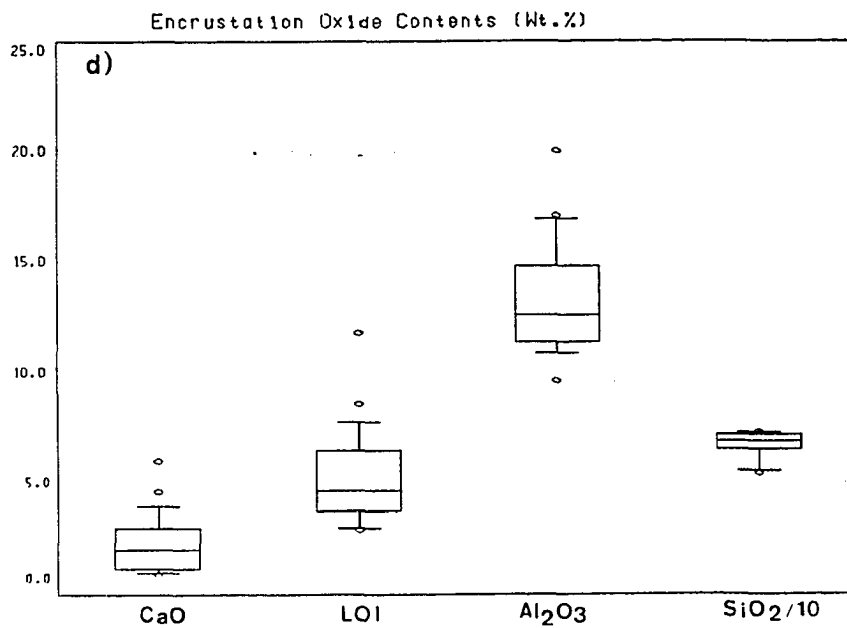
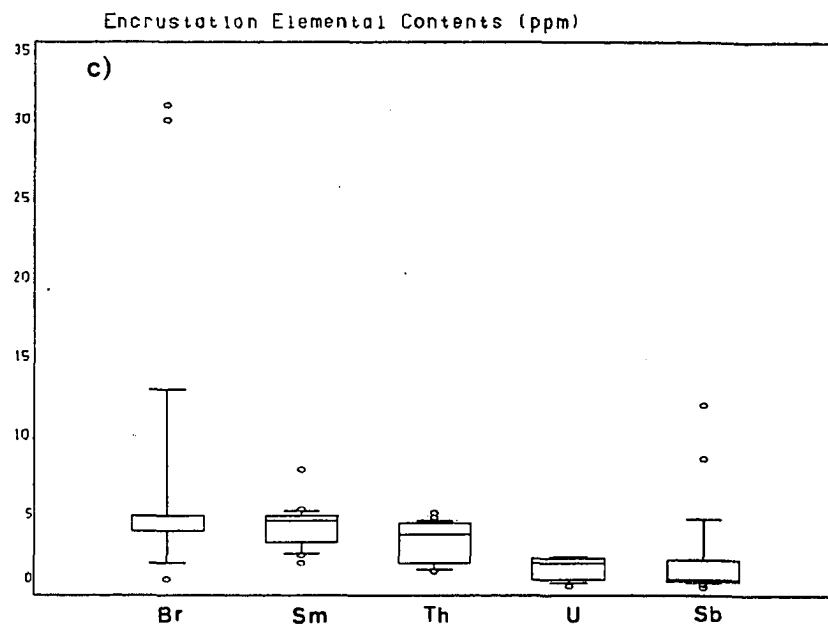


Fig. 29c-d Box plots of the VTTS encrustation chemistry. c) Br, Sm, Th, U, Sb. d) CaO, LOI, Al<sub>2</sub>O<sub>3</sub>, SiO<sub>2</sub>/10.

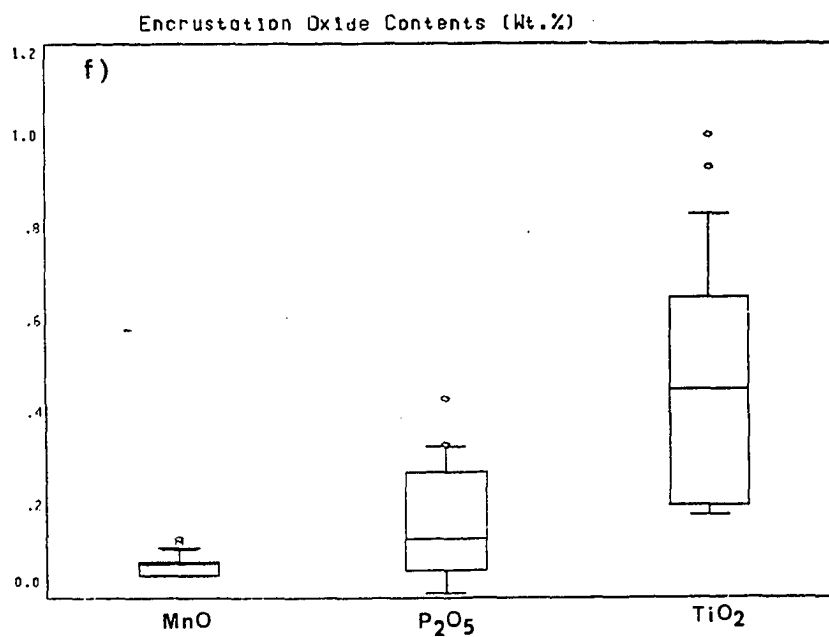
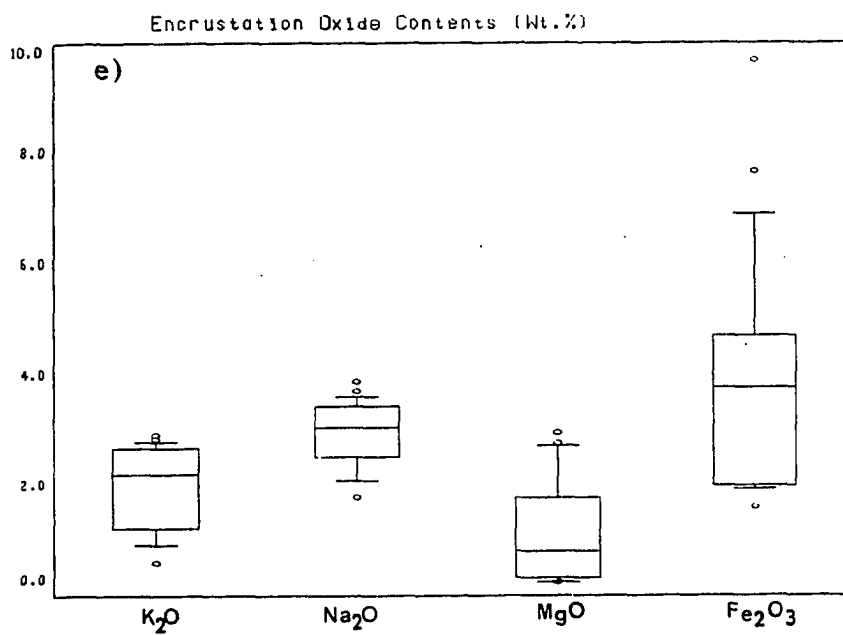


Fig. 29e-f Box plots of the VTTS encrustation chemistry. e) K<sub>2</sub>O, Na<sub>2</sub>O, MgO, Fe<sub>2</sub>O<sub>3</sub>. f) MnO, P<sub>2</sub>O<sub>5</sub>, TiO<sub>2</sub>.

imply that Au is not enriched in the VTTS encrustations but instead is present at or below background levels ( $\approx$  3-6 ppb for crustal rocks, Rose et al. 1979). To check the homogeneity of the Au distribution in these samples, another 5 encrustation samples were submitted to Bondar-Clegg as a separate sample suite. Three to four splits of each of these samples were analyzed under different sample designations. Only one of these samples contained Au in concentrations (6 ppb) above the lower analytical detection limit of 5 ppb.

The samples analyzed at the University of Alaska Fairbanks followed the same trend with one major exception. Of these analyses, 4 were above the lower detection limit of 10 ppb. The lowest value (16 ppb) is similar to the values obtained from Bondar-Clegg. The two intermediate values (150 ppb and 160 ppb) suggest moderate enrichment of Au in these samples. In contrast, sample 5.1S yielded a Au value of 7.36 ppm. This sample was taken from a low-temperature active fumarole within Novarupta's ejecta ring. Interestingly, a split of this sample contained one of the highest levels of Hg<sup>o</sup> (4501 ppb) observed in the surficial deposit Hg<sup>o</sup> survey. Marked enrichment of Hg is typically found in the alteration products associated with precious metal epithermal ore deposits (Silberman and Berger 1985).

During the Au analyses, two checks of the CMA-1 Au standard did not differ from its listed concentration by more than 4.5% (3.3% and 4.2% respectively). However, another split of sample 5.1S was determined by Bondar-Clegg to contain < 5 ppb Au. This suggests that the Au content of sample 5.1S is either highly inhomogeneously distributed, or that one of the analytical values for this sample is incorrect. Whether sample 5.1S contains Au in elevated concentrations or not, both analytical procedures imply that Au concentrations in the overwhelming majority of the VTTS encrustations are at or below detection.

### *Enrichment factors*

Elemental enrichment factors were then calculated for the alteration products. Lepel et al. (1978) have defined the enrichment factor (EF) as:

$$EF_{sample} = (X/R)_{sample} / (X/R)_{reference}$$

where EF is the enrichment of the element in the sample,  $(X/R)_{sample}$  is the ratio of the element to a reference element R in the sample, and  $(X/R)_{reference}$  is the ratio of the element to the reference element in a reference material. For the lower VTTS encrustation samples, a sample of visibly unaltered distal ash-flow tuff (A30.1, Appendix 4) was chosen for the reference material. The mean chemical analysis of 2 unaltered dacitic/andesitic upper VTTS air-fall samples (B5.1 and B5.2, Appendix 4) was chosen as the reference material for the upper VTTS encrustation samples. For the altered Naknek Formation samples (collected from near the summit of Baked Mountain), the mean chemical analysis of 3 unaltered samples of Naknek Formation (32.1, 32.2, A3.5, Appendix 4) was selected as the reference material. Finally, a visibly unaltered sample of the rhyodacitic Novarupta dome (FD, Appendix 4) was used as the reference material for an altered dome sample. In all cases, Ti was chosen as the reference element because it is considered one of the least reactive elements in acid gases (Symonds et al. 1987). Papike et al. (1991) used the isocon method of Grant (1986) to quantify the chemical losses and gains for the major oxides from alteration zones surrounding 3 lower VTTS fumaroles. In every case, Ti exhibited the lowest mobility (average gain of 0.1 g TiO<sub>2</sub>/100 g unaltered rock). The choice of Ti as the reference element for the VTTS alteration products seems a good one, particularly for the encrustation samples.

Figure 30 (a-d) illustrates the calculated mean enrichment factors for the encrustations, altered Naknek, and altered Novarupta dome samples. An enrichment factor of 1 would signify no elemental enrichment in the altered samples, an EF of > 1 or < 1 would indicate,



respectively, enrichment or depletion of the element in the altered sample in comparison to the unaltered reference material.

The lower VTTS encrustations (Figure 30a) have enrichment factors  $> 1$  for seven elements (As, Cr, Sb, Cu, Ni, Pb, Fe) and loss on ignition (LOI), an indirect measure of the structural and nonstructural water content of the sample. Under active fumarolic conditions, the elements As, Sb, Fe, Cu, Ni, and Pb have either relatively high volatilities as halide (Cl, Br, F) gas species (Symonds et al. 1987) and/or relatively high mobilities as aqueous halide complexes (Barnes 1979). In contrast, Cr has an extremely low volatility; its presence in fumarolic encrustations is believed to result from the attack of acidic condensate on fumarolic wall rock (Symonds et al. 1987). These late-stage, relatively low-temperature, water-rich reactions would favor the Cr being fixed in the encrustations as a relatively immobile oxide or hydroxide phase. The fact that Cr has the highest EF in the lower VTTS encrustations suggests that a significant fraction of the more volatile and aqueous mobile elements have been removed from these deposits via weathering processes. Since As, Sb, Cu, Ni, Zn and Pb are moderately to highly volatile as halide species over the common range of active fumarole temperatures, initial deposition of these elements as amorphous or crystalline halides would favor their subsequent removal by surficial weathering processes. The LOI enrichment factor suggests hydration reactions have affected these samples. As previously mentioned, chlorides and fluorides were abundant in the initial VTTS fumarolic encrustations (Shipley 1920; Zies 1924) but weathering processes have removed these species, resulting in their absence from the present-day VTTS encrustations (Keith 1991). With the exception of Fe, Symonds et al. (1987) found much higher enrichments ( $\approx 5$ - $\approx 1500$  times) of Pb, Zn and Cu (As, Sb and Ni were not measured) relative to Cr in actively-forming encrustations at Merapi volcano. This is further support for the idea that the lower VTTS encrustations have been severely degraded by weathering.

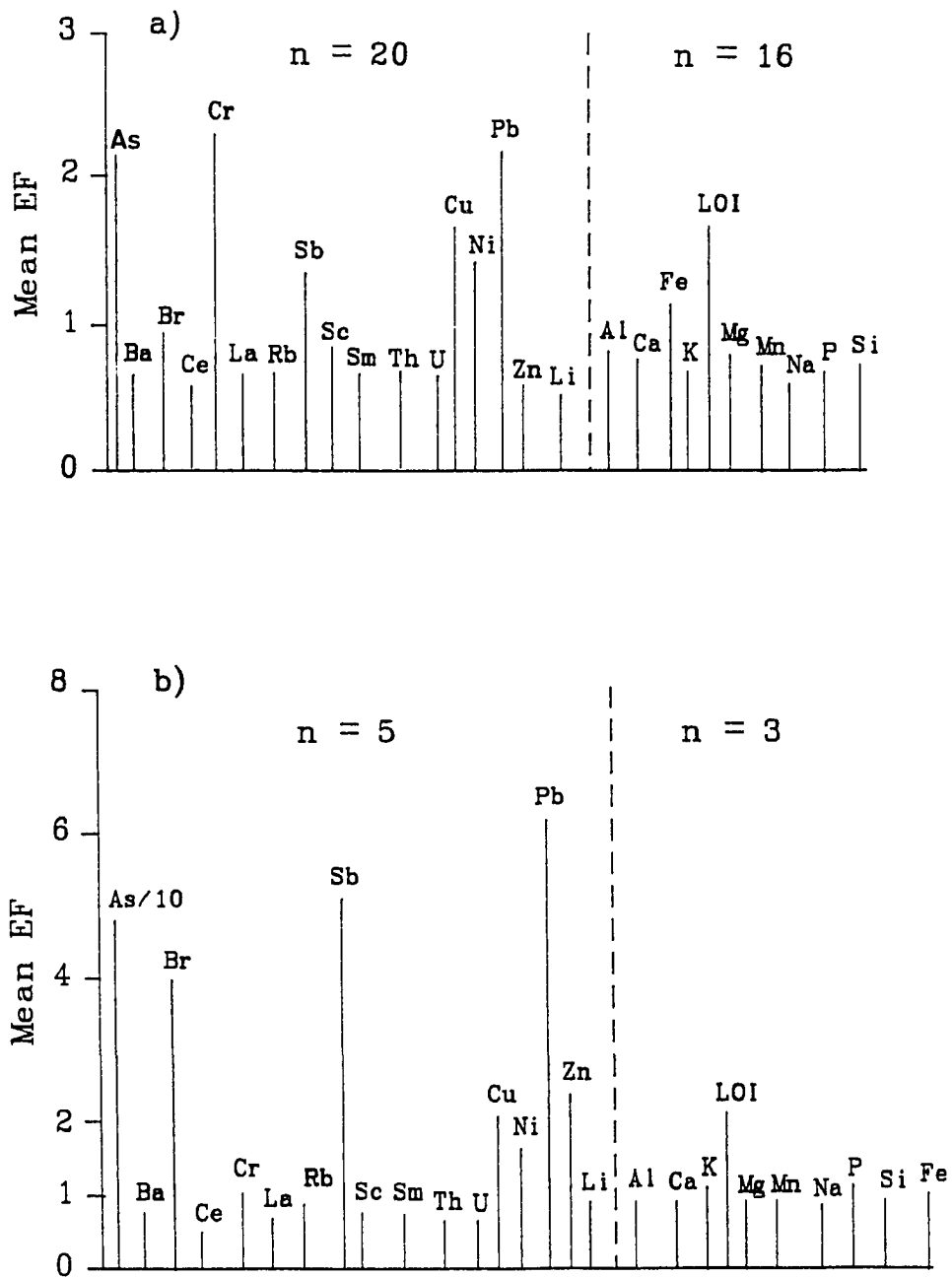


Fig. 30a-b Mean enrichment factors (EF) for the VTTS alteration products.  
 a) Lower VTTS encrustations. b) Upper VTTS encrustations.

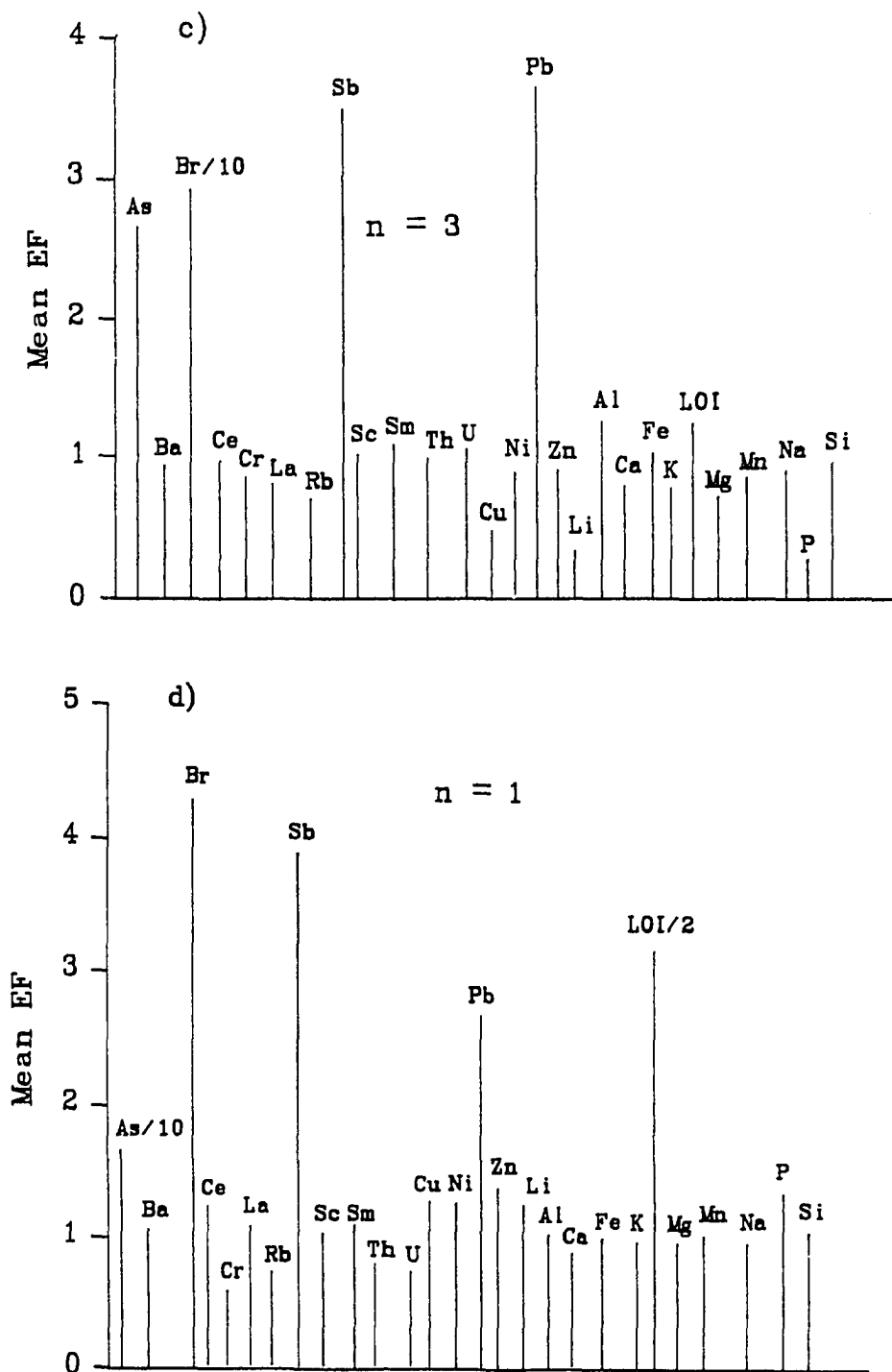


Fig. 30c-d Mean enrichment factors (EF) for the VTTS alteration products.  
 c) Altered Naknek Formation. d) Altered Novarupta dome.

The upper VTTS encrustations (Figure 30b) have enrichment factors substantially > 1 for As, Br and Sb and Pb. All of these elements, with the exception of Pb, are highly volatile as halide species while Pb is moderately volatile as a halide species and relatively mobile as an aqueous halide complex. The EF of 48 for As is the largest EF observed in any of the VTTS alteration products. The EF's for Cr, Si, and Al are approximately 1. Of the remaining elements, enrichment factors are close to 1 except for a few species (Ce, Sm, Th, U). Although the LOI EF suggests hydration reactions have affected these deposits, the sampled upper VTTS encrustations apparently have been less degraded by weathering than the lower VTTS encrustations. Four of the five upper VTTS encrustation samples come from a fossil fumarole whose color zonation pattern fits that of the magnetite-rich vents described by Keith (1991). Such vents should have a higher concentration of preserved primary fumarolic constituents than the non-magnetite-rich vents. Support for this idea stems from the fact that the sampled upper VTTS magnetite-rich vent yielded the highest concentration of As (1060 ppm) and Mo (130 ppm), and the second (452 ppm) and third highest (413 ppm) concentrations of W found in this study. Still, the maximum enrichment factors for the upper VTTS encrustations are one to nearly three orders of magnitude less than what Symonds et al. (1987) found in actively-forming encrustations.

Similar to the upper VTTS encrustations, the three altered Naknek Formation samples exhibit EF's significantly greater than 1 for As, Br, Sb and Pb. The EF for Br (29.5) is the second highest EF observed in the VTTS alteration products. These enrichments probably represent portions of volatile elements deposited from the vapor phase via gas-rock reactions. The enrichment factors for the majority of the remaining elements are near 1. Exceptions are the extremely low EF's seen for Cu, Li and P. These large depletions relative to unaltered rock, and smaller depletions for Mg and Rb, suggest that gas-Naknek Formation and liquid-Naknek Formation reactions could be one source of some of the elements (particularly Cu, Li and P) found in the VTTS encrustations.

The one altered Novarupta dome sample preserves evidence of probable vapor phase alteration through its high EF's for As, Br, Sb, and Pb. Most of the remaining elements have enrichment factors near 1. Chromium shows the largest relative depletion. Water-rich reactions (e.g., glass hydration) with this sample, as implied by the LOI EF, may have leached some Cr from the original unaltered sample.

#### *Elemental correlation patterns*

The encrustation data base was investigated for correlations between elements using the statistical software package SOLO.† Table 14 is a raw and log-transformed chemical data correlation matrix for the VTTS encrustation samples. The values in Table 14 correspond to the correlation coefficient ( $r$ ) which is a measure of the linear relationship between two variables (Davis 1986). Of the major elements, those typically enriched (compared to silica-rich igneous rocks) in mafic rocks and magmas, Ca, Fe, Mg, Mn, and Ti, exhibit fairly high positive correlations with each other. Likewise, Si and K, usually concentrated in more silica-rich magmas and rocks, also show high positive correlations with each other. These two groups also exhibit high negative intercorrelations. This suggests that these two groups of elements have different primary sources or different concentration mechanisms operating on them. Aluminum, P and Na do not show high positive correlations with any of the other major oxide elements, but Al does exhibit high negative correlations with Si and K. In addition, Na shows a high negative correlation with LOI. Sodium initially deposited as halide or other water-soluble phases would be prone to removal from the encrustations via aqueous fluids reacting with the encrustations. The relatively high EF for LOI in the VTTS

---

† SOLO is a personal computer adaptation of the statistical package BMDP developed at the University of California at Davis.



Figure 31 (a-d). The patterns of covariance suggest the isomorphic substitution of these elements for more abundant cations in the alteration phases.

High positive correlations are also shown for Ba, Rb, Th, and U with Si and for Th and U with K. Although Th and U may possess the same ionic charge as Si, their ionic radii are markedly different relative to that of Si. Both the ionic size and charge of Rb and Ba differs greatly from that of Si. Similarly, the ionic charge and ionic radii of Th and U differ significantly from that of K. These relationships are definitely not compatible with the isomorphic substitution of elements into pure encrustation phases. Instead they simply reflect that the encrustation samples, as proposed by Keith (1991), are impure. For instance, the high positive correlations for Ba, K, Rb, Th, and U with Si and K can be explained by the high concentrations of these elements typically present in volcanic glass. As reviewed earlier, Hildreth (1983) has shown that the VTTS ejecta are glass-rich, particularly the lower VTTS ejecta which may contain up to 98% glass. Therefore the dominant alteration reactions involve glass and the just-discussed covariances probably reflect various degrees of alteration of the Si- and K-rich encrusted glass. The moderately low enrichment factors ( $\approx 0.65$ ) for Th, U, Rb and Ba imply that a portion of these elements have been selectively leached from the volcanic glass and carried away from the fumarolic deposits. Smith et al. (1982) have suggested that glass dissolution is the dominant process by which uranium is initially mobilized from volcanic ash.

Of the analyzed cations, the most perplexing correlation pattern is that of Cr. This element is present in fairly high concentrations ( $\approx 150$ -300 ppm) in the encrustation samples yet does not possess an absolute value correlation  $> 0.37$  with any of the other analyzed species. This may indicate that Cr is present in the encrustations as a separate trace mineral. Using SOLO, stepwise multiple regression analysis was undertaken with Cr as the dependent variable and the major oxides and LOI as the independent variables entered into the regression equation in the order  $\text{SiO}_2$ ,  $\text{K}_2\text{O}$ ,  $\text{Al}_2\text{O}_3$ ,  $\text{CaO}$ ,  $\text{MgO}$ ,  $\text{MnO}$ ,  $\text{Fe}_2\text{O}_3$ ,

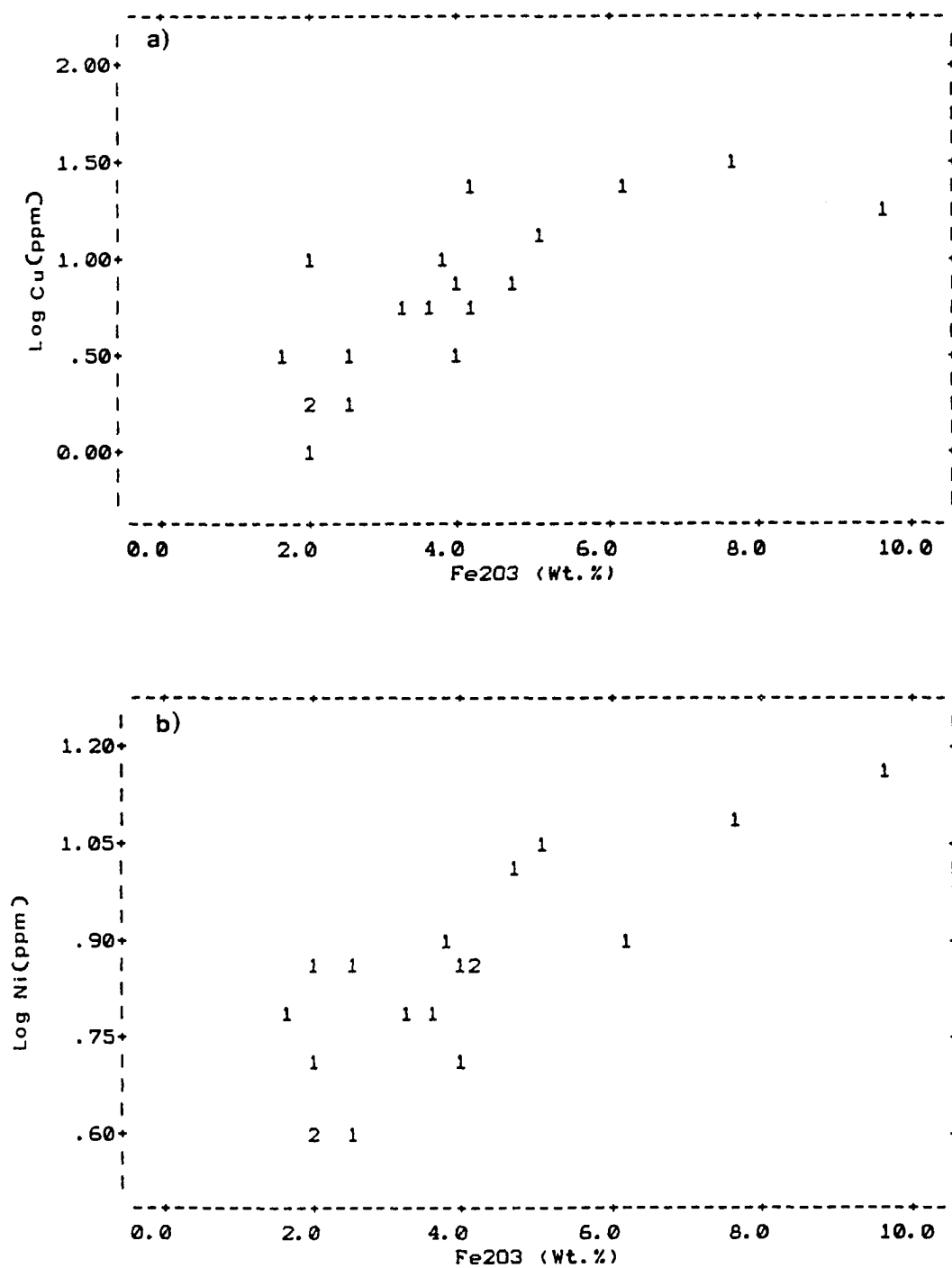


Fig. 31a-b Scatter plots illustrating elemental covariance in the VTTS encrustations. a) Log Cu vs. Fe<sub>2</sub>O<sub>3</sub>. b) Log Ni vs. Fe<sub>2</sub>O<sub>3</sub>. Numerals correspond to the number of plotted points.



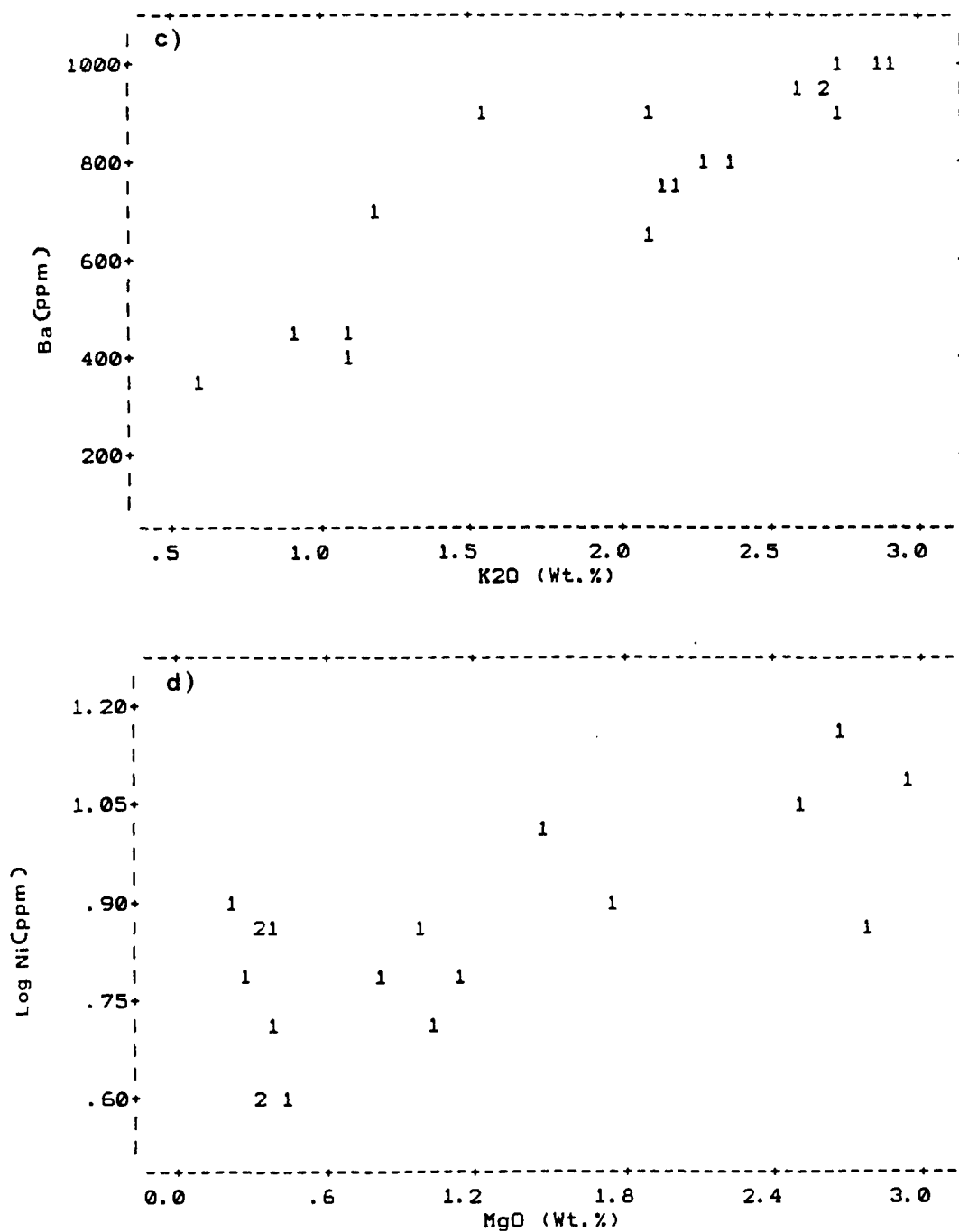


Fig. 31c-d Scatter plots illustrating elemental covariance in the VTTS encrustations. c) Ba vs. K<sub>2</sub>O d) Log Ni vs. MgO. Numerals correspond to the number of plotted points.

Na<sub>2</sub>O, TiO<sub>2</sub>, Log LOI, P<sub>2</sub>O<sub>5</sub>. The results of this analysis paralleled the relationships seen in the correlation matrix. The highest simple R<sup>2</sup>, a goodness-of-fit estimator of the simple linear regression between one dependent and one independent variable, was found between Cr and Log LOI and was extremely low ( $\approx 0.1 R^2$ ). The largest changes in sequential R<sup>2</sup>, the cumulative R<sup>2</sup> resulting from the stepwise addition of independent variables into the regression equation, were found for CaO (+ 0.23 R<sup>2</sup> increase) and P<sub>2</sub>O<sub>5</sub> (+ 0.39 R<sup>2</sup> increase). An analysis of variance revealed the regression to be significant at  $\alpha = 0.05$  but with a relatively low adjusted R<sup>2</sup> (0.62).

#### *Factor analysis and canonical correlation*

Factor analysis of the encrustation data set was done in an attempt to discern the geochemical factors controlling element distribution in the encrustations. Factor analysis is a multivariate statistical technique related to regression, but it does not require one variable to be dependent and the other independent. It is a method of placing similarly behaving variables (in this case elements) into independent groups called factors. The variables within a factor are closely correlated, while the independent factors are not. The different factors can then be examined for significance in terms of geological processes, sample type, or other geochemical or geological information.

Factor analysis with varimax rotation, also known as R-mode factor analysis, was conducted on the encrustation data using the statistical package SOLO. R-mode factor analysis is a method of expressing the data into fewer and/or more meaningful factors. A comprehensive review of the theory and application of factor analysis can be found in Davis (1986).

The factor analysis algorithm requires a greater number of observations (samples) than variables (analyzed species). Since the database employed contained 28 variables, the data were split into major oxide element (19 samples, 11 variables) and trace-element (25 samples, 17 variables) subsets and both subsets factor analyzed. The factor analysis model

requires the number of factors be known prior to analysis. Since this is seldom the case, two alternatives are commonly employed (Davis 1986). The simplest approach is to assume some prior number of factors. Many statisticians recommend retaining all factors that have eigenvalues greater than one; this results in retaining all factors that contain greater data variance than the original standardized variables. Dan Hawkins (pers. commun. 1990) has suggested this basic approach with one modification. In this method, a factor with an eigenvalue near to, but less than one, may be retained if it explains five or more percent of the cumulative variance in the data set. Factor retention is particularly recommended if the added factor can be readily explained in light of some geological process or information. The modified approach of Hawkins was followed in the factor analysis of the data subsets of this study.

Tables 15 and 16 list rotated factor loadings and factor scores for the major oxides and trace elements. The factor loading is the numerical entry under each factor column which corresponds to the listed variable. The magnitude of the factor loading indicates the importance of that factor in explaining the the variance of the variable in the data set; the square of the factor loading is the percentage variance of the variable explained by the factor. Factor loadings  $> \approx 0.39$  ( $\approx 15\%$  of variance explained) are typically selected (Rose et al. 1979) as those loadings important for the attachment of a real parameter to the factor. The sign of the factor loading is relative; for instance, if the real parameter is based on factor loadings with negative signs, then factor loadings of positive sign will be negatively correlated with this factor and vice versa. The factor score can be thought of as a quantitative measure of the variable about a factor mean value (D. Hawkins pers. commun. 1990). A factor score of 0 signifies equality with the factor mean, factor scores of 1 and -1 indicate, respectively, one positive standard deviation and one negative standard deviation from the factor mean. Also shown in the tables are the factor communalities. The

**Table 15** Factor loadings and scores for the major oxide data.

Rotated Factor Loadings					
Variable	Factor 1	Factor 2	Factor 3	Factor 4	Communality
Al <sub>2</sub> O <sub>3</sub>	0.2811	0.3131	0.6128	0.5569	0.8627
CaO	0.8480	-0.1139	0.3031	0.3564	0.9509
Fe <sub>2</sub> O <sub>3</sub>	0.4078	0.0295	-0.0250	0.8808	0.9437
K <sub>2</sub> O	-0.7731	-0.4455	-0.3070	-0.2836	0.9708
Log LOI	0.1424	0.9536	0.1508	0.0680	0.9571
MgO	0.8772	0.1113	0.1559	0.3975	0.9641
Na <sub>2</sub> O	-0.0614	-0.9373	0.0499	-0.0911	0.8930
P <sub>2</sub> O <sub>5</sub>	0.1301	-0.0184	0.9513	0.0071	0.9223
SiO <sub>2</sub>	-0.5454	-0.2924	-0.4428	-0.6413	0.9904
TiO <sub>2</sub>	0.8199	0.4944	0.0066	-0.0014	0.9168
MnO	0.9320	0.0147	0.0695	0.3114	0.9706

Factor Scores					
Sample	Factor 1	Factor 2	Factor 3	Factor 4	
A1.2A	-0.97	-0.32	-0.70	0.40	
A1.2C	-0.47	0.37	1.08	-0.09	
A1.2D	-0.13	-0.94	-0.04	-0.03	
A1.2E	0.20	-0.42	0.49	-0.24	
A1.3P	-0.77	-0.71	0.72	-0.89	
A1.3R	-1.40	0.06	-0.66	1.42	
A1.3U	-0.57	-1.30	0.02	-0.40	
A1.3W	-0.82	-0.16	0.26	-0.75	
A1.3Y	-0.77	-0.76	0.22	-0.30	
A2.1CZ	-0.55	1.14	0.10	-1.03	
A2.1WZ	-0.51	-0.05	-0.93	-0.53	
A2.1O	0.36	-0.93	-0.97	0.70	
A3.4C	-0.00	2.36	1.83	0.33	
A3.4B	0.36	1.18	-0.93	2.83	
A3.4P	-0.35	0.91	-1.10	-0.64	
A5.1S	0.98	0.74	-0.84	-0.66	
A6.7U	2.40	0.58	-1.45	-1.43	
A7.2P	1.94	-1.75	0.85	1.13	
A7.2R	1.10	-0.00	2.06	0.18	

communality is the percentage cumulative variance of a variable explained by the factors and is equal to the sum of the squared factor loadings for that variable.

The factor loadings and factor scores were used to attach preliminary geological parameters to the factors. Factor 1 of the major oxides has very high positive loadings on Ca, Mg, Mn, and Ti and a moderate positive loading on Fe. It also possesses high negative loadings on Si and K. This factor is interpreted as reflecting a mafic mineral component.

**Table 16** Factor loadings and scores for the trace-element data.

Variable	Rotated Factor Loadings				Communality
	Factor 1	Factor 2	Factor 3	Factor 4	
Log As	0.7099	-.2029	0.1423	-.5263	0.8424
Ba	-.8756	0.3043	0.1367	0.0465	0.8801
Log Br	-.0442	0.1444	0.0386	-.8803	0.7992
Ce	-.8141	0.1656	-.4311	-.0527	0.8789
Cr	0.0415	0.0226	0.8793	-.0777	0.7814
La	-.9067	0.2192	-.2862	-.1507	0.9748
Rb	-.7834	0.4332	0.0834	0.0727	0.8137
Log Sb	0.2867	-.5045	0.4847	-.5004	0.8222
Sc	0.5672	-.6671	-.2454	0.2217	0.8761
Sm	-.8320	-.0177	-.3497	-.1672	0.8428
Th	-.8292	0.5280	0.0433	0.0273	0.9689
U	-.8239	0.5030	0.0190	0.0943	0.9411
Log Cu	0.1285	-.7267	-.3194	0.3453	0.7658
Log Ni	0.1910	-.7839	0.2927	-.0523	0.7393
Log Pb	0.1365	-.8447	0.1790	-.2157	0.8107
Log Zn	0.2378	-.8650	-.0774	0.1568	0.8353
Li	-.7492	-.1004	0.2494	0.3291	0.7419
Sample	Factor Scores				
	Factor 1	Factor 2	Factor 3	Factor 4	
A1.2A	-.87	0.36	-.99	-.32	
A1.2C	-.28	-.38	-1.29	0.58	
A1.2D	-.48	0.36	-.23	0.24	
A1.2E	-.26	0.25	-.71	0.24	
A1.3P	-1.04	0.45	-.05	-.19	
A1.3P <sub>ur</sub>	-.76	-.02	1.28	-.80	
A1.3R	-1.00	-.51	-.88	0.13	
A1.3U	-1.01	0.06	-.33	0.31	
A1.3W	-.43	0.96	0.45	0.16	
A1.3Y	-.68	0.65	0.10	0.11	
A1.4P	1.26	-1.57	-.02	-2.34	
A2.1CZ	-.28	1.42	0.35	-.24	
A2.1P	-.13	-.17	2.70	-.49	
A2.1R	-.38	-.06	0.64	0.58	
A2.1WZ	-.45	1.07	0.35	-.14	
A2.1O	-.53	-.37	1.06	1.12	
A3.4C	1.86	0.27	-1.26	2.05	
A3.4B	-.56	-1.74	-2.19	-1.15	
A3.4P	0.02	1.29	-.48	0.26	
A5.1S	-.72	-.08	-.32	-1.01	
A6.7U	1.97	0.71	-.47	0.63	
A7.2B	2.33	1.51	0.24	-2.06	
A7.2P	0.20	-2.55	0.98	0.32	
A7.2R	1.39	-.78	0.07	0.06	
A7.2W	0.83	-1.13	1.02	1.96	

High positive factor scores are found for the upper VTTS samples where the altered ejecta is more mafic and contains a greater concentration of mafic mineral phenocrysts. The highest positive factor score is observed for the least visibly altered sample (A6.7U). This suggests that factor 1 is indicative of the chemistry of the matrix upon which the encrustations are forming. All but two of the lower VTTS encrustation samples exhibit moderate to high negative factor scores. This is expected since the lower VTTS encrustations are forming on Si- and K-rich, mafic-mineral-poor rhyolitic ejecta.

Factor 2 shows an extremely high positive loading for Log LOI, in fact, 91% of the variance in the LOI data is accounted for by this factor. Positive factor scores are found for this variable in both the upper and lower VTTS encrustation samples. This factor represents a hydration effect; aqueous reactions leading to the formation of hydrous crystalline and amorphous phases are responsible for the high positive factor scores. The moderately positive factor loading for Ti implies that Ti is fairly immobile and is concentrated during these reactions relative to more soluble phases. About 10% of the variance in the Al data set can also be explained by this mechanism. In contrast, Na exhibits an extremely high negative correlation (high negative factor loading) with LOI as was previously observed in the correlation matrix. Eighty-eight percent of the variance in the Na data set can be accounted for by this factor. This is further evidence that Na is soluble during these reactions and is prone to removal from the fumarolic deposits and glass matrix. Nearly 20% of the variance in the K data can also be accounted for by this mechanism.

Positive loadings on factor 3 explain about 38% and 91% of the variance, respectively, in the Al and P data. Positive factor scores are observed throughout the VTTS samples. Hildreth (1983) has reported that some of the ubiquitous plagioclase phenocrysts within the VTTS ejecta contain inclusions of apatite. Apparently, these apatite inclusions can account for nearly all of the variance in the P data. The highest positive factor scores are consistently found in encrustation samples taken from the central (A3.4C, A1.2C, A1.3P) or near-central

(A7.2R) portions of the fumarolic conduit. Keith (1991) notes that the most extensively altered VTTS ejecta are found immediately adjacent to the main fumarolic conduit. This suggests that factor 3 represents the dissolution of apatite-bearing plagioclase phenocrysts and the release of P and Al for possible incorporation into the encrustation phases.

A large fraction of the variance of Fe, and smaller amounts of the variance of Al and Mg can be accounted for by their positive loadings on factor 4. Positive factor scores are noted in the encrustation samples which, by their color (e.g., orange, red, black) or XRD patterns, are thought to contain Fe-oxides. Minor amounts of Al and Mg are probably co-precipitated with these Fe-oxides. The moderately high negative factor loading for Si indicates its exclusion from these Fe-oxide phases. Negative factor scores are found in samples where there is no sign of the presence of Fe-oxides.

A four factor solution was also selected for the trace elements. To see if any of these factors correlate with the major oxide factors, another statistical technique known as canonical correlation was employed. Canonical correlation is a multivariate technique with the same computational basis as factor analysis but which is closely related to multiple regression (Davis 1986). Canonical correlation examines the relationship between a set of X variables (in this case the trace elements) and Y variables (the major oxides) and attempts to find linear combinations of the X and Y variables that give the highest correlation between the two data sets. These linear combinations are known as canonical variables (Davis 1986). In other words, this technique can be used to decide whether any of the major oxide factors are the same as those selected by the trace element factor solution model.

Tests for canonical correlation were conducted using the BMDP statistical package available on the University of Alaska Fairbanks VAX computer system. Separate computer runs were done to check for correlation between the four trace element factors and each of the four major oxide factors - a total of 16 computer trials. Statistically significant correlation

was found between factor 1 of the major oxides with factor 2 of the trace elements and for factor 4 of the major oxides with factor 1 of the trace elements.

Two different tests can be used to evaluate the significance of the canonical correlation. These will be examined for the canonical correlation between factor 1 of the major oxides and factor 2 of the trace elements. Bartlett's Test for Remaining Eigenvalues (Table 17) indicates the statistically significant number of canonical variables necessary to express the dependency between the two sets of variables. As the data in Table 17 show, at an  $\alpha$  of 0.01, one canonical variable (i.e., one canonical variable for the first set of variables and one canonical variable for the second set of variables) would be considered necessary for the example case. The squared multiple correlations of each variable in one set with all the other variables in the other set can also be used to test the significance of the canonical correlation. All of the squared multiple correlations of each variable in factor 1 of the major oxides with all variables of factor 2 of the trace elements are significant at an  $\alpha$  of  $\leq 0.05$  (Table 17). Similarly, all squared multiple correlations of each variable in factor 2 of the trace elements with all variables of factor 1 of the major oxides are significant at an  $\alpha$  of  $\leq 0.07$ . A cross-plot of the canonical variable for factor 1 of the major oxides against the canonical variable for factor 2 of the trace elements (Figure 32) shows the nearly perfect ( $R^2 = 0.994$ ) linear relationship between these two sets of variables.

The correlation of these two factors is explainable in view of the matrix chemistry parameters previously proposed for factor 1 of the major oxides. The factor loadings suggest that about 57% of the variance of Ni and Cu and approximately 73% of the variance of Pb and Zn can be accounted for by the encrustation matrix chemistry. With one exception, the largest positively correlated factor scores (negative in sign) correspond to the mafic mineral richer upper VTTS ejecta. In addition, some of the lower VTTS samples show minor positive correlations with this factor. All of these are from samples whose colors suggest they contain hematite and/or magnetite. Therefore, a minor amount of isomorphic substitution



**Table 17 Example of statistical parameters for canonical correlation.**

<b>Bartlett's Test for Remaining Eigenvalues</b>		
Number of Eigenvalues	1 Tail Probability	
	0.0007	
1	0.2053	
2	0.5882	
3	0.7916	
4	0.7538	
5	0.8093	
6	0.6396	
<b>Squared Multiple Correlations</b>		
<b>Each Variable In First Set With All Variables In Second Set</b>		
Variable	R <sup>2</sup>	Probability Value
CaO	0.958	0.0000
Fe <sub>2</sub> O <sub>3</sub>	0.779	0.0417
K <sub>2</sub> O	0.955	0.0001
MgO	0.947	0.0001
MnO	0.884	0.0035
SiO <sub>2</sub>	0.891	0.0028
TiO <sub>2</sub>	0.800	0.0286
<b>Squared Multiple Correlations</b>		
<b>Each Variable In Second Set With All Variables In First Set</b>		
Variable	R <sup>2</sup>	Probability Value
Rb	0.900	0.0001
Log Cu	0.635	0.0660
Log Sb	0.631	0.0690
Log Ni	0.860	0.0006
Sc	0.958	0.0000
Th	0.943	0.0000
Log Zn	0.739	0.0141
U	0.956	0.0000
Log Pb	0.853	0.0008

of elements like Cu and Ni for Fe probably occurs in the VTTS encrustations. An alternative explanation is that the Cu, Ni, Pb, and Zn data variances reflect the presence of tiny sulfide inclusions containing these elements in primary magnetite crystals. This explanation is not favored, because although Ramdohr (1962) observed tiny sulfide inclusions in a few VTTS magnetite crystals, Keith (pers. commun. 1990), in a more comprehensive study of the VTTS encrustations, has not been able to verify their presence.

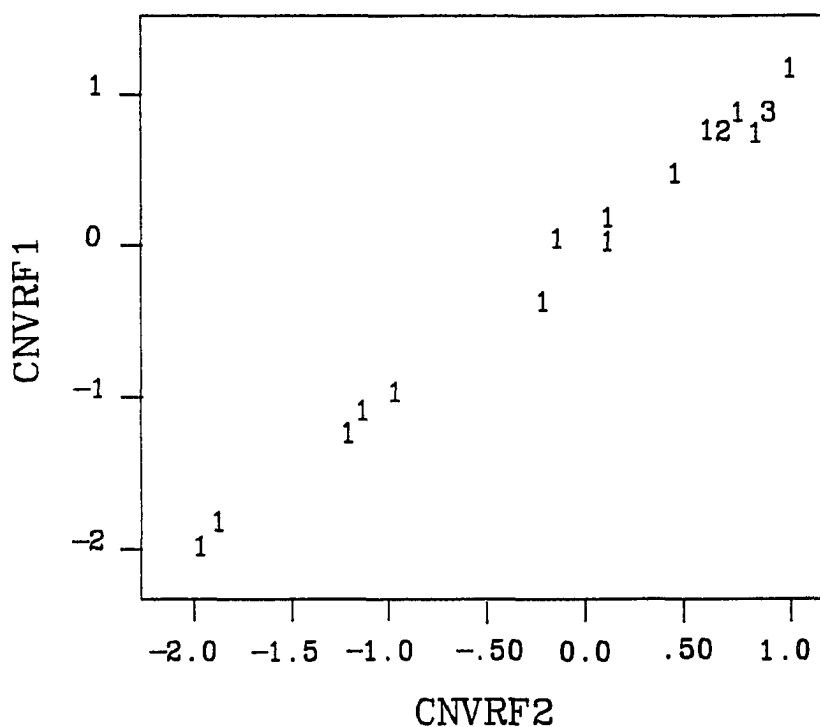


Fig. 32 Cross-plot of the canonical variable derived from factor 1 of the major oxides (CNVRF1) against the canonical variable derived from factor two of the trace elements (CNVRF2).  $R^2 = 0.994$ . Numerals correspond to the number of plotted points.

The correlation of factor 4 of the major oxides with factor 1 of the trace elements (Figure 33) can be explained by considering this as an iron oxide/altered ash factor. The lithophile elements, including the Rare Earths, of this factor correlate positively with  $\text{SiO}_2$  and  $\text{K}_2\text{O}$  but correlate negatively with the rest of the major oxides of the factor. This implies that the source of these elements is the volcanic glass of the ejecta. The range of negative factor scores for the trace-element subset suggests that the volcanic glass has experienced various degrees of alteration. The highest positive factor scores are found for

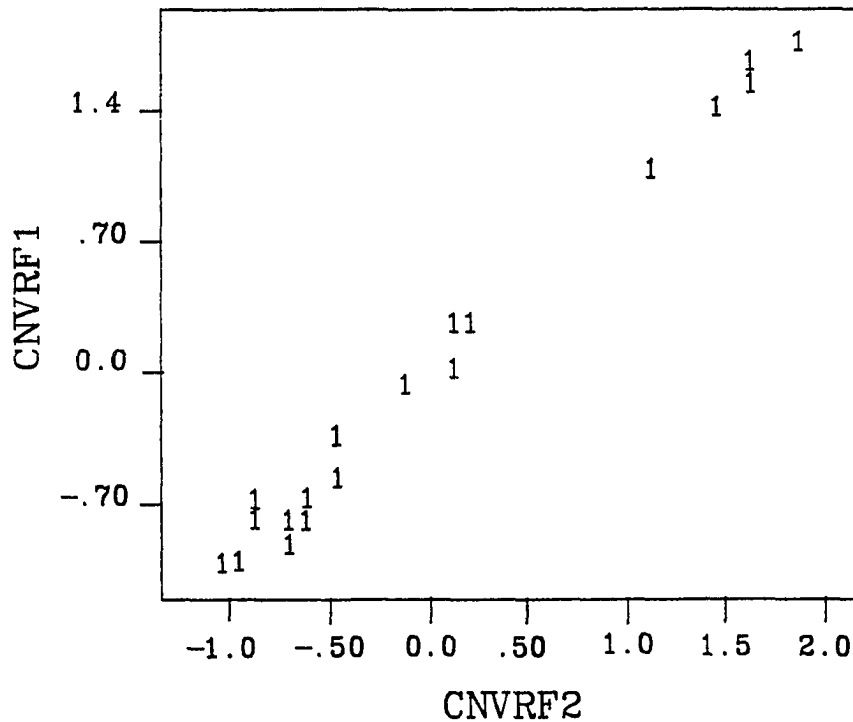


Fig. 33 Cross-plot of the canonical variable derived from factor 4 of the major oxides (CNVRF1) against the canonical variable derived from factor 1 of the trace elements (CNVRF2).  $R^2 = 0.986$ . Numerals correspond to the number of plotted points.

samples (with one exception) with probable high iron oxide (mostly hematite) content. Fe-bearing acidic solutions probably leached the volcanic glass and phenocryst phases and subsequently precipitated the Fe-oxide phases. It appears that approximately 50% of the variance of As can be accounted for by co-precipitation of As with the Fe-oxides.

Factors 3 and 4 of the trace elements do not exhibit statistically significant canonical correlations with any of the major oxide factors. Chromium has a very high positive loading on factor 3. Antimony also possesses a moderately positive loading on this factor. While

these are the only important positive loadings, Ni, Pb, Li, As and Ba show minor positive loadings on factor 3. Since Cr in fumarolic deposits is thought to be derived by the attack of acidic condensate on fumarolic wall rock, this distribution of elements may reflect their relatively high mobilities in aqueous solutions as halide complexes. The moderately negative loading for Ce, and the other elements with negative loadings, suggest that the transport of these species as aqueous halide complexes was not important. However, Cu and Zn load negatively on this factor, and it is hard to imagine conditions where these elements would be immobile as halide complexes while Cr, Sb, Ni and Pb would be mobile as halide complexes. Therefore, the interpretation of the factor 3 trace-element loadings may be incorrect.

Factor 4 of the trace elements has important negative loadings for Br, As, and Sb. These three elements are highly volatile as gaseous halides. Approximately 25% of the variance of As and Sb, and about 78% of the variance of Br can be accounted for by this factor. These data, as well as the previously discussed enrichment factor patterns, support that vapor phase transport of As, Sb, and Br was significant in the VTTS fumaroles.

## Discussion

Factor analysis and canonical correlation of the VTTS encrustation chemical data not only corroborated the chemical trends exhibited in the univariate statistics, but these multivariate statistical techniques suggest that nearly all (low of 74% for Li to high of 99% for Si) the variance in the encrustation chemistries can be explained by six factors. The percentage of the element and oxide variance (the squared factor loadings of Tables 15 and 16) explained by these factors is given in Table 18.

Inspection of the sample factor scores was useful in attaching reasonable geological mechanisms to the factors. Apparently, the largest amount of the data variance for CaO,

K<sub>2</sub>O, TiO<sub>2</sub>, MnO, Sb, Sc, Cu, Ni, Pb and Zn is the result of natural variation in the chemistry of the ejecta on which the encrustations formed. This interpretation is supported by Keith's (1991) observations that the VTTS encrustations are impure samples that typically include 50 - 90% ejecta in various stages of alteration. In addition, since a large majority of the variance in the data of Ni, Cu, Pb and Zn are explained by this factor, this suggests that the galena, sphalerite and copper sulfides observed in the VTTS fissure vents in 1923 by Zies (1929) have been effectively removed from the VTTS deposits. Effective dissolution of these phases would also explain why none of them were detected in fifty XRD analyses of the encrustations.

The plagioclase/apatite dissolution factor illustrates the efficiency of the fumarolic fluids in altering the ejecta. Nearly all the variance (91%) in the P data and a significant amount (38%) of the variance in the Al data can be explained by the dissolution of apatite inclusions in plagioclase phenocrysts present in the ejecta. This interpretation is supported by the observations that the highest positive factor scores for this factor are found in samples taken from the central, most altered portions of the fumarolic conduits, and that none of the X-rayed samples exhibited apatite patterns.

The correlation of factor 4 of the major oxides with factor 1 of the trace elements probably indicates alteration of the ejecta to various degrees by Fe-rich acidic solutions coupled with subsequent precipitation of Fe-oxides. Solutions of this nature would have been formed as the fumaroles cooled to the point where condensation of acidic vapors could take place. Primary fumarolic magnetite dissolved by the acidic condensate would have contributed Fe to these solutions. Seventy-seven percent of the variance in the Fe data can be explained by this factor. Close to 50% of the As data variance can be accounted for by co-precipitation of As with the Fe-oxides. Keith (1991) has reported that As and Fe are often enriched in the encrusted VTTS dacitic fallout relative to the underlying leached ash-flow tuff. The data of Keith (1991) therefore support the interpretation of this factor.

**Table 18 Percentage of data variance explained by individual factors.**

Variable	Selected Factor and Percentage Data Variance Explained					
	Matrix Chemistry	Hydration/ Leach	Plag/Apatite Dissolution	Fe-oxide/ Leach	Vapor Transport	Resistant Cr/Leach
Al <sub>2</sub> O <sub>3</sub>	7.9	9.8	37.6	31.0	—	—
CaO	71.9	1.3	9.2	12.7	—	—
Fe <sub>2</sub> O <sub>3</sub>	16.6	0.09	0.06	77.6	—	—
K <sub>2</sub> O	59.8	19.8	9.4	8.0	—	—
Log LOI	2.0	90.9	2.3	0.46	—	—
MgO	76.9	1.2	2.4	15.5	—	—
Na <sub>2</sub> O	0.4	87.8	0.25	0.82	—	—
P <sub>2</sub> O <sub>5</sub>	1.7	0.03	90.5	0.00	—	—
SiO <sub>2</sub>	29.7	8.5	19.6	41.1	—	—
TiO <sub>2</sub>	67.2	24.4	0.00	0.00	—	—
MnO	86.9	0.02	0.48	9.7	—	—
Log As	4.1	—	—	49.1	27.7	2.0
Ba	9.2	—	—	76.7	0.2	1.9
Log Br	2.1	—	—	0.20	77.5	0.1
Ce	2.7	—	—	66.2	0.28	18.6
Cr	0.05	—	—	0.17	0.60	77.3
La	4.8	—	—	82.2	2.3	8.2
Rb	18.7	—	—	61.4	0.50	0.70
Log Sb	25.4	—	—	8.2	25.0	23.5
Sc	44.5	—	—	32.2	4.9	6.0
Sm	0.03	—	—	69.2	2.6	12.2
Th	27.8	—	—	68.8	0.07	0.20
U	25.3	—	—	67.9	0.89	0.04
Log Cu	52.8	—	—	1.7	11.9	10.2
Log Ni	61.4	—	—	3.6	0.3	8.6
Log Pb	71.4	—	—	1.9	4.6	3.2
Log Zn	74.5	—	—	5.6	2.5	0.6
Li	1.0	—	—	56.1	10.8	6.2

The univariate statistics indicated that Cr exhibits virtually no correlation with any of the other analyzed elements or oxides in the VTTS encrustations. Factor analysis revealed that Cr has a very high positive loading on factor 3 of the trace elements. Slightly over 77% of the Cr data variance can be accounted for by this factor. Antimony (23% of variance explained) is the only other trace element which has even a slightly positive loading on this factor. This factor has been tentatively interpreted as representing another leaching event. Keith (1991) has shown that Cr is often extremely depleted in the VTTS ash-flow

tuff immediately adjacent to the fumarole walls, indicating that Cr is mobilized from the tuff by the fumarolic fluids.

The enrichments of Cr in the samples of this study (as shown by the positive factor scores of Table 16) exhibit no consistent spatial distribution. These Cr enrichments suggest that Cr may now be present in the VTTS encrustations as a weather-resistant (oxide) trace mineral or as a trace element in a weather-resistant phase. Other elements originally transported with the Cr but deposited as less chemically-resistant phases would be preferentially removed from the encrustations by subsequent weathering. The elemental enrichment factors support such reactions taking place. This is further evidence that the chemical patterns in the VTTS encrustations are the result of a complex series of primary and secondary alteration processes.

Additional evidence of the solubility of some of the encrustation chemical components is shown by the hydration/leach factor. Nearly all of the LOI variance is explained by this factor. X-ray data are available for five samples (A1.3R, A3.4C, A3.4B, A6.7U, A7.2R) which have positive factor scores for this factor. Within the detection range of the X-ray equipment, three of these samples are amorphous, one contains only  $\alpha$ -cristobalite, and one contains only hematite (Appendix 1). This implies that a low-temperature hydration and leaching encouraged the formation of hydrated amorphous phases. Nearly all the variance in the Na data and about 20% of the variance in the K data can be explained by the leaching of primary soluble (e.g., halides, sulfates) phases. Some of the soluble Na and K may also be derived from hydration of the glass ejecta. A sizable portion ( $\approx 25\%$ ) of the data variance for Ti and lesser amounts of the variances of Al and Si can be explained by these elements becoming locally enriched in the encrustations, relative to the more soluble phases, during the hydration/leach process.

Factor 4 of the trace elements illustrates that the VTTS encrustations preserve a signature of significant vapor phase element transport. Close to 78% of the data variance of

Br and nearly 25% of the data variances of As and Sb are explained by this factor. The high loading of Br on this factor suggests that As and Sb were transported in the vapor phase as halide or oxyhalide species. The observation by Keith (1991) of Cl enrichment in the intensely leached walls of two representative VTTS fossil fumaroles also supports this idea. Keith (1991) proposes that residual magmatic volatiles (e.g., SO<sub>2</sub>, H<sub>2</sub>S, F, Cl) were released from the ash-flow tuff through glass devitrification and subsequently incorporated into the fumarolic gases.

The highest positive factor scores for the vapor phase transport factor are found in three dark purple to dark black encrustation samples (A1.4P, A3.4O, A7.2B). Keith (1991) reported that vapor phase magnetite typically imparts the black colors to the cores of the magnetite-rich VTTS fumaroles. Two of the high factor score samples (A1.4P and A3.4B) were X-rayed. Magnetite was tentatively identified in sample A1.4P, while sample A3.4B is apparently amorphous (Appendix 1).

The data of this study and that of Keith (1991) thus confirm that the VTTS fossil fumarolic encrustations are mostly composed of relatively insoluble secondary minerals and amorphous phases. Univariate and multivariate statistical analysis reveals that the encrustation chemistries integrate a complex history of primary and secondary fumarolic processes and weathering reactions. The factor analysis and canonical correlation proved to be useful in sorting out the elements with similar geochemical behaviors. Even after 40-75 years of weathering, the VTTS fossil fumarolic encrustations still preserve a signature of the processes responsible for their formation and evolution. These data indicate that the fossil fumarolic encrustations are valuable, especially when integrated with the earlier VTTS encrustations studies, for evaluating the long-term evolution of fumarolic deposits.

The current VTTS fossil fumarole chemical data base does not appear to be appropriate for quantitative modeling of epithermal ore-forming processes. Data from this study show



that the fossil fumarole primary encrustations have been severely degraded by a series of low-temperature leaching and weathering processes.

The advanced argillic alteration assemblages abundant in the warm ground patches of Novarupta Basin are consistent with mineral alteration patterns associated with volcanic rock-hosted precious metal ore deposits. Unfortunately, there are no active, high gas flux fumaroles in Novarupta Basin that can be sampled to evaluate whether epithermal ore element deposition may have been initiated beneath Novarupta. One sample collected from a supergene alteration zone surrounding a low-temperature Novarupta Basin fumarole yielded a highly anomalous gold concentration (7.36 ppm). However, a second analysis of this sample exhibited only a background Au concentration. Interestingly, a sample split from this site contained one of the highest  $\text{Hg}^0$  concentrations (4501 ppb) found in the surficial  $\text{Hg}^0$  survey, confirming that some degree of vapor phase elemental transport is actively occurring beneath Novarupta. Two moderately Au-anomalous samples (150 ppb, 160 ppb) and one slightly Au-anomalous sample (27 ppb) suggest that Au mobilization and deposition did occur in the other VTTS fumaroles, including the fossil systems.

The problem in using bulk encrustations from the VTTS to model epithermal ore-formation lies in trying to differentiate the magnitude and efficiency of the various fumarolic mechanisms responsible for element transport and concentration. Degradation of the fossil fumarolic encrustations by weathering has further complicated the problem. In addition, since the bulk encrustations vary in their degree of purity, a method for subtracting out the contribution of ejecta to the elemental concentration patterns would be necessary.

The best hope of using the VTTS fossil fumarolic encrustations to further model epithermal ore deposition apparently rests with the primary fumarolic magnetite. Since the vapor phase magnetite typically exists as a very thin coating coating on fallout clasts (Keith 1991), large volume sample collection followed by magnetite concentration would be necessary before wet chemical analysis. Magnetic separation processes, together with

heavy-liquid concentration, may provide enough suitably pure magnetite for wet chemical analysis. Non-destructive (electron microprobe) or partially destructive (ion microprobe) analysis could be undertaken on much smaller amounts of isolated magnetite or even the magnetite-encrusted ejecta. The ion microprobe and electron microprobe methods, however, have significantly higher detection limits for most metals and metalloids compared to the wet chemical techniques. If an accurate determination can be made from the magnetite samples of the magnitude of vapor phase metal/metalloid transport and deposition, then bulk encrustation data from the fossil fumaroles could be used to assess the amount of metals/metalloids potentially remobilized from the fumarolic deposits by low-temperature alteration and/or weathering processes.

## CHAPTER 6:

### DISCUSSION AND CONCLUSIONS

---

The Mount St. Augustine volcanic/magmatic system appears to possess some unique characteristics. The restored composition of a 1987 gas sample collected from a summit rooted fumarole at Mount St. Augustine by Symonds et al. (1990) contained HCl in a concentration an order of magnitude greater than that in any previously reported volcanic gas analysis. Chlorine concentrations in crystal-hosted glass inclusions (Johnston 1980), and chlorine contents retained in degassed pumices (Johnston 1980, this study) from Mount St. Augustine's eruptive products, are also the highest ever reported for a volcanic center. The 1979-1984 gas chemistry and condensate stable isotope data of this study suggest that seawater is a possible source of these anomalously high Cl concentrations.

The Mount St. Augustine gas data suggest that the  $fO_2$  of the high-temperature fumarolic emissions increased dramatically from 1979 (near NNO) to 1984 ( $\approx 1.5$  to 2 log units above NNO). To the author's knowledge, such a trend has not been reported from any other volcano. This work contends that the increase with time in gas  $fO_2$  is due to open system cooling of the gases in a more oxidizing environment resulting from seawater influx into Mount St. Augustine's volatile source region. Symonds et al. (1990) observed that two restored 1987 high-temperature fumarolic gas samples from Mount St. Augustine have  $fO_2$  values near NNO; these values are very similar to the  $fO_2$  values of the 1979 and 1982 gases. Whether the  $fO_2$  of the high-temperature fumarolic gases will increase following the 1986 eruption of Mount St. Augustine is an interesting question. Discovery of a cyclicity in the high-temperature gas  $fO_2$  may shed additional light on Mount St. Augustine's post-eruptive magmatic processes. If changes in the high-temperature gas  $fO_2$

are found to be consistent, then monitoring of the high-temperature gas  $fO_2$  could possibly serve as another volcanic hazard forecasting tool for this site.

A number of independent lines of evidence support a phreatomagmatic component in the eruption mechanism of Mount St. Augustine. This study proposes that a seawater-magma interaction may actually trigger some of the early explosive phases of Mount St. Augustine's eruptive cycle. The gas and stable isotope data apparently indicate that seawater influences the high-temperature fumarolic emissions long after Mount St. Augustine's eruptive cycle is complete. The gas chemistries suggest that resupply of magma to any near-surface storage chamber through 1984 (the last sampling period prior to the 1986 eruption) was insignificant.

In summary, the 1979-1984 gas chemistry trends and condensate stable isotope patterns are best explained by continued outgassing of a small volume of near-surface unerupted magma coupled with an increase in the proportions of seawater in the high-temperature fumarolic emissions. If Mount St. Augustine's volcanic/magmatic system is significantly influenced by seawater-magma or seawater-gas interaction, then the question must be raised as to why Mount St. Augustine would be prone to subvolcanic seawater infiltration. As previously described, Mount St. Augustine is built upon uplifted continental basement and its volcanic edifice is deeply fractured. Large-scale tectonism may have produced an extensive subvolcanic fracture system.

Large-scale tectonic forces may be concentrated near Mount St. Augustine as a result of where it is situated in the Aleutian arc. Kienle and Swanson (1983) reported that the alignment of volcanoes in the eastern Aleutian arc indicates that this portion of the Aleutian arc is segmented. The two main segments, the Cook and Katmai segments, are offset by approximately  $35^\circ$  (Kienle and Swanson 1983). Although the exact segment boundary is not known, Mount St. Augustine lies near the projected point of intersection of the Cook and Katmai trends. Fisher et al. (1981) include Mount St. Augustine in an arc-transverse

tectonic zone between the two segments, and Kienle et al. (1983) have proposed Mount St. Augustine as a segment boundary volcano.

According to Fisher et al. (1981), arc-transverse tectonic boundaries are characterized by large-scale crustal disruption (e.g., fracturing) in the subducting plate. However, Kienle and Swanson (1983) contend that since subduction is oblique in the eastern Aleutian arc, fracturing of the subducting plate should not create any localized zones of disruption in the overlying plate. Kienle and Swanson (1983) also report that the overriding plate in this portion of the Aleutian arc possesses a brittle top layer characterized by diffuse seismicity. Although the current evidence suggests that warping of the subducting plate would not generate a significant shallow fracture system beneath Mount St. Augustine, it is an intriguing possibility that the unique gas signatures of this volcano are somehow related to its location near a tectonic plate segment boundary.

Study of the Mount St. Augustine rooted fumaroles shows that an integrated approach, combining thermodynamic evaluation of gas chemistries with gas and condensate stable isotope analyses, will produce the most valid and interpretable fumarolic emissions data. As an example, thermodynamic modeling of the 1984 NaOH gas samples implied that the CH<sub>4</sub> measured in sample 84A4 was from a nonmagmatic source. Stable isotope values of the gas ( $\delta^{13}\text{C} - \text{CH}_4$ ,  $\delta^{13}\text{C} - \text{CO}_2$ ) and condensate ( $\delta^{18}\text{O} - \text{H}_2\text{O}$ ) from this vent provided independent, corroborating evidence that the source of the CH<sub>4</sub> was nonmagmatic. Since most, if not all, sampled gases are chemical disequilibrium assemblages, raw gas data should never be interpreted without prior testing of the equilibrium hypothesis.

Numerous rootless fumaroles formed on pyroclastic flows and a lava flow soon after their emplacement during the 1986 eruptive cycle of Mount St. Augustine. The location and morphology of the rootless fumaroles were controlled by pre-eruption drainage and topography, and by compaction and settling of the flow deposits. Varying amounts of encrustations were observed around every fumarolic conduit type. Since the encrustations were collected from

active vents, it was easier to provide a more pure, less degraded sample for analysis than when encrustations are collected from fossil fumaroles. Sulfates and native sulfur are the most abundant crystalline encrustation phases. Cl-rich, hydrated amorphous phases are also abundant in the encrustations. Many of these amorphous phases are metastable and upon cooling of the fumarole lose non-structural water and crystallize to more stable forms.

The high halogen contents of the rootless fumarolic condensates (Symonds et al. 1990), and the mineralogy, chemistry, and morphology of the encrustations support leaching of the andesitic ash and lava flow as the primary source for the chemical components contained in the encrustations. The chemical data suggest that zinc, and to a lesser degree cobalt and nickel, were transported in the vapor phase, probably as halide species. Apparently, some trace-element distributions in the encrustation phases were controlled by isomorphic substitution for major elements.

Unfortunately, the 1986 Mount St. Augustine eruptive deposits degassed too rapidly to allow suitable gas samples to be collected concurrently with encrustations from the rootless vents. As discussed in Chapter 3, encrustation chemistries of the 1986 rootless fumaroles cannot be directly compared to the gas chemistries of the 1979-1984 summit rooted fumaroles. However, the rapid cooling of the 1986 eruptive deposits, and therefore the short time period over which volatile element transport and concentration processes could have taken place, suggests the encrustation chemistries can be used to interpret the nature of the rootless fumarolic gases. The relative abundance of S-rich and Cl-rich encrustation phases implies that the rootless fumarolic gases were also S- and Cl-rich. This interpretation is supported by analyses of condensates collected from three 1986 pyroclastic flow fumaroles (Symonds et al. 1990).

From a technical standpoint, the reconnaissance survey of  $\text{Hg}^{\circ}$  in the VTTS surficial deposits was very effective. No correlation was observed between the topography and  $\text{Hg}^{\circ}$  values at either the 5 cm or 15 cm sample depth along two Novarupta Basin sample

traverses. This indicates that downslope accumulation of  $\text{Hg}^{\circ}$  by particle creep or water percolation was negligible. Replicate sample analyses support that the  $\text{Hg}^{\circ}$  is homogeneously distributed within the sampled VTTS surficial deposits.

Statistically-derived  $\text{Hg}^{\circ}$  threshold and  $\text{Hg}^{\circ}$  contrast values allowed the differentiation between relict and actively accumulating  $\text{Hg}^{\circ}$  in the VTTS regolith. The restriction of high  $\text{Hg}^{\circ}$  contrast sites to Novarupta Basin, together with the presence of warm ground patches and minor, low-temperature fumarolic activity in this area, suggests that an incipient hydrothermal system has developed at shallow levels beneath Novarupta.

Results of this study, coupled with previously available geological and geophysical data, support the Turtle being underlain by an igneous intrusion. Based on the  $\text{Hg}^{\circ}$  data, the preferred Novarupta vent model is one generated by collapse of supporting vent walls after the major eruptive phase into a cored-out explosive vent. A series of deep-extending faults act as slip planes for the supporting vent walls. These faults subsequently serve as multiple pathways for  $\text{Hg}^{\circ}$  migration to the surface whereupon the  $\text{Hg}^{\circ}$  is concentrated in the regolith. The process of piecemeal vent wall collapse produces a funnel-like vent morphology with subsidence concentrated in the narrow funnel center.

Interpretation of more recently acquired geophysical (Goodliffe et al. 1991) and geological (Wallmann 1991) data from the Novarupta region supports both the presence of a shallow intrusion beneath the Turtle and the preferred vent model proposed from the  $\text{Hg}^{\circ}$  survey. These independent data confirm that volatile element surveys are a reliable, low-cost tool for the investigation of post-eruptive magmatic processes in the VTTS.

In the author's opinion, a rare opportunity was missed during the recent CSDP-sponsored investigations of the Novarupta vent region. The  $\text{Hg}^{\circ}$  data of this study suggested that near-surface amorphous silica deposits apparently are effective at preventing the migration of  $\text{Hg}^{\circ}$  to the surface. A detailed  $\text{Hg}^{\circ}$  survey, utilizing the same surveyed grid as the CSDP investigations, would have complemented the gravity and magnetic surveys of

the Novarupta vent region. Comparison of the geologic structures maps derived from these different studies could have shown which structures have been effectively silicified (i.e., low  $Hg^0$  contrast over the structures identified by the geophysical techniques). Such knowledge would be very useful in determining the nature and extent of a developing hydrothermal system beneath Novarupta.

Chemical patterns exhibited by the VTTS fossil fumarolic encrustations show that these deposits have been severely degraded from their primary state by secondary alteration and weathering processes. Surprisingly, even 40 - 75 years after the cessation of fumarolic activity, the fossil encrustations preserve a signature of a complex series of elemental transport, deposition and remobilization processes. Factor analysis suggests that vapor phase transport of the metalloids As and Sb, probably as halide or oxyhalide species, was significant in the VTTS fumaroles. The data enrichment factors imply that Pb, Cu, Zn, and Ni were also transported in the vapor phase, an interpretation supported by the observation of well-formed crystals of Cu- Pb- and Zn-sulfides in the VTTS early fumarolic deposits (Zies 1924, 1929). Unfortunately, as the fumaroles cooled, condensed acidic vapors effectively removed these deposits as well as the vast majority of the earlier-deposited vapor phase magnetite. The effectiveness of the dissolution reactions is illustrated by the factor analysis loadings; 53 - 75% of the data variance for Cu, Pb, Zn, and Ni in the analyzed bulk encrustations is apparently controlled by natural variation in the chemistry of the ejecta on which the encrustations are found.

Statistical analysis of the bulk encrustation data can help discern the various processes responsible for the evolution of the fumarolic deposits. These techniques, however, cannot be used to estimate the magnitude and efficiency of the various processes due to their complex overprinting. As proposed in Chapter 5, careful collection, concentration, and analysis of primary fumarolic magnetite still preserved in the VTTS fossil encrustations should enable identification of the concentration range of metallic/metalloid elements in



the magnetite. If an estimate can be made of the magnitude and efficiency of vapor phase metal/metalloid transport, then the bulk encrustation data of this study can be used to estimate the amount of metals/metalloids that were remobilized by secondary fumarolic alteration and weathering processes. Both sets of data are required to better constrain the role of fumarolic processes in epithermal ore formation.

Similarities were found between the encrustations collected from the active vents on the 1986 Mount St. Augustine eruptive products and the fumarolic deposits formed early in the cooling of the 1912 VTTS ash-flow sheet. At both of these locations, leaching of the ejecta by acidic fumarolic condensate provided the bulk of the chemical components for encrustation development. Sulfates and sulfur, the most abundant crystalline phases in the encrustations collected from active rootless fumaroles at Mount St. Augustine, were noted in significant amounts around active VTTS fumaroles in 1917 (Shipley 1920). Chlorides were present in large concentrations in the VTTS encrustations. Electron microscopy and EDAX scans identified minor amounts of a number of Cl-rich amorphous phases in the Mount St. Augustine encrustations, and halite was observed in an apparent sublimate sample.

Noticeable differences were also found between the Mount St. Augustine encrustations and the early-formed VTTS encrustations. Mounds, several feet high, of amorphous silica were common in the 1917 VTTS fumarolic deposits. Only minor amounts of tridymite were noted in the 1986 Mount St. Augustine encrustations. No vapor phase magnetite or sulfides, nor any of the more rare mineral phases observed in the 1917 and 1919 VTTS fumarolic deposits, were noted in the Mount St. Augustine encrustations. Extremely high F concentrations, up to 15 wt.% F, were found in the 1917 - 1919 VTTS encrustations. No fluoride mineral phases were noted in the Mount St. Augustine encrustations. However, F may have been present in some of the amorphous phases since the EDAX method used to scan these phases cannot detect F. Symonds et al. (1990) noted F contents of 50, 260, and

1100 ppm, respectively, in condensate from three 1986 Mount St. Augustine pyroclastic flow fumaroles. Many of the differences in the quantities, mineralogies and chemistries between the 1917 - 1919 VTTS encrustations and the 1986 Mount St. Augustine encrustations can be rationalized in terms of the physical characteristics of the VTTS and Mount St. Augustine pyroclastic deposits. The VTTS ash-flow fumaroles used for comparison to the 1986 Mount St. Augustine vents had already been active for up to seven years when they were sampled in 1917 and 1919. The 1917 and 1919 VTTS encrustations obviously integrated a much longer time period, compared to the 1986 Mount St. Augustine fumaroles, of element transport, deposition and remobilization processes. The VTTS vents were initially hotter than the Mount St. Augustine rootless fumaroles and, in general, their temperatures declined much less rapidly than the thin, non-welded pyroclastic flows of Mount St. Augustine. This suggests the Mount St. Augustine fumaroles experienced higher  $fO_2$  conditions compared to the young VTTS fumarolic vents.

In addition to the physical differences between the VTTS and Mount St. Augustine pyroclastic deposits, it is interesting to speculate whether bulk composition or fractionation trends in the respective magma chambers significantly influenced the chemistries of the fumarolic encrustations at these two sites. According to Smith (1979), all caldera-forming ash-flow sheets should show some degree of vertical compositional (chemical and/or mineralogical) zoning. Smith (1979) and Hildreth (1979) contend that the compositional zonation in the eruptive deposits reflects a similar compositional zonation in the large-volume silicic magma chambers prior to eruption. Hildreth (1979) postulates that the compositional zonation in the magma is produced by differentiation in the liquid state by the process of "convection-driven thermogravitational diffusion". In this mechanism, convection in the magma drives chemical diffusion in a nonisothermal multicomponent liquid. As this process continues, compositional zoning is established throughout the magma chamber. Hildreth (1979) speculates that this process results in the roofward migration and concentration of

volatile species/elements in the magma chamber and conversely, the downward enrichment of non-volatile species. As an example, H<sub>2</sub>O, Cl, F, Br, Nb, Sb, Mo, Sn, W, U and Th should be significantly enriched toward the magma chamber roof in this model, whereas Mg, P, Ti, Fe, Cu, Zr, Ba, Co and Au should be enriched downward in the magma chamber. Hildreth (1979) proposes that magmatic systems capable of producing large-volume ash-flows probably require 10<sup>5</sup> - 10<sup>6</sup> years for this differentiation to take place, but in small caldera-forming stratovolcanoes the differentiation process may be accomplished in approximately 10<sup>3</sup> years.

The VTTS ash-flow exhibits compositional zonation (Hildreth 1983, 1987). According to the convection-driven thermogravitational diffusion model, significant concentrations of roofward-enriched volatile species/elements should have been released during the emplacement and early degassing of the 1912 ash-flow sheet. It is reasonable to assume that the fumarolic encrustations should also exhibit high concentrations of many of these species/elements. The extremely high concentrations of F and Cl in the early-formed VTTS encrustations supports this model. As noted earlier, Zies (1929) reported that in 1919 small areas of the fumarolically altered ash-flow sheet contained 0.1 - 0.5 wt.% MoO<sub>3</sub> (≈670 - 3350 ppm Mo). Keith (1984) observed maximum Sn and Sb contents of 1000 ppm and 50 ppm, respectively, in the VTTS fossil fumarolic encrustations. No data exist for concentrations of W in the early-formed VTTS encrustations. Tungsten concentrations in the fossil fumarolic encrustations of this study vary greatly (nearly half of the analyzed samples contain W below detection limits); the maximum W concentration observed was 523 ppm.

In the convection-driven thermogravitational diffusion model, the magmas of volcanoes that frequently erupt small-volume pyroclastic flows should not have sufficient time to develop roofward enrichments of elements like Mo, W, Sn or Sb. Systems like Mount St. Augustine should therefore exhibit low concentrations in their fumarolic emissions and encrustations of the elements enriched roofward in the large-volume highly silicic magmas. Data for Mo, Sn, W or Sb concentrations do not exist for the 1986 Mount St. Augustine

rootless fumarolic encrustations. However, Symonds et al. (1990) observed that Mo, relative to unaltered 1986 ash, was enriched in condensate from the three 1986 pyroclastic flow fumaroles by a factor of nearly 630. In addition, Lepel et al. (1978) found the following maximum enrichment factors, calculated relative to 1976 ash chemistries, in aerosols collected from Mount St. Augustine's 1976 eruptive plumes: W - 11; Sb - 1820.

Similar geochemical behavior was observed at Merapi volcano. Merapi is a very active andesitic stratovolcano located in the Indonesian volcanic arc. Historically recent volcanic activity at this site has been characterized by successive extrusions of lava domes followed by glowing avalanches (LeGuern and Bernard 1982). Symonds et al. (1987) collected condensates, sublimates (collected in silica tubes) and encrustations from high-temperature summit fumaroles at Merapi. The maximum concentrations of Mo (1800 ppm), Sn (3000 ppm) and W (1700 ppm) are similar to (in the case of Mo) or significantly greater (in the case of Sn and W) than the concentrations of these elements observed in the early-formed VTTS encrustations (Zies 1929) and the VTTS fossil fumarolic encrustations (Keith 1984; this study). Maximum enrichment factors for these elements in the Merapi encrustations ranged from a low of 330 for Mo to a high of 5200 for W. Sublimates from this site possessed even larger concentrations and greater enrichments of Mo, W, and Sn (Symonds et al. 1987).

The preceding data illustrate some interesting points concerning ore-forming processes in igneous systems. The Augustine and Merapi data suggest that emanations from andesitic systems may be significantly enriched in elements (e.g., Mo, Sn, W, Sb) which are commonly thought to be preferentially enriched in more evolved, highly silicic magmas. If this is true, it implies that availability of abundant elemental complexing agents (e.g., hydroxyl groups, halides, oxyhalides) is more important than bulk magma composition or processes like thermogravitational diffusion in determining the type and amount of ore elements released by magmatic devolatilization. This hypothesis would be discredited if the Sn, Mo, W, and Sb concentrations in the VTTS encrustations were initially much higher than those observed

by Zies (1929), Keith (1984) and the author. This study indicates that the VTTS fumarolic deposits have been severely degraded by secondary alteration and weathering processes. Significant quantities of Mo, W, Sn, and Sb may have been removed from the initial VTTS fumarolic deposits, even by as early as 1919, if these elements were originally deposited as water-soluble compounds. Unfortunately, no trace-element analyses were conducted on the early-formed VTTS encrustations rich in F and Cl. More accurate knowledge of the magnitude and efficiency of vapor phase element transport in highly silicic systems is required to discern the critical factors controlling element concentration during magma devolatilization.

## CHAPTER 7:

### RECOMMENDATIONS FOR FUTURE WORK

---

The data of this thesis illustrate how the study of fumarolic systems can provide valuable information on magmatic and volcanic processes. Based on this work, a number of recommendations for additional studies can be made.

A review of the literature suggests that the study of volcanic gases in the Aleutian arc has received less attention than similar studies in any of the world's major volcanic arcs. Given the important role of volatiles in igneous processes, this situation needs to be remedied. Its frequent historic eruptions and proximity to transport routes and significant population centers makes Mount St. Augustine the most logical site to initiate a permanent gas sampling program in the Aleutian arc. The fact that definite chemical trends were observed in the 1979-1984 Mount St. Augustine fumarolic gases supports the continued sampling of the high-temperature summit vents at this location.

Initially, yearly sampling of the high-temperature summit vents should be undertaken to determine if fumarolic emissions following the 1986 eruption indicate degassing trends similar to those found after the 1976 eruption. The summit gas samples collected by Robert Symonds in 1986, 1987, and 1989 can serve as the baseline data for this continued monitoring. Since Mount St. Augustine's seismicity and edifice deformation are actively monitored, long-term changes in gas chemistry could be checked for correlation to any significant changes in the geophysical data. The ability to check for correlations with geophysical data is another reason why it makes sense to establish the first permanent gas sampling program in the Aleutian arc at Mount St. Augustine. Such a multidiscipline approach holds the most promise for tracking the long-term evolution of Mount St. Augustine's magmatic/volcanic system.

If gas data are to be used for shorter-term eruption forecasting at Mount St. Augustine, it is necessary to ascertain whether there are time lags between changes in gas chemistry and the geophysical data. If possible, repeated gas sampling should be done during a period of increased seismicity. If no changes in gas chemistry are observed, the summit vents should be resampled soon after the seismicity patterns return to more normal levels. Developments in the technology of electrochemical gas sensors should be closely watched. The Alaska Volcano Observatory should consider testing the currently available  $fO_2$  gas sensors at Mount St. Augustine. If these sensors prove to be durable, real-time data of at least one component of the gases could be compared concurrently to the geophysical data.

Continued gas sampling is also necessary to unravel the causes of the anomalously high HCl concentrations in the high-temperature fumarolic gases at Mount St. Augustine. Chlorine stable isotope analyses of high-temperature fumarolic condensates may provide more direct evidence of seawater influx into the Mount St. Augustine volatile source region. Establishing the major source of the anomalously high HCl levels in the high-temperature gases is important since the visible, physical characteristics of Mount St. Augustine, when compared to other convergent plate volcanoes, are in no way unusual. This information is vital for refining models of Mount St. Augustine's eruption mechanism.

As shown by this study, the chemistries of actively-forming fumarolic encrustations can be used to qualitatively estimate the chemistries of fumarolic gases. More work is required to quantitatively establish the relationship between the chemistries of fumarolic gases, condensates, isolated sublimates and encrustations. Recent advances in thermodynamic modeling (e.g., the computer code SOLVGAS) enable the prediction of the chemistry of sublimates and their sequence of deposition from saturated gases. Additional silica tube sublimates should be collected, and compared to gas chemistries from the same vents, to field test the computer models and provide data for their refinement. Realistically, then the modeling should be able to be done in reverse; analyses of sublimates should be able to be

used to quantitatively estimate the gas chemistry and conditions responsible for sublimate deposition.

The high-temperature active summit fumaroles at Mount St. Augustine would make a very suitable site for the collection of silica tube sublimates. A small-scale collection of silica tube sublimates has already been conducted at Mount St. Augustine (Symonds et al. in press), suggesting that this is a workable approach. Samples of condensates and bulk encrustations should also be taken from the summit vents. Chemical data from these samples would help to determine the degree of equilibrium maintained between the gas and sublimate deposits as well as the potential for post-depositional remobilization of elements from the encrustation phases.

To the author's knowledge, little attention has been given to the potential of using active fumaroles as natural laboratories for gas-rock interaction and liquid-rock interaction experiments. The active summit fumaroles at Mount St. Augustine could be used for this purpose. Samples of various lithologies could be suspended within active fumarolic vents. The gas chemistry, flux, temperature, condensation rate and condensate pH could be easily measured at these vents. The major drawback to such studies is site access and the inability to monitor experimental conditions anywhere near as closely in synthetic laboratory situations. However, it is conceivable that in natural systems experiments could be run for months or even years; experimental runs of this length are not practical or economically feasible for mechanical laboratory equipment.

The success of the reconnaissance  $Hg^0$  survey of this study supports further volatile element surveys in the Aleutian arc. An ideal opportunity still exists for the application of detailed  $Hg^0$  surveys in the VTTS. Unfortunately, only 17 survey markers were left in the ground following the CSDP-sponsored gravity and magnetic surveys of Novarupta Basin (Eichelberger et al. 1990). Results of a  $Hg^0$  survey conducted over a sampling grid similar to that used in the geophysical data collection could be compared to results of the



geophysical studies. The presence or absence of  $Hg^0$  anomalies above structures delineated by the geophysical studies could identify whether these structures are relatively sealed (e.g., by silicification) or open. This information is important for modeling the nature and extent of any developing hydrothermal system beneath Novarupta.

Detailed  $Hg^0$  sample traverses perpendicular to the orientation of a proposed magma feeder dike between Novarupta and Trident could evaluate if hydraulic transfer of magma from beneath Trident to Novarupta has occurred. A further application of detailed VTTS  $Hg^0$  surveys lies in the detection of zones of near-surface high heat flow. Initial results (Eichelberger et al. 1990) of a conductive heat flow survey undertaken with the 1989 geophysical surveys reveal the technique of using buried heat flow sensors to be largely inconclusive. Detailed  $Hg^0$  surveys would probably provide a more homogeneous, interpretable data base for delineating zones of anomalous near-surface heat flow in the VTTS.

The bulk encrustations from the VTTS fossil fumaroles are valuable for delineating the processes operative over the long-term evolution of these deposits. However, to further constrain the role vapor phase element transport played in the degassing of the 1912 ash-flow sheet, detailed studies of the primary fumarolic magnetite should be undertaken. Detailed chemical studies of chemically and/or mechanically separated magnetite samples would identify the range of metallic/metalloid species in the magnetite. Field observation records of the VTTS early investigations could be used to estimate the time (at the very least the maximum amount) required to generate the magnetite deposits. Crude chemical analyses of gas samples taken from active vents in 1918 and 1919 are available (Allen and Zies 1923). The collection method of these gas samples allows a rough approximation of the fluxes of the major gas species, plus Cl and F, out of individual fumarolic vents. All of the preceding data could then be used to estimate volatile element fluxes and the efficiency of vapor phase element transport in the VTTS fumaroles.

The amounts of primary fumarolic magnetite preserved in the VTTS surficial deposits are very minor. However, a ground magnetometer survey in the VTTS by Tribble (1972) implies that significant quantities of fumarolic magnetite remain preserved in the zone of abundant fossil fissures (middle VTTS) at shallow depths ( $\approx$  1-2 m). Excavation at these sites may recover sufficient amounts of primary fumarolic magnetite to enable successful undertaking of the proposed work. Magnetite recovered from this excavation should be minimally affected by secondary alteration and weathering processes.

The proposed drilling within the VTTS should also return valuable data on volatile element fluxes and the efficiency of vapor phase elemental transport. Recently revised plans (T. Keith pers. commun. 1991) call for two holes; one drilled on a slant beneath Novarupta dome and the other drilled into the ash-flow sheet in the middle VTTS. Analyses of volatile elements retained in the drill core materials from these two markedly different crystallization regimes will be made. These data can be compared to the volatile element contents found in the fumarolic magnetite samples. A more complete picture of the pre- and post-eruptive devolatilization history of this site will then be available. Given the paucity of similar information for rhyolitic magmatic/volcanic systems, these data will have wide applicability.

## References

---

- Allen ET, Zies EG (1923) A chemical study of the fumaroles of the Katmai region. *Nat Geograph Soc Contrib Tech Pap Katmai Ser 2*: 75-155
- Anderson AT (1975) Some basaltic and andesitic gases. *Rev Geophys Space Phys 13*: 37-55
- Anma K (1971) An aeromagnetic survey in the Valley of Ten Thousand Smokes, Alaska. MS thesis Univ of Alaska Fairbanks: 1-97
- Aramaki S (1984) Formation of the Aira Caldera, southern Kyushu about 22,000 years ago. *J Geophys Res 89*: 8485-8501
- Bacon CR (1989) Crystallization of accessory phases in magmas by local saturation adjacent to phenocrysts. *Geochim Cosmochim Acta 53*: 1055-1066
- Barnes HL (1979) Solubilities of ore minerals. In Barnes HL (Ed) *Geochemistry of Hydrothermal Ore Deposits - Second Edition*. John Wiley and Sons New York: 404-460
- Barnes I (1984) Volatiles of Mount St. Helens and their origins. *J Volcanol Geotherm Res 22*: 136-146
- Beget J (1986) Prehistoric tephra eruptions, debris avalanches, and tsunamis at Mt. St. Augustine: the geologic record. *EOS Trans Amer Geophys Un 67*: 1260
- Benhamou G, Allard P, Sabroux JC, Vitter G, Dajlevic D, Creusot A (1988) Oxygen fugacity of gases and rocks from Momotombo Volcano, Nicaragua: application to volcanological monitoring. *J Geophys Res 93*: 14872-14880
- Berg E, Kubota S, Kienle J (1967) Preliminary determination of the crustal structure in Katmai National Monument, Alaska. *Bull Seismol Soc Am 57*: 1367-1392
- Bernard A (1985) Les mecanismes de condensation des gaz volcaniques (chimie, mineralogie et equilibres des phases condenses majeures et mineures). PhD thesis Univ Bruxelles Belgium
- Bernard A, LeGuern F (1986) Condensation of volatile elements in high-temperature gases of Mount St Helens. *J Volcanol Geotherm Res 28*: 91-105
- Bingqiu Z, Zhang J, Zhu L, Zheng Y (1986) Mercury, arsenic, antimony, bismuth and boron as geochemical indicators for geothermal areas. *J Geochem Explor 25*: 379-388
- Bottinga Y (1969) Calculated fractionation factors for carbon and oxygen isotopic exchange in the system calcite-carbon dioxide-graphite-methane-hydrogen-water vapor. *Geochim Cosmochim Acta 33*: 49-64

- Bowen HJM (1979) *Environmental Chemistry of the Elements*. Academic Press New York NY: 333 pp
- Buffler RT (1976) Geologic map of south Augustine Island, Lower Cook Inlet, Alaska. Alaska Div Geol Geophy Surveys AOF-96: 1-3 map
- Burnham CW (1979) The importance of volatile constituents. In Yoder HS Jr (Ed) *The Evolution of Igneous Rocks*. Princeton Univ Press Princeton: 439-482
- Casadevall TJ, Johnston DA, Harris DM, Rose WI, Malinconico LL, Stoiber RE, Bornhorst TJ, Williams SN, Woodruff L, Thompson JM (1982) SO<sub>2</sub> emission rates at Mount St. Helens from March 29 through December, 1980. US Geol Surv Prof Pap 1250: 193-200
- Christensen OD, Capuano RA, Moore JN (1983) Trace-element distribution in an active hydrothermal system, Roosevelt Hot Springs thermal area, Utah. *J Volcanol Geotherm Res* 16: 99-129
- Cioni R, Corazza E (1981) Medium-temperature fumarolic gas sampling. *Bull Volcanol* 44: 23-29
- Cox ME (1983) Summit outgassing as indicated by radon, mercury and pH mapping, Kilauea volcano, Hawaii. *J Volcanol Geotherm Res* 16: 131-151
- Craig H (1953) The geochemistry of the stable carbon isotopes. *Geochim Cosmochim Acta* 3: 53-92
- Craig H (1961) Isotopic variation in meteoric waters. *Sci* 133: 1702-1703
- Crenshaw WB, Williams SN, Stoiber RE (1982) Fault location by radon and mercury detection at an active volcano in Nicaragua. *Nature* 300: 345-346
- Curtis GH (1968) The stratigraphy of the ejecta from the eruption of Mount Katmai and Novarupta, Alaska. In Coats RR, Hay RL, Anderson CA (Eds) *Studies in Volcanology*. Geol Soc Am Mem 116: 153-210
- Davis JC (1986) *Statistics and Data Analysis in Geology - Second Edition*. John Wiley and Sons New York: 646 pp
- D'Amore F, Panichi C (1980) Evaluation of deep temperatures of hydrothermal systems by a new gas geothermometer. *Geochim Cosmochim Acta* 44: 549-556
- Desborough GA, Rostad O (1980) Hydrated aluminum hydroxy-fluoride, a ralstonite-like mineral at Big Southern Butte, Snake River Plain, Idaho. *Am Miner* 65: 1057-1058
- Detterman RL (1973) Geologic map of the Iliamna B-2 quadrangle, Augustine Island, Alaska. US Geol Surv Map GQ-1068

- Devine JD, Sigurdsson H, Davies AN, Self S (1984) Estimates of sulfur and chlorine yield to the atmosphere from volcanic eruptions and potential climatic effects. *J Geophys Res* 89: 6309-6325
- Donhan Geothermal Energy, Ltd (1984) Geothermal development in the Nigorikawa area, Hokkaido, Japan. Unpubl Rept Morioka Japan: 1-17
- Eichelberger JC, Hildreth W (1986) Research drilling at Katmai, Alaska. *EOS Trans Amer Geophys Un* 67: 778-780
- Eichelberger JC, Ballard S, Carrigan CR, Goodliffe A, Hildreth W, Iwatsubo E, Kasameyer PW, Keith TEC, Kienle J, Papike JJ, Pollard DD, Stone DB, Wallmann PC, Ward PL, Wilt M, Yount ME (1990) Geophysical expedition to Novarupta volcano, Katmai National Park, Alaska. *EOS Trans Amer Geophys Un* 71: 733-735
- Escher BG (1929) On the formation of calderas. *Leidsche Geol Meded* 3: 183-219
- Evans WC, Banks NG, White LD (1981) Analyses of gas samples from the summit crater. *US Geol Surv Prof Pap* 1250: 227-232
- Fang SC (1978) Sorption and transformation of mercury vapor by dry soil. *Environ Sci Technol* 12: 285-288
- Fenner CN (1920) The Katmai region, Alaska, and the great eruption of 1912. *J Geol* 28: 569-606
- Fenner CN (1923) The origin and mode of emplacement of the great tuff deposit of the Valley of Ten Thousand Smokes. *Nat Geograph Soc Contrib Tech Pap Katmai Ser* 1: 1-74
- Fisher MA, Bruns TR, Von Huene R (1981) Transverse tectonic boundaries near Kodiak Island, Alaska. *Geol Soc Am Bull* 92: 10-18
- Fournier RO (1973) Silica in thermal waters: laboratory and field investigations. In *Proc Int Symp Hydrogeochem and Biogeochem Japan 1970*. *Hydrogeochemistry* 1: 122-129
- Fournier RO (1985) The behavior of silica in hydrothermal solutions. In Berger BR, Bethke PM (Eds) *Geology and Geochemistry of Epithermal Systems*. *Rev Econ Geol* 2 *Econ Geol Publ Comp El Paso Tx*: 45-59
- Gantes M, Sabroux JC, Vitter G (1983) Chemical sensors for monitoring volcanic activity. In Tazieff H, Sabroux JC (Eds) *Forecasting Volcanic Events*. *Elsevier Sci Publ The Netherlands*: 409-424

- Gedney L, Matteson C, Forbes RB (1970) Seismic refraction profiles of the ash flow in the Valley of Ten Thousand Smokes, Katmai National Monument, Alaska. *J Geophys Res* 75: 2619-2624
- Gerlach TM (1979) Evaluation and restoration of the 1970 volcanic gas analyses from Mt Etna, Sicily. *J Volcanol Geotherm Res* 6: 165-178
- Gerlach TM (1980) Evaluation of volcanic gas analyses from Kilauea Volcano. *J Volcanol Geotherm Res* 7: 295-317
- Gerlach TM (1981) Restoration of new volcanic gas analyses from basalts of the Afar region: further evidence of CO<sub>2</sub> trends. *J Volcanol Geotherm Res* 10: 83-91
- Gerlach TM (1982) Interpretation of volcanic gas data from tholeiitic and alkaline mafic magmas. *Bull Volcanol* 45(3): 235-244
- Gerlach TM (1983) Intrinsic chemical variations in high-temperature volcanic gases from basic lavas. In Tazieff H, Sabroux JC (Eds) *Forecasting Volcanic Events*. Elsevier Sci Publ The Netherlands: 323-336
- Gerlach TM, Casadevall TJ (1986a) Evaluation of gas data from high-temperature fumaroles at Mt. St. Helens, 1980-1982. *J Volcanol Geotherm Res* 28: 107-140
- Gerlach TM, Casadevall TJ (1986b) Fumarole emissions at Mount St. Helens volcano, June 1980 to October 1981: Degassing of a magma-hydrothermal system. *J Volcanol Geotherm Res* 28: 141-160
- Gerlach TM, Nordlie BE (1975a) The C-O-H-S gaseous system, part I: composition limits and trends in basaltic gases. *Am J Sci* 275: 353-376
- Gerlach TM, Nordlie BE (1975b) The C-O-H-S gaseous system, part II: temperature, atomic composition, and molecular equilibria in volcanic gases. *Am J Sci* 275: 377-394
- Gerlach TM, Nordlie BE (1975c) The C-O-H-S gaseous system, part III: magmatic gases compatible with oxides and sulfides in basaltic magmas. *Am J Sci* 275: 395-410
- Giggenbach WF (1975) A simple method for the collection and analysis of volcanic gas samples. *Bull Volcanol* 39: 132-145
- Giggenbach WF (1982) Carbon-13 exchange between CO<sub>2</sub> and CH<sub>4</sub> under geothermal conditions. *Geochim Cosmochim Acta* 46: 159-165
- Giggenbach WF (1987) Redox processes governing the chemistry of fumarolic gas discharges from White Island, New Zealand. *Applied Geochem* 2: 143-161
- Giggenbach WF, LeGuern F (1976) The chemistry of magmatic gases from Erta Ale, Ethiopia. *Geoch Cosmochim Acta* 40: 25-30

- Goodliffe AM, Stone DB, Kienle J, Kasameyer P (1991) The vent of the 1912 Katmai eruption: gravity and magnetic measurements. *Geophys Res Lettr* 18 no. 8: 1521-1524
- Grant JA (1986) The isocon diagram - a simple solution to Gresens' equation for metasomatic alteration. *Econ Geol* 81: 1976-1982
- Griggs RF (1919) Are the Ten Thousand Smokes real volcanoes? *Ohio J Sci* 19: 97-116
- Griggs RF (1922) The Valley of Ten Thousand Smokes. *Nat Geograph Soc Washington DC*: 340 pp
- Hampton CM, Bailey KD (1985) Sublimates obtained during fusion of volcanic glasses. *J Volcanol Geotherm Res* 25: 145-155
- Harris DM, Rose WI, Bornhorst T, Casadevall TJ (1980) Variations of SO<sub>2</sub> and CO<sub>2</sub> emission rates at Mount St Helens, July 22 to August 29, 1980. *EOS Trans Amer Geophys Un* 61: 1139
- Harris G (in prep - MS thesis Univ of Alaska Fairbanks) Petrology and petrography of the 1986 eruption of Mount St. Augustine.
- Heald EF, Naughton JJ, Barnes IL (1963) The chemistry of volcanic gases. 2. Use of equilibrium calculations in the interpretation of volcanic gas samples. *J Geophys Res* 68: 545-557
- Henley RW (1985) Geothermal framework for epithermal ore deposits. In Berger BR, Bethke PM (Eds) *Geology and Geochemistry of Epithermal Systems*. *Rev Econ Geol* 2 *Econ Geol Publ Comp El Paso Tx*: 1-21
- Henley RW, Ellis AJ (1983) Geothermal systems ancient and modern - a geochemical review. *Earth Sci Rev* 19: 1-50
- Henley RW, Truesdall AH, Barton PB Jr, Whitney JA (1984) Fluid-Mineral Equilibria in Hydrothermal Systems. *Rev Econ Geol* 1 *Econ Geol Publ Comp El Paso Tx*: 267 pp
- Hildreth W (1979) The Bishop Tuff: evidence for the origin of compositional zonation in silicic magma chambers. In *Ash-Flow Tuffs*, Chapin CE, Elston WE (Ed.) *Geol Soc Am Spec Pap* 180: 43-75.
- Hildreth W (1983) The compositionally zoned eruption of 1912 in the Valley of Ten Thousand Smokes, Katmai National Park, Alaska. In Aramaki S, Kushiro J (Eds) *Arc Volcanism*. *J Volcanol Geotherm Res* 18: 1-56
- Hildreth W (1987) New perspectives on the eruption of 1912 in the Valley of Ten Thousand Smokes, Katmai National Park, Alaska. *Bull Volcanol* 49: 680-693

- Hobbs PV, Radke LF, Stith JL (1977) Eruptions of St. Augustine Volcano: airborne measurements and observations. *Sci* 195: 871-873
- Hoffmann DJ, Rosen JM (1983) Sulfuric acid droplet formation and growth in the stratosphere after the 1982 eruptions of El Chichon. *Sci* 222: 325-327
- Huebner JS, Sato M (1970) The oxygen fugacity-temperature relationships of manganese oxide and nickel oxide buffers. *Am Mineral* 55: 934-952
- Hughes JM, Stoiber RE (1985) Vanadium sublimates from the fumaroles of Izalco Volcano, El Salvador. *J Volcanol Geotherm Res* 24: 283-291
- Ivosevic SW (1987) *Gold. Min Enginrng* 39 no 5: 346
- Iwasaki I, Hiramaya M, Katsura T, Ozawa T, Ossaka J, Kamada M, Matsumoto H (1964) Alteration of rocks by volcanic gas in Japan. *Bull Volcanol* 27: 65-78
- Johnson KE (1986) Isotope geochemistry of Augustine Volcano, Alaska. MS thesis, Southern Methodist University
- Johnson KE, Harmon RS, Moorbath S, Strong DF, Morris JD (in press - *Contr Miner Petr*) Augustine volcano: isotopic and trace element constraints on magmatic components.
- Johnston DA (1978) Volatiles, magma mixing, and the mechanism of eruption of Augustine Volcano, Alaska. PhD thesis, Univ of Washington: 1-177
- Johnston DA (1979) Onset of volcanism at Augustine Volcano, Lower Cook Inlet. *US Geol Surv Circ* 804-B: 878-880
- Johnston DA (1980) Volcanic contribution of chlorine to the stratosphere: more significant to ozone than previously estimated? *Sci* 209: 491-492
- Jonasson JR, Boyle RW (1972) Geochemistry of mercury and origin of contamination of the environment. *Trans Can Inst Min Metall* 75: 8-15
- Kama W, Siegel SM (1980) Volatile mercury release from vascular plants. *Org Geochem* 2: 99-101
- Kauffman RS, Long A, Campbell DC (1988) Chlorine isotope distribution in formation waters, Texas and Louisiana. *Amer Assoc Petrol Geol Bull* 72: 839-844
- Keith TEC (1983) Mineralogical and chemical changes in fumarolic deposits with time at surface conditions. *Proc 4th Int Symp on Water-Rock Interaction Misasa Japan*: 231-234
- Keith TEC (1984) Preliminary observations on fumarole distribution and alteration, Valley of 10,000 Smokes, Alaska. *US Geol Surv Circ* 939: 82-85



- Keith TEC (1991) Fossil and active fumaroles in the 1912 eruptive deposits, Valley of Ten Thousand Smokes, Alaska. *J Volcanol Geotherm Res* 45: 227-254
- Keith TEC, Casadevall TJ, Johnston DA (1981) Fumarole encrustations: occurrence, mineralogy, and chemistry. *US Geol Surv Prof Pap* 1250: 239-250
- Kennedy GC (1948) Equilibrium between volatiles and iron oxides in igneous rocks. *Am J Sci* 148: 529-549
- Kienle J (1969) Gravity survey in the general area of Katmai National Monument. PhD thesis Univ Alaska Fairbanks: 151 pp
- Kienle J (1970) Gravity traverses in the Valley of Ten Thousand Smokes, Katmai National Monument, Alaska. *J Geophys Res* 75: 6641-6649
- Kienle J (1991) Depth of the ash flow deposit in the Valley of Ten Thousand Smokes, Katmai National Park, Alaska. *Geophys Res Lettr* 18 no. 8: 1533-1536
- Kienle J, Lalla DJ, Pearson CF, Barnett SA (1979) Search for shallow magma accumulations at Augustine Volcano. Fin Rept by Geophys Inst Univ of AK, College, AK to US Dept Ener, Wash DC: 157 pp
- Kienle J, Shaw GE (1979) Plume dynamics, thermal energy and long distance transport of vulcanian eruption clouds from Augustine Volcano, Alaska. *J Volcanol Geotherm Res* 6: 139-164
- Kienle J, Swanson SE (1980) Volcanic hazards from future eruptions of Augustine Volcano, Alaska. *Geophys Inst Univ of Alaska Rept UAG R-275*: 1-122
- Kienle J, Swanson SE (1983) Volcanism in the eastern Aleutian arc: Late Quaternary and Holocene centers, tectonic setting, and petrology. *J Volcanol Geotherm Res* 17: 393-432
- Kienle J, Swanson SE, Pulpan H (1983) Magmatism and subduction in the eastern Aleutian arc. In *Arc Volcanism: Physics and Tectonics*, Shimozuru D, Yokoyama I (Ed.) Terra Scientific Publishing Co, Tokyo: 191-224
- Kienle J, Davies JN, Miller TP, Yount ME (1986) 1986 eruption of Augustine Volcano: Public safety response by Alaskan volcanologists. *EOS Trans AGU* 67: 580-582
- Kiyosu Y (1983) Hydrogen isotope compositions of hydrogen and methane from some volcanic areas in northeastern Japan. *Earth Planet Sci Let* 62(1): 41-52
- Kiyosu Y, Kurahashi M (1983) Origin of sulfur species in acid sulfate-chloride thermal waters, northeastern Japan. *Geochim Cosmochim Acta* 47: 1237-1245
- Klusman RW, Landress RA (1978) Secondary controls on mercury in soils of geothermal areas. *J Geochem Explor* 9: 75-91

- Klusman RW, Landress RA (1979) Mercury in soils of the Long Valley, California, geothermal system. *J Volcanol Geotherm Res* 5: 49-65
- Kodosky LG (1989) Surface mercury geochemistry as a guide to volcanic vent structure and zones of high heat flow in the Valley of Ten Thousand Smokes, Katmai National Park, Alaska. *J Volcanol Geotherm Res* 38: 227-242
- Kodosky LG, Keskinen M (1987) Mercury distribution within the Valley of Ten Thousand Smokes, Katmai National Park, Alaska. *EOS Trans Amer Geophys Un* 68: 1537
- Kodosky LG, Keskinen M (1990) Fumarole distribution, morphology, and encrustation mineralogy associated with the 1986 eruptive products of Mount St Augustine, Alaska. *Bull Volcanol* 52: 175-185
- Kodosky LG, Motyka RJ, Symonds RB (1991) Fumarolic emissions from Mount St Augustine, Alaska, 1979-1984: Degassing trends, volatile sources and their possible role in eruptive style. *Bull Volcanol* 53: 381-394
- Krauskopf KB (1964) The possible role of volatile metal compounds in ore genesis. *Econ Geol* 59: 22-45
- Krauskopf KB (1979) *Introduction to Geochemistry - Second Edition*. McGraw-Hill Inc New York: 617 pp
- Landa ER (1978) The retention of metallic mercury vapor by soils. *Geochim Cosmochim Acta* 42: 1407-1411
- LeGuern F, Bernard A (1982) A new method for sampling and analyzing volcanic sublimates - application to Merapi volcano, Java. *J Volcanol Geotherm Res* 12: 133-146
- LeGuern F, Gerlach TM, Nohl A (1982) Field gas chromatograph analyses of gases from a glowing dome at Merapi Volcano, Java, Indonesia, 1977,1978,1979. *J Volcanol Geotherm Res* 14: 223-245
- Lepel EA, Stefansson KM, Zoeller WH (1978) The enrichment of volatile elements in the atmosphere by volcanic activity: Augustine Volcano, 1976. *J Geophys Res* 83: 6213-6220
- Limke AJ, Beget JE (1986) Emplacement velocities and rheological properties of pyroclastic flows during the March 27-April 8 eruption of Mt St Augustine. *EOS Trans Amer Geophys Un* 67: 1259
- Lovering TS (1957) Halogen-acid alteration of ash at fumarole no. 1, Valley of Ten Thousand Smokes, Alaska. *Bull Geol Soc Amer* 68: 1585-1604

- Magaritz M, Gat JR (1981) Review of the natural abundance of hydrogen and stable isotopes. In *Stable Isotope Hydrology*, Tech Rept Ser 210, Int Atomic Ener Agen Vienna: 85-98
- Mathez EA (1976) Sulfur solubility and magmatic sulfides in submarine basalt glass. *J Geophys Res* 81: 4269-4276
- Matlick JS, Buseck PR (1976) Exploration for geothermal areas using mercury: A new geochemical technique. *UN Symp on Develop and Use of Geotherm Res 2nd Proc* 1: 785-792
- Matlick JS, Shiraki M (1981) Evaluation of the mercury soil mapping geothermal exploration techniques. *Geotherm Res Council Trans* 5: 95-98
- Matsuo S, Suzuoki T, Kusakabe M, Wada H, Suzuki M (1974) Isotopic and chemical compositions of volcanic gases from Satsuma-Iwojima, Japan. *Geochem J* 8: 165-173
- Matumoto T (1971) Seismic body waves observed in the vicinity of Mt. Katmai, Alaska, and evidence for the existence of molten chambers. *Geol Soc Am Bull* 82: 2905-2920
- McNeal JM, Rose WA (1974) The geochemistry of mercury in sedimentary rocks and soils in Pennsylvania. *Geochim Cosmochim Acta* 38: 1759-1784
- McNearny JJ, Buseck PR, Hanson JC (1972) Mercury detection by means of thin gold films. *Sci* 178: 611-612
- Mizutani Y, Sugiura T (1982) Variations in chemical and isotopic composition of fumarolic gases from Showashinzan Volcano, Hokkaido, Japan. *Geochem J* 16: 63-71
- Morgan JD (1986) Mining 1985. *Min Enginrng* 38 no 5: 331-339
- Motyka RJ, Kodosky LG, Evans W (1986) A review of gas sampling at Augustine Volcano, Alaska: 1982-1986. *EOS Trans Amer Geophy Un* 67: 1260
- Nakamura K (1977) Volcanoes as possible indicators of tectonic stress orientation, principle and practice. *J Volcanol Geotherm Res* 2: 1-16
- Naughton JJ, Greenberg VA, Goguel R (1976) Incrustations and fumarolic condensates at Kilauea Volcano, Hawaii: field, drill-hole and laboratory observations. *J Volcanol Geotherm Res* 1: 149-165
- Naughton JJ, Lewis VA, Hammond D, Nishimoto D (1974) The chemistry of sublimates collected directly from lava fountains at Kilauea Volcano, Hawaii. *Geochim Cosmochim Acta* 38: 1679-1690
- Noguchi K, Kamiya H (1963) Prediction of volcanic eruption by measuring the chemical compositions and amounts of gases. *Bull Volcanol* 25: 367-368

- Officer CB, Drake CL (1985) Terminal Cretaceous environmental events. *Sci* 227: 1161-1163
- Ohmoto H, Rye RD (1979) Isotopes of sulfur and carbon. In Barnes HL (Ed) *Geochemistry of Hydrothermal Ore Deposits - Second Edition*. John Wiley and Sons New York: 509-567
- Oskarsson N (1981) The chemistry of Icelandic lava incrustations and the latest stages of degassing. *J Volcanol Geotherm Res* 10: 93-111
- Papike JJ, Keith TEC, Spilde MN, Galbreath KC, Shearer CK, Laul JC (1991) Geochemistry and mineralogy of fumarolic deposits, Valley of Ten Thousand Smokes, Alaska: bulk chemical and mineralogical evolution of dacite-rich protolith. *Amer Mineral* 76: 1662-1673
- Phelps DW, Buseck PR (1978) Natural concentrations of Hg in the Yellowstone and Coso geothermal fields. *Geotherm Res Council Trans* 2: 521-522
- Pineau F, Javoy M (1983) Carbon isotopes and concentrations in mid-ocean ridge basalts. *Earth Planet Sci Let* 62: 239-257
- Poreda R, Craig H (1989) Helium isotope ratios in circum-Pacific volcanic arcs. *Nature* 338: 473-478
- Power J (1988) Seismicity associated with the 1986 eruptions of Augustine Volcano, Alaska. MS thesis Univ. of Alaska Fairbanks: 142 pp
- Ramdohr P (1962) Erzmikroskopische unersuchungen an magnetiten der exhalationen in Valley of the 10,000 Smokes. *Neus Jahrbuch fur Mineralogie Monatshefte* 314: 49-59
- Rampino MR, Self S (1984) The atmospheric effects of El Chichon. *Sci Amer* 250: 48-57
- Richet P, Bottinga Y, Javoy M (1977) A review of hydrogen, carbon, nitrogen, oxygen, sulphur, and chlorine stable isotope fractionation among gaseous molecules. *Annu Rev Earth Planet Sci* 5: 65-110
- Rose AW, Burt DM (1979) Hydrothermal alteration. In Barnes HL (Ed) *Geochemistry of Hydrothermal Ore Deposits - Second Edition*. John Wiley and Sons New York: 173-236
- Rose AW, Hawkes HE, Webb JS (1979) *Geochemistry in Mineral Exploration - Second Edition*. Academic Press New York: 657 pp
- Rose WI, Chuan RL, Kyle PR (1985) Rate of sulfur dioxide emissions from Erebus Volcano, Antarctica. *Nature* 316: 710-712
- Rose WI, Heiken G, Wohletz K, Eppler D, Barr S, Miller T, Chuan RL, Symonds RB (1988a) Direct rate measurements of Mt. St. Augustine eruption plumes: a problem of scaling up uncontrolled variables. *Hawaii Symp How Volcanoes Work Abstr Vol*: 212

- Rose WI, Heiken G, Wohletz K, Eppler D, Barr S, Miller T, Chuan RL, Symonds RB (1988b) Direct rate measurements of Mt. St. Augustine eruption plumes: a problem of scaling up uncontrolled variables. *J Geophys Res* 93: 4485-4499
- Rose WI, Wunderman RL, Hofmann MF, Gale L (1983) A volcanologist's review of atmospheric hazards of volcanic activity: Fuego and Mount St. Helens. *J Volcanol Geotherm Res* 17: 133-158
- Sackett WM, Chung HM (1979) Experimental confirmation of the lack of carbon isotope exchange between methane and carbon oxides at high temperatures. *Geochim Cosmochim Acta* 43: 273-276
- Sakai H, Ueda A, Casadevall TJ, Moore JG (1981) The isotopic ratios and chemistry of sulfur at Kilauea volcano, Hawaii, and Satsuma Iwojima, Southern Kyushu. In *The Volcanological Society of Japan and IAVCEI (Eds) Arc Volcanism. Abstr 1981 IAVCEI Symp Tokyo and Hakone Japan*: 312-313
- Sato M, Moore JG (1973) Oxygen and sulfur fugacities of magmatic gases directly measured in active vents of Mount Etna. *Philos Trans R Soc Lond Ser A* 274: 137-146
- Sato M, Wright TL (1966) Oxygen fugacities directly measured in magmatic gases. *Sci* 153: 1103-1105
- Sayre JD, Hagelbarger PR (1919) A study of temperatures in the Valley of Ten Thousand Smokes. *Ohio J Sci* 19: 249-278
- Shepherd ES (1938) Gases in rocks and some related problems. *Amer J Sci* 235: 311-351
- Sheppard DS, Giggenbach WF (1985) Methods for the analysis of geothermal and volcanic gases and waters. Rep no. CD 2364, Chem Div Dept Scientific and Industrial Res Lower Hutt NZ: 78pp
- Sheppard SMF, Nielsen RL, Taylor HP (1969) Oxygen and hydrogen isotope ratios of clay minerals from porphyry copper deposits. *Econ Geol* 64: 755-777
- Sheridan MF (1970) Fumarolic mounds and ridges of the Bishop Tuff, California. *Geol Soc Amer Bull* 81: 851-868
- Shieh YN, Taylor HP Jr (1969) Oxygen and carbon isotope ratios of contact metamorphism of carbonate rocks. *J Petrol* 10: 307-331
- Shipley JW (1920) Some chemical observations on the volcanic emanations and incrustations in the Valley of Ten Thousand Smokes, Katmai, Alaska. *Am J Sci* 50: 141-153

- Silberman ML, Berger BR (1985) Relationship of trace-element patterns to alteration and morphology in epithermal precious-metal deposits. In Berger BR, Bethke PM (Eds) *Geology and Geochemistry of Epithermal Systems*. Rev Econ Geol 2 Econ Geol Publ Comp El Paso Tx: 203-232
- Silberman ML, White DE, Keith TEC, Doctor RD (1979) Duration of hydrothermal activity at Steamboat Springs, Nevada from ages of spatially associated volcanic rocks. US Geol Surv Prof Pap 458-D: 13 pp
- Sinclair AJ (1974) Selection of threshold values in geochemical data using probability graphs. *J Geochem Explor* 3: 129-149
- Smith DB, Zielinski RA, Rose WI Jr (1982) Leachability of uranium and other elements from freshly erupted volcanic ash. *J Volcanol Geotherm Res* 13: 1-30
- Smith RL (1979) Ash-flow magmatism. In *Ash-Flow Tuffs*, Chapin CE, Elston WE (Ed.) Geol Soc Am Spec Pap 180: 5-27
- Stevens RK, Mulik JD, O'Keefe AE, Krost KJ (1971) Gas chromatography of reactive sulfur gases in air at the part-per-billion level. *Anal Chem* 43: 827-831
- Stoiber RE, Legget DC, Jenkins TF, Murrmann RP, Rose WI (1971) Organic compounds in volcanic gas from Santiaguito Volcano, Guatemala. *Geol Soc Am Bull* 82: 2299-2302
- Stoiber RE, Rose WI (1970) The geochemistry of Central American volcanic gas condensates. *Geol Soc Amer Bull* 81: 1891-1911
- Stoiber RE, Rose WI (1974) Fumarole incrustations at active Central American volcanoes. *Geochim Cosmochim Acta* 38: 495-516
- Stoiber RE, Williams SN, Huebert B (1987) Annual contribution of sulfur dioxide to the atmosphere by volcanoes. *J Volcanol Geotherm Res* 33: 1-8
- Stoiber RE, Williams SN, Malinconico LL, Johnston DA, Casadevall TJ (1981) Mt. St. Helens: evidence of increased magmatic gas component. *J Volcanol Geotherm Res* 11: 203-212
- Strothers RB, Rampino MR (1983) Volcanic eruptions in the Mediterranean before A.D. 630 from written and archeological sources. *J Geophys Res* 88: 6357-6372
- Suhr NH, Gong H (1983) Some procedures for the chemical and mineralogical analysis of coals. Final Rept to US Dept of Energy DOE-30013-53 Part 3: 21
- Swanson SE, Kienle J (1988) The 1986 eruption of Mt. St. Augustine: field test of a hazard model. *J Geophys Res* 93: 4500-4520

- Symonds RB, Reed MH, Rose WI (in press - *Geochim Cosmochim Acta*) Speciation and fluxes of gases at Augustine Volcano, Alaska: metal transport in a Cl-rich gas phase.
- Symonds RB, Rose WI, Gerlach TM, Briggs PH, Harmon RS (1990) Evaluation of gases, condensates, and SO<sub>2</sub> emissions from Augustine Volcano, Alaska: the degassing of a Cl-rich volcanic system. *Bull Volcanol* 52: 355-374
- Symonds RB, Rose WI, Reed MH, Lichte FE, Finnegan DL (1987) Volatilization, transport and sublimation of metallic and non-metallic elements in high temperature gases at Merapi Volcano, Indonesia. *Geochim Cosmochim Acta* 51: 2083-2101
- Tedesco D, Sabroux JC (1987) The determination of deep temperatures by means of the CO-CO<sub>2</sub>-H<sub>2</sub>-H<sub>2</sub>O geothermometer: an example using fumaroles in the Campi Flegrei, Italy. *Bull Volcanol* 49: 381-387
- Thomas DM, Naughton JJ (1979) Helium/Carbon dioxide ratios as premonitors of volcanic activity. *Sci* 204: 1195-1196
- Thomas E, Varekamp JC, Buseck PR (1982) Zinc enrichment in the phreatic ashes of Mt. St. Helens, April 1980. *J Volcanol Geotherm Res* 12: 339-359
- Trible MC (1972) Ground magnetometer survey in the Valley of Ten Thousand Smokes, Alaska. MS thesis Univ Alaska Fairbanks: 210 pp
- Truesdell AH, Hulston JR (1980) Isotopic evidence on environments of geothermal systems. In Fritz P, Fontes JC (Eds) *Handbook of Environmental Geochemistry (1): The terrestrial environment*. Elsevier Amsterdam: 179-226
- Van Kooten GK (1987) Geothermal exploration using surface mercury geochemistry. *J Volcanol Geotherm Res* 31: 269-280
- Varekamp JC, Buseck PR (1983a) Hg anomalies in soils: a geochemical exploration method for geothermal areas. *Geothermics* 12: 29-47
- Varekamp JC, Buseck PR (1983b) The speciation of mercury in hydrothermal systems, with applications to ore deposition. *Geochim Cosmochim Acta* 48: 177-185
- Varekamp JC, Buseck PR (1984) Changing mercury anomalies in Long Valley, California: Indication for magma movement or seismic activity. *Geol* 12: 283-286
- Vigliano JA, Harmon RS, Borthwick J, Nehring NL, Motyka RJ, White LD, Johnston DA (1985) Stable isotope evidence for a magmatic component in fumarole condensates from Augustine Volcano, Cook Inlet, Alaska, USA. *Chem Geol* 49: 141-157
- Walker GPL (1984) Downsag calderas, ring faults, caldera sizes, and incremental caldera growth. *J Geophys Res* 89: 8407-8416

- Wallmann PC (1991) Structure and vent geometry of the Novarupta basin, Valley of Ten Thousand Smokes, Katmai National Park, Alaska. PhD thesis Stanford University: 176pp
- Welhan JA (1981) Carbon and hydrogen gases in hydrothermal systems: the search for a mantle source. PhD thesis Univ. of California San Diego: 216 pp
- White DE (1955) Thermal springs and epithermal ore deposits. In Bateman AM (Ed) Economic Geology 50th Anniversary Volume: 99-154
- White DE, Waring GA (1963) Volcanic emanations. US Geol Surv Prof Pap 440-K: 1-27
- Williams H (1954) Preliminary notes on geological work done on Mount Katmai and in the Valley of Ten Thousand Smokes. In Lutney RS (Ed) Interm Rept Katmai Proj Katmai Nat Mon AK: 55-62
- Williams SN (1985) Soil radon and elemental mercury distribution and relation to magmatic resurgence at Long Valley Caldera. Sci 229: 551-553
- Wones DR, Guilbert MC (1969) The fayalite-magnetite-quartz assemblage between 600° and 800°C. Am J Sci 267A: 480-488
- Woods C, Chuan RL, Rose WI (1985) Halite particles injected into the stratosphere by the 1982 El Chichon eruption. Sci 230: 170-172
- Yount ME, Miller TP, Gamble BM (1987) The 1986 eruptions of Augustine Volcano, Alaska: hazards and effects. US Geol Surv Circ 998: 3-13
- Zies EG (1924) The fumarolic incrustations of the Valley of Ten Thousand Smokes. Nat Geograph Soc Contrib Tech Pap Katmai Ser 3: 157-179
- Zies EG (1929) The Valley of Ten Thousand Smokes: I. The fumarolic incrustations and their bearing on ore deposition. II. The acid gases contributed to the sea during volcanic activity. Nat Geograph Soc Contrib Tech Pap Katmai Ser 4: 1-79
- Zoller WH, Parrington JR, Kotra JMP (1983) Iridium enrichment in airborne particles from Kilauea volcano: January 1983. Sci 222: 1118-1121



## Appendix 1

### Results of X-ray Diffraction Analyses

---

VTTS Samples		
<u>Sample</u>	<u>Identified Minerals</u>	<u>Location</u>
A1.3P	Sulfur(?), hematite	Lower VTTS
A1.3R	Hematite	Lower VTTS
A1.4O	Magnetite	Lower VTTS
A1.4P	$\alpha$ -cristobalite, alunite, magnetite(?)	Lower VTTS
A1.5Pur	Amorphous	Lower VTTS
A2.1R	Hematite	Lower VTTS
A2.5W	Fluorite	Lower VTTS
A2.5O	Hematite	Lower VTTS
A2.5P	Hematite	Lower VTTS
A2.6O	Sulfur, hematite	Lower VTTS
A3.4B	Amorphous	Lower VTTS
A3.4C	$\alpha$ -cristobalite	Lower VTTS
A6.2W	Amorphous	Upper VTTS
A6.2O	Hematite	Upper VTTS
A6.4P	Hydrated aluminum hydroxy-fluoride	Upper VTTS
A6.7U	Amorphous	Upper VTTS
A6.7P	Amorphous	Upper VTTS
A6.8R	Hydrated aluminum hydroxy-fluoride	Upper VTTS
A7.1IW	$\alpha$ -cristobalite	Upper VTTS
A7.1IR	$\alpha$ -cristobalite	Upper VTTS
A7.2R	Amorphous	Middle VTTS
A7.4R	Hematite	Upper VTTS
A7.5R	$\beta$ -cristobalite, hematite	Upper VTTS
A7.7B	$\beta$ -cristobalite	Middle VTTS
A8.1R	$\chi$ -cristobalite, hydrated aluminum hydroxy-fluoride	Middle VTTS
A8.1G	Amorphous	Middle VTTS
A8.1CF	$\alpha$ -cristobalite	Middle VTTS
A8.1C	$\alpha$ -cristobalite, sulfur	Middle VTTS
A8.1S	Sulfur	Middle VTTS
A8.3R	Hydrated aluminum hydroxy-hydrate	Middle VTTS
A8.3C	Hydrated aluminum hydroxy-hydrate	Middle VTTS
DFB8E*	Unidentified peaks	Upper VTTS
DFB6*	Amorphous	Upper VTTS
A5.5IW	$\alpha$ -cristobalite	Novarupta Basin
A5.5IB	Amorphous	Novarupta Basin
A5.5S	Amorphous	Novarupta Basin

<u>Sample</u>	<u>Identified Minerals</u>	<u>Location</u>
A6*	Amorphous	Novarupta Basin
A8*	Kaolinite	Novarupta Basin
F3*	Amorphous	Novarupta Basin
F2.1	Kaolinite, goethite, alunite, hematite	Novarupta Basin
F2.2	Kaolinite, hematite	Novarupta Basin
F9.1	Amorphous	Novarupta Basin
F9.2	Amorphous	Novarupta Basin
F5.1	Amorphous	Novarupta Basin
F5.2	Pyrite, kaolinite, alunite, mixed layer illite-smectite	Novarupta Basin
F5.3	Kaolinite, natroalunite, mixed layer illite-smectite	Novarupta Basin
F6	Alunite, natroalunite	Novarupta Basin
F3.1	Kaolinite, alunite	Novarupta Basin
F8.2	Amorphous	Novarupta Basin
F5.4	Kaolinite, hematite, natroalunite	Novarupta Basin
<b>Mount St. Augustine Samples</b>		
FL1	Amorphous	
F1	Amorphous	
FL2	Amorphous	
FL3	Sulfur	
PF2.1CL	Sulfur	
PF3.1C	Gypsum, anhydrite	
PF3.1W	Gypsum, anhydrite	
PF3.2B	Amorphous	
PF3.3R	Tridymite	
PF4.2W	Gypsum	
PF4.2R	Gypsum	
PF4.4Y	Gypsum	
PF4.5U	Sulfur	
PF4.5Y	Sulfur, halite	
PF4.5R	Tridymite	
PF4.5GY	Tridymite	
L1	Soda alum	

---

\* 1971 VTTS samples collected by Dr. Dan Hawkins.

## Appendix 2

### Geochemistry of the Mount St. Augustine Samples\*

Encrustations												
Sample	SiO <sub>2</sub>	Al <sub>2</sub> O <sub>3</sub>	Fe <sub>2</sub> O <sub>3</sub>	MgO	CaO	Na <sub>2</sub> O	K <sub>2</sub> O	TiO <sub>2</sub>	MnO	P <sub>2</sub> O <sub>5</sub>	LOI	Total
F1	60.26	17.84	5.06	3.56	7.51	2.56	0.82	0.62	0.12	0.05	3.06	101.41
FL1	59.58	15.93	5.55	3.75	6.83	2.55	0.81	0.58	0.13	0.10	1.65	97.46
FL2	58.23	16.93	5.66	3.59	6.95	3.48	0.78	0.56	0.12	0.19	0.97	97.46
FL3	59.32	14.57	4.41	3.40	6.42	2.14	0.82	0.59	0.11	0.07	5.46	97.31
PF4.2W	31.73	6.47	2.45	1.41	18.69	1.44	0.39	0.28	0.05	0.03	13.00	75.94
PF4.2C	56.31	15.59	5.34	3.34	5.64	2.33	0.82	0.54	0.11	0.10	7.33	97.45
PF4.2R	62.31	11.48	6.34	2.26	3.44	2.13	0.95	0.62	0.08	0.10	7.37	97.08
PF4.5R1	46.74	14.75	5.34	3.63	7.10	2.04	0.71	0.35	0.12	0.01	16.10	96.89
PF4.5R2	46.96	14.78	5.32	3.64	7.16	2.91	0.72	0.35	0.12	0.01	15.10	97.07
PF4.5GY	63.52	10.82	3.57	2.69	3.92	2.47	0.87	0.48	0.09	0.02	12.20	100.65
PF4.5Y	4.61	3.11	0.72	1.46	3.00	41.3	0.87	0.08	0.10	0.22	29.10	84.57
PU3.1GP	61.74	15.99	4.88	2.45	6.18	3.38	0.98	0.54	0.10	0.07	1.60	97.91
L1	66.77	15.86	3.71	1.30	4.72	3.60	1.41	0.45	0.07	0.19	1.17	99.25
PF3.2B	61.13	16.71	6.08	3.82	7.28	1.76	1.01	0.60	0.13	0.13	2.17	100.82
PF3.2BW	55.75	15.73	6.40	3.92	8.19	1.77	1.29	0.62	0.12	0.08	2.33	96.20
Sample	Ba	Sr	Cr	Ni	Co	V	Cu	Zr	Zn	Pb		
F1	405	329	57	29	81	150						
FL1	372	281	68	34	149	136						
FL2	386	317	68	29	150	195						
FL3	389	268	49	29	137	90						
PF4.2W	255	405	26	16	132	52						
PF4.2C	398	275	71	45	124	117			96			
PF4.2R	445	214	47	22	93	151			82			
PF4.5R1	399	345	59	25	52	176						
PF4.5R2	393	343	63	28	52	178			1245			
PF4.5GY	417	174	31	21	87	85			222			
PF4.5Y	127	274	22	99	211	25	<2		99	60		
PU3.1GP	451	272	53	28	149	134						
L1	654	244	30	24	110	87						
PF3.2B	396	252	85	82	80	165	23	87	59	20		
PF3.2BW	329	250	114	124	75	190	34	88	50	20		

Sample	SiO <sub>2</sub>	Al <sub>2</sub> O <sub>3</sub>	Fe <sub>2</sub> O <sub>3</sub>	MgO	CaO	Na <sub>2</sub> O	K <sub>2</sub> O	TiO <sub>2</sub>	MnO	P <sub>2</sub> O <sub>5</sub>	LOI	Total
<b>Unaltered Ash</b>												
PF4.2U	58.73	16.71	6.26	4.04	7.46	2.65	0.74	0.61	0.14	0.19	0.17	97.70
PU3.1U	59.23	17.21	6.32	3.94	7.62	3.52	0.73	0.60	0.13	0.15	0.56	100.01
PF4.5U1	57.79	17.02	5.92	3.70	7.56	2.89	0.76	0.61	0.12	0.15	0.57	97.15
PF4.5U2	59.42	17.08	5.97	3.79	7.55	2.78	0.78	0.63	0.12	0.15	0.32	98.60
Sample	Ba	Sr	Cr	Ni	Co	V	Cu	Zr	Zn	Pb		
PF4.2U	355	311	73	35	110	163						
PU3.1U	341	310	72	39	176	150			70			
PF4.5U1	366	305	69	35	129	170			65			
PF4.5U2	337	277	74	38	123	168			75			

\* Elements in ppm, oxides in wt.%, blanks indicate no data. All analyses were performed at the Mineral Industries Research Laboratory of the University of Alaska Fairbanks using the procedure outlined in Chapter 3. Lower limits of analytical detection were as follows: Ba - 10 ppm; Sr - 10 ppm; Cr - 5 ppm; Ni - 5 ppm; Co - 10 ppm; Cu - 2 ppm; Zr - 10 ppm; Zn - 5 ppm; Pb - 5 ppm; all oxides - 0.01 wt.%.

## Appendix 3

### VTTS Hg<sup>o</sup> and Au Data

---

#### VTTS Hg<sup>o</sup> Data

##### Encrustations

Sample	Hg <sup>o</sup> (ppb)	Sample	Hg <sup>o</sup> (ppb)
A1.1F	81*	A1.2A	62
A1.3P	44	A1.2D	20
A1.3W	69	A1.2E	82*
A1.3Pur	40	A1.4W	29
A1.3R	50*	A1.4P	36
A1.3Y	40*	A1.4O	99
A1.5O	45	A2.1R	76*
A2.5T	44	A2.1W	33
A2.5W	35	A2.1O	84
A2.5P	55*	A2.6O	60*
A2.5O	35	A3.2R <sup>y</sup>	29
A3.4P	38	A3.2W	40*
P3.2S2	40	A3.2B	38
A6.1O	37	A3.2T <sup>y</sup>	25
A6.1C	37	A3.2T	44
A6.1T	35	A3.2R <sup>y</sup>	37
A6.2P	38	A3.2OR	29
A6.2R	87*	A6.3W	48
A6.2W	45	A6.3R	51
A6.2T	45	A6.6TG	30*
A6.7R	106*	A6.6OR	27
A6.7U	22	A6.6RO	27
A6.7PK	50	A6.6RB	32
A6.7P	38	A6.6B	30
A6.7O	40*	A6.6B1	29
A6.8U	33	A6.6T	31*
A6.8R	27	A7.1W	201*
A7.2P	312*	A7.1B	63*
A7.2W	248	A7.1R	266
A7.2B	185	A7.5O	147
A8.1R	61	A7.5Y	143
A8.1G	56	A7.5P	87
A8.1W	39	A8.3U	52
A9.3S	36	A8.3R	170
A9.3C	30*	A8.3P	29

Sample	Hg <sup>o</sup> (ppb)	Sample	Hg <sup>o</sup> (ppb)
A9.3SW	29*	A7.3W'	124
A7.4W	194	A7.3P	79
A7.4W'	414*	A7.3R	130*
A7.4R	168*	A7.3W	62
A7.7	397*	f18.1	27
f19.1	60	f18.2	33
f19.2	24	f18.3	45
f19.3	20	f20.1	20
f21	60	f20.2	20
f22	22	f20.3	25
f23	36	f24.1	12
f25.1	16	f24.2	26
f25.2	29	f24.3	16
f25.3	20	f26	24
f25.4	19	f27.1	24
f28.1	33	f27.2	21
f28.2	17	f27.3	256*
f29.1	16	A30.1	19
f29.2	16	f31.1	24
f29.3	25	f31.2	20
f29.4	16	A5.1R	6913
f29.5	17	A5.1B	1473
f29.6	28	A5.1S	4501
A5.2W	495	A5.6W	378*
A5.2R	657*	A5.6T	2076
A5.2S	2404	A5.6R	5335*
A5.8B	314*	A5.7R	205*
A5.8W	335	A5.7O	175
A5.8O	285*	A5.7T	81
A5.8R	391*	A9.43	19
A5.8RW	427	f1.1	249
A5.8O'	843	f1.2	206
f2.1	371	f3.1	1897
f2.2	6057	f3.2	3072
f9T	45	f10.1	881
f9.1	1457	f10.2	5447
f9.2	210*	f11T	933
f12.1	108	f11.1	424
f12.2	128	f11.2	652
f13T	2219	f11.3	358
f13.1	2239	f16.1	6144
f13.2	3042	f16.2	5231
f17.1	23	f35.1	30
f17.2	740	f35.2	30
f14.1	25	f15.1	29

Sample	Hg <sup>o</sup> (ppb)	Sample	Hg <sup>o</sup> (ppb)
f14.2	37	f15.2	20*
f5.1	41	f6	25
f5.2	24	f7	79
f5.3	47	f8.1	127
f5.4	134	f8.2	48
f5.5	32	f8	209
82K63H	24*	84K127A	138*
82K63E	31	84K127D	1435
82K64B	21	86K167B	34
82K105B	21		

**Novarupta Basin Sample Traverses**

A1.1	34	A1.5-1	53
A1.2	71	A1.5-2	19
A2.1	28	A2.5-1	23
A2.2	23	A2.5-2	27
A3.1	36	A4.1	98
A3.2	23	A4.2	347
A4.5-1	33	A5.1	107*
A4.5-2	41	A5.2	65
A6.1	39	A7.1	24
A6.2	41	A7.2	23
A8.1	45	A9.1	26
A8.2	24	A9.2	no sp.
A10.1	24	A11.1	48
A10.2	27	A11.2	41
A12.1	22	A13.1	23
A12.2	26	A13.2	26
A14.1	51	A15.1	20
A14.2	no sp.	A15.2	24
A16.T	20	A17.1	23
A16.1	38	A17.2	49
A16.2	41	A18.1	25
A19.1	128	A18.2	33
A19.2	147	A20.1	53
A21.1	40	A20.2	54
A21.2	29	A22.1	29
A23.1	47	A22.2	29
A23.2	30	A24.1	48
A25.1	57	A24.2	180*
A25.2	53		
B1.1	161*	B2.1	372
B1.2	287	B2.2	149
B3.1	428	B4.1	52
B3.2	574	B4.2	878*
B5T	64	B6T	64

Sample	Hg <sup>o</sup> (ppb)	Sample	Hg <sup>o</sup> (ppb)
B5.1	1008	B6.1	112
B5.2	3609*	B6.2	33
B7.1	18	B8.1	92
B7.2	33	B8.2	220
B9.1	29	B10.1	25
B9.2	33	B10.2	23
B11.1	22	B12.1	23
B11.2	26	B12.2	22
B13.1	34	B14.1	42
B13.2	28	B14.2	23
B15.1	32	B16.1	22
B15.2	33	B16.2	18
B17.1	25	B18.1	29
B17.2	18	B18.2	34
B19.1	37	B20.1	19
B19.2	22	B20.2	14
B21.1	1753	B22.1	18
B21.2	1084	B22.2	no sp.
B23.1	150	B24.1	33
B23.2	18	B24.2	19
B25.1	23	B26.1	28
B25.2	22	B26.2	85
B27.1	26	B28.1	29
B27.2	23	B28.2	38

\* Average value of replicate analyses; see Hg<sup>o</sup> replication data. All Hg<sup>o</sup> analyses were performed at the Geophysical Institute of the University of Alaska Fairbanks using the procedure outlined in Chapter 4.

#### Hg<sup>o</sup> Replication Data

Sample	Analyses (ppb)	Average (ppb)	Sample	Analyses (ppb)	Average (ppb)
<b>Same Analytical Session</b>					
A1.2E	82, 82	82	A1.1F	73, 91	81
A2.1R	84, 67	76	A2.6O	63, 57	60
A5.6W	396, 360	378	A5.7R	207, 203	205
A5.8B	323, 304	314	A3.2W	45, 34	40
A7.2P	310, 314	312	A5.2R	657, 657	657
A6.2R	87, 87	87	A6.6TG	36, 25	30
A9.3C	31, 29	30	A9.3SW	29, 29	29
A7.4R	173, 163	168	A7.4W'	321, 506	414
A7.7R	412, 382	397	A7.3R	141, 118	130
f9.2	208, 213	210	B4.2	948, 809	878
A5.1	127, 87	107	B1.1	172, 151	161
f27.3	259, 253	256	f15.2	20, 20	20
82K63H	24, 25	24	84K127A	120, 156	138



**Between Analytical Sessions**

Sample	Analyses (ppb)	Average (ppb)	Sample	Analyses (ppb)	Average (ppb)
A1.3R	52, 47	50	A1.3Y	40, 39	40
A5.2R	657, 761	709	A7.1B	70, 56	63
A6.7R	135, 77	106	A5.8O	284, 286	285
A5.7R	255, 205	230	A2.5P	51, 59	55
A1.2E	82, 77	80	A7.1W	197, 206	201
A5.8R	482, 300	391	A6.7O	41, 38	40
A5.6R	5654, 5016	5335	A24.2	218, 143	180
B5.2	3313, 3905	3609	B1.1	165, 151	158

**VTTS Au Data\***

Sample	Au (ppb)	Sample	Au (ppb)	Sample	Au (ppb)
<b>Encrustations</b>					
A1.3W	<10	A2.1O	<10	A2.1G	<10
A2.6O	<10	A9.3C	<10	A3.2T	<10
A3.2W	<10	A3.2R''	<10	A3.3W	<10
A5.8B	<10	A5.8O	<10	A5.8O'	16
A5.1S	7360	A5.1B	<10	A5.6W	<10
A5.6R	<10	A3.4O	<10(2)	A3.4P	<10
A5.2S	160	A5.7R	<10	A6.4R	<10
A2.2P	<10	A1.2	<10(2)	A6.1T	<10
A6.1O	<10	A1.5Pur	150		
<b>Altered Naknek Formation</b>					
A2.7AN	<10				
<b>Unaltered Naknek Formation</b>					
A3.5	<10				
<b>Altered Novarupta Dome</b>					
A5.3AR	<10				
<b>Unaltered Novarupta Dome</b>					
FD	<10				
<b>Siliceous Sinter</b>					
A8.1C	27(2)	A5.5S	<10(2)		

\* These Au analyses were performed at the Mineral Industries Research Laboratory of the University of Alaska Fairbanks using the procedure outlined in Chapter 5. Values followed by parentheses represent averages of the number of analyses contained within the parentheses. For Bondar-Clegg Au values, see Appendix 4.

## Appendix 4

### Geochemistry of the VTTS Samples

VTTS - Gold + 46 Elements*													
Sample	Au	As	Ba	Br	Ce	Co	Cr	Cs	Eu	Hf	Ir	La	Mo
<b>Encrustations</b>													
A1.2A	0.007	17	980	4	39	<10	96	2	<2	4	<0.1	17	<2
A1.2C	<0.005	13	670	3	33	<10	91	2	<2	4	<0.1	15	<2
A1.2D	0.006	15	920	4	30	<10	160	2	<2	4	<0.1	15	<2
A1.2E	<0.005	12	740	4	32	<10	130	<1	<2	<2	<0.1	14	<2
A1.3P	0.007	15	1000	4	38	65	160	2	<2	<2	<0.1	17	3
A1.3Pur	0.007	59	900	5	33	<10	260	2	<2	<2	<0.1	14	<2
A1.3R	0.006	15	960	4	39	34	120	2	<2	<2	<0.1	16	<2
A1.3U	0.007	15	950	5	31	37	120	2	<2	<2	<0.1	15	3
A1.3W	<0.005	14	940	4	26	41	200	2	<2	<2	<0.1	15	<2
A1.3Y	<0.005	12	990	5	24	37	120	3	<2	<2	<0.1	14	<2
A1.4P	<0.005	439	370	13	14	48	160	<1	<2	<2	<0.1	9	<2
A2.1CZ	<0.005	12	800	4	28	<10	150	2	<2	6	<0.1	14	<2
A2.1P	<0.005	19	700	11	17	<10	320	2	<2	3	<0.1	10	<2
A2.1R	<0.005	14	870	4	23	<10	210	2	<2	4	<0.1	12	<2
A2.1WZ	<0.005	15	890	6	28	<10	190	2	<2	4	<0.1	14	<2
A2.1O	<0.005	12	750	3	33	<10	280	2	<2	4	<0.1	12	<2
A3.4C	<0.005	11	350	<1	19	22	120	<1	<2	3	<0.1	6	<2
A3.4B	<0.005	25	430	10	39	15	98	<1	2	3	<0.1	15	<2
A3.4P	<0.005	10	790	4	29	<10	140	2	<2	4	<0.1	14	<2
A5.1S	<0.005	10	900	31	32	<10	190	<1	<2	5	<0.1	16	<2
A6.7U	<0.005	149	400	3	12	11	160	<1	<2	3	<0.1	7	<2
A7.2B	<0.005	1060	360	30	<10	92	200	<1	<2	<2	<0.1	6	<2
A7.2P	0.012	87	700	2	<10	65	170	<1	<2	<2	<0.1	8	130
A7.2R	<0.005	114	450	4	13	42	170	<1	<2	<2	<0.1	7	3
A7.2W	<0.005	31	470	<1	<10	63	190	<1	<2	<2	<0.1	7	9
<b>Novarupta Basin Warm Ground Patches</b>													
f1.1	<0.005	3	740	<1	32	20	82	<1	<2	5	<0.1	17	<2
f1.2	<0.005	10	800	2	37	11	61	<1	<2	6	<0.1	18	<2
f5.1	<0.005	11	630	2	34	<10	<50	1	<2	4	<0.1	15	<2
f5.2	<0.005	11	690	2	31	19	<50	2	<2	4	<0.1	14	<2
f5.3	<0.005	12	590	2	33	<10	<50	1	<2	3	<0.1	13	<2
f5.4	<0.005	18	600	<1	32	<10	<50	<1	<2	5	<0.1	16	<2
f9T	<0.005	7	490	2	15	18	94	<1	<2	3	<0.1	9	<2

Sample	Au	As	Ba	Br	Ce	Co	Cr	Cs	Eu	Hf	Ir	La	Mo
f9.1	<0.005	13	530	2	15	14	97	<1	<2	3	<0.1	10	<2
f9.2	<0.005	11	520	2	24	13	95	1	<2	3	<0.1	11	<2
Sample	Rb	Sb	Sc	Se	Sm	Sn	Ta	Th	Tb	U	Te	W	Yb
Encrustations													
A1.2A	75	1	7.9	<10	5.1	<200	<1	4.7	1	2.4	<20	<2	<5
A1.2C	41	1	14	<10	4.5	<200	<1	3.8	<1	1.8	<20	<2	<5
A1.2D	57	0.9	10	<10	4.7	<200	<1	4.2	1	2.2	<20	4	<5
A1.2E	44	0.8	12	<10	4.8	<200	<1	3.8	<1	2	<20	<2	5
A1.3P	56	0.9	7.4	<10	5.4	<200	<1	5.2	1	2.4	<20	523	<5
A1.3P <sub>ur</sub>	60	2.2	8	<10	5	<200	<1	4.5	1	2.3	<20	28	<5
A1.3R	56	1	6.2	<10	5	<200	<1	4.1	1	2.3	<20	322	<5
A1.3U	67	1	6.9	<10	5.3	<200	<1	4.5	1	2.2	<20	286	<5
A1.3W	49	0.9	5.9	<10	5	<200	<1	4.7	1	2.2	<20	320	<5
A1.3Y	65	0.9	7.2	<10	5.1	<200	<1	4.6	<1	2.4	<20	359	<5
A1.4P	<10	12	24	<10	3.1	<200	<1	1.5	<1	0.8	<20	245	<5
A2.1CZ	63	2.4	5.8	<10	4.7	<200	<1	4.9	<1	2.3	<20	6	<5
A2.1P	33	4.8	7.3	<10	3.7	<200	<1	3.6	<1	1.6	<20	15	<5
A2.1R	56	0.9	10	<10	4.6	<200	<1	3.8	<1	2.1	<20	<2	<5
A2.1WZ	64	1.1	6.3	<10	4.9	<200	<1	4.5	<1	2.3	<20	3	<5
A2.1O	53	0.8	13	<10	4.3	<200	<1	3.8	<1	1.9	<20	<2	<5
A3.4C	<10	0.5	26	<10	2.6	<200	<1	2	<1	1.2	<20	<2	<5
A3.4B	22	1.2	21	<10	7.9	<200	<1	2.2	1	1	<20	<2	<5
A3.4P	50	0.7	7	<10	4.3	<200	<1	4.3	<1	2.1	<20	<2	<5
A5.1S	31	0.8	11	<10	4.7	<200	<1	4.4	<1	2	<20	<2	<5
A6.7U	17	0.8	20	<10	2.6	<200	<1	1.9	<1	0.9	<20	9	<5
A7.2B	22	2.7	4.9	<10	2	<200	<1	1.6	<1	0.8	<20	452	<5
A7.2P	27	8.6	21	<10	3.3	<200	<1	1.6	<1	0.9	<20	356	<5
A7.2R	27	2.6	21	<10	2.5	<200	<1	1.5	<1	0.6	<20	247	<5
A7.2W	23	1.9	20	<10	2.6	<200	<1	1.8	<1	1	<20	413	<5
Novarupta Basin Warm Ground Patches													
f1.1	<10	0.4	28	<10	6	<200	<1	4.1	1	1.7	<20	<2	<5
f1.2	11	0.6	22	>10	5.8	<200	<1	4.1	1	1.8	<20	<2	<5
f5.1	27	0.7	16	<10	4.1	<200	<1	3.1	<1	1.4	<20	<2	<5
f5.2	30	0.7	15	<10	4.3	<200	<1	2.9	<1	1.4	<20	<2	<5
f5.3	23	0.8	16	<10	3.9	<200	<1	2.9	<1	1.4	<20	<2	<5
f5.4	18	0.9	19	<10	6.2	<200	<1	3.3	<1	1.1	<20	<2	<5
f9T	31	0.6	20	<10	3.4	<200	<1	2.4	<1	1.2	<20	<2	<5
f9.1	32	0.6	22	<10	3.7	<200	<1	2.4	<1	1.1	<20	<2	<5
f9.2	28	0.7	20	<10	3.7	<200	<1	2.3	<1	1.2	<20	<2	<5

Sample	Ag	Zr	Lu	Cd	Cu	Ni	Pb	Zn	B	Li	Al <sub>2</sub> O <sub>3</sub>	CaO	Fe <sub>2</sub> O <sub>3</sub>
<b>Encrustations</b>													
A1.2A	<0.1	<500	<0.5	<0.2	6	7	7	8	42	29	11.4	1.05	4.21
A1.2C	<0.1	<500	<0.5	<0.2	21	7	7	16	42	40	13.9	2.15	4.12
A1.2D	<0.1	<500	<0.5	<0.2	5	6	6	13	35	36	12.6	2.05	3.58
A1.2E	<0.1	<500	<0.5	<0.2	3	5	8	18	45	40	13.3	2.76	4
A1.3P	<0.1	<500	<0.5	<0.2	2	7	7	8	35	42	11.4	1.04	1.93
A1.3Pur	<0.1	<500	<0.5	<0.2	2	10	13	10	IS	34	IS	IS	IS
A1.3R	<0.1	<500	<0.5	<0.2	27	8	8	18	34	37	12.5	0.92	6.16
A1.3U	<0.1	<500	<0.5	<0.2	9	5	6	14	38	55	12.6	1.25	1.98
A1.3W	<0.1	<500	<0.5	<0.2	3	6	5	5	32	39	11.9	0.99	1.6
A1.3Y	<0.1	<500	<0.5	<0.2	2	7	6	8	33	45	12.4	1.18	2.51
A1.4P	<0.1	<500	<0.5	<0.2	4	14	61	38	IS	10	IS	IS	IS
A2.1CZ	<0.1	<500	<0.5	<0.2	1	4	5	4	35	40	11.7	1.44	1.99
A2.1P	<0.1	<500	<0.5	<0.2	3	16	9	7	IS	47	IS	IS	IS
A2.1R	<0.1	<500	<0.5	<0.2	7	10	7	16	IS	37	IS	IS	IS
A2.1WZ	<0.1	<500	<0.5	<0.2	2	4	6	7	38	41	11.3	1.3	1.97
A2.1O	<0.1	<500	<0.5	<0.2	8	10	6	24	31	46	13.1	3.01	4.7
A3.4C	<0.1	<500	<0.5	<0.2	11	8	6	19	29	15	20	2.56	3.76
A3.4B	<0.1	<500	<0.5	<0.2	20	14	12	18	37	41	16.8	3.28	9.68
A3.4P	<0.1	<500	<0.5	<0.2	3	4	6	5	32	34	10.9	1.59	2.5
A5.1S	<0.1	<500	<0.5	<0.2	6	6	10	15	30	43	14.8	2.19	3.32
A6.7U	<0.1	<500	<0.5	<0.2	7	7	5	11	20	23	9.64	3.32	4.05
A7.2B	<0.1	<500	<0.5	<0.2	3	6	4	8	IS	12	IS	IS	IS
A7.2P	0.1	<500	<0.5	0.5	35	12	99	55	23	42	16.3	5.99	7.67
A7.2R	<0.1	<500	<0.5	<0.2	14	11	18	24	71	23	17.1	4.64	5.18
A7.2W	<0.1	<500	<0.5	0.2	17	13	15	29	IS	49	IS	IS	IS
<b>Novarupta Basin Warm Ground Patches</b>													
f1.1	<0.1	<500	<0.5	<0.2	5	7	11	33	<10	44	23.8	4.45	5.58
f1.2	<0.1	590	<0.5	<0.2	5	7	11	21	<10	34	23	2.92	5.95
f5.1	<0.1	<500	<0.5	<0.2	14	4	6	6	15	25	19.64	0.95	3.61
f5.2	<0.1	<500	<0.5	<0.2	40	8	5	7	20	22	19.20	0.77	3.52
f5.3	<0.1	<500	<0.5	<0.2	23	4	6	5	19	19	20	0.74	4.03
f5.4	<0.1	<500	<0.5	<0.2	9	7	8	22	25	20	21	0.71	8.43
f9T	<0.1	<500	<0.5	<0.2	8	8	6	19	20	29	16.7	5.87	6.58
f9.1	<0.1	<500	<0.5	<0.2	11	8	7	26	16	33	16.6	5.76	7.04
f9.2	<0.1	<500	<0.5	<0.2	6	6	8	27	18	32	15.5	4.71	6.55

Sample	K <sub>2</sub> O	LOI	MgO	MnO	Na <sub>2</sub> O	P <sub>2</sub> O <sub>5</sub>	SiO <sub>2</sub>	TiO <sub>2</sub>	Total
<b>Encrustations</b>									
A1.2A	2.91	4.66	0.32	0.05	3.23	0.08	71	0.22	99.13
A1.2C	2.1	6.36	1	0.05	2.9	0.32	65.1	0.48	98.48
A1.2D	2.1	3.78	0.81	0.06	3.7	0.13	68.6	0.31	98.16
A1.2E	2.12	5.04	1.01	0.07	3.41	0.23	65.9	0.52	98.36
A1.3P	2.85	4.06	0.3	0.05	3.43	0.27	72.5	0.19	98.02
A1.3Pur	IS	IS	IS	IS	IS	IS	IS	IS	IS
A1.3R	2.66	4.44	0.24	0.05	2.7	0.11	68.5	0.18	98.46
A1.3U	2.68	3.03	0.39	0.05	3.88	0.11	72	0.19	98.16
A1.3W	2.59	4.53	0.25	0.05	3.04	0.18	72.4	0.18	97.71
A1.3Y	2.73	3.78	0.37	0.05	3.48	0.17	71.2	0.2	98.07
A1.4P	IS	IS	IS	IS	IS	IS	IS	IS	IS
A2.1CZ	2.27	6.44	0.32	0.05	2.08	0.2	71.1	0.45	98.05
A2.1P	IS	IS	IS	IS	IS	IS	IS	IS	IS
A2.1R	IS	IS	IS	IS	IS	IS	IS	IS	IS
A2.1WZ	2.73	4.63	0.46	0.05	3.02	<0.01	72.8	0.3	98.56
A2.1O	2.2	3.55	1.49	0.08	3.39	<0.01	65.9	0.37	97.79
A3.4C	0.61	11.81	1.76	0.08	1.78	0.33	55.4	0.73	98.82
A3.4B	1.07	8.59	2.68	0.1	2.27	0.06	54.3	0.65	97.45
A3.4P	2.37	6.76	0.35	0.05	2.51	<0.01	71.6	0.47	99.10
A5.1S	1.55	6.24	1.14	0.08	2.98	<0.01	66	1	99.30
A6.7U	1.07	6.46	2.76	0.12	2.47	0.08	68	0.93	98.90
A7.2B	IS	IS	IS	IS	IS	IS	IS	IS	IS
A7.2P	1.2	2.93	2.95	0.13	3.51	0.32	57.2	0.64	98.84
A7.2R	0.92	6.92	2.49	0.1	3.12	0.43	55.9	0.65	97.45
A7.2W	IS	IS	IS	IS	IS	IS	IS	IS	IS
<b>Novarupta Basin Warm Ground Patches</b>									
f1.1	0.32	11.02	2.64	0.16	2.62	0.25	49.6	0.95	101.39
f1.2	0.68	13.75	2.16	0.11	2.38	0.33	48.1	0.87	100.25
f5.1	1.63	14.65	0.45	0.03	1.54	0.46	56.8	0.59	100.35
f5.2	1.53	15.46	0.40	0.03	1.37	0.34	54.8	0.57	97.99
f5.3	1.46	15.12	0.37	0.03	1.43	0.10	54.9	0.55	98.73
f5.4	0.80	13.87	0.75	0.03	0.94	0.41	50.6	0.71	98.25
f9T	1.31	2.09	2.96	0.12	3.62	0.28	59.9	0.67	100.10
f9.1	1.16	2.86	3.09	0.14	3.55	0.30	57.6	0.66	98.76
f9.2	1.20	3.49	2.53	0.12	3.35	0.31	59.9	0.67	98.33

Sample	Au	As	Ba	Br	Ce	Co	Cr	Cs	Eu	Hf	Ir	La	Mo
<b>Altered Naknek Formation</b>													
A2.3AN	<0.005	17	360	<1	15	37	80	<1	<2	<2	<0.1	8	<2
A2.4SAN	0.01	12	1200	<1	29	10	170	1	<2	3	<0.1	14	<2
A2.7AN	<0.005	57	620	99	21	15	<50	1	<2	4	<0.1	11	<2
<b>Unaltered Naknek Formation</b>													
32.1	<0.005	6	1100	<1	22	16	100	1	<2	3	<0.1	14	<2
32.2	<0.005	15	530	<1	24	20	110	3	<2	3	<0.1	15	<2
A3.5	<0.005	12	860	<1	24	16	160	<1	<2	4	<0.1	13	<2
<b>Altered Novarupta Dome</b>													
A5.3AR	0.008	153	610	8	29	20	82	1	<2	3	<0.1	11	2
<b>Unaltered Novarupta Dome</b>													
FD	<0.005	10	640	2	25	23	150	1	<2	3	<0.1	11	<2
<b>Unaltered Upper VTTS Ejecta</b>													
B5T	<0.005	11	500	1	20	14	97	<1	<2	3	<0.1	10	<2
B5.1	<0.005	8	560	2	20	14	200	<1	<2	3	<0.1	9	<2
B5.2	<0.005	5	560	2	22	12	110	1	<2	3	<0.1	10	<2
B13.1	<0.005	17	490	9	14	10	180	1	<2	3	<0.1	9	<2
B13.2	<0.005	24	510	27	20	<10	120	<1	<2	4	<0.1	8	<2
<b>Unaltered Lower VTTS Ejecta</b>													
A30.1	<0.005	11	940	4	36	<10	<50	4	<2	3	<0.1	<16	<2
<b>Siliceous Sinter</b>													
A8.1CH	<0.005	41	<100	6	<10	270	160	<1	<2	<2	<0.1	<5	3
A5.5S	<0.005	8	490	16	<10	310	210	<1	<2	<2	<0.1	<5	3

Sample	Rb	Sb	Sc	Se	Sm	Sn	Ta	Th	Tb	U	Te	W	Yb
<b>Altered Naknek Formation</b>													
A2.3AN	<10	0.4	20	<10	4.2	<200	<1	1.0	<1	0.6	<20	<2	<5
A2.4SAN	46	0.6	15	<10	3.6	<200	<1	3.4	<1	1.4	<20	<2	<5
A2.7AN	38	11.0	23	<10	4.1	<200	<1	3.9	<1	1.6	<20	18	<5
<b>Unaltered Naknek Formation</b>													
32.1	55	0.5	16	<10	3.4	<200	<1	3.4	<1	1.1	<20	<2	<5
32.2	51	0.6	23	<10	4.1	<200	<1	2.2	<1	1.6	<20	3	<5
A3.5	44	3.0	14	<10	3.0	<200	<1	3.6	<1	1.2	<20	45	<5
<b>Altered Novarupta Dome</b>													
A5.3AR	25	7.2	17	<10	4.1	<200	<1	3.0	<1	1.4	<20	92	<5
<b>Unaltered Novarupta Dome</b>													
FD	37	2.0	18	<10	4.2	<200	<1	4.0	<1	1.9	<20	85	<5
<b>Unaltered Upper VTTS Ejecta</b>													
B5T	28	0.7	18	<10	3.5	<200	<1	2.2	<1	1.2	<20	10	<5
B5.1	32	0.5	19	<10	3.3	<200	<1	2.7	<1	1.2	<20	2	<5
B5.2	20	0.5	23	<10	3.8	<200	<1	2.3	<1	1.0	<20	<2	<5
B13.1	31	0.8	17	<10	3.1	<200	<1	2.5	<1	1.2	<20	<2	<5
B13.2	22	1.5	15	<10	2.8	<200	<1	2.4	<1	1.3	<20	<2	<5
<b>Unaltered Lower VTTS Ejecta</b>													
A30.1	59	0.9	8.1	<10	5.3	<200	<1	4.6	<1	2.5	<20	<2	<5
<b>Siliceous Sinter</b>													
A8.1CH	<10	3.8	0.8	10	0.2	<200	<1	<0.5	<1	<0.5	<20	259	<5
A5.5S	<10	0.4	1	<10	0.3	<200	<1	<0.5	<1	<0.5	<20	401	<5

Sample	Ag	Zr	Lu	Cd	Cu	Ni	Pb	Zn	B	Li	Al <sub>2</sub> O <sub>3</sub>	CaO	Fe <sub>2</sub> O <sub>3</sub>
<b>Altered Naknek Formation</b>													
A2.3AN	<0.1	<500	<0.5	<0.2	12	23	8	42	88	21	19.4	5.89	15
A2.4SAN	<0.1	<500	<0.5	<0.2	20	20	6	46	36	38	13.7	3.70	4.80
A2.7AN	<0.1	<500	<0.5	<0.2	4	11	81	47	153	32	23.4	1.16	5.47
<b>Unaltered Naknek Formation</b>													
32.1	<0.1	<500	<0.5	<0.2	24	16	7	44	26	61	14.3	3.46	5.74
32.2	0.5	<500	<0.5	0.2	36	27	8	64	49	162	14.9	5.43	9.07
A3.5	<0.1	<500	<0.5	<0.2	22	16	12	48	29	56	13.6	3.58	6.18
<b>Altered Novarupta Dome</b>													
A5.3AR	0.2	<500	<0.5	<0.2	12	8	25	33	89	32	15.2	4.46	6.09
<b>Unaltered Novarupta Dome</b>													
FD	<0.1	<500	<0.5	<0.2	10	7	10	26	19	27	16.1	5.76	6.35
<b>Unaltered Upper VTTS Ejecta</b>													
B5T	<0.1	<500	<0.5	<0.2	9	8	7	23	15	28	16.2	4.96	7.19
B5.1	<0.1	<500	<0.5	<0.2	5	6	4	9	13	32	15.9	5.38	5.25
B5.2	<0.1	<500	<0.5	<0.2	9	6	5	12	11	28	15.8	5.28	5.28
B13.1	<0.1	<500	<0.5	<0.2	3	3	4	6	15	26	11.8	3.79	3.60
B13.2	<0.1	<500	<0.5	<0.2	1	2	7	3	27	26	10.1	2.94	3.42
<b>Unaltered Lower VTTS Ejecta</b>													
A30.1	0.1	<500	<0.5	<0.2	3	4	3	16	33	59	11.8	1.56	2.14
<b>Siliceous Sinter</b>													
A8.1CH	<0.1	<500	<0.5	<0.2	3	7	5	5	19	5	0.43	0.10	0.34
A5.5S	<0.1	<500	<0.5	<0.2	2	4	4	5	151	3	0.69	0.09	0.47



Sample	K <sub>2</sub> O	LOI	MgO	MnO	Na <sub>2</sub> O	P <sub>2</sub> O <sub>5</sub>	SiO <sub>2</sub>	TiO <sub>2</sub>	Total
<b>Altered Naknek Formation</b>									
A2.3AN	0.56	5.12	3.3	0.16	2.93	0.13	46.6	0.86	99.95
A2.4SAN	1.91	3.26	1.90	0.10	2.88	0.18	65.7	0.50	98.63
A2.7AN	1.45	12.18	0.86	0.04	1.63	<0.01	52.5	0.57	99.26
<b>Unaltered Naknek Formation</b>									
32.1	2.04	4.30	2.22	0.10	3.06	0.22	61.8	0.55	97.79
32.2	1.53	9.01	3.68	0.12	2.41	1.04	49.8	0.72	97.71
A3.5	1.93	2.90	2.09	0.10	2.90	<0.01	64.2	0.62	98.00
<b>Altered Novarupta Dome</b>									
A5.3AR	1.55	2.91	2.27	0.11	3.57	0.20	61.8	0.62	98.88
<b>Unaltered Novarupta Dome</b>									
FD	1.76	<0.05	2.65	0.12	4.09	0.16	62.4	0.68	100.07
<b>Unaltered Upper VTTS Ejecta</b>									
B5T	1.40	3.03	2.54	0.11	3.63	0.38	60.8	0.70	100.94
B5.1	1.42	2.62	2.72	0.12	3.72	0.10	59.8	0.67	97.70
B5.2	1.26	4.22	2.91	0.13	3.39	0.36	58	0.65	97.28
B13.1	1.27	2.89	2.22	0.10	3.27	0.20	69.2	0.60	98.94
B13.2	1.22	4.38	1.75	0.09	2.81	0.28	70.1	0.76	97.85
<b>Unaltered Lower VTTS Ejecta</b>									
A30.1	2.76	2.08	0.55	0.06	4.09	0.15	72.2	0.22	97.61
<b>Siliceous Sinter</b>									
A8.1CH	0.05	19.41	0.05	<0.01	0.07	0.19	77.2	0.04	97.88
A5.5S	0.05	3.82	0.05	<0.01	0.09	0.12	92.4	0.41	98.19

\* Elements in ppm, oxides in wt.%, "IS" denotes insufficient sample. All analyses were obtained from Bondar-Clegg analytical services in Vancouver, B.C., Canada. In the reported chemical data, Au through Zr were analyzed by Neutron Activation, Cd through Li (except B) were analyzed by Atomic Absorption Spectrometry, Al<sub>2</sub>O<sub>3</sub> through TiO<sub>2</sub> (except LOI) plus B were analyzed by DCP, and LOI was analyzed by Gravimetry. The lower limits of analytical detection were as follows: Au - 0.005 ppm; As - 1 ppm; Ba - 100 ppb; Br - 1 ppm; Ce - 10 ppm; Co - 10 ppm; Cr - 50 ppm; Cs - 1 ppm; Eu - 2 ppm; Hf - 2 ppm; Ir - 0.1 ppm; La - 5 ppm; Mo - 2 ppm; Rb - 10 ppm; Sb - 0.2 ppm; Sc - 0.5 ppm; Se - 10 ppm; Sm - 0.1 ppm; Sn - 200 ppm; Ta - 1 ppm; Tb - 1 ppm; Te - 20 ppm; Th - 0.5 ppm; U - 0.5 ppm; W - 2 ppm; Yb - 5 ppm; Ag - 0.1 ppm; Cd - 0.2 ppm; Cu - 1 ppm; Ni - 2 ppm; Pb - 2 ppm; Zn - 1 ppm; B - 10 ppm; Li - 1 ppm; all oxides - 0.01 wt.%.